

**INSIGHTS INTO THE CATALYTIC MECHANISM OF A
RETAINING XYLANASE FROM *CELLULOMONAS FIMI***

by

JACQUELINE WICKI

B.Sc., The University of British Columbia, 1998

A THESIS SUBMITTED IN PARTIAL FULFILLMENT OF
THE REQUIREMENTS FOR THE DEGREE OF
DOCTOR OF PHILOSOPHY

in

THE FACULTY OF GRADUATE STUDIES

(Chemistry)

THE UNIVERSITY OF BRITISH COLUMBIA

July 2007

ABSTRACT

The family 10 xylanase from *Cellulomonas fimi* (Cex) is an important model enzyme on which numerous mechanistic studies have been performed. This enzyme catalyzes the hydrolysis of β -glycosidic linkages via a double-displacement mechanism involving the formation and subsequent breakdown of a covalent glycosyl-enzyme intermediate with net retention of stereochemistry at the centre undergoing substitution. The finer details of the mechanism of this enzyme were investigated in three studies in order to gain a better understanding of this family of enzymes.

In the first study presented in *Chapter 2*, the roles of key active-site residues in the catalytic mechanism of Cex were investigated by utilizing site-directed mutagenesis in combination with steady state kinetic analyses and pH-rate dependencies. The rate-determining step for the aryl substrates tested remains deglycosylation for many of the enzymes, while the altered pH profiles demonstrate a role for these highly conserved residues in the hydrogen-bond network responsible for maintaining the ionization state of the two catalytic residues.

In *Chapter 3*, a second study addresses a fundamental enquiry of mechanistic enzymology; that is, how distal and proximal substrate interactions influence catalysis. By systematically removing hydrogen-bonding interactions through modification, individually, of substrate and enzyme, deep insight is gained into the effects of these modifications on each step of the hydrolysis reaction catalyzed by Cex and a family 11 xylanase (Bcx). The data obtained provide significant insight into the contributions of hydrogen-bonding interactions at the distal and proximal sites. The strongest bond energies were measured in the proximal site, suggesting that these interactions are critical

for substrate binding and bond hydrolysis. A particularly important finding of this study is that both 'uniform' and 'differential' binding interactions are recruited in the active site of a single enzyme.

The third study, presented in *Chapter 4*, examines how well a series of five high affinity inhibitors mimic the transition state of Cex as a function of the sp^2 - or sp^3 - hybridization state of the "anomeric carbon". Kinetic parameters for *o*-nitrophenyl β -xylobioside were determined, and very good correlations were observed in logarithmic plots relating the K_i value for the sp^2 -hybridized class of inhibitor with 10 mutants and k_{cat}/K_m for the hydrolysis of the substrate by the corresponding mutants. The dependence was significantly less in the plot of $\log(k_{cat}/K_m)$ versus $\log(1/K_i)$ for the sp^3 -hybridized class of inhibitor, indicating that the sp^2 -hybridized class of inhibitors more closely mimics the geometry of the transition state than does the sp^3 -hybridized class of inhibitors.

TABLE OF CONTENTS

ABSTRACT.....	ii
TABLE OF CONTENTS.....	iv
LIST OF TABLES	xi
LIST OF FIGURES.....	xiii
LIST OF ABBREVIATIONS	xix
ACKNOWLEDGEMENTS	xxi
DEDICATION	xxii
1 GENERAL INTRODUCTION	2
1.1 GLYCOSIDASES.....	3
1.1.1 Traditional classification systems	4
1.1.2 Subsite nomenclature.....	6
1.1.3 Glycosidase families	7
1.2 CATALYTIC MECHANISM OF RETAINING β -GLYCOSIDASES.....	7
1.2.1 Oxocarbenium ion-like transition states	11
1.2.2 Nature of the covalent glycosyl-enzyme intermediate.....	14
1.2.3 Nucleophilic participation	18
1.2.4 Acid/base catalysis.....	22
1.2.5 Non-covalent interactions.....	28
1.2.6 Substrate distortion.....	30
1.3 BIODEGRADATION OF CELLULOSE AND XYLAN.....	34
1.3.1 <i>Cellulomonas fimi</i> xylanase	36
1.3.2 <i>Bacillus circulans</i> xylanase	42
1.4 AIMS OF THIS THESIS	46

TABLE OF CONTENTS

ABSTRACT.....	ii
TABLE OF CONTENTS.....	iv
LIST OF TABLES	xi
LIST OF FIGURES.....	xiii
LIST OF ABBREVIATIONS	xix
ACKNOWLEDGEMENTS	xxi
DEDICATION	xxii
1 GENERAL INTRODUCTION	2
1.1 GLYCOSIDASES.....	3
1.1.1 Traditional classification systems	4
1.1.2 Subsite nomenclature.....	6
1.1.3 Glycosidase families	7
1.2 CATALYTIC MECHANISM OF RETAINING β -GLYCOSIDASES.....	7
1.2.1 Oxocarbenium ion-like transition states.....	11
1.2.2 Nature of the covalent glycosyl-enzyme intermediate.....	14
1.2.3 Nucleophilic participation	18
1.2.4 Acid/base catalysis.....	22
1.2.5 Non-covalent interactions.....	28
1.2.6 Substrate distortion.....	30
1.3 BIODEGRADATION OF CELLULOSE AND XYLAN.....	34
1.3.1 <i>Cellulomonas fimi</i> xylanase	36
1.3.2 <i>Bacillus circulans</i> xylanase	42
1.4 AIMS OF THIS THESIS	46

2	CHARACTERIZATION OF HIGHLY CONSERVED RESIDUES IN THE ACTIVE SITE OF <i>CELLULOMONAS FIMI</i> XYLANASE	49
2.1	INTRODUCTION	49
2.2	RESULTS	52
2.2.1	Generation of mutants of Cex	52
2.2.2	Production, purification, and physical characterization	53
2.2.3	Kinetic analysis: pH dependence of k_{cat}/K_m	54
2.2.4	Kinetic analysis: steady state kinetics	56
2.2.4.1	Probing the -2 subsite: steady state kinetic analyses of Glu43, Asn44, and Lys47 mutants	62
2.2.4.2	Probing the -1 subsite: steady state kinetic analyses of His80 mutants	67
2.2.4.3	Probing the -1 subsite: steady state kinetic analyses of Asn126 and Asn169 mutants	71
2.3	DISCUSSION	73
2.3.1	Effects of mutations on glycosylation and deglycosylation	73
2.3.2	A second look at the rate-limiting step in the hydrolysis reaction by Cex and mutants: diffusion-controlled rate constants	78
2.3.3	Importance of -2 subsite amino acids Glu43, Asn44, and Lys47	81
2.3.3.1	Role of Glu43	81
2.3.3.2	Role of Asn44	82
2.3.3.3	Role of Lys47	83
2.3.3.4	Role of His80	84
2.3.4	Amino acids that influence the catalytic residues	85
2.3.4.1	Role of Asn126	85
2.3.4.2	Role of Asn169	86
2.3.5	Analyses of the pH profiles for Cex variants	87
2.3.6	Activity of family 10 enzymes	90
2.4	CONCLUSIONS	92

3	AN ASSESSMENT OF THE BINDING ENERGY CONTRIBUTION OF HYDROGEN BONDS AT THE TRANSITION STATE USING DEOXYGENATED SUBSTRATES AND SITE-DIRECTED MUTAGENESIS	94
3.1	INTRODUCTION	94
3.1.1	Hydrogen-bonding energetics in water	96
3.1.2	Hydrogen bonding to fluorine.....	99
3.1.3	Electronic effects	100
3.1.4	Objectives.....	102
3.2	RESULTS AND DISCUSSION	103
3.2.1	Binding energy contributions probed by using substrate analogues	103
3.2.1.1	Kinetic analysis of family 10 <i>C. fimi</i> xylanase.....	104
3.2.1.2	Kinetic analysis of family 11 <i>B. circulans</i> xylanase	112
3.2.1.3	Comparison of results for two xylanases from distinct families	118
3.2.2	Binding energy contributions probed by using mutant enzymes	123
3.2.2.1	Design of the mutations.....	124
3.2.2.2	Subsite -2 interactions	125
3.2.2.3	Subsite -1 interactions	129
3.2.3	Uniform and differential binding interactions	130
3.3	CONCLUSIONS.....	133

4	INQUIRY INTO THE TRANSITION-STATE ANALOGY OF A SERIES OF IMINOSUGAR INHIBITORS FOR A XYLANASE.....	136
4.1	INTRODUCTION	136
4.1.1	Transition-state theory	136
4.1.2	Enzyme catalysis	138
4.1.3	Experimental approaches to enzymatic transition-state structure	140
4.1.3.1	KIE to determine TS structure.....	140
4.1.3.2	Computational approaches to the transition state.....	141
4.1.3.3	TS analogues	142
4.1.4	Criteria for transition-state analogy	143
4.1.4.1	Strong inhibition.....	144
4.1.4.2	Slow inhibition	144
4.1.4.3	Free energy relationships.....	147
4.1.4.4	Thermodynamic parameters	150
4.1.4.5	pH profiles	151
4.1.5	Inhibitors of glycoside hydrolysis.....	152
4.1.6	Inhibitors of Cex.....	156
4.1.7	Aims of this study.....	158
4.2	RESULTS AND DISCUSSION	159
4.2.1	Inhibition of Cex mutants by iminosugar inhibitors	160
4.2.2	How good a transition-state analogue is the inhibitor?	163
4.2.3	The pK_a values of <i>xylobio</i> -derived inhibitors.....	168
4.2.4	The pH dependence of the binding of <i>xylobio</i> -derived inhibitors.....	171
4.2.4.1	<i>Xylobio</i> -derived lactam oxime, imidazole, and isofagomine lactam	172
4.2.4.2	<i>Xylobio</i> -derived deoxynojirimycin and isofagomine	174
4.3	CONCLUSION: TRANSITION-STATE MIMICS OR FORTUITOUS BINDERS?	175

5	MATERIALS AND METHODS.....	178
5.1	MOLECULAR BIOLOGY	178
5.1.1	Reagents, enzymes, and bacterial strains.....	178
5.1.2	Oligonucleotides	178
5.1.3	Site-directed mutagenesis by linear amplification	180
5.1.4	Site-directed mutagenesis by PCR.....	183
5.1.5	Overexpression and purification by active-site mutants of Cex	186
5.1.6	Protein mass determination	188
5.2	ENZYME KINETICS.....	188
5.2.1	General materials and procedures	188
5.2.2	Steady state kinetics	189
5.2.3	pH stability studies.....	191
5.2.4	pH dependence studies.....	192
5.2.5	Kinetics of inhibition.....	193
5.2.6	pK_a determinations for inhibitors.....	195
5.2.7	Determination of extinction coefficients	195
	REFERENCES	198
	APPENDICES	228

A	GRAPHICAL REPRESENTATION OF DATA	228
A.1	STEADY STATE KINETICS FOR THE HYDROLYSIS OF XYLOBIOSIDES OR CELLOBIOSIDES	228
A.1.1	Native Cex	228
A.1.2	Cex E43A	231
A.1.3	Cex N44A	235
A.1.4	Cex K47A	239
A.1.5	Cex H80A	242
A.1.6	Cex H80N	246
A.1.7	Cex H80Q	250
A.1.8	Cex Q87M	254
A.1.9	Cex Q87Y	257
A.1.10	Cex N126A	260
A.1.11	Cex E127A	263
A.1.12	Cex N169A	264
A.1.13	Cex H205N	267
A.2	STEADY STATE KINETICS FOR INHIBITION BY IMINO SUGAR INHIBITORS	269
A.2.1	Cex E43A	269
A.2.2	Cex N44A	271
A.2.3	Cex K47A	273
A.2.4	Cex H80A	275
A.2.5	Cex H80N	277
A.2.6	Cex H80Q	279
A.2.7	Cex Q87M	281
A.2.8	Cex Q87Y	283
A.2.9	Cex N126A	285
A.2.10	Cex E127A	287
A.2.11	Cex N169A	289
A.3	PH DEPENDENCIES OF K_{CAT}/K_M FOR THE HYDROLYSIS OF XYLOBIOSIDES OR CELLOBIOSIDES BY NATIVE AND MUTANT CEX	292

B	COMPILATION OF CEX DATA.....	298
B.1	TABLES.....	298
B.2	REFERENCES.....	310
C	FUNDAMENTALS OF ENZYME KINETICS.....	312
C.1	BASIC ENZYME KINETICS	312
C.2	THE SIGNIFICANCE OF MICHAELIS–MENTEN PARAMETERS.....	316
C.3	ENZYME INHIBITION	322
C.3.1	Competitive inhibition	322
C.3.2	Noncompetitive, uncompetitive, and mixed inhibition	323
C.4	BINDING ENERGY AND ENZYME CATALYSIS	325
C.5	THE PH DEPENDENCE OF ENZYME CATALYSIS.....	327
C.5.1	The Michaelis–Menten mechanism	328
C.5.2	Modifications and breakdown of the Michaelis–Menten mechanism	330

LIST OF TABLES

Table 2.1: Total yields of Cex mutants produced.....	54
Table 2.2: Determination of molecular weight by mass spectrometry.....	54
Table 2.3: pH Dependence of k_{cat}/K_m for <i>C. fimi</i> xylanase and mutants.....	56
Table 2.4: Michaelis–Menten parameters for the hydrolysis of various aryl glycoside substrates by <i>C. fimi</i> xylanase.....	61
Table 2.5: Michaelis–Menten parameters for the hydrolysis of various aryl glycoside substrates by several family 10 xylanases.....	62
Table 2.6: Michaelis–Menten parameters for the hydrolysis of aryl glycosides by the <i>C. fimi</i> xylanase (Cex) and mutants E43A, N44A, and K47A.....	63
Table 2.7: Michaelis–Menten parameters for the hydrolysis of aryl glycosides by the <i>C. fimi</i> xylanase (Cex) and mutants H80A, H80N, and H80Q.....	68
Table 2.8: Michaelis–Menten parameters for the hydrolysis of aryl glycosides by the <i>C. fimi</i> xylanase (Cex) and mutants N126A and N169A.....	72
Table 2.9: Kinetic parameters for the glycosylation and deglycosylation steps of the hydrolysis reaction by variants of Cex.....	74
Table 2.10: Free energy changes at the glycosylation and deglycosylation steps of the hydrolysis reaction by variants of Cex.....	76
Table 3.1: Kinetic parameters for the hydrolysis of deoxy/deoxyfluoro analogues by wild-type <i>C. fimi</i> xylanase.....	105
Table 3.2: Summary of hydrogen-bonding interactions between the xylobiosyl intermediate and protein residues in the active site of the 2-deoxy-2-fluoroxyllobiosyl–enzyme complex of Cex.....	110
Table 3.3: Kinetic parameters for the hydrolysis of deoxy/deoxyfluoro analogues of PNPX ₂ by wild-type <i>B. circulans</i> xylanase.....	113
Table 3.4: Summary of hydrogen-bonding interactions between the xylobiosyl intermediate and protein residues in the active site of the 2-deoxy-2-fluoroxyllobiosyl–enzyme complex of Bcx (81).....	118

Table 3.5: Binding energy contribution $\Delta\Delta G^\ddagger$ (kcal mol ⁻¹) of individual hydroxyl groups in the hydrolysis of PNPX ₂ by Cex and Bcx.	120
Table 3.6: Kinetic parameters for the hydrolysis of PNPX ₂ by wild-type and mutant <i>C. fimi</i> xylanase.	126
Table 3.7: Apparent binding energy contribution, $\Delta\Delta G^\ddagger$ (kcal mol ⁻¹), of individual substrate hydroxyl groups in the hydrolysis of deoxy/deoxyfluoro analogues of PNPX ₂ by wild-type <i>C. fimi</i> xylanase and selected mutants.....	128
Table 4.1: Inhibition constants (K_i) for Cex and Bcx with various <i>xylobio</i> -derived iminosugars.....	157
Table 4.2: Inhibition constants (K_i) for <i>C. fimi</i> xylanase and mutants with various <i>xylobio</i> -derived iminosugars.	161
Table 4.3: <i>Xylobio</i> -derived inhibitor pK _a values of the conjugate acid.	170
Table 4.4: Parameters determined from the pH profile for the binding of <i>xylobio</i> -derived inhibitors to wild-type Cex.....	172
Table 5.1: Primers used in the mutagenesis of <i>C. fimi</i> xylanase.....	179
Table 5.2: pH Incubation mixture for enzyme stability studies.....	191
Table 5.3: Standard assay conditions for enzyme stability.....	192
Table 5.4: Standard assay conditions for pH profiles.....	193
Table 5.5: Extinction coefficients of substituted phenols at 37°C in sodium phosphate buffer, pH 7.00.	196

LIST OF FIGURES

Figure 1.1: Glycone and aglycone moieties of a β -glucoside are shown with the arrow indicating the scissile glycosidic bond.....	3
Figure 1.2: Reactions catalyzed by retaining and inverting β -glucosidases.....	5
Figure 1.3: A schematic depiction of <i>endo</i> and <i>exo</i> sites of cleavage of an oligosaccharide by glycosidases.....	5
Figure 1.4: Schematic drawing of sugar-binding subsites in two glycosidases. By convention, the non-reducing end of the substrate is drawn on the left while the reducing end is drawn on the right. The arrow placed between the -1 and +1 subsites indicates the point of cleavage.	6
Figure 1.5: The hydrolysis reactions catalyzed by retaining and inverting glycosidases.....	8
Figure 1.6: General double-displacement mechanism for a retaining glycosidase.	10
Figure 1.7: Inactivation and reactivation by 2-deoxy-2-fluoro glycosides. (A) Inactivation by formation of the fluoroglycosyl-enzyme intermediate. (B) Reactivation by transglycosylation of the fluoroglycosyl-enzyme intermediate.....	16
Figure 1.8: Structures of several classes of the fluoro sugars that function as mechanism-based inactivators.....	17
Figure 1.9: Nucleophilic fluorination of 2,4-dinitrophenyl β -mannoside by the β -mannosidase nucleophile mutant (Glu519Ser) from <i>Cellulomonas fimi</i>	21
Figure 1.10. The <i>anti</i> orientation of the acid catalytic residue and protonation trajectory as the basis for rationalizing the relative potency of two triazole inhibitors. (A) <i>Anti</i> -protonation of the glycosidic oxygen. (B) Absence of any possible hydrogen bonding to the 1,2,3-triazole inhibitor. (C) Possible <i>anti</i> -protonation of the 1,3,4-triazole inhibitor.....	23
Figure 1.11: Depiction of the pH dependence of k_{cat}/K_m for Bcx Asn35Asp mutant as the product of titration curves of catalytic residues derived from ^{13}C -NMR. Although only 1% of the mutant is in the correct ionization state for catalysis, it is 20% more active than the wild-type enzyme.....	27

- Figure 1.12: The Asn35Asp mutant of Bcx increases the inherent catalytic efficiency by at least 100-fold over the wild-type enzyme by forming a strong hydrogen bond between Asp35 and Glu172. 28
- Figure 1.13: Partial map of pyranoside interconversions adapted from Stoddart (78). Potential transition-state conformations that possess a coplanar arrangement of C5, O5, C2 and C1 atoms are shown boxed. 32
- Figure 1.14: Orientation of the lone pairs on the endocyclic oxygen relative to the glycosidic oxygen of the leaving group. (A) The 4C_1 ground state conformation of many common glycosides and covalent intermediate structures. This conformation features a lone pair on the ring oxygen that is antiperiplanar to the C1–OR bond in an α -configured glycoside. (B) The 4H_3 conformation proposed as a possible transition-state conformation. (C) The ${}^{4,1}B$ or 4E conformation and (D) the skew-boat 1S_3 conformation that features a lone pair on the ring oxygen that is antiperiplanar to the C1–OR bond in a β -configured glycoside, as required for the optimal effect of the antiperiplanar lone pair hypothesis (ALPH)..... 34
- Figure 1.15: Three-dimensional structure of Cex with bound 2F-X₂ (76). The overall structure of Cex is depicted as a protein cartoon in divergent (wall-eyed) stereo, with α -helices coloured green, β -strands blue and loops red. The bound 2F-X₂ is drawn as a stick model, with atoms coloured according to atom type, carbon in grey, oxygen in red, and fluorine in yellow. The water molecules in the active site have been removed for clarity. This figure and subsequent molecular representations were prepared with Chem3D Ultra 10.0 (<http://www.cambridgesoft.com>). 37
- Figure 1.16: Active site of the *Cellulomonas fimi* xylanase trapped as a covalent 2-deoxy-2-fluorocellobiosyl–enzyme intermediate. Adapted from (32)..... 40
- Figure 1.17: Hydrogen bonding at the transition state..... 42
- Figure 1.18: Three-dimensional structure of Bcx with bound 2F-X₂ (81). The overall structure of Bcx is depicted as a protein cartoon in divergent (wall-eyed) stereo, with α -helices coloured green, β -strands blue and loops red. The bound 2F-X₂ is drawn as a stick model, with atoms coloured according to atom type, carbon in grey, oxygen in red, and fluorine in yellow. The water molecules in the active site have been removed for clarity. This figure was prepared with Chem3D Ultra 10.0 (<http://www.cambridgesoft.com>)..... 43
- Figure 1.19: Active site of the *Bacillus circulans* xylanase trapped as a covalent 2-deoxy-2-fluoroxyllobiosyl–enzyme intermediate. 44

Figure 1.20: The 2-deoxy-2-fluoroxyllobiosyl–enzyme intermediate formed on the <i>Bacillus circulans</i> xylanase. Green dashes represent hydrogen bonds, the blue dash depicts a non-hydrogen bond interaction, and the R group represents the saccharide unit bound in the –2 subsite of the active site. Adapted from Sidhu <i>et al.</i> (81).....	46
Figure 2.1: Scheme of protein–carbohydrate interactions in the active site region of 2F-xylobiosyl–Cex-cd complex observed by three-dimensional structural analysis (76). Hydrogen-bonding interactions between heteroatoms are in Angstroms. The distance between 2F and the carbonyl oxygen of Glu233 is 2.6 Å (not shown).....	51
Figure 2.2: Overview of the QuikChange™ Site-Directed Mutagenesis Kit.....	53
Figure 2.3: Data for the hydrolysis of <i>o</i> -nitrophenyl xylobioside by wild-type Cex plotted in (A) and (B) Michaelis–Menten form; and (C) and (D) Lineweaver–Burk form. Kinetic parameters for the hydrolysis reaction were obtained by fitting data obtained at lower substrate concentrations (unbroken line), while those for the hydrolysis reaction were obtained by fitting data obtained at higher substrate concentrations (dashed line).....	60
Figure 2.4: pH profiles of wild-type (○) and Glu43, Asn44, and Lys47 mutants of Cex. The pH dependence of wild-type Cex was measured using 2,4DNPC where $pK_{a1} = 3.9$ and $pK_{a2} = 7.7$. (A) The E43A (●) mutant enzyme activity was measured using 2,4DNPC where $pK_{a1} = 3.7$ and $pK_{a2} = 6.9$. (B) The N44A (■) mutant enzyme activity was measured using 2,4DNPC where $pK_{a1} = 3.9$ and $pK_{a2} = 8.0$. (C) The K47A (▲) mutant enzyme activity was measured using 2,5DNPX ₂ where $pK_{a1} = 3.9$ and $pK_{a2} = 6.0$	66
Figure 2.5: pH profiles of wild-type (○) and His80 mutants of Cex. The pH dependence of wild-type Cex was measured using 2,4DNPC where $pK_{a1} = 3.9$ and $pK_{a2} = 7.7$. (A) The H80A (●) mutant enzyme activity was measured using PNPX ₂ where $pK_{a1} = 4.6$ and $pK_{a2} = 6.2$. (B) The H80N (■) mutant enzyme activity was measured using PNPX ₂ where $pK_{a1} = 4.6$ and $pK_{a2} = 6.3$. (C) The H80Q (▲) mutant enzyme activity was measured using PNPX ₂ where $pK_{a1} = 4.6$ and $pK_{a2} = 7.0$	70
Figure 2.6: pH profiles of wild-type (○) and Asn126 and Asn169 mutants of Cex. The pH dependence of wild-type Cex was measured using 2,4DNPC where $pK_{a1} = 3.9$ and $pK_{a2} = 7.7$. (A) The N126A (●) mutant enzyme activity was measured using 2,4DNPC where $pK_{a1} = 4.4$ and $pK_{a2} = 8.5$. (B) The N169A (■) mutant enzyme activity was measured using 2,4DNPC where $pK_{a1} = 4.0$ and $pK_{a2} = 8.2$	73

- Figure 2.7: (A) Comparison of rate constants for glycosylation of PNPC and PNPX₂ by variants of Cex. A slope of $m = 1.0$ and correlation coefficient of $r = 0.87$ was observed. (B) Comparison of rate constants for deglycosylation of cellobiosyl–enzyme intermediates and xylobiosyl–enzyme intermediates of variants of Cex. A slope of $m = 0.94$ and correlation coefficient of $r = 0.95$ was observed. (C) Comparison of rate constants for glycosylation and deglycosylation reactions for the hydrolysis of ONPX₂ by variants of Cex. Open circles correspond to mutations within the –2 subsite; and closed circles correspond to mutations within the –1 subsite of Cex. A slope of $m = 0.97$ and correlation coefficient of $r = 0.62$ was observed. 77
- Figure 3.1: The hydroxyl can act as a hydrogen-bond donor or acceptor, whereas fluorine can only act as a hydrogen-bond acceptor. 95
- Figure 3.2: Chromogenic synthetic substrates. PNPX₂, 2'-deoxy-PNPX₂, 2'-deoxy-2'-fluoro-PNPX₂, 3'-deoxy-PNPX₂, 3'-deoxy-3'-fluoro-PNPX₂, 4'-deoxy-PNPX₂, and 4'-deoxy-4'-fluoro-PNPX₂ were prepared by Dr. Johann Schloegl. 3'-Deoxy-3'-fluoro-PNPX₂ was prepared by Dr. Chris A. Tarling. 104
- Figure 3.3: Schematic representation of proposed intermolecular hydrogen-bond interactions between 4-nitrophenyl β -xylobioside and Cex based on substrate analogue data, X-ray crystallography and NMR studies. 109
- Figure 3.4: Scheme of protein–carbohydrate interactions in the active site region of the 2-fluoroxxylobiosyl–Bcx complex observed by three-dimensional structural analysis (81). Hydrogen-bonding interactions between heteroatoms are in Angstroms. 115
- Figure 3.5: Binding energy contribution $\Delta\Delta G^\ddagger$ (kcal mol⁻¹) plot for a series of deoxy- and deoxyfluoro- β -xylobioside analogues with *B. circulans* xylanase (Bcx) and *C. fimi* xylanase (Cex). 121
- Figure 3.6: Scheme of protein–carbohydrate interactions in the active site region of 2F-xylobiosyl–Cex-cd complex observed by three-dimensional structural analysis (76). Hydrogen-bonding interactions between heteroatoms are in Angstroms. The distance between 2F and the carbonyl oxygen of Glu233 is 2.6 Å (not shown). 123
- Figure 3.7: Reaction coordinate diagram showing the consequences of modifications to the (a) distal sugar and (b) proximal sugar. 132
- Figure 4.1: A reaction profile. The horizontal axis is the reaction coordinate and the vertical axis is the potential or Gibbs free energy. The transition state corresponds to the maximum of the Gibbs free energy. 137

Figure 4.2: Reaction coordinate diagram to show how an enzyme can increase the rate of reaction of a bound substrate by stabilizing the transition state.....	139
Figure 4.3: Two potential mechanisms for slow-binding inhibition.....	145
Figure 4.4: Thermodynamic box illustrating the relationship between ground-state and transition-state binding. The designations E, S, and P refer to enzyme, substrate in the ground state form, and product, respectively, while S^\ddagger represents the transition state structure.....	147
Figure 4.5: Structures of some naturally occurring and synthetic glycosidase inhibitors in the <i>gluco</i> -configuration.	153
Figure 4.6: Structures of the 5 iminosugars studied.	160
Figure 4.7: Inhibition of Cex N169A by <i>xylobio</i> -imidazole at varying concentrations of 2,4DNPC. Plot A is the Michaelis–Menten plot, plot B is the Lineweaver–Burk plot, and plot C is the Eadie–Hofstee plot. The concentrations of <i>xylobio</i> -imidazole were 0 (○), 0.123 (●), 0.370 (□), 0.925 (■), and 2.47 μ M (Δ).....	162
Figure 4.8: Transition state analogy plots for <i>C. fimi</i> xylanase Cex. Comparison between k_{cat}/K_m for ONPX ₂ and inhibitor K_i values for <i>xylobio</i> -derived (A) lactam oxime 1; (B) imidazole 2; (C) isofagomine lactam 3; (D) deoxynojirimycin 4; and (E) isofagomine 5.....	167
Figure 4.9: Titration curves for the conjugate acid forms of the <i>xylobio</i> -derived lactam oxime (●), imidazole (■), deoxynojirimycin (▼), and isofagomine (◆). <i>Note:</i> amides are strong bases (conjugated acid pK_a between -6 and -10); therefore, the pK_a of the <i>xylobio</i> -isofagomine lactam is likely well below -5	169
Figure 4.10: pH dependence of k_{cat}/K_m for Cex (●), $1/K_i$ for <i>xylobio</i> -derived lactam oxime pK_a 4.9 (●), imidazole pK_a 5.9 (■), isofagomine lactam $pK_a < -5$ (▲), deoxynojirimycin pK_a 6.9 (▼), and isofagomine pK_a 8.8 (◆). Fits to “bell-shaped” profiles are shown for k_{cat}/K_m (dashed line) and $1/K_i$ (coloured solid lines).	171

Figure 5.1: Introducing mutations by the QuikChange™ Site-Directed Mutagenesis method. A supercoiled dsDNA vector with an insert of interest (—●—) and two synthetic oligonucleotide primers (—^—) containing the desired mutation are mixed. The oligonucleotide primers, each complementary to opposite strands of the vector, are extended during temperature cycling using *Pfu* DNA polymerase to generate mutated plasmid containing staggered nicks. Following temperature cycling, the methylated, nonmutated parental DNA template is digested with *Dpn* I. The circular, nicked dsDNA is transformed into XL1-Blue supercompetent cells. After transformation, the nicks in the mutated plasmid are repaired by the XL1-Blue supercompetent cells. 181

Figure 5.2: Restriction map of pUC12-1.1*cex*(PTIS)..... 183

Figure 5.3: Introducing mutations by in vitro overlap-extension PCR. Two PCRs are performed to produce two fragments that carry overlapping sequences. These two fragments are then mixed, denatured, and annealed to obtain mutant DNAs in a further PCR. 184

LIST OF ABBREVIATIONS

ALPH	antiperiplanar lone pair hypothesis
Bcx	<i>Bacillus circulans</i> xylanase (family 11)
BcXyn11A	<i>Bacillus circulans</i> xylanase (family 11)
BSA	bovine serum albumin
CAZy	carbohydrate-active enzyme database
Cex	<i>Cellulomonas fimi</i> xylanase (family 10)
CfXyn10A	<i>Cellulomonas fimi</i> xylanase (family 10)
DEGLY	deglycosylation
EC	Enzyme Commission (classification number) of the International Union of Biochemistry
ESI-MS/MS	electrospray ionization tandem mass spectrometry
GLY	glycosylation
HEWL	hen egg white lysozyme
HPLC	high performance liquid chromatography
IPTG	isopropyl β -D-thiogalactoside
IUBMB	International Union of Biochemistry and Molecular Biology
kDa	kiloDalton
M	mutant enzyme
MS/MS	tandem mass spectrometry
NMR	nuclear magnetic resonance
PDB	protein data bank
RP-HPLC	reverse phase high performance liquid chromatography
TS	transition state
WT	wild-type enzyme

Substrates

3F-PNPX ₂	<i>p</i> -nitrophenyl 3-deoxy-3-fluoro- β -xylobioside
2'H-PNPX ₂	<i>p</i> -nitrophenyl 2'-deoxy- β -xylobioside
2'F-PNPX ₂	<i>p</i> -nitrophenyl 2'-deoxy-2'-fluoro- β -xylobioside
3'H-PNPX ₂	<i>p</i> -nitrophenyl 3'-deoxy- β -xylobioside
3'F-PNPX ₂	<i>p</i> -nitrophenyl 3'-deoxy-3'-fluoro- β -xylobioside
4'H-PNPX ₂	<i>p</i> -nitrophenyl 4'-deoxy- β -xylobioside
4'F-PNPX ₂	<i>p</i> -nitrophenyl 4'-deoxy-4'-fluoro- β -xylobioside
2F-DNPC	2,4-dinitrophenyl 2-deoxy-2-fluoro- β -cellobioside
DNPC	2,4-dinitrophenyl β -cellobioside
PNPC	<i>p</i> -nitrophenyl β -cellobioside
PNPX ₂	<i>p</i> -nitrophenyl β -xylobioside
ONPX ₂	<i>o</i> -nitrophenyl β -xylobioside
2,5DNPX ₂	2,5-dinitrophenyl β -xylobioside

Amino Acid Abbreviations

Ala	A	alanine
Arg	R	arginine
Asn	N	asparagine
Asp	D	aspartic acid
Cys	C	cysteine
Glu	E	glutamic acid
Gln	Q	glutamine
Gly	G	glycine
His	H	histidine
Ile	I	isoleucine
Leu	L	leucine
Lys	K	lysine
Met	M	methionine
Phe	F	phenylalanine
Pro	P	proline
Ser	S	serine
Thr	T	threonine
Trp	W	tryptophan
Tyr	Y	tyrosine
Val	V	valine

ACKNOWLEDGEMENTS

First and foremost, I would like to express my sincere gratitude to my supervisor, Professor Stephen G. Withers, for all of his guidance, encouragement, and tremendous patience. His insights and enthusiasm were a source of inspiration for me and I consider it a great privilege to have been part of his research group.

I wish to thank all the members of the Withers group, past and present, for their friendship and all their assistance. The technical support of Shouming He, Ms. Karen Rupitz, and Ms. Emily Kwan is also greatly appreciated.

I would like to extend my gratitude to the following people who contributed to this work: Professor Spencer Williams for a fruitful collaboration on the TSA project and for synthesizing the iminosugar inhibitors; Dr. Johann Schloegl for a fruitful collaboration on the deoxysugar project and for synthesizing all distal deoxy/deoxyfluoro xylobioside substrates; Dr. Chris Tarling for synthesizing the proximal xylobioside substrate; and Professor R. Anthony Warren for access to his "Cellulase" lab.

And finally, to all my family and friends, thank you for your support and steadfast belief in me.

*Mamie mojej Grażynie,
której nieustająca cierpliwość i oddanie sprawiły,
że powstanie tej pracy stało się możliwe.*

CHAPTER 1

GENERAL INTRODUCTION

1 General Introduction

Carbohydrates comprise a diverse array of simple and complex biological molecules. They are the most abundant class of organic molecules found in living organisms. Unlike the other major classes of biopolymers such as proteins and nucleic acids, carbohydrate compounds are not synthesized according to a template, and this, in large part, accounts for their remarkable diversity. The vast assortment of biological functions expressed by carbohydrates is, at least in part, a consequence of the immense variety of distinctive structural motifs generated by synthetic enzymes.

Carbohydrate polymers such as starch and glycogen are traditionally recognized as major sources of metabolic energy, while polymers such as cellulose and chitin are suitable for the maintenance of physical structures. Various oligosaccharides are ubiquitous as components of lipids, proteins, nucleic acids, and other complex biomolecules. The role of carbohydrates in molecular recognition and signal transduction is critical to the performance of biological systems. As a result of their biological importance and potential medical applications, carbohydrates, along with the enzymes responsible for their metabolism, are now the subjects of extensive research efforts. Glycosidases are one such group of enzymes, and are responsible for the transfer of glycosyl moieties from a glycoside to water, the result being hydrolysis. Due to the biologically widespread process of glycoside cleavage, glycosidase inhibitors have potential therapeutic value. An understanding of the mechanism by which these enzymes hydrolyse glycosidic bonds and of how to inhibit them is fundamental to their application in medicine and industry.

1.1 Glycosidases

Glycosidases, alternatively known as glycoside hydrolases, comprise a large family of enzymes that catalyze the transfer of a glycosyl moiety from a donor sugar to an acceptor water molecule. These enzymes are typically involved in the biodegradation of complex polymeric carbohydrate molecules to their simple sugar constituents. The glycosidic bonds that join polysaccharides display formidable stability, as is demonstrated by the five million year half-life of a common glycosidic linkage under neutral aqueous conditions (1). Hydrolysis of the glycosidic scissile bond occurs between the glycone, which is typically a carbohydrate moiety, and the aglycone, which commonly consists of another saccharide unit, but may also be an alcohol, phosphate, or thiol group (Figure 1.1). Glycosidases catalyze the breakdown of such linkages by factors on the order of 10^{17} -fold, representing one of the largest rate accelerations attained by any class of enzyme. Furthermore, these enzymes are relatively promiscuous with regards to aglycone specificity; consequently, a detailed kinetic analysis may be carried out using a wide array of synthetic substrates.

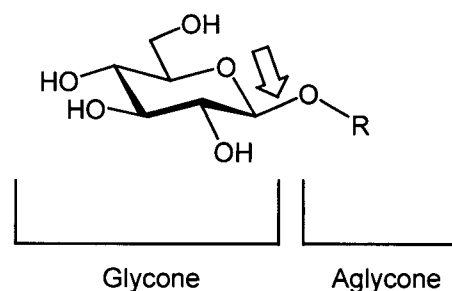


Figure 1.1: Glycone and aglycone moieties of a β -glucoside are shown with the arrow indicating the scissile glycosidic bond.

1.1.1 Traditional classification systems

A number of methods have been devised to classify glycosidases. A simple system derived by the International Union of Biochemistry and Molecular Biology (IUBMB) classifies enzymes primarily according to the reaction they catalyze, and this, together with the name(s) of the substrate(s) provides a basis for classification of individual enzymes. Nevertheless, IUBMB rules are of limited value in that they do not provide any detailed information on the reaction mechanism. Several other classification systems exist, based on three criteria: glycone specificity, the anomeric configuration of the glycosidic linkage that is formed or broken, and the stereochemical outcome of the reaction.

- Regarding the glycone specificity, the classification is dependent on the sugar moiety for which the glycosidase is most reactive. For instance, glucosidases would be specific for a glucose moiety as the glycone while galactosidases would prefer a galactose unit as the glycone.
- Glycosidases may also be classified as either “ α ” or “ β ” according to the absolute specificity for the anomeric configuration that is broken in the substrate. For instance, a β -glycosidase will only cleave β -glycosides and not α -glycosides.
- Glycosidases are classified as “inverting” or “retaining” depending on whether the enzyme cleaves the glycosidic bond with net retention or inversion of anomeric configuration (Figure 1.2). For example, a retaining β -glycosidase cleaves a β -glycosidic linkage to yield a hemiacetal with the β -configuration,

while an inverting β -glycosidase cleaves a β -glycosidic linkage to generate an α -hemiacetal.

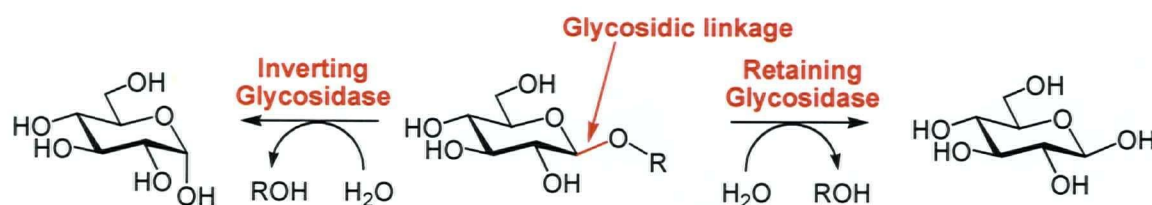


Figure 1.2: Reactions catalyzed by retaining and inverting β -glycosidases.

- Furthermore, the terms “*exo*” and “*endo*” are used to categorize glycosidases that act on polymeric substrates such as cellulose and xylan. Enzymes that cleave terminal sugar residues from either end of the oligosaccharide chain, typically releasing mono- or disaccharides, are known as *exo*-glycosidases. Other enzymes that cleave at sites in the middle of the oligosaccharide chain are known as *endo*-glycosidases. This distinction serves to indicate substrate specificity of a glycosidase and has been found to correlate with the tertiary structure of certain enzymes.

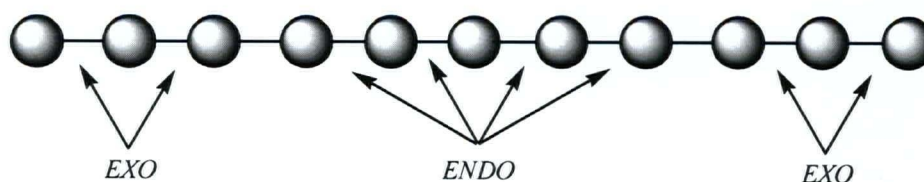


Figure 1.3: A schematic depiction of *endo* and *exo* sites of cleavage of an oligosaccharide by glycosidases.

1.1.2 Subsite nomenclature

Glycosidases have evolved to bind the saccharide residues of oligo- and polysaccharides in distinct subsites. The expansive growth of available three-dimensional structures has led to the identification of these binding subsites and consequently necessitated a more reliable system of nomenclature. Under a system put forth by Davies *et al.* (2), the position of the subsite relative to the point of cleavage is assigned by labelling subsites from $-n$ to $+n$ (where n is an integer). Subsites are labelled such that the $-n$ represents the non-reducing end and $+n$ the reducing end, with cleavage taking place between the -1 and $+1$ subsites. Glucoamylase, for example, cleaves a monosaccharide from the non-reducing end of the oligosaccharide chain (Figure 1.4A). Alternatively, *T. reesi* cellobiohydrolase I cleaves disaccharide units from the reducing end of the substrate (Figure 1.4B).

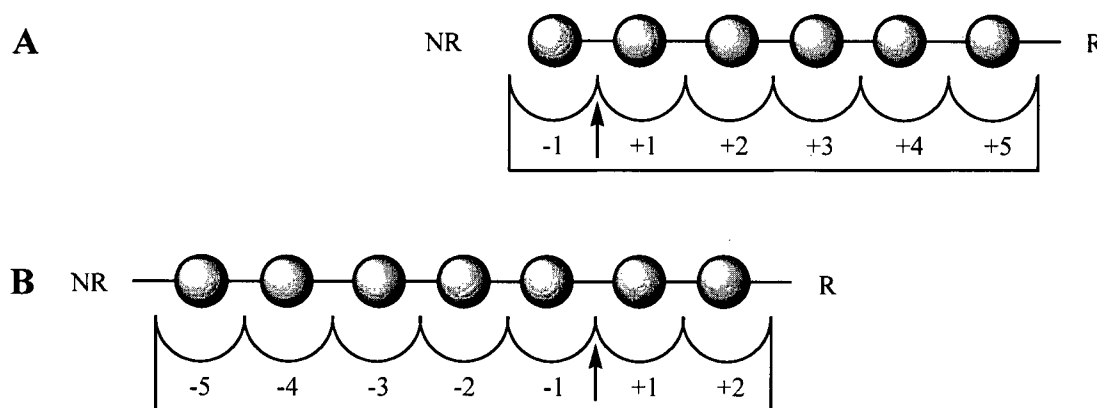


Figure 1.4: Schematic drawing of sugar-binding subsites in two glycosidases. By convention, the non-reducing end of the substrate is drawn on the left while the reducing end is drawn on the right. The arrow placed between the -1 and $+1$ subsites indicates the point of cleavage.

1.1.3 Glycosidase families

In addition to traditional criteria for classification, glycosidases have been grouped into distinct families by Henrissat based on amino acid sequence similarities and tertiary structure as evaluated through hydrophobic cluster analysis and other methods of sequence comparison (3-5). A recent compilation of carbohydrate-transforming enzymes is available from the continuously updated carbohydrate-active enzyme database (CAZy) at <http://www.cazy.org/>. To date, the CAZy classification lists ~100 sequence-derived glycoside hydrolase families and there are three-dimensional structural representatives for over 60 of these (6). The similarity of the tertiary structures and conserved chemical mechanisms amongst enzymes within the same family has long established the discriminatory power of this classification method. Although more information is required before one is able to infer structural information and reaction mechanism based solely on sequence, experimental results have confirmed the identity of key catalytic residues by extrapolation to all members of a particular family. Furthermore, enzymes belonging to different families have been grouped into different clans based on similar tertiary structure and location of catalytic residues, despite low sequence similarity. Therefore, useful insights into the evolution of these enzymes may be obtained by grouping into clans and families.

1.2 Catalytic Mechanism of Retaining β -Glycosidases

Glycosidases perform catalysis via two distinct mechanisms (7), originally proposed by Koshland (8), resulting in inversion or retention of anomeric configuration (Figure 1.5). In the case of inverting glycosidases, hydrolysis of the glycosidic bond

occurs in a single step with inversion of anomeric configuration through the general base-catalyzed attack of water at the sugar anomeric centre, with general acid-catalyzed departure of the aglycone.

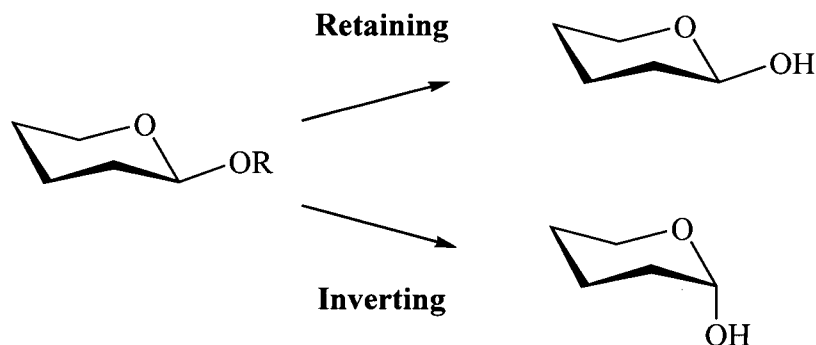


Figure 1.5: The hydrolysis reactions catalyzed by retaining and inverting glycosidases.

In contrast, retaining glycosidases catalyze the hydrolysis of the glycosidic bond with net retention of anomeric configuration. The reaction follows a double-displacement mechanism involving the formation and hydrolysis of a covalent glycosyl-enzyme intermediate via oxocarbenium ion-like transition states, as illustrated in Figure 1.6. Binding and stabilization of the transition-state complexes is achieved through non-covalent binding interactions between the substrate and a number of amino acids within the active site of the enzyme. Two key amino acid residues play particularly important roles: the catalytic nucleophile and the acid/base catalyst. The acid/base catalyst facilitates bond cleavage by donating a proton to the glycosidic oxygen during the formation of the glycosyl-enzyme intermediate. The glycosylation step involves the development of a covalent bond between the carboxyl group of the catalytic nucleophile

and the anomeric carbon of the sugar substrate, while the deglycosylation step involves the hydrolysis of the glycosyl–enzyme intermediate. In this second step, the acid/base catalyst deprotonates the catalytic water which displaces the catalytic nucleophile resulting in a sugar product with retention of the original anomeric configuration.

A crucial structural difference between retaining and inverting glycosidases is the difference in the distance separating their two key catalytic residues (9, 10). In inverting glycosidases, the general-base and the general-acid carboxyl groups are typically separated by an average distance of 7-11 Å (O to O) in order to accommodate the nucleophilic water molecule, whereas in retaining glycosidases the nucleophile and acid/base catalyst are found approximately 5 Å apart.

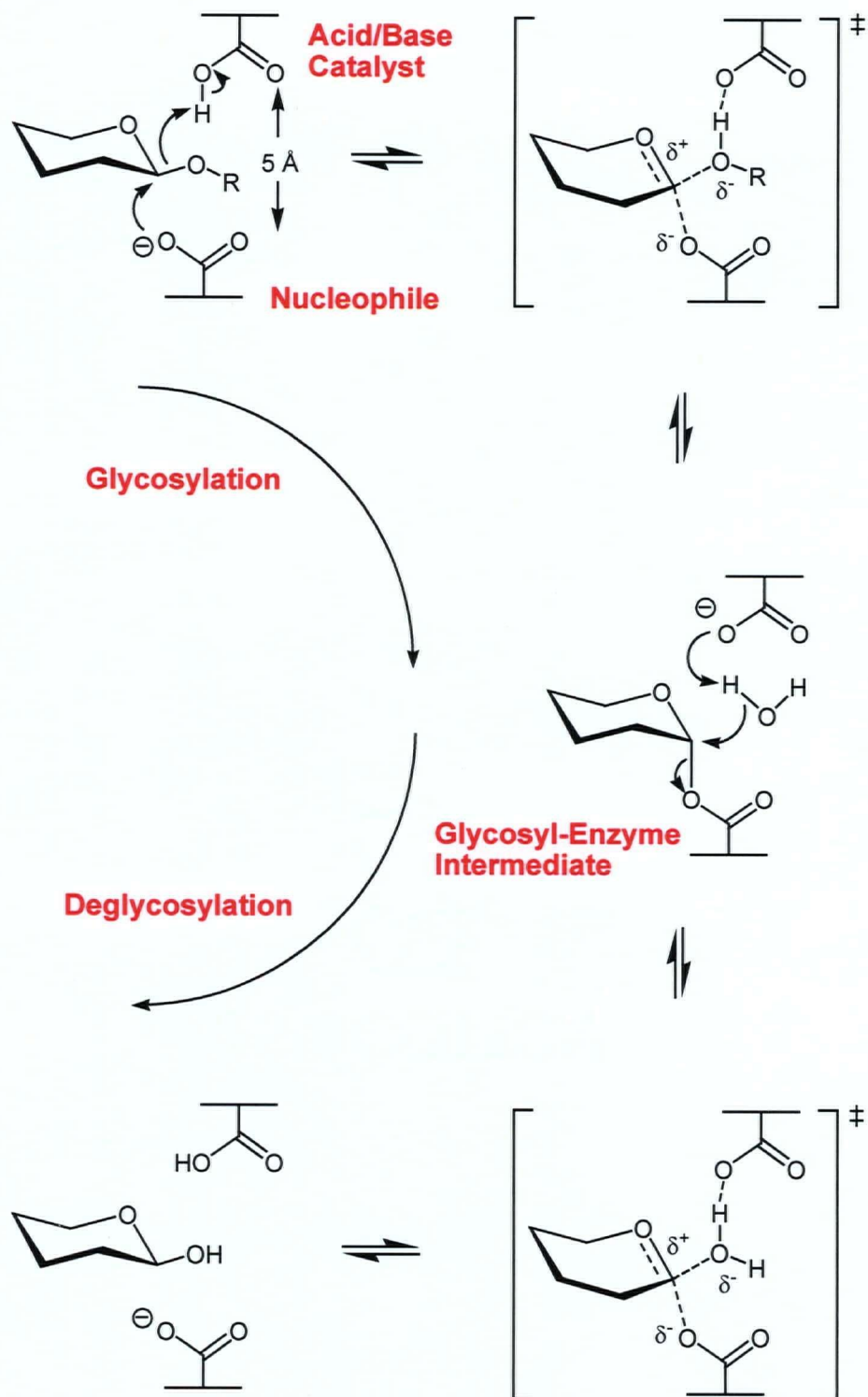


Figure 1.6: General double-displacement mechanism for a retaining glycosidase.

An alternative mechanism for β -N-acetyl hexosaminidases that utilizes acetamido-group participation during hydrolysis has been established wherein the 2-acetamido group of the substrate acts as an intramolecular nucleophile to displace the leaving group, forming a bicyclic oxazolinium-ion intermediate. Such a mechanism has been graphically demonstrated through determination of the structure of a family GH-20 hexosaminidase in complex with the inhibitor GlcNAc-thiazoline, which mimics the covalent oxazolinium intermediate of the substrate-assisted retentive hydrolysis (11). Another recent example of an enzyme utilizing substrate-assisted catalysis via acetamido-group participation is that of family 56 hyaluronidase, a major allergen of bee venom (12).

The essential features of the general mechanism of action of glycosidases have been discussed in recent reviews (6, 13-17). A variety of experimental strategies including kinetic isotope effects, crystal structure analyses of wild-type and mutated glycosidases and of their complexes with ligands, and structural and kinetic analyses of transition-state analogues have been employed to decipher the mechanistic details of catalysis. The key points that have been the focus of most of the mechanistic studies have been the nature of the intermediate and the transition state, the extent of nucleophilic participation, the role and nature of acid/base catalysis, and the role of substrate distortion in catalysis.

1.2.1 Oxocarbenium ion-like transition states

A key feature of the double-displacement mechanism for glycosidase-catalyzed cleavage is the structure of the oxocarbenium ion-like transition state through which

glycosylation and deglycosylation are postulated to proceed. The transition state occurs on the reaction coordinate somewhere between a distorted substrate and a species where the glycosidic bond is substantially elongated while the bond to the enzyme is hardly formed. A characteristic of bond cleavage in each step of the reaction includes the development of a positive charge on the C1 and O5 atoms of the sugar ring in the -1 subsite. To distribute the positive charge across both C1 and O5, the pyranose ring adopts a half-chair or boat conformation to accommodate an effective overlap of the lone pair of electrons on the endocyclic oxygen with the resulting vacant *p*-orbital at the reaction centre. The majority (>75%) of the accumulating positive charge was shown to reside on the endocyclic oxygen of 2,4-dinitrophenyl β -D-glycopyranosides during spontaneous hydrolysis (18). The characteristics of the oxocarbenium ion-like transition states for retaining glycosidases have been explored extensively through kinetic isotope effects and inhibition studies with transition-state analogues (19).

Much of the evidence for positive charge development in the transition state has been derived from measurement of positive secondary α -deuterium kinetic isotope effects ($k_H/k_D > 1$). Through careful selection of the aglycone, thereby controlling rate-limiting steps, these measurements have been reported for both the glycosylation and deglycosylation steps of the double-displacement mechanism. A normal kinetic isotope effect ($k_H/k_D > 1$) is associated with a change in the hybridization state of the anomeric centre from sp^3 to sp^2 as the substrate goes from the ground state to the transition state, which is consistent with transition states for the formation and hydrolysis of the intermediate having significant oxocarbenium ion character. Conversely, an inverse kinetic isotope effect ($k_H/k_D < 1$) would be expected for a hypothetical ion-pair

intermediate in cases where the second step of the reaction, which would necessarily involve a change in hybridization from sp^2 in the ion pair to sp^3 in the product, is rate determining.

Nevertheless, in every known case, kinetic isotope effect measurements determined for the glycosidase-catalyzed hydrolysis of the substrates have been normal ($k_H/k_D > 1$) regardless of which step is rate determining, consistent with oxocarbenium ion character at both transition states. For example, kinetic isotope effects measured on the glycosylation transition state include values of $k_H/k_D = 1.15$ -1.20 for *Escherichia coli* (*lacZ*) β -galactosidase (20), $k_H/k_D = 1.05$ -1.07 for *Agrobacterium* sp. β -glucosidase (21), and $k_H/k_D = 1.06$ -1.12 for *Cellulomonas fimi* xylanase (22). Similarly, kinetic isotope effects for the deglycosylation transition state have been measured and include values of $k_H/k_D = 1.20$ -1.25 for *E. coli* β -galactosidase (23) and $k_H/k_D = 1.10$ -1.12 for *C. fimi* xylanase (22).

Further evidence for the existence of the oxocarbenium ion-like transition states is obtained from studies with transition-state analogue inhibitors. Transition-state analogues that closely resemble the proposed structure of the transition state will bind tighter to the active site of glycosidases than do the normal glycoside substrates since they mimic the transition state. The characteristic features proposed for an oxocarbenium ion-like transition state include a positive charge at the positions corresponding to either O5 or C1, an sp^2 -hybridized centre at the position corresponding to C1 and a conformation where the atoms corresponding to C5, O5, C1 and C2 are coplanar, typically a half-chair. Evidence for the existence of oxocarbenium ion-like transition

states may be inferred through the tight binding by the enzyme to analogues that possess some or all of the characteristics discussed above.

Physical organic studies have shown that although glycosyl oxocarbenium ions appear to have a finite lifetime in aqueous solution, they cannot exist in the presence of a closely located nucleophile, particularly when that nucleophile is anionic (24). The corresponding transition states of the glycosidase-catalyzed hydrolysis mechanism can therefore be expected to exhibit oxocarbenium ion *character*, with the nucleophile and leaving group maintaining partial covalency to the anomeric carbon.

1.2.2 Nature of the covalent glycosyl–enzyme intermediate

A second feature of the nucleophilic substitution reaction characterizing glycoside cleavage is the presence of a covalent glycosyl–enzyme intermediate, as opposed to a stabilized oxocarbenium ion-pair intermediate. As alluded to earlier, strong evidence for the nature of the intermediate may be obtained from secondary α -deuterium kinetic isotope effect studies that provide insight regarding the changes in the geometry at the anomeric centre in the rate-limiting step of the reaction as it proceeds from the ground state to the transition state. A glycosyl–enzyme intermediate has more sp^3 character than the preceding and following transition states. A positive kinetic isotope effect on the deglycosylation step, whose value for k_H/k_D falls between 1.1 and 1.3, reflects significant sp^3 to sp^2 rehybridization at the anomeric centre, consistent with the proposed geometry for the covalent glycosyl–enzyme intermediate. Conversely, an inverse isotope effect with a k_H/k_D of less than unity would be observed for a change in geometry from sp^2 to sp^3 .

Direct evidence for the existence of a covalent intermediate comes via the trapping of a relatively stable glycosyl-enzyme intermediate through a variety of different methods. One highly successful approach involves the use of mechanism-based inactivators such as the fluoro sugar inhibitors that function via the formation and accumulation of a relatively stable glycosyl-enzyme intermediate. Several classes of these mechanism-based inactivators have been developed to destabilize *both* transition states through the incorporation of a highly electron withdrawing fluorine substituent adjacent to the site of positive charge development, resulting in a decrease in the rate of both the formation and the hydrolysis of the intermediate. Accumulation of the intermediate is achieved by the incorporation of a good leaving group such as fluoride ion or 2,4-dinitrophenolate, which accelerates the glycosylation step of the reaction, but not deglycosylation (Figure 1.7A). The intermediate that forms breaks down very slowly, with typical half-lives for hydrolytic turnover measured in days. Reactivation of the enzyme occurs much faster by a transglycosylation reaction in the presence of a suitable glycosyl acceptor sugar according to Figure 1.7B.

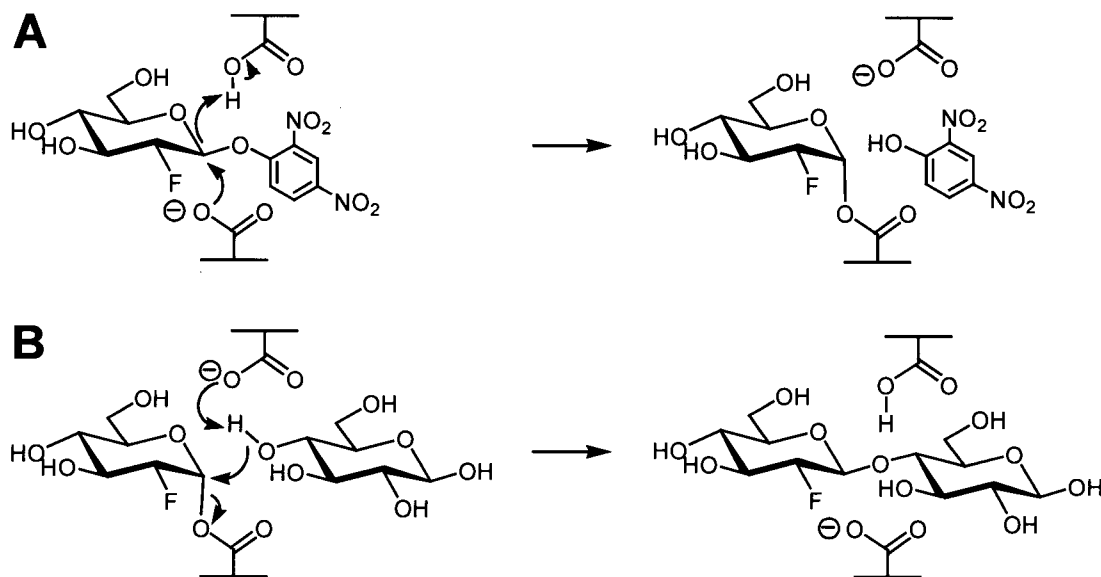


Figure 1.7: Inactivation and reactivation by 2-deoxy-2-fluoro glycosides. (A) Inactivation by formation of the fluoroglycosyl-enzyme intermediate. (B) Reactivation by transglycosylation of the fluoroglycosyl-enzyme intermediate.

The first generation of such mechanism-based inhibitors, involving the replacement of the 2-hydroxyl with a 2-fluorine substituent, were the 2-deoxy-2-fluoro-β-D-glycosyl fluorides (25) and the 2,4-dinitrophenyl 2-deoxy-2-fluoro-β-D-glycosides (26). The removal of key hydrogen bonding interactions with the 2-position hydroxyl has the additional effect of destabilizing the transition states in the retaining β-glycosidase catalyzed hydrolysis of glycosides since interactions at this position have been shown to contribute up to 10 kcal mol⁻¹ to transition-state stabilization (27-29). The fluorine group therefore destabilizes the transition state both through its significant inductive effects and also by removal of important interactions at the 2-position.

The development of alternative approaches was initiated due to the failure of the 2-fluoro sugar compounds to function as inactivators of α-retaining glycosidases, serving

rather as slow substrates for which the rate-determining step is formation of the glycosyl-enzyme intermediate. One approach to further slow the glycosylation step involved the installation of a second fluorine at C2 along with the simultaneous incorporation of a still better leaving group such as 2,4,6-trinitrophenol and resulted in the development of 2-deoxy-2,2-difluoro glycosides that form extremely stable glycosyl-enzyme intermediates on α -retaining enzymes (30). A similar strategy that involves substitution of fluorine at C5 in place of the hydrogen was developed by McCarter and Withers (31). These 5-fluoro-glycosyl fluorides inactivate the glycosyl-enzyme intermediate of both α - and β -retaining glycosidases by formation of a stabilized fluoroglycosyl-enzyme intermediate through a mechanism analogous to that of the 2-deoxy-2-fluoro glycosides. The three-dimensional structures of a growing number of these glycosyl-enzyme intermediates have been solved by single crystal X-ray diffraction. The 2-deoxy-2-fluorocellobiosyl-enzyme intermediate formed on the xylanase Cex from *Cellulomonas fimi* was the first such structure solved (32).

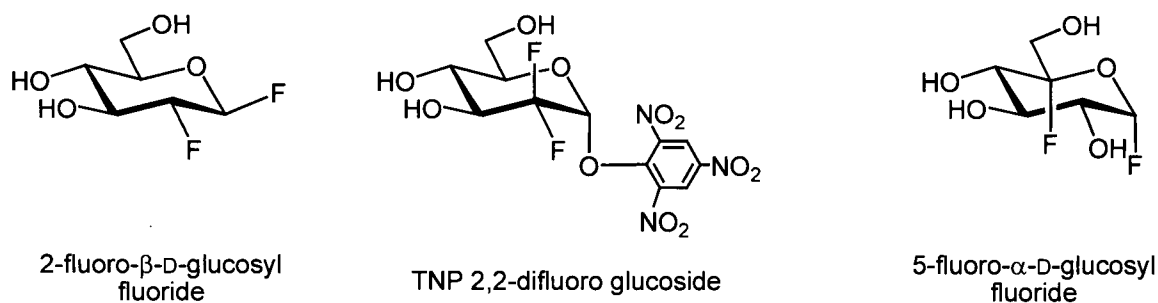


Figure 1.8: Structures of several classes of the fluoro sugars that function as mechanism-based inactivators.

An alternate method of trapping the intermediate has been achieved by modification of key enzyme residues through mutation. Using this approach, the covalent glycosyl–enzyme intermediate of a xylanase from *C. fimi* was the first to be trapped without disrupting important interactions at the 2-position. The X-ray structure of this glycosylated enzyme once again confirmed that the intermediate is indeed covalent (33). Vocadlo *et al.* revealed that hen egg white lysozyme (HEWL) performs catalysis via the formation of a covalent intermediate in common with other retaining glycosidases (34). The accumulation of a covalent 2-fluorochitobiosyl–enzyme intermediate on the wild-type enzyme, as well as the nonfluorinated chitobiosyl–enzyme intermediate on the acid/base mutant, was demonstrated by mass spectrometry. The formation of a covalent intermediate was further confirmed by the X-ray crystallographic structural analysis of a trapped 2-fluorochitobiosyl–enzyme intermediate on an acid/base mutant of lysozyme. The mechanism of hen egg white lysozyme was unequivocally shown to proceed through a covalent glycosyl–enzyme intermediate and not a stabilized oxocarbenium ion pair as had long been held.

1.2.3 Nucleophilic participation

Retaining glycosidases perform nucleophilic catalysis with extraordinary ability. The identification of the essential nucleophilic residue involved in the double-displacement mechanism may be achieved through sequence alignments of enzymes within a family and identification of conserved amino acid residues as possible candidates to function in such a capacity. Site-directed mutagenesis studies followed by detailed kinetic analyses may lead to the correct assignment of catalytic residues.

Essential residues in an enzyme may also be predicted using a high resolution, three-dimensional image obtained through X-ray crystallography. Crystallographic studies on retaining glycosidases have identified carboxyl residues appropriately located within the active site to function as nucleophiles. More substantial evidence for the correct assignment of a catalytic carboxyl group is derived from glycosidases co-crystallized with either an inhibitor or a substrate bound within the active site of the enzyme. Despite the fact that X-ray crystallography has provided many useful insights into the structures and functions of a diverse number of glycosidases, this technique does not unequivocally identify the important catalytic residues, and furthermore, is not always available for every enzyme. Although, group-specific labels have been used to identify catalytic groups in labelling experiments, a more popular and reliable approach to identifying and assigning the roles of the catalytic residues is the use of mechanism-based inactivators.

Mechanism-based inactivators have been successfully applied in labelling experiments to identify the catalytic nucleophiles in the active sites of a number of retaining glycosidases. A common approach involves proteolytic digestion of the labelled enzyme to yield a mixture of short peptides, followed by separation of the resultant mixture by RP-HPLC and analysis by ESI-MS/MS (electrospray ionization tandem mass spectrometry). The labelled peptide is characterized within the peptide mixture by a tandem mass spectrometry method known as a neutral loss scan which detects those peptides that lose a characteristic reporter group by collision-induced fragmentation (35). Isolated, labelled peptides are subsequently sequenced by further MS/MS analysis, or by Edman degradation. This approach has been used successfully to

identify the catalytic nucleophile in *Bacillus subtilis* xylanase as Glu78 (36) and human glucocerebrosidase as Glu340 (37). Leading references to this approach may be found in the following publications and reviews (26, 38-41).

Mutagenesis studies involving replacement of specific side chain residues to function as alternative nucleophiles have led to insight into mechanistic details of catalysis. For instance, the replacement of specific side chain residues can result in a change of enzymatic mechanism. An example of an inverting glycosidase being converted into a retaining enzyme is that of the inverting T4 phage lysozyme (42). In the wild-type inverting enzyme, the hydroxyl side chain of Thr26 hydrogen bonds to the attacking water molecule, which is deprotonated by the neighbouring Asp20 during hydrolysis. The crystal structure shows that mutating Thr26 to a histidine residue results in a mutant that occupies the position normally assumed by the water molecule. It has been rationalized that the imidazole group acts as a nucleophile to form a covalent glycosyl-imidazolium-ion intermediate that is subsequently hydrolysed to form a product of retained configuration. Conversely, converting a retaining β -glycosidase to an inverting enzyme by shortening a nucleophilic glutamate by substitution with aspartate has not been achieved (43, 44). Rather, these enzymes function as retaining enzymes, albeit at reduced rates relative to the wild-type enzymes. Replacement of the glutamic acid or aspartic acid by alanine, glycine or serine virtually eliminates all nucleophilic activity. Addition of small, external anions such as azide, which do not require general base catalytic assistance, can result in cleavage of the glycosidic bond of activated substrates such as 2,4-dinitrophenyl β -glycosides with inversion of configuration, yielding the α -glycosyl azide product. Rate accelerations upon addition of azide (2 M)

have been observed, with the catalytic rate constant (k_{cat}) rising from $1 \times 10^{-5} \text{ s}^{-1}$ to 1 s^{-1} for the Glu358Ala mutant of *Agrobacterium* sp. β -glucosidase (45). In addition to formate and azide, halides have been shown to act as effective substitute nucleophiles. Indeed, the serine, glycine and alanine nucleophile mutants of *Agrobacterium* sp. β -glucosidase and *Cellulomonas fimi* β -mannosidase (46) were effective in catalyzing nucleophilic fluorination of 2,4-dinitrophenyl β -glycosides to form the corresponding α -glycosyl fluorides (Figure 1.9, first step). The glycosyl fluoride, in turn, is used to glycosylate a second equivalent of substrate in a transglycosylation reaction, thereby forming glycosidic bonds (Figure 1.9, second step).

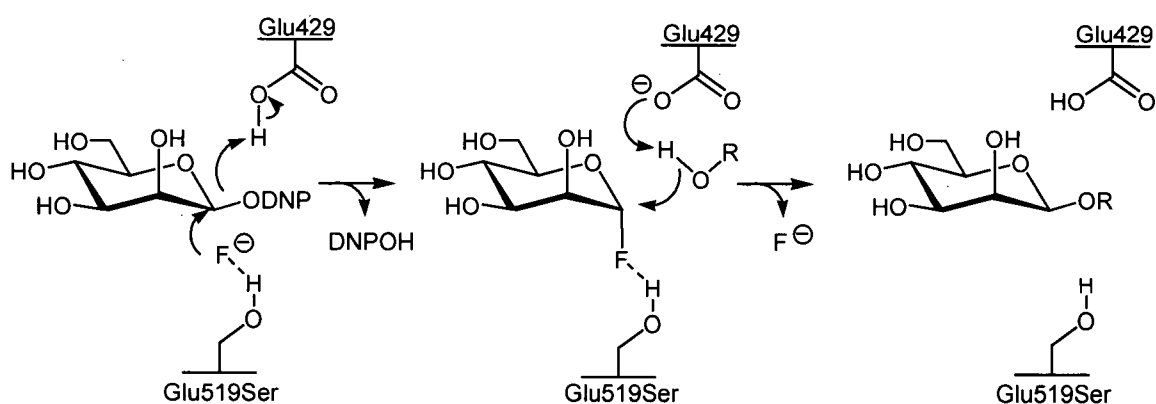


Figure 1.9: Nucleophilic fluorination of 2,4-dinitrophenyl β -mannoside by the β -mannosidase nucleophile mutant (Glu519Ser) from *Cellulomonas fimi*.

One application of mechanistic studies has led to the development of synthetically useful mutants termed glycosynthases (47). Mutation of the catalytic nucleophile of retaining glycosidases results in enzymes that catalyze the synthesis of oligosaccharides by using glycosyl fluorides as glycosyl donors (48-50).

1.2.4 Acid/base catalysis

In Koshland's mechanism for inverting and retaining glycosidases, the hydrolysis of the glycosidic linkage proceeds with general acid/base assistance. As stated earlier, in the glycosylation step for retaining glycosidases, an enzymic carboxyl group acts as an acid catalyst to facilitate the departure of the aglycone. Indeed, X-ray crystal structures of several glycosidases reveal carboxyl group residues in one of two positions that could function as proton donor groups. Crystallographic analysis of glycosidases in complex with ligands has revealed two protonation trajectories, termed either *anti* or *syn* by Vasella and coworkers (19). The definition of the protonation trajectory is based on the orientation of the lone pair on the glycosidic oxygen with respect to the catalytic acid. The protonation trajectory is defined as *anti* if the catalytic acid is opposite to the endocyclic oxygen on the side of a plane formed from C1, O1, and H1. When the catalytic acid is on the same side of this plane as the endocyclic oxygen, then the protonation trajectory is defined as *syn*. The large discrepancy in the degree of inhibition by competitive triazole inhibitors with enzymes from different families of glycosidases has been explained to result from these two differences in the protonation trajectory (Figure 1.10). Inhibition kinetics and crystallographic analysis of the family 10 xylanase from *Cellulomonas fimi* (Cex) in complex with a *xylobio*-imidazole inhibitor and the *xylobio*-lactam oxime substantiates *anti*-protonation. The family 11 xylanase from *Bacillus circulans* (Bcx) interacted only weakly with these inhibitors. The weak inhibition was correlated with the proposed *syn*-protonation by family 11 glycosidases (51, 52). Predictably, because there is significant resemblance of the active site within glycosidase families, members within one family may thus be categorised as *anti*-

protonators (GH-families 1, 2, 5, 10, 18 and 20) or *syn*-protonators (GH-families 7, 11, 12, 16, 22, 23 and 45).

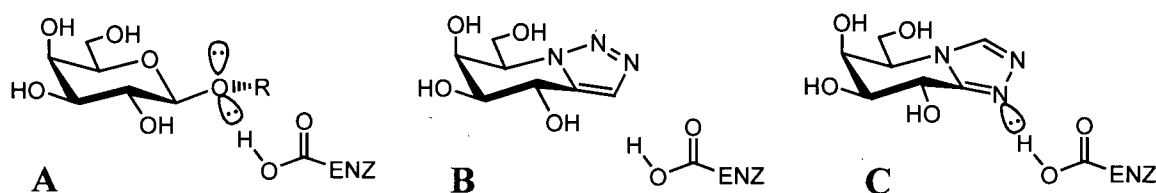


Figure 1.10. The *anti* orientation of the acid catalytic residue and protonation trajectory as the basis for rationalizing the relative potency of two triazole inhibitors. (A) *Anti*-protonation of the glycosidic oxygen. (B) Absence of any possible hydrogen bonding to the 1,2,3-triazole inhibitor. (C) Possible *anti*-protonation of the 1,3,4-triazole inhibitor.

The role of the acid/base catalyst has been probed extensively in several enzymes through mutagenesis studies. In the absence of a crystal structure, highly conserved carboxyl group residues can be identified using sequence alignment data, followed by site-directed mutagenesis and kinetic studies. Using this approach, Glu170 was identified as the acid/base catalyst in *Agrobacterium* sp. β -glucosidase (53). Detailed kinetic analysis using substrates having poor leaving groups compared with substrates not requiring acid assistance may be performed on enzymes that have had the proposed residue mutated to confirm its role as the acid/base catalyst. For substrates having poor leaving groups that require efficient acid catalysis, deletion of the carboxyl group of the general acid/base catalytic residue results in a significant decrease in the rate of the glycosylation step of the hydrolysis reaction, which is reflected in a reduction in the second-order rate constant ($k_{\text{cat}}/K_{\text{m}}$). Conversely, for activated substrates that do not require acid catalysis, the formation of the glycosyl-enzyme intermediate will occur at

rates close to that of the wild-type enzyme. Accumulation of the glycosyl-enzyme intermediate is the net result observed when these acid/base mutants hydrolyse reactive substrates because the deglycosylation step of the double-displacement mechanism is also slowed upon deletion of the general acid/base catalytic residue. This accumulation of the intermediate is reflected in the kinetic analysis by an initial “burst” of the activated leaving group and an extremely low K_m value.

Mutagenesis studies, where the position of the catalytic residue is changed in the active site, have demonstrated the flexibility of acid/base catalysis in glycosidases. This has been demonstrated in the xylanase from *Bacillus circulans* by changing the length of the acid/base catalyst (54), while incorporation of an appropriately positioned acid catalyst into the substrate was able to restore the activity of the acid/base mutant of *Agrobacterium* sp. β -glucosidase (Glu170Gly) (55). Additionally, oxidation of a mutant of glucoamylase in which the general base had been replaced by cysteine to convert it to cysteinesulfinic acid, and observation of activity demonstrates that acid/base catalysts are not limited to carboxyl groups (56, 57).

The first step in the hydrolysis mechanism for retaining glycosidases, glycosylation, benefits from acid catalysis. Although the pK_a of a typical carboxylic acid is 4.5, the pK_a of the acid catalyst within the active site of many glycosidases is perturbed upward to a value between 6 and 8. This shift in pK_a is presumed to arise from an electrostatic field exerted by the nucleophilic carboxyl group that is held in close proximity to the acid/base residue. A pK_a value above that of the medium pH is necessary to maintain a favourable protonation state of the general acid/base catalytic residue. The deglycosylation step of the hydrolysis reaction similarly benefits from base

catalysis. The deprotonated residue that formerly acted as a general acid catalyst is now poised to act as a general base catalyst in the deglycosylation step of the reaction. In fact, the general acid/base catalytic residue has been observed to be hydrogen bonded to a well-ordered water molecule positioned near the anomeric centre in the crystal structures of several glycosidases in which the glycosyl–enzyme intermediate has been trapped. The same residue that previously functioned as a general acid with a pK_a of 6–8 now fulfills that role of general base due to a drop in pK_a resulting from electrostatic field effects. An electrostatic basis for pK_a cycling of the acid/base residue has been extensively studied in *Bacillus circulans* xylanase (Bcx) through a series of elegant experiments that involved direct ^{13}C -NMR titrations of the enzyme that had been ^{13}C labelled in the carboxyl group side chains of both the acid/base and the nucleophilic residues. The pK_a of the catalytic acid/base residue was found to be 6.7 in the free enzyme. Upon formation of a stable xylobiosyl–enzyme intermediate, thus neutralizing the charge on the nucleophile, the pK_a of the acid/base catalytic residue dropped by 2.5 units to 4.2 in order to provide the ionization state required to act as a general base.

Furthermore, the effect of hydrogen bonding interactions on the acid/base catalyst of *Bacillus circulans* xylanase (Bcx) has also been extensively studied through a series of elegant experiments. In the wild-type enzyme, Asn35 forms a hydrogen bond (3.1 Å) to the acid/base catalyst Glu172. This hydrogen bond is maintained at 3.2 Å by the mutation Asn35Asp, but the pH optimum is shifted from 5.7 to 4.6 while increasing the activity by 20% (see Figure 1.11). The pH dependence of k_{cat}/K_m for the Asn35Asp mutant followed pK_a values of 3.5 and 5.8. These pK_a values were determined by ^{13}C -NMR titrations on the enzyme to arise from Asp35 ($pK_a = 3.7$) and the nucleophile

Glu78 ($pK_a = 5.7$), but not the acid/base catalyst Glu172 ($pK_a = 8.4$). These pK_a values indicate that only 1% of the enzyme was in the correct ionization state. Thus, the active form of the Asn35Asp mutant was inherently 100 times more active than the wild-type enzyme. The increase in activity has been attributed to the Asn35Asp–Glu172 hydrogen bond. Crystallographic studies on the Asn35Asp mutant trapped as the 2-fluoroxymylobiosyl covalent intermediate revealed that this hydrogen bond had shortened substantially to 2.7 Å in the intermediate. Likewise, ^{13}C -NMR titrations on the trapped intermediate determined a primary ionization pK_{a1} of 2.6 for the Asn35–Asp172 pair, indicating that the pK_a of Glu172 had effectively dropped 5.8 units upon formation of the intermediate, corresponding to an energy difference of $\sim 8 \text{ kcal mol}^{-1}$. This is dramatically greater than the pK_a drop found in the wild-type enzyme, in which the pK_a of Glu172 shifts only 2.5 units ($3.5 \text{ kcal mol}^{-1}$) upon forming the covalent intermediate. Therefore, the formation of a stronger hydrogen bond in the covalent intermediate drives the formation of that intermediate by making proton donation by Glu172 to the departing glycosidic oxygen increasingly more favourable.

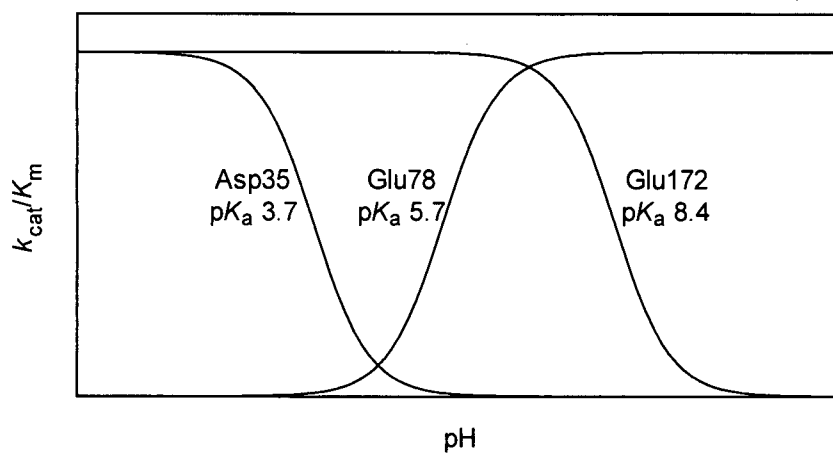


Figure 1.11: Depiction of the pH dependence of k_{cat}/K_m for Bcx Asn35Asp mutant as the product of titration curves of catalytic residues derived from ^{13}C -NMR. Although only 1% of the mutant is in the correct ionization state for catalysis, it is 20% more active than the wild-type enzyme.

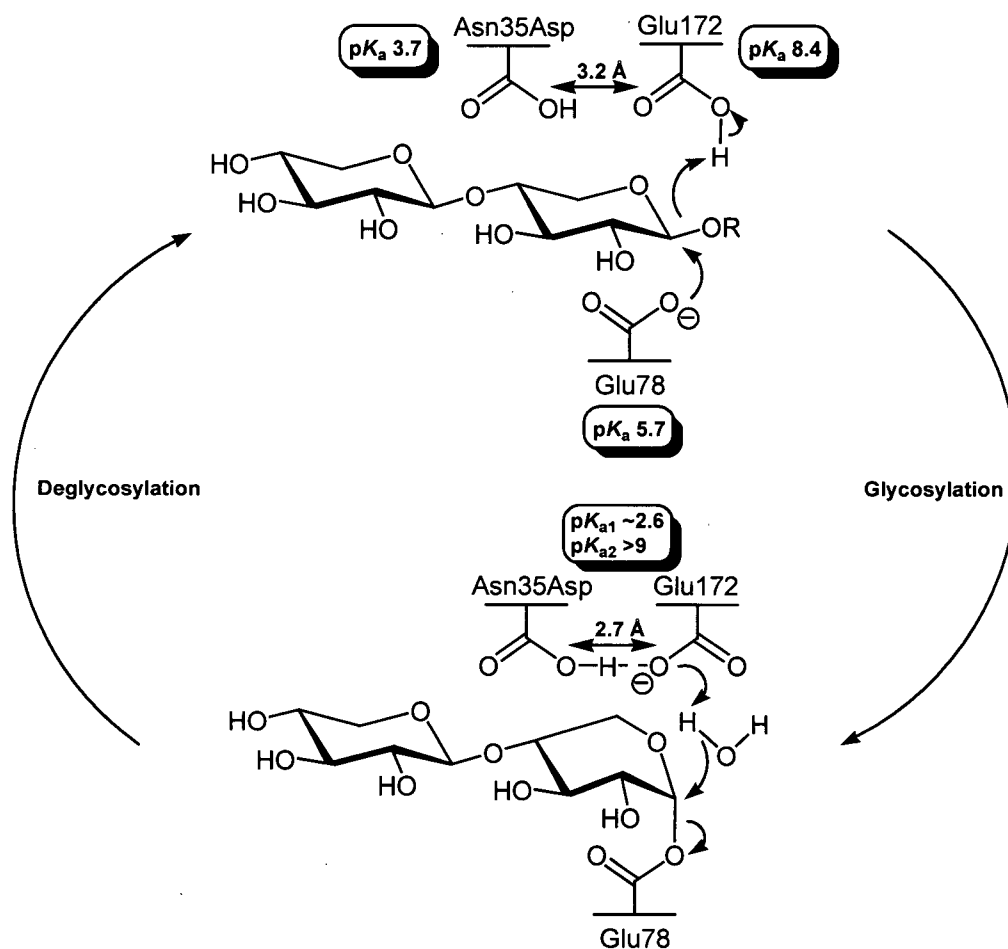


Figure 1.12: The Asn35Asp mutant of Bcx increases the inherent catalytic efficiency by at least 100-fold over the wild-type enzyme by forming a strong hydrogen bond between Asp35 and Glu172.

1.2.5 Non-covalent interactions

Non-covalent interactions between enzyme and substrate have been proposed to account for the majority of the catalytic power of enzymes by Pauling. The binding energy derived from these interactions leads to a decrease in the activation energy of the reaction by stabilizing the geometry and charge of the transition state preferentially over that of the ground state, thereby resulting in rate acceleration. X-ray crystal structures of

carbohydrate-binding proteins and glycosidases have identified interactions between the hydroxyl groups of the sugar ligand and the enzyme, most of which represent hydrogen bonds. A systematic approach to explore the importance of individual non-covalent interactions has been achieved in which site-directed mutagenesis is carried out to remove the side chain residue on the protein that was interacting with the substrate. Another approach has been through the use of modified substrates in which each hydroxyl group has been replaced by a hydrogen or fluorine to correlate structure and activity. Kinetic parameters are then measured on the modified system in each case.

Modified deoxy- and deoxyfluoro-glycoside substrates have been utilized to identify and quantify important non-covalent interactions in the catalytic mechanism of glycosidases. For example, upon removal of the hydroxyl group of glucose at the 2-position and replacement by hydrogen, the rate of hydrolysis by *Aspergillus wentii* β -glucosidase drops by at least a factor of 10^6 , corresponding to $>7 \text{ kcal mol}^{-1}$ of stabilization (58). The hydroxyl group at position 4 is also important, with 4-deoxy substrates being hydrolysed 10^4 to 10^5 -fold slower relative to the unmodified substrates (58). The importance of interactions at the 2-position is revealed through similar studies with *E. coli* β -galactosidase, in view of the fact that enzymatic hydrolysis of 2-deoxy-galactosides is 10^5 -fold slower than is hydrolysis of the unmodified substrate (59). Interactions at the 4- and 6-positions appear to be less important, with rate reductions of only 500 and 1000-fold being observed with 4-deoxy and 6-deoxy substrates (27). The interactions with the 3- and 6-hydroxyl groups during the chemical steps of the *Agrobacterium* sp. β -glucosidase catalyzed reaction each provide $2.2 \text{ kcal mol}^{-1}$ towards stabilization of the transition state (28). Hydrogen-bonding interactions at the 2-position

appear to be most important and provide 5 kcal mol^{-1} worth of transition state stabilization, with rate reductions of approximately 5000-fold being observed for the hydrolysis of 2-deoxy-glucosides (28). Likewise, the rate of hydrolysis of the 2-deoxy-cellobiosyl-enzyme intermediate is 10^6 -fold lower than that for the corresponding cellobiosyl-enzyme in *C. fimi* xylanase, revealing the importance of non-covalent interactions at position 2 for stabilization of the transition state (35). The formation of low-barrier hydrogen bonds, although controversial, has been proposed to account for significant rate accelerations (60). The formation of these specific, strong hydrogen bonds in enzyme transition states and intermediate complexes is effectively accomplished within the shielded environment of the enzyme active site.

1.2.6 Substrate distortion

Many aspects of the function and catalytic mechanism of glycosidases remain controversial despite the fact that the first X-ray structure of an enzyme was that of a glycosidase, hen egg white lysozyme (HEWL). Hydrolysis by these enzymes is performed via transition states that display considerable oxocarbenium ion-like character as the anomeric carbon becomes sp^2 hybridized. Such hybridization requires a planar arrangement of C5, O5, C1 and C2 at or near the transition state (61). The resulting conformation for the transition state can only be accommodated by 4H_3 and 3H_4 half-chair and ${}^{2,5}B$ and $B_{2,5}$ classical boat conformations (62). Support for the planar transition state has come from X-ray structural analysis of enzymes trapped in various states along the reaction coordinate that reveal distortion of the pyranosyl ring at the -1 subsite from its standard 4C_1 conformation (63). This distortion was originally proposed in the late 1960s

by Phillips and co-workers on the basis of the analysis of oligosaccharide complexes of HEWL (64), and later verified by the high-resolution structure determinations of a HEWL tetrasaccharide lactone derivative (65). Similar work on product and pseudo product complexes of HEWL (66, 67) and a mutant T4 lysozyme product complex (68) revealed distorted sugars. The high-resolution crystal structures of "Michaelis" complexes of two structurally unrelated *endo*-glucanases from families GH-5 and GH-7 (69-72) and a family GH-20 hexosaminidase (73) have been unambiguously observed. For these β -retaining enzymes, the unhydrolysed substrates in the -1 subsite adopt a 1S_3 skew-boat conformation (or the closely related 4E envelope conformation), while the subsequent covalent intermediates have been observed as undistorted 4C_1 chairs (33, 34, 74-77). This implies a ${}^1S_3 \rightarrow {}^4H_3 \rightarrow {}^4C_1$ pseudorotational itinerary for the glycosylation step of the retaining mechanism (Figure 1.13).

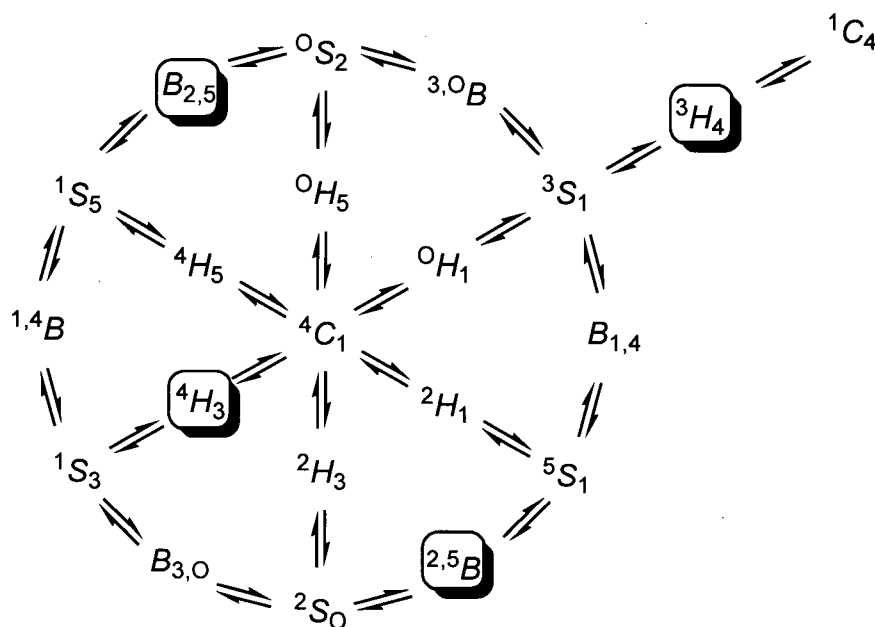


Figure 1.13: Partial map of pyranoside interconversions adapted from Stoddart (78). Potential transition-state conformations that possess a coplanar arrangement of C5, O5, C2 and C1 atoms are shown boxed.

Other potential transition-state conformations have been observed. For instance, evidence of a $^{2,5}B$ boat conformation for the transition state has been observed for family GH-11 xylanases that display a covalent xylobiosyl-enzyme intermediate in a $^{2,5}B$ conformation (79-81). Catalysis in this enzyme family presumably proceeds along a $^4C_1 \rightarrow ^2H_3 \rightarrow ^2S_0 \rightarrow ^{2,5}B$ itinerary. Furthermore, recent trapping of a family 26 β -mannanase in a 1S_5 conformation and its subsequent covalent intermediate in a 0S_2 conformation suggest a different catalytic strategy via a $B_{2,5}$ transition state (82) along a $^1S_5 \rightarrow B_{2,5} \rightarrow ^0S_2$ pseudorotational itinerary for the glycosylation step for this class of enzyme. Similarly, the structures of three different covalent glycosyl-enzyme intermediates for the family 38 Golgi α -mannosidase II from *Drosophila melanogaster* trapped by use of fluorinated sugar analogues revealed sugar intermediates bound in a

distorted 1S_5 skew boat conformation (83). Increasing evidence confirms that, despite sharing a common mechanism, glycosidases could utilize different transition state and intermediate structures due to substantial substrate distortion at the -1 subsite of the active site.

Distortion of the -1 subsite sugar from the preferred ground state 4C_1 chair conformation toward a boat or skew-boat form in which the glycosidic bond and leaving group become axial has been proposed to be driven by the extra interactions that develop within the $+1$ subsite. This distortion confers numerous catalytic benefits to the enzyme both in allowing a direct 'in-line' attack on the sugar anomeric centre by the nucleophile, concomitant with leaving group departure, and in removing potential repulsive interactions upon distortion to a boat or skew-boat form. As the substrate moves closer to the conformation of the oxocarbenium ion transition state, the interaction between a pseudoequatorial 2-hydroxyl substituent and the carbonyl group of the catalytic nucleophile, which in some cases is believed to contribute in excess of 10 kcal mol^{-1} (28), is enhanced. Additionally, the pseudoaxial bond orientation is consistent with the dictates of stereoelectronic theory (84), which require an antiperiplanar arrangement of the sp^3 lone pair electrons on the ring oxygen and the glycosidic bond in order to facilitate electron donation to the transition state, and thus enhance the rate of hydrolysis (85). The antiperiplanar lone pair hypothesis (ALPH) requires a conformational change of the pyranosyl ring from a chair to a skew-boat or boat resulting in a pseudoaxial orientation of the aglycone (Figure 1.14).

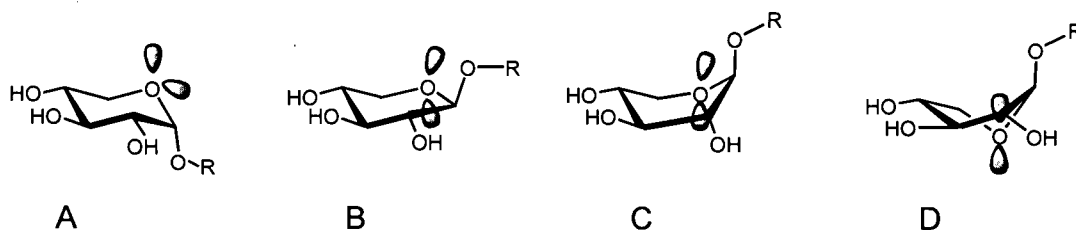


Figure 1.14: Orientation of the lone pairs on the endocyclic oxygen relative to the glycosidic oxygen of the leaving group. (A) The 4C_1 ground state conformation of many common glycosides and covalent intermediate structures. This conformation features a lone pair on the ring oxygen that is antiperiplanar to the C1–OR bond in an α -configured glycoside. (B) The 4H_3 conformation proposed as a possible transition-state conformation. (C) The ${}^{4,1}B$ or 4E conformation and (D) the skew-boat 1S_3 conformation that features a lone pair on the ring oxygen that is antiperiplanar to the C1–OR bond in a β -configured glycoside, as required for the optimal effect of the antiperiplanar lone pair hypothesis (ALPH).

Analysis of pyranoside ring conformations along the reaction pathway opens the capacity for the selective design of transition-state analogue inhibitors, which are highly valuable as mechanistic probes and potential therapeutic agents.

1.3 Biodegradation of Cellulose and Xylan

Cellulose and xylan, which are linear polymers of β -1,4-linked glucopyranosyl and xylopyranosyl residues respectively, are the most abundant polysaccharides on earth and are the major components of plant cell walls. Biodegradation of these β -1,4-glycans is achieved through the action of β -1,4-glycosidases or β -1,4-xylosidases, hydrolytic enzymes which act cooperatively to convert these largely insoluble polymeric substrates into their simple constituent sugars. The depolymerization of cellulose occurs in a synergistic manner by the action of *endo*- and *exo*-glucanases. *Endo*-glucanases cleave the internal β -1,4 bonds of cellulose, thereby increasing the number of free non-reducing

ends, which are sites for hydrolysis by *exo*-glucanases. The resulting product of cellulose degradation, cellobiose, is then hydrolysed to glucose by β -glucosidases.

Xylan degradation involves similar xylanolytic enzymes for its complete hydrolysis that include *endo*-1,4-xylanases (EC 3.2.1.8) and β -xylosidases (EC 3.2.1.37). Xylan is a heteropolysaccharide containing substituent groups of acetyl, 4-*O*-methyl-D-glucuronosyl and α -arabinofuranosyl residues linked to the xylan backbone. *Endo*-xylanases depolymerise xylan by the random hydrolysis of the xylan backbone and β -D-xylosidases hydrolyse small oligosaccharides. The side groups present in xylan are liberated by α -L-arabinofuranosidase, α -D-glucuronidase, and acetyl xylan esterase, among others.

A variety of microorganisms, mainly bacteria and fungi, along with plants are reported to produce xylanases (86-88). Many of these enzymes have a modular organization and comprise both catalytic and non-catalytic domains. On the basis of amino acid sequence alignment of their catalytic domains, they may be assigned to a specific family of β -glycosidases that displays similar catalytic mechanism and specificity. Most known xylanases belong to GH families 10 and 11 (over 300 gene sequences are known), and about 20 more xylanase genes are distributed between families 5, 8 and 43.

Xylanases are fast becoming a major group of industrial enzymes (89), finding significant application in the biobleaching of wood pulp (86, 87, 90, 91). However, the use of xylanases is not restricted to the paper and pulp industry. Potential applications of xylanases in biotechnology include treating animal feed to increase digestibility (92, 93),

clarification of juices and wines (94) and bioconversion of agricultural wastes to fermentation products (95). The xylanolytic enzymes also have an application in rye baking where they are used as dough strengtheners and result in an increased volume of baked bread (96-99). Processes used to produce ethanol as an alternative source of energy from biomass are an intensive area of research owing to the high cost and inevitable depletion of the world's petroleum supplies (100, 101). There are reports regarding the production of ethanol from hemicellulose wastes by incorporating xylanase treatment (95, 102, 103).

Future work on the application of these enzymes in the biotechnology industry requires a complete understanding of the structure/function relationships obtained from biochemical and structural studies. An extensively studied family 10 enzyme is the β -1,4-*endo*-glycanase from the soil bacterium *Cellulomonas fimi*. Family 10 members function primarily as 1,4-xylanases, although activity against cellobiosides has been reported. Members of GH-11 function exclusively as xylanases, of which the xylanase from *Bacillus circulans* is a representative enzyme.

1.3.1 *Cellulomonas fimi* xylanase

The β -1,4-glycanase from the soil bacterium *Cellulomonas fimi* is an extensively studied enzyme. The gene encoding the glycanase has been cloned, expressed into *E. coli*, and subsequently sequenced. The enzyme is glycosylated when produced in *C. fimi*, whereas the recombinant form expressed in *E. coli* is not. The main function of glycosylation appears to be protection against proteolysis, and has no apparent effect on catalytic activity. Also known as CfXyn10A, the glycanase enzyme is a 47 kDa protein

comprising an N-terminal catalytic domain (35 kDa) and a C-terminal cellulose-binding domain (12 kDa) connected by a proline and threonine-rich linker peptide (104). When separated by limited proteolysis, the domains of Cex retain their respective catalytic and cellulose binding properties. The catalytic domain (Cex-cd) is a member of family 10 of the glycoside hydrolases (105, 106).

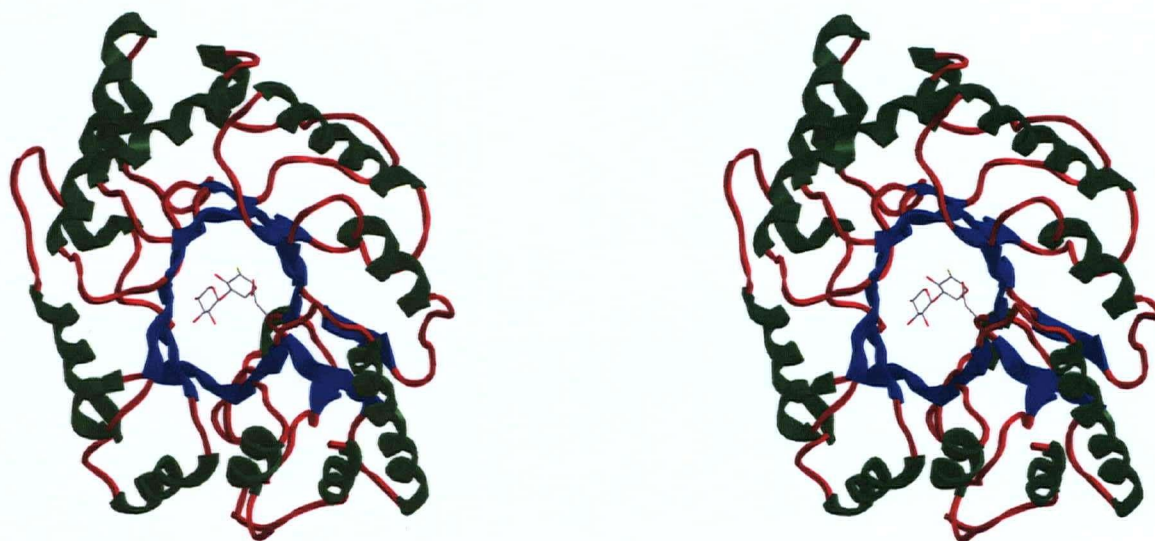


Figure 1.15: Three-dimensional structure of Cex with bound 2F-X₂ (76). The overall structure of Cex is depicted as a protein cartoon in divergent (wall-eyed) stereo, with α -helices coloured green, β -strands blue and loops red. The bound 2F-X₂ is drawn as a stick model, with atoms coloured according to atom type, carbon in grey, oxygen in red, and fluorine in yellow. The water molecules in the active site have been removed for clarity. This figure and subsequent molecular representations were prepared with Chem3D Ultra 10.0 (<http://www.cambridgesoft.com>).

Cex is catalytically active on cellulose, xylan, and a range of soluble aryl β -D-glycosides (22, 106). Stereochemical studies using ¹H-NMR revealed a “retaining” enzyme that utilizes a double-displacement mechanism involving the formation and hydrolysis of a covalent glycosyl–enzyme intermediate via oxocarbenium ion-like

transition states during the hydrolysis of substrates (107). The catalytic nucleophile is Glu233, identified by trapping of a covalent 2-deoxy-2-fluoro-glycosyl-enzyme intermediate and sequencing of the purified glycopeptide (35, 108). The assignment of the nucleophilic residue was later confirmed by mutagenesis followed by kinetic analysis (22). The acid/base catalyst was identified as Glu127 by detailed kinetic analysis of site-directed mutants (105, 109).

Insight into the kinetic mechanism was obtained through a detailed kinetic study which allowed the identification of rate-limiting steps, as well as investigation of the transition-state structure for each step. Support for the double-displacement mechanism of Cex was derived from pre-steady and steady state kinetics, Brønsted relationships, kinetic isotope effect measurements, inactivation experiments, and pH studies (22, 33, 35, 76, 105, 108-111).

The X-ray crystal structure of the catalytic domain of Cex (112) revealed an eight-stranded parallel α/β -barrel, with an open cleft at the carboxyl-terminal end, proposed to be the active site (Figure 1.15). The two catalytic residues, Glu233 and Glu127, are separated by a distance of 5.5 Å on either side of the cleft, consistent with a retaining mechanism as is presumably optimal for the efficient formation of a glycosyl-enzyme intermediate by Glu233 and the concomitant protonation of the aglycone by Glu127. Highly conserved residues within family 10 enzymes were identified that form the environments around the key catalytic carboxyl groups and likely, therefore, play important roles in catalysis. For example, His205 was hydrogen bonded to both the nucleophile, Glu233, and to Asp235.

Additional insights into the interactions at the active site that are fundamental to the catalytic mechanism and substrate specificity may be obtained from crystallographic analysis of the structure of a glycosyl–enzyme intermediate complex. The formation of a covalent 2-deoxy-2-fluorocellobiosyl–enzyme intermediate was achieved by the diffusion of the mechanism-based inactivator 2,4-dinitrophenyl 2-deoxy-2-fluorocellobioside into the crystals of the catalytic domain of Cex (Cex-cd), followed by the determination of the structure of this glycosyl–enzyme complex by X-ray crystallography (32). No significant structural change was observed within the protein upon formation of the glycosyl–enzyme. The structure of the seemingly rigid cavity identified the amino acid residues involved in binding and catalysis. Amino acid side chains interacting with the 6-hydroxyl, and thus likely responsible for determining the cellulose/xylan specificity, were revealed in the structure (Figure 1.16). Subsequent determination of the structure of the 2-deoxy-2-fluoroxyllobiosyl–enzyme revealed that two of the residues that had moved position slightly in the fluorocellobiosyl–enzyme complex no longer moved, consistent with the higher specificity for xylan (76). However, when mutations at one of these positions were made there was no significant effect upon the cellulose/xylan specificity.

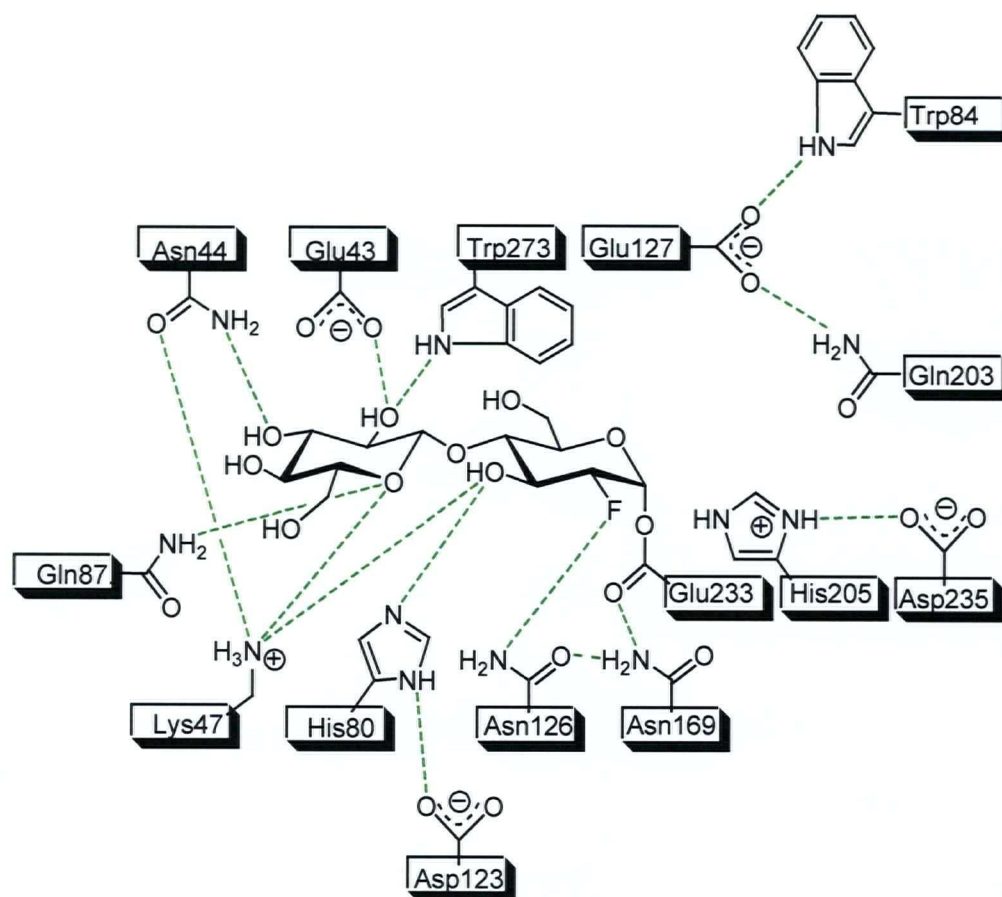


Figure 1.16: Active site of the *Cellulomonas fimi* xylanase trapped as a covalent 2-deoxy-2-fluorocellobiosyl-enzyme intermediate. Adapted from (32).

Insights into the source of the very strong interactions at the 2-position were provided by the three-dimensional structure of stable intermediates formed from 2-deoxy-2-fluoro glycosides (32, 76). The highly conserved Asn125 residue and the carbonyl oxygen of the nucleophile itself were observed to be closest to the fluorine of the substrate moiety. Interactions at the 2-position are extremely important to transition-state stabilization of a number of glycosidases (28), contributing at least 10 kcal mol^{-1} in the case of Cex (32). Subsequent mutational studies have shown that interactions with the amide moiety of Asn126 contribute only approximately $2.5 \text{ kcal mol}^{-1}$ to the stability of

the transition state. Therefore, the most likely source of the remainder of this large interaction energy seems to be with the nucleophile. However, since the 2-position is substituted by fluorine in these trapped complexes, the interactions involved at this position have been impossible to unequivocally identify.

To directly address the nature of the interactions between the enzyme and the 2-hydroxyl of the proximal cellobiosyl moiety, the catalytic domain of the Cex double mutant His205Asn/Glu127Ala was trapped with 2,4-dinitrophenyl cellobioside to form an unsubstituted cellobiosyl-enzyme complex and the crystal structure was subsequently solved to 1.8 Å (33). The overall structure proved to be very similar to that of the wild-type enzyme in its 2-deoxy-2-fluorocellobiosyl-enzyme form, with only minor changes observed in the positioning of the nucleophile and in the hydrogen bonding patterns as a consequence of the mutations. The carbonyl oxygen of the nucleophile was involved in a short (2.37 Å) hydrogen bond with the sugar 2-hydroxyl which was implicated to contribute $>10 \text{ kcal mol}^{-1}$ to transition-state stabilization. Because the structure solved is that of the reactive intermediate, presumably, this interaction is optimized at the transition state both geometrically, as the ring flattens, and electronically, as the positive charge develops at the anomeric centre, acidifying the 2-hydroxyl and thereby increasing its hydrogen bond donor capability, as shown in Figure 1.17.

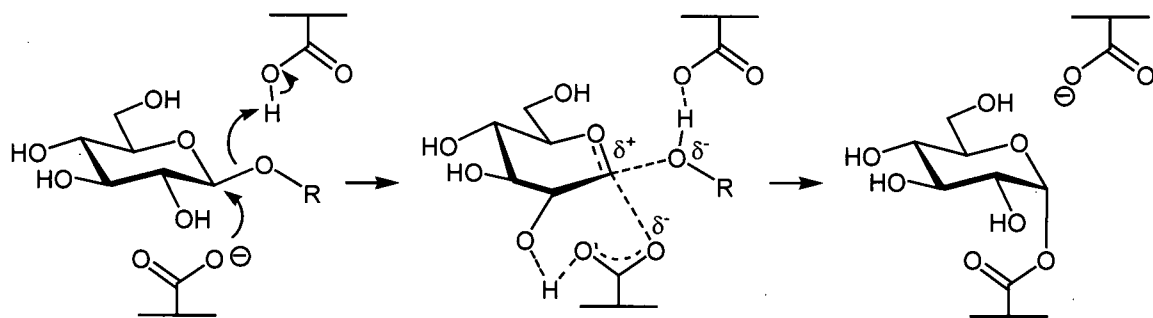


Figure 1.17: Hydrogen bonding at the transition state.

1.3.2 *Bacillus circulans* xylanase

The xylanase from *Bacillus circulans* (Bcx or BcXyn11A) is a 20.4 kDa protein that is a member of the low molecular mass family 11 xylanases (113). Members of this family derive from both eukaryotic and bacterial species and share sequence identity varying from 40-90 %. This “alkaline” xylanase has been extensively characterized using a combination of structural, spectroscopic, and enzymatic techniques (36, 44, 54, 81, 114, 115). Previous studies have determined that Glu78 functions as the nucleophile while Glu172 functions as the general acid/base catalyst in a double-displacement mechanism (36, 81, 115). The pK_a values of all the carboxyl (115, 116) and imidazole (117) groups have been determined by NMR spectroscopy. Specifically, the pK_a values of Glu78 and Glu172 are 4.6 and 6.7, respectively, determined directly using ^{13}C -NMR spectroscopy and in close agreement with those determined from the bell-shaped pH-activity profile of this enzyme (115).

The pH optima of family 11 xylanases range from 2 to 11 and are often correlated with the nature of the residue adjacent to the acid/base catalyst. An alkaline pH optimum is observed in xylanases where the amino acid hydrogen bonded to the catalytic acid/base

is an asparagine residue, whereas an acid pH optimum is observed when this residue is aspartic acid. Substitution of Asn35 with Asp in Bcx resulted in an increase in activity of approximately 20% accompanied by a reduction of the pH optimum from 5.7 to 4.6 (118). A detailed study of this mutant demonstrated that this shift in the pH optimum, together with the formation of a strong hydrogen bond between Asp35 and Glu172 in the glycosyl-enzyme intermediate, was the result of a reverse protonation mechanism, as discussed earlier.

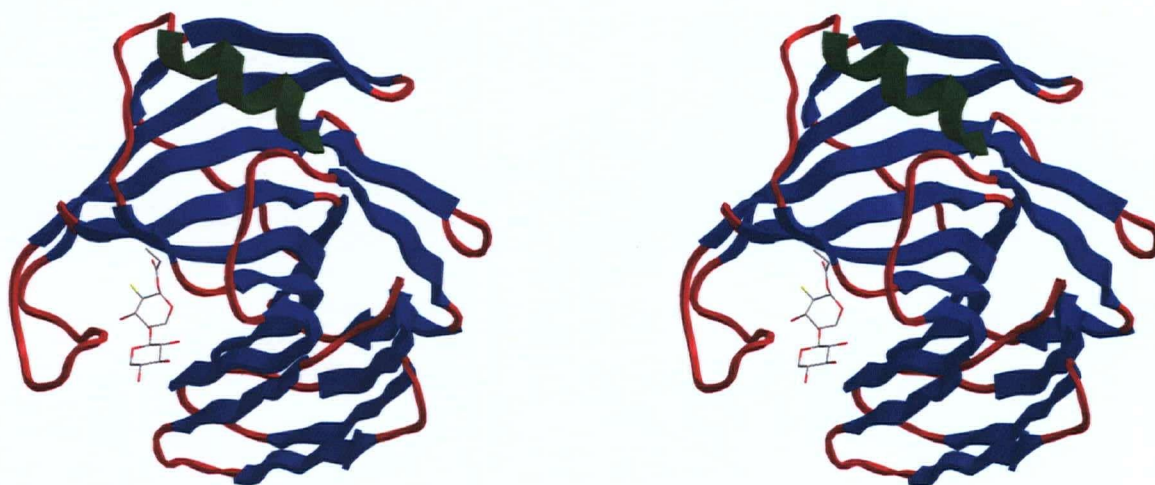


Figure 1.18: Three-dimensional structure of Bcx with bound 2F-X₂ (81). The overall structure of Bcx is depicted as a protein cartoon in divergent (wall-eyed) stereo, with α -helices coloured green, β -strands blue and loops red. The bound 2F-X₂ is drawn as a stick model, with atoms coloured according to atom type, carbon in grey, oxygen in red, and fluorine in yellow. The water molecules in the active site have been removed for clarity. This figure was prepared with Chem3D Ultra 10.0 (<http://www.cambridgesoft.com>).

Structures of the native enzyme, a non-covalent Michaelis complex, and the glycosyl-enzyme intermediate of Bcx have been solved by X-ray crystallography (Figure 1.18) (81, 119). The structure of the active site of Bcx revealed several highly conserved

residues arranged in an intricate network of hydrogen bonds surrounding the two catalytically essential acidic residues, Glu78 and Glu172 (119). The structure of the 2-deoxy-2-fluoroxyllobiosyl–enzyme intermediate formed on Bcx revealed the sugar in the –1 subsite distorted into a ${}^{2,5}B$ boat conformation (81), unlike the 4C_1 conformations seen in other cases (Figure 1.19). This conformation places C5, O5, C1 and C2 in a plane, as is required at the oxocarbenium ion-like transition state of the double-displacement mechanism. Analysis of the conformation of the intermediate also provides insight into specificity, as such a conformation is more readily accessible for xylan derivatives since sugars with bulky hydroxymethyl substituents at C5 would be forced axial resulting in steric clashes with the enzyme.

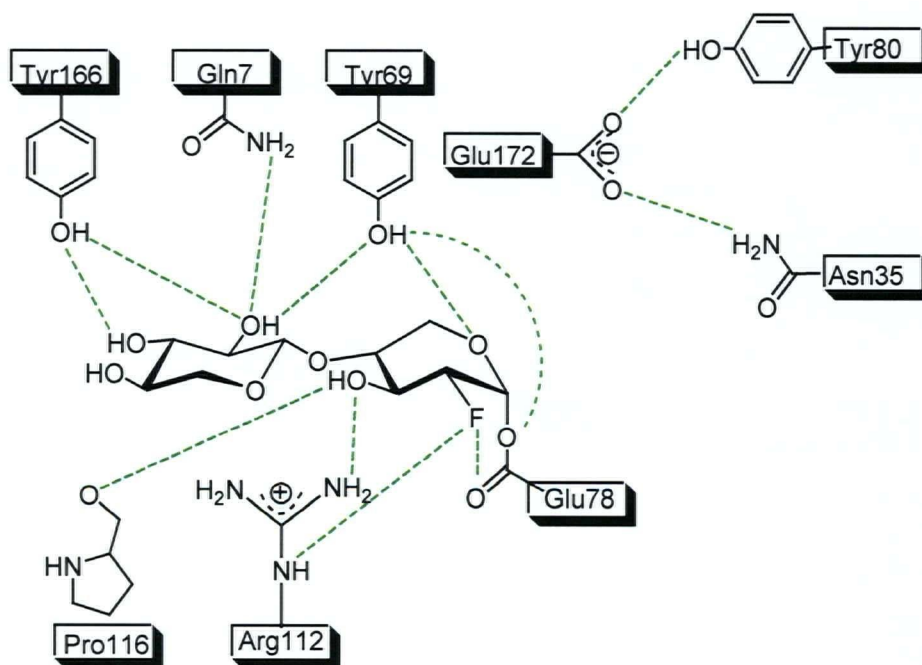


Figure 1.19: Active site of the *Bacillus circulans* xylanase trapped as a covalent 2-deoxy-2-fluoroxyllobiosyl–enzyme intermediate.

A number of interesting observations are revealed by comparison of this structure of the glycosyl-enzyme intermediate and that of a non-covalent Michaelis complex (119). Most notably, the hydroxyl group of conserved residue Tyr69 forms a bifurcated hydrogen bond interaction with the endocyclic oxygen of the xylose residue in the -1 subsite and the oxygen of Glu78 in its ester linkage with the sugar (Figure 1.20). Indeed, mutation of Tyr69 to Phe leads to complete loss of enzyme activity (119), indicating a very important role for this hydroxyl group. It seems probable that a full hydrogen bonding interaction develops from Glu78 to Tyr69, while a stabilizing electrostatic or dipolar interaction develops between the endocyclic oxygen and the hydroxyl group of Tyr69 as the glycosidic bond in this intermediate cleaves, resulting in negative charge development on Glu78 and the generation of positive charge on the sugar ring oxygen at the transition state. Other interesting observations on this complex include the close approach of the fluorine at C2 to the carbonyl oxygen of the nucleophile. Additionally, the conserved residue Tyr80 is involved in a hydrogen bonding interaction with an ordered water molecule held in place for nucleophilic attack at the sugar anomeric centre through hydrogen bonding interaction with the acid/base catalyst Glu172 (Figure 1.20).

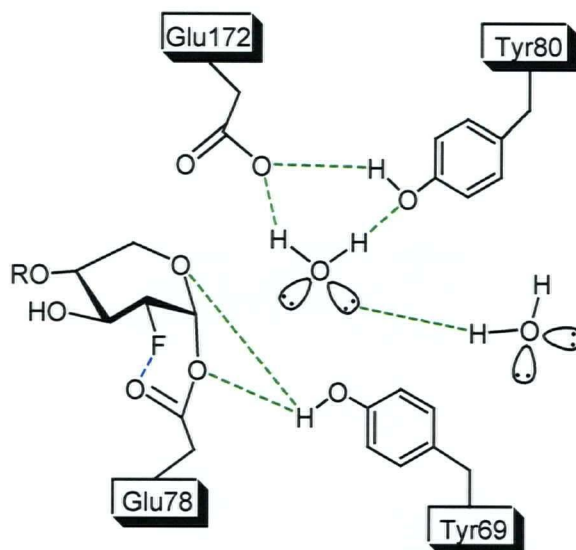


Figure 1.20: The 2-deoxy-2-fluoroxyllobiosyl-enzyme intermediate formed on the *Bacillus circulans* xylanase. Green dashes represent hydrogen bonds, the blue dash depicts a non-hydrogen bond interaction, and the R group represents the saccharide unit bound in the -2 subsite of the active site. Adapted from Sidhu *et al.* (81).

1.4 Aims of this Thesis

Numerous studies of the glycanase Cex from *Cellulomonas fimi* have classified the enzyme as a dual xylanase/cellulase retaining β -glycosidase. The overall objective of this study is to contribute to a better understanding of the catalytic mechanism of the glycanase through a combination of studies.

Structural analysis of the catalytic domain of Cex reveals an intricate network of amino acid residues that participate in the catalytic mechanism. Aside from the catalytic nucleophile and acid/base catalyst, the complex architecture of the active site reveals amino acid residues that may be important in substrate recognition and specificity. The first part of this thesis will consist of a detailed kinetic analysis of a number of active site mutants. Mechanistic investigations of these mutants may help clarify the roles of the

corresponding residues. This will involve steady state kinetic analysis, linear free energy relationship studies, and pH dependence studies. Linear free energy relationship studies should give insight into the rate-determining step and provide information on the degree of negative charge accumulation on the phenolate oxygen at the glycosylation transition state. Furthermore, pH dependence studies may provide insights into the ionization state of the residues at the active site of this enzyme.

Bcx has been characterized extensively using a wide range of structural, spectroscopic, and enzymatic techniques. In this study, Bcx will be further characterized using modified deoxy- and deoxyfluoro-substrates to determine the individual contributions of hydroxyl groups to enzyme catalysis.

An evaluation of the transition-state mimicry of imino-sugar inhibitors may shed light on the structural details of the mechanism of action. Furthermore, rigorous criteria to establish the nature of enzyme inhibition through kinetic studies will aid in the development of therapeutic agents.

In these combined biochemical studies, we hope to reveal the principles of catalysis and specificity for these enzymes.

CHAPTER 2

CHARACTERIZATION OF HIGHLY CONSERVED RESIDUES IN THE ACTIVE SITE OF *CELLULOMONAS FIMI* XYLANASE

2 Characterization of Highly Conserved Residues in the Active Site of *Cellulomonas fimi* Xylanase

2.1 Introduction

The three-dimensional structure of the Cex catalytic domain provides a structural basis for the clarification of the wealth of biochemical information that is currently available for the enzyme. Family 10 xylanases studied to date all consist of 8-fold parallel α/β barrels containing deep active site grooves, consistent with an *endo*-mode of hydrolysis. Members of this family cleave glycosidic bonds by a double-displacement mechanism involving formation and hydrolysis of a covalent glycosyl-enzyme intermediate via oxocarbenium ion-like transition states. During the glycosylation step of the reaction mechanism, a xylose residue at the -1 subsite becomes covalently linked to the enzyme's nucleophile, assisted by general acid-catalyzed protonation of the glycosidic oxygen as it departs. In the deglycosylation step, the covalent glycosyl-enzyme intermediate is hydrolyzed by an activated water molecule that is simultaneously deprotonated by the acid/base catalyst through a general base-catalyzed process. The location of the two key catalytic residues, the nucleophile and acid/base catalyst, is conserved in all family 10 enzymes (120). A series of studies have identified the nucleophile and acid/base catalyst in the family 10 xylanase from Cex using a combination of mechanism-based inactivators, site-directed mutagenesis and detailed kinetic analysis (105, 108). Elucidation of the mechanism of action was achieved through identification of the rate-limiting steps, followed by an investigation of the transition-state structure for each step of the mechanism. This was derived from pre-steady and steady state kinetics, Brønsted relationships, kinetic isotope effect

measurements, inactivation experiments, and pH studies. These data are compiled in *Appendix B*, page 298.

The topology of the active sites of family 10 glycanases was investigated by Charnock *et al.* by testing the rate and pattern of xylooligosaccharide cleavage (121). Data obtained showed that Cex contained three glycone binding sites and two aglycone binding sites. The free energies of productive binding determined for a range of oligosaccharides in the subsites of Cex showed that the -2 subsite plays an important role in substrate binding. Furthermore, productive complexes were generally only formed when xylotrioside and xyloetraoside substrates occupied the -2 and -1 subsites of the xylanase. Residues that have the potential to play an important role in ligand binding through hydrogen bonding with sugar hydroxyl groups or hydrophobic stacking interactions with the pyranose rings have been identified at the -1 and -2 subsites. The three-dimensional structures of several family 10 xylanases have revealed highly conserved residues on the surface of the active-site cleft (112, 122-129). In particular, structural analysis of family 10 xylanases covalently linked to mechanism-based cellobiosyl and xylobiosyl inhibitors has facilitated the identification of active-site amino acids that play important roles in substrate binding and catalysis (Figure 2.1). Specifically, structural analysis of Cex shows that Glu43, Asn44, Lys47, His80, Gln87, Asn126, and Asn169 are part of an important hydrogen bond network involved in substrate recognition (32, 33, 76, 125). The high-resolution structures of the ligand-enzyme complexes have also revealed amino acids that influence the positions and ionization states of the two key catalytic residues; for example, Asn126 and Asn169 are in the vicinity of the two catalytic residues. These residues, based on amino acid

sequence alignments and structural analysis, have been a target for mutagenesis and kinetic analysis in order to gain insight into the reaction mechanism of glycosidases. In order to investigate the role of these active-site residues in the structure and function of Cex, mutant enzymes were produced at each position, namely, E43A, N44A, K47A, H80A, H80N, H80Q, N126A, and N169A.

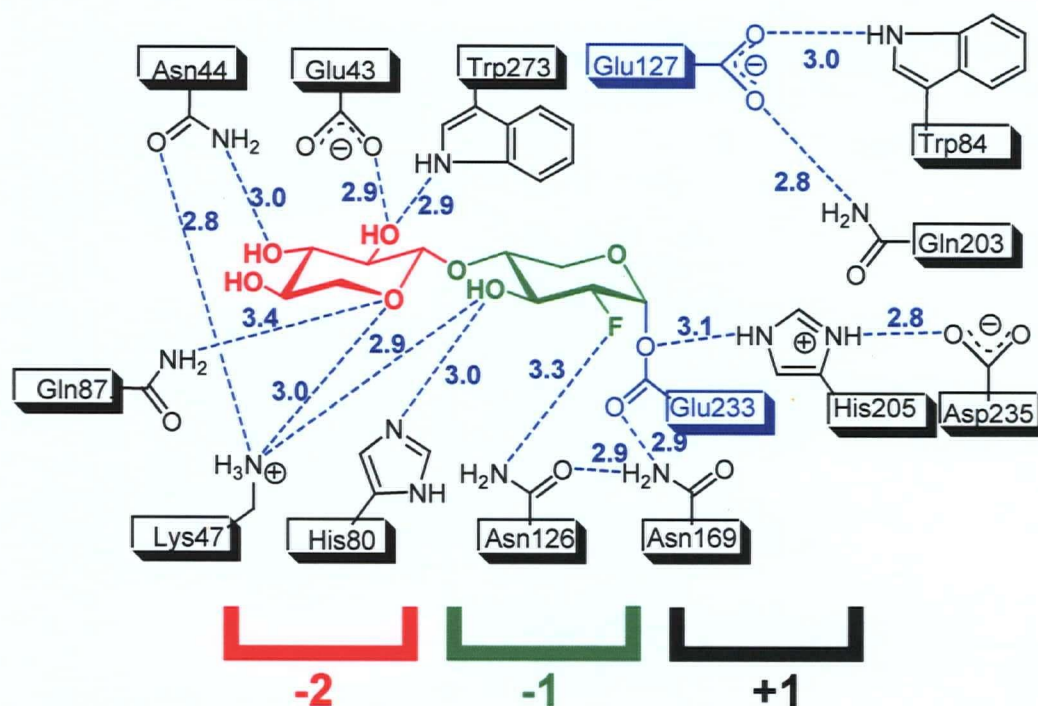


Figure 2.1: Scheme of protein-carbohydrate interactions in the active site region of 2F-xylobiosyl-Cex-cd complex observed by three-dimensional structural analysis (76). Hydrogen-bonding interactions between heteroatoms are in Angstroms. The distance between 2F and the carbonyl oxygen of Glu233 is 2.6 Å (not shown).

The primary aim of this study is to investigate the roles of highly conserved residues in the -2 and -1 binding subsites of Cex. The biochemical properties of Cex and variants of Cex will be evaluated to achieve this objective through detailed steady state kinetic analyses and pH studies. The information derived from studies presented in this section will provide the basis for further work presented in the upcoming chapters of this thesis.

2.2 Results

2.2.1 Generation of mutants of Cex

A linear amplification, site-directed mutagenesis method was used to produce E43A, N44A, K47A, H80A, H80N, and H80Q variants of Cex. The N126A and N169A mutants were produced by a similar procedure by Dr. Valerie Notenboom (University of Toronto), and generously provided for this study. The procedure, based on the QuikChange site-directed mutagenesis kit by Stratagene, utilized pUC12-1.1*cex*(PTIS) as the vector containing the 1.4 kb *cex* gene and two synthetic oligonucleotide primers (Figure 2.2). The complementary oligonucleotide primers were extended using *Pwo* DNA polymerase to generate a mutated plasmid containing staggered nicks. Following temperature cycling, the reaction mixture was treated with the *Dpn* I endonuclease which is specific for methylated and hemimethylated DNA, and was thereby used to select for mutated synthesized DNA by digesting the methylated, nonmutated parental DNA template. The circular, nicked vector DNA was then transformed into XL1-Blue electrocompetent cells that repaired the nicks in the mutated plasmid. The plasmid DNA was isolated and subjected to restriction analysis to reveal positive clones, which were

then sequenced to verify the correct mutations. The recombinant pUC12-1.1*cex*(PTIS) was subsequently transformed into electrocompetent *E. coli* JM101 cells for expression of mutant protein.

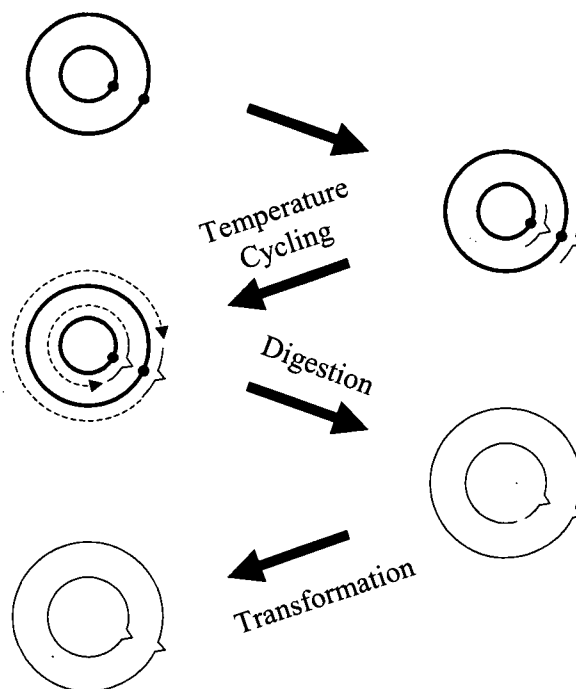


Figure 2.2: Overview of the QuikChange™ Site-Directed Mutagenesis Kit.

2.2.2 Production, purification, and physical characterization

The mutant proteins were produced and purified as described in *Materials and Methods*. No significant differences in behaviour were observed during purification. The mutant proteins eluted at approximately the same position as wild-type enzyme from the cellulose affinity column. The purified protein ran as a single band on SDS-PAGE at the same position (47 kDa) as the native enzyme with greater than 95% purity by inspection. Final protein yield ranged from 5 to 20 mg L⁻¹ of liquid culture (Table 2.1). Mass

spectrometric analysis confirmed the molecular masses of the mutant proteins (Table 2.2).

Table 2.1: Total yields of Cex mutants produced.

Enzyme	Total Yield (mg)
Cex E43A	17
Cex N44A	12
Cex K47A	13
Cex H80A	7.3
Cex H80N	6.0
Cex H80Q	5.2

Table 2.2: Determination of molecular weight by mass spectrometry.

Enzyme	Observed M_r (Da)	Observed ΔM_r (Da)	Expected ΔM_r (Da)
Native Cex	47124 \pm 3	0	0
Cex E43A	47064 \pm 3	60 \pm 5	58
Cex N44A	47082 \pm 3	42 \pm 5	43
Cex K47A	47070 \pm 3	54 \pm 5	57
Cex H80A	47058 \pm 3	66 \pm 5	66
Cex H80N	47100 \pm 3	24 \pm 5	23
Cex H80Q	47114 \pm 3	10 \pm 5	9

2.2.3 Kinetic analysis: pH dependence of k_{cat}/K_m

Michaelis–Menten parameters for the hydrolysis of aryl cellobioside and xylobioside substrates as a function of pH were measured to characterize the mutant

xylanases. Substrates were chosen with high K_m values to enable k_{cat}/K_m to be determined from a single experiment at a substrate concentration well below K_m . An initial concentration of about $K_m/5$ was hydrolyzed by the enzymes to give a first-order increase in absorbance as the products were released with rate constant $(k_{cat}/K_m) \times [E]_0$. The pH dependence of k_{cat}/K_m determined in this way agrees well with that determined from Michaelis–Menten plots. The method is experimentally easier, and more reproducible and accurate (130) because it eliminates the need to correct for the variation of extinction coefficient of the substrate with pH, thereby reducing errors associated with the determination of substrate concentration. The parameter k_{cat}/K_m was chosen to be monitored, rather than k_{cat} or K_m individually, in order to be able to interpret the pH dependence in terms of ionization events related specifically to the unbound enzyme, since k_{cat}/K_m is the second-order rate constant for the reaction of free enzyme and substrate. The first-order rate constant k_{cat} reflects bound species including the enzyme–substrate, –intermediate, and –product complexes. Since k_{cat}/K_m reflects the events up to and including the first irreversible step in the mechanism, its value will not be influenced by potential changes in the rate-determining step from glycosylation to deglycosylation or *vice versa*. Additionally, transglycosylation reactions may occur at elevated substrate concentrations making it experimentally difficult to extract K_m and k_{cat} values individually. Conversely, a pseudo-first-order analysis of the reaction velocity under conditions of limited substrate accurately measures k_{cat}/K_m .

The pH dependence plots for k_{cat}/K_m were fit to a bell-shaped activity profile, described by equation 2.1, to provide two pK_a values (pK_{a1} and pK_{a2}), as summarized in Table 2.3.

$$\frac{k_{\text{cat}}}{K_m} = \left(\frac{k_{\text{cat}}}{K_m} \right)_{\text{max}} \left(\frac{K_{a1}[\text{H}^+]}{(K_{a1} + [\text{H}^+])(K_{a2} + [\text{H}^+])} \right) \quad (2.1)$$

Table 2.3: pH Dependence of k_{cat}/K_m for *C. fimi* xylanase and mutants.^a

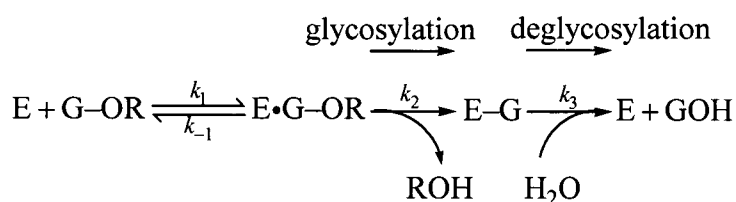
Enzyme	$\text{p}K_{a1}$	$\text{p}K_{a2}$	pH Optimum	Conditions	
				Substrate	pH Range
Wild-Type	3.9	7.7	5.8	2,4DNPC	3.5-8.5
E43A	3.7	6.9	5.3	2,4DNPC	3.5-8.5
N44A	3.9	8.0	5.9	2,4DNPC	3.5-8.5
K47A	3.9	6.0	4.9	2,5DNPX ₂	3.5-8.0
H80A	4.6	6.2	5.4	PNPX ₂	3.5-7.5
H80N	4.6	6.3	5.5	PNPX ₂	3.5-7.5
H80Q	4.6	7.0	5.8	PNPX ₂	4.0-7.5
Q87M	4.0	8.1	6.1	2,4DNPC	3.5-8.5
Q87Y	3.9	8.3	6.1	2,4DNPC	3.5-8.5
N126A	4.4	8.5	6.4	2,4DNPC	4.0-8.5
N169A	4.0	8.2	6.1	2,4DNPC	3.5-8.5

^a Graphical representation of this data is given in *Appendix A*, page 292. An error of ± 0.1 pH units was estimated from a non-linear fit by GraFit 4.0 (131).

2.2.4 Kinetic analysis: steady state kinetics

In order to investigate the role of highly conserved active-site residues in the mechanism of Cex, kinetic parameters for a range of substrates were determined for mutant enzymes of Cex; namely, E43A, N44A, K47A, H80A, H80N, H80Q, N126A, and N169A. The kinetic parameters for these mutant enzymes may help reveal the importance of these residues for the catalytic function of Cex.

The initial kinetic characterization of the active-site mutants of Cex consisted of comparisons to the wild-type enzyme with respect to the fundamental steady state kinetic constants: k_{cat} , the turnover number; K_m , the apparent dissociation constant; and k_{cat}/K_m , the apparent second-order rate constant, often referred to as the specificity constant. Assessment of these kinetic parameters will yield insight into how particular mutations affect the rates of the individual glycosylation and deglycosylation steps. The generally accepted double-displacement mechanism for Cex can be expressed as follows:



where,

E = unbound enzyme

G-OR = unbound glycoside substrate

E·G-OR = Michaelis enzyme-substrate complex

E-G = glycosyl-enzyme intermediate

ROH = leaving group phenol

GOH = sugar product

k_1 = second-order rate constant for association

k_{-1} = first-order rate constant for dissociation

k_2 = first-order rate constant for glycosylation

k_3 = first-order rate constant for deglycosylation

As discussed in *Appendix C*, the kinetic parameters, k_{cat} , K_m , and k_{cat}/K_m , can be defined in terms of the individual rate constants as follows:

$$k_{\text{cat}} = \frac{k_2 k_3}{k_2 + k_3} \quad (2.2)$$

$$K_m = \frac{k_3 (k_{-1} + k_2)}{k_1 (k_2 + k_3)} \quad (2.3)$$

$$\frac{k_{\text{cat}}}{K_m} = \frac{k_1 k_2}{k_{-1} + k_2} \quad (2.4)$$

Mutations that reduce the rate of deglycosylation (relative to glycosylation) will result in accumulation of the glycosyl-enzyme intermediate. Therefore, provided deglycosylation is the rate-determining step ($k_3 \ll k_2$), the K_m reduces to

$$K_m = \frac{k_3}{k_2} \left(\frac{k_{-1} + k_2}{k_1} \right) = \frac{k_3}{k_2} K_s \quad (2.5)$$

Therefore, the K_m decreases as the ratio k_3/k_2 . Correspondingly, a relative reduction in the rate of glycosylation would be expected to increase the K_m . The effect of a mutation on the rate of the glycosylation step can also be estimated by analysis of k_{cat}/K_m , which reflects the first irreversible step in the reaction. Detailed interpretations of k_{cat} , K_m , and k_{cat}/K_m are given in *Appendix C*.

Nitrophenyl cellobiosides and xylobiosides with aglycones having different pK_a values were evaluated as substrates for Cex and its mutants. The enzymatic hydrolysis rates were measured by spectrophotometric detection of phenol release under the standard assay conditions described in *Materials and Methods*. The enzyme concentrations employed were those which gave a sufficiently large absorbance change to ensure accurate determination of rates, yet resulted in less than 10% conversion of the substrate to product to ensure linear kinetics. The maximum velocities (V_{max}) and the apparent dissociation constants (K_m) were determined when the highest substrate concentration assayed was greater than $2K_m$ by fitting the initial rates and substrate concentrations to the Michaelis-Menten equation using the program GraFit 4.0 (131). At low substrate concentration, when no saturation was reached ($[S]_{\text{max}} < 2K_m$), k_{cat}/K_m was evaluated as

the slope of the linear region of V_0 versus $[S]$. Alternatively, k_{cat}/K_m was determined using the substrate depletion method using very little substrate ($[S] < 0.2K_m$). Regardless of the method employed, all values are numerically equivalent, confirming the validity of this approach for these studies.

In various cases, the Lineweaver–Burk plots for the xylobioside substrates were biphasic (Figure 2.3), revealing a rate enhancement over that expected at higher substrate concentrations. Such behaviour is likely due to transglycosylation of the xylobiosyl–enzyme intermediate to a second substrate molecule bound in the aglycone site at higher substrate concentrations. This has been observed to occur with *Agrobacterium* sp. β -glucosidase (Abg) with PNPX (21). Values of k_{cat} and K_m for both the hydrolytic reaction and the transglycosylation reaction were estimated by drawing a straight line through the two regions of the Lineweaver–Burk plot. Such an approach was used to estimate these two parameters for Abg (21). Thus, kinetic parameters determined at low substrate concentrations are those of the simple hydrolysis process, while those at high substrate concentration are for the transglycosylation process; the high K_m value reflecting the relatively poor binding at the aglycone site.

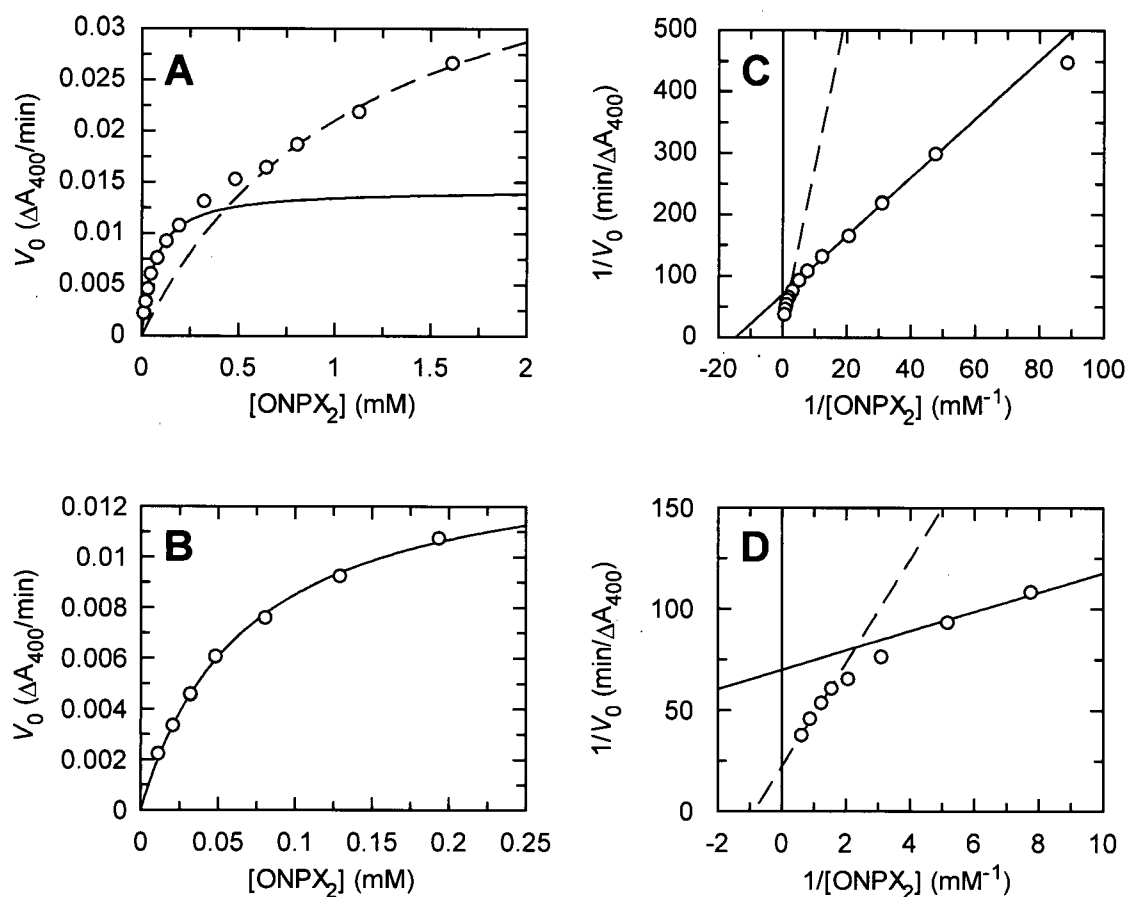


Figure 2.3: Data for the hydrolysis of *o*-nitrophenyl xylobioside by wild-type Cex plotted in (A) and (B) Michaelis–Menten form; and (C) and (D) Lineweaver–Burk form. Kinetic parameters for the hydrolysis reaction were obtained by fitting data obtained at lower substrate concentrations (unbroken line), while those for the hydrolysis reaction were obtained by fitting data obtained at higher substrate concentrations (dashed line).

Cex displays significant activity against soluble cellulose and xylan, and, as shown in previous studies and assembled in Table 2.4, is highly active against a range of aryl β -glucosides (22, 132). The enzyme displays considerably higher activity with aryl β -xylobiosides and β -xylosides, compared with the corresponding β -cellobiosides and β -glucosides, respectively.

Table 2.4: Michaelis–Menten parameters for the hydrolysis of various aryl glycoside substrates by *C. fimi* xylanase.

Substrate	k_{cat} (s^{-1})	K_{m} (mM)	$k_{\text{cat}}/K_{\text{m}}$ ($\text{s}^{-1} \text{mM}^{-1}$)
PNPG ^a	0.033	8.3	0.0041
PNPX ^a	2.6	20	0.13
PNPC ^a	15.8	0.60	26
PNPX ₂ ^a	40	0.018	2200
2,4DNPG ^a	18	1.9	9.5
2,4DNPC ^a	12.9	0.11	117

^a Data taken from Tull and Withers (22).

The substrate specificities of family 10 enzymes vary considerably. Cex cleaves cellulosic substrates with significantly higher activity than do several other family 10 xylanases, as presented in Table 2.5. Although the xylanases from *Streptomyces lividans* and *Cellvibrio japonicus* cleave cellobiosides, the enzymes display far lower activity than Cex (121, 126). There is also some variability in terms of the rate-limiting steps in the double-displacement reaction mechanism. For example, for Cex the rate-limiting step for hydrolysis of either PNPC or 2,4DNPC is deglycosylation (22). However, the rate-limiting step in the hydrolysis of 2,4DNPC by Xyn10A from *Cellvibrio japonicus* is glycosylation, as substantiated by the absence of a pre-steady state burst of DNP release (133).

Table 2.5: Michaelis–Menten parameters for the hydrolysis of various aryl glycoside substrates by several family 10 xylanases.

Substrate	Enzyme	k_{cat} (s^{-1})	K_m (mM)	k_{cat}/K_m ($s^{-1}mM^{-1}$)
PNPG	Cex, <i>C. fimi</i> ^a	0.033	8.3	0.0041
	Xyn10A, <i>S. lividans</i> ^b	0.011	180	0.00069
	Xyn10A, <i>C. japonicus</i> ^c	ND ^d	ND ^d	ND ^d
PNPX	Cex, <i>C. fimi</i> ^a	2.6	20	0.13
	Xyn10A, <i>S. lividans</i> ^b	0.32	380	0.00081
	Xyn10A, <i>C. japonicus</i> ^c	0.15	310	0.00048
PNPC	Cex, <i>C. fimi</i> ^a	15.8	0.60	26
	Xyn10A, <i>S. lividans</i> ^b	3.6	51	0.071
	Xyn10A, <i>C. japonicus</i> ^c	2.6	50	0.052
PNPX ₂	Cex, <i>C. fimi</i> ^a	40	0.018	2200
	Xyn10A, <i>S. lividans</i> ^b	29	0.58	51
	Xyn10A, <i>C. japonicus</i> ^c	86	0.57	150

^a Data taken from Tull and Withers (22).^b Data taken from Ducros *et al.* (126).^c Data taken from Charnock *et al.* (121).^d ND, not detectable.

2.2.4.1 Probing the –2 subsite: steady state kinetic analyses of Glu43, Asn44, and Lys47 mutants

Residues in the active site are highly conserved among members of family 10 glycoside hydrolases. For instance, the residues Glu43, Asn44, Lys47 are highly conserved in the –2 subsite of the binding cleft of family 10 enzymes (Figure 2.1). Lys47 also interacts extensively with the –1 subsite. To evaluate the importance of conserved residues located at the –2 subsite of Cex, the effect on enzyme activity of creating E43A, N44A, and K47A mutations will be assessed. Cex E43A and N44A display very similar

k_{cat} values to those of native Cex, whereas K47A is significantly less active against the aryl β -glucosides, particularly those with poorer leaving groups (Table 2.6).

Table 2.6: Michaelis–Menten parameters for the hydrolysis of aryl glycosides by the *C. fimi* xylanase (Cex) and mutants E43A, N44A, and K47A.^b

Enzyme	Substrate	Michaelis–Menten Parameters			Rate-Limiting Step (k_{cat}) (DEGLY or GLY)
		k_{cat} (s^{-1})	K_{m} (mM)	$k_{\text{cat}}/K_{\text{m}}$ ($\text{s}^{-1} \text{mM}^{-1}$)	
Native Cex	2,4DNPC	8.46 ± 0.07	0.068 ± 0.002	124 ± 5	DEGLY
	PNPC	9.24 ± 0.07	0.58 ± 0.01	15.9 ± 0.5	DEGLY
	2,5DNPX ₂	29.9 ± 0.6	0.0145 ± 0.0009	2100 ± 200	DEGLY
	PNPX ₂	32.0 ± 0.4	0.0219 ± 0.0007	1500 ± 70	DEGLY
	ONPX ₂	(i) 38.1 ± 0.8^a	(i) 0.068 ± 0.003^a	(i) 560 ± 40^a	DEGLY
		(ii) 121 ± 8^a	(ii) 1.2 ± 0.1^a	(ii) 100 ± 20^a	
Cex E43A	2,4DNPC	4.92 ± 0.02	0.185 ± 0.003	26.6 ± 0.5	DEGLY
	PNPC	1.29 ± 0.03	12.8 ± 0.5	0.101 ± 0.007	DEGLY/GLY
	2,5DNPX ₂	(i) 19.5 ± 0.2^a	(i) 0.063 ± 0.001^a	(i) 310 ± 10^a	DEGLY
		(ii) 35 ± 1^a	(ii) 0.35 ± 0.04^a	(ii) 100 ± 20^a	
	PNPX ₂	27.4 ± 0.8	5.4 ± 0.3	5.1 ± 0.4	DEGLY
	ONPX ₂	(i) 47 ± 3^a	(i) 1.6 ± 0.2^a	(i) 30 ± 5^a	DEGLY
		(ii) 151 ± 7^a	(ii) 7.8 ± 0.6^a	(ii) 19 ± 2^a	
Cex N44A	2,4DNPC	9.36 ± 0.06	0.070 ± 0.002	134 ± 4	DEGLY
	PNPC	10.1 ± 0.2	1.74 ± 0.07	5.8 ± 0.4	DEGLY
	2,5DNPX ₂	(i) 43.1 ± 0.5^a	(i) 0.038 ± 0.001^a	(i) 1130 ± 50^a	DEGLY
		(ii) 80 ± 3^a	(ii) 0.27 ± 0.03^a	(ii) 300 ± 50^a	
	PNPX ₂	(i) 89 ± 7^a	(i) 3.6 ± 0.4^a	(i) 25 ± 4^a	DEGLY
		(ii) 170 ± 10^a	(ii) 8.9 ± 0.7^a	(ii) 20 ± 2^a	
Cex K47A	ONPX ₂	(i) 80 ± 8^a	(i) 0.64 ± 0.10^a	(i) 130 ± 30^a	DEGLY
		(ii) 430 ± 30^a	(ii) 7.4 ± 0.9^a	(ii) 60 ± 10^a	
	2,4DNPC	4.20 ± 0.06	2.6 ± 0.1	1.6 ± 0.1	DEGLY
	PNPC	0.020 ± 0.002	29 ± 3	0.00071 ± 0.00015	GLY
	2,5DNPX ₂	(i) 59 ± 2^a	(i) 0.20 ± 0.01^a	(i) 300 ± 20^a	DEGLY
		(ii) 120 ± 10^a	(ii) 0.76 ± 0.12^a	(ii) 150 ± 30^a	
	PNPX ₂	0.36 ± 0.01	9.6 ± 0.3	0.038 ± 0.002	GLY
	ONPX ₂	9.7 ± 0.2	8.5 ± 0.3	1.15 ± 0.06	GLY

^a Parameters are for the (i) hydrolysis and (ii) transglycosylation reactions.

^b Graphical representation of this data is given *Appendix A*, page 228. Errors were estimated from a non-linear fit by GraFit 4.0 (131).

For substrates that show no significant dependence of k_{cat} on phenol leaving group ability, the initial bond-cleavage step is unlikely to be rate limiting; thus, the deglycosylation step is the rate-limiting step for these substrates. Deglycosylation must be rate determining for substrates where transglycosylation is observed at elevated substrate concentrations. Conversely, for substrates that show a significant dependence of k_{cat} on leaving group ability, the glycosylation step is likely to be the rate-limiting step for these substrates.

The k_{cat} values for hydrolysis of xylobioside substrates by the E43A variant are essentially unchanged relative to those of the wild-type enzyme, indicating that the mutation does not affect the deglycosylation step, which remains rate determining. Hydrolysis of cellobioside substrates follows a somewhat different pattern, with k_{cat} for 2,4DNPC and PNPC being 2- and 7-fold lower, respectively, than for wild-type enzyme, implying that the rate-limiting step changes from deglycosylation to glycosylation, at least for PNPC. This is supported by the much higher K_{m} value observed.

The k_{cat} values for hydrolysis of cellobioside and xylobioside substrates by the N44A variant are relatively unchanged, indicating that the mutation does not affect the rate-limiting deglycosylation step. Lys47 hydrolyzed aryl cellobioside and xylobioside substrates with modest leaving groups with significantly lower k_{cat} and higher K_{m} values than the wild-type enzyme. However, the values of k_{cat} for the more activated substrates 2,4DNPC and 2,5DNPX₂, were similar to those of the wild-type enzyme. The mutation changes the rate-limiting step for PNPC, as well as PNPX₂ and ONPX₂ hydrolysis from deglycosylation to glycosylation. Such a change in rate-limiting step is not seen for the more activated substrates since the glycosylation step is inherently faster in those cases.

As shown in Figure 2.4, the three variant enzymes have simple bell-shaped pH profiles, where the pK_a of the acidic limb of the profile, corresponding to the ionization of the nucleophile, is largely unaffected. The basic limb, corresponding to the acid/base catalyst, is affected differently in each case. No significant shift is seen for the N44A enzyme, whereas the pK_a corresponding to ionization of the acid/base catalyst for Cex E43A and Cex K47A shifted to 6.9 and 6.0, respectively, compared to the wild-type value of 7.7 as shown in Table 2.3.

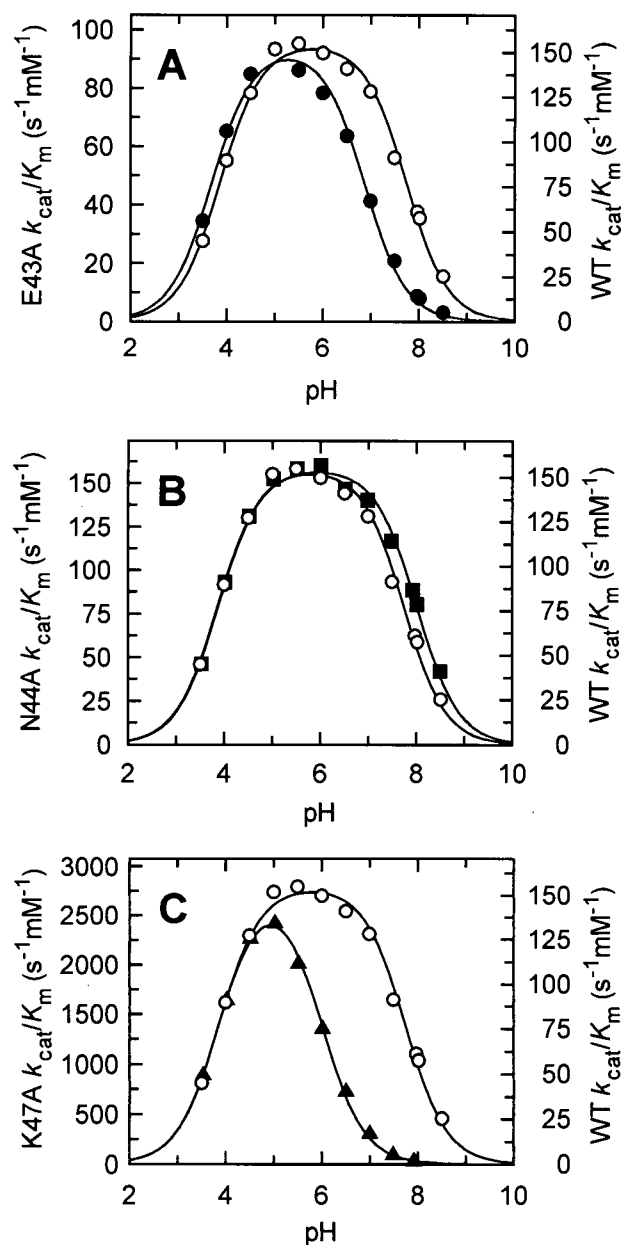


Figure 2.4: pH profiles of wild-type (O) and Glu43, Asn44, and Lys47 mutants of *Cex*. The pH dependence of wild-type *Cex* was measured using 2,4DNPC where $pK_{a1} = 3.9$ and $pK_{a2} = 7.7$. (A) The E43A (●) mutant enzyme activity was measured using 2,4DNPC where $pK_{a1} = 3.7$ and $pK_{a2} = 6.9$. (B) The N44A (■) mutant enzyme activity was measured using 2,4DNPC where $pK_{a1} = 3.9$ and $pK_{a2} = 8.0$. (C) The K47A (▲) mutant enzyme activity was measured using 2,5DNPX₂ where $pK_{a1} = 3.9$ and $pK_{a2} = 6.0$.

2.2.4.2 Probing the -1 subsite: steady state kinetic analyses of His80 mutants

In order to investigate the role of the His80 residue in the structure and function of Cex, three mutant enzymes were produced; namely, H80A, H80N, and H80Q. The properties of Cex H80A do not distinguish between its role as a hydrogen-bond (proton) donor or as an acceptor because Ala is capable of neither of these functions. Asn and Gln variants may distinguish between the models because these residues can participate in hydrogen bonding interactions that mimic the His nitrogens, but they cannot mimic the acid/base properties.

The specific activity of these mutant enzymes is reduced by a significant amount, revealing the importance of this residue for the catalytic function of Cex. Fortunately, they retain sufficient activity to determine their kinetic parameters on the synthetic aryl glycoside substrates (Table 2.7).

The properties of the H80A and H80N variants are nearly indistinguishable, while the activity of the H80Q mutant is further impaired by roughly 10-fold. These results indicate that the presence of an amide side chain at position 80 is not sufficient to restore Cex activity. Geometric limitations may hinder the amide-containing residues from mimicking the hydrogen-bonding contributions of His80, especially since it also interacts with Asp123 in a manner reminiscent of a Ser—His—Asp triad in proteases.

For the His80 mutations, deglycosylation remained the rate-limiting step for the hydrolysis of xylobioside substrates. For the cellobioside substrates, glycosylation may start to become rate limiting with PNPC.

Table 2.7: Michaelis–Menten parameters for the hydrolysis of aryl glycosides by the *C. fimi* xylanase (Cex) and mutants H80A, H80N, and H80Q.^b

Enzyme	Substrate	Michaelis–Menten Parameters			Rate-Limiting Step (k_{cat}) (DEGLY or GLY)
		k_{cat} (s^{-1})	K_m (mM)	k_{cat}/K_m ($s^{-1} mM^{-1}$)	
Native Cex	2,4DNPC	8.46 ± 0.07	0.068 ± 0.002	124 ± 5	DEGLY
	PNPC	9.24 ± 0.07	0.58 ± 0.01	15.9 ± 0.5	DEGLY
	2,5DNPX ₂	29.9 ± 0.6	0.0145 ± 0.0009	2100 ± 200	DEGLY
	PNPX ₂	32.0 ± 0.4	0.0219 ± 0.0007	1500 ± 70	DEGLY
	ONPX ₂	(i) 38.1 ± 0.8^a	(i) 0.068 ± 0.003^a	(i) 560 ± 40^a	DEGLY
		(ii) 121 ± 8^a	(ii) 1.2 ± 0.1^a	(ii) 100 ± 20^a	
Cex H80A	2,4DNPC	0.088 ± 0.004	0.0071 ± 0.0003	12 ± 1	DEGLY
	PNPC	0.048 ± 0.002	13 ± 1	0.0037 ± 0.0004	DEGLY/GLY
	2,5DNPX ₂	(i) 0.25 ± 0.01^a	(i) 0.0021 ± 0.0002^a	(i) 120 ± 20^a	DEGLY
		(ii) 0.73 ± 0.03^a	(ii) 0.32 ± 0.02^a	(ii) 2.3 ± 0.3^a	
	PNPX ₂	0.42 ± 0.02	0.59 ± 0.03	0.72 ± 0.07	DEGLY
	ONPX ₂	(i) 0.33 ± 0.02^a	(i) 0.039 ± 0.002^a	(i) 8.4 ± 0.8^a	DEGLY
		(ii) 2.9 ± 0.2^a	(ii) 3.4 ± 0.2^a	(ii) 0.84 ± 0.08^a	
Cex H80N	2,4DNPC	0.056 ± 0.003	0.0051 ± 0.0003	11 ± 2	DEGLY
	PNPC	0.040 ± 0.002	6.6 ± 0.4	0.0060 ± 0.0006	DEGLY
	2,5DNPX ₂	(i) 0.12 ± 0.01^a	(i) 0.0012 ± 0.001^a	(i) 99 ± 10^a	DEGLY
		(ii) 0.22 ± 0.02^a	(ii) 0.15 ± 0.03^a	(ii) 1.5 ± 0.3^a	
	PNPX ₂	(i) 0.13 ± 0.01^a	(i) 0.099 ± 0.02^a	(i) 1.3 ± 0.3^a	DEGLY
		(ii) 0.29 ± 0.03^a	(ii) 0.58 ± 0.06^a	(ii) 0.51 ± 0.1^a	
Cex H80Q	2,4DNPC	(i) 0.14 ± 0.01^a	(i) 0.016 ± 0.002^a	(i) 8.6 ± 1^a	DEGLY
		(ii) 0.75 ± 0.07^a	(ii) 2.0 ± 0.2^a	(ii) 0.38 ± 0.1^a	
	2,4DNPC	0.012 ± 0.002	0.0019 ± 0.0002	6.1 ± 1	DEGLY
	PNPC	0.0064 ± 0.0006	3.1 ± 0.3	0.0021 ± 0.0004	DEGLY
	2,5DNPX ₂	(i) 0.034 ± 0.01^a	(i) 0.00062 ± 0.0001^a	(i) 54 ± 10^a	DEGLY
		(ii) 0.068 ± 0.01^a	(ii) 0.17 ± 0.02^a	(ii) 0.40 ± 0.08^a	
Cex H80Q	PNPX ₂	(i) 0.037 ± 0.01^a	(i) 0.062 ± 0.006^a	(i) 0.61 ± 0.1^a	DEGLY
		(ii) 0.10 ± 0.01^a	(ii) 0.63 ± 0.07^a	(ii) 0.16 ± 0.03^a	
	ONPX ₂	(i) 0.039 ± 0.01^a	(i) 0.010 ± 0.001^a	(i) 3.8 ± 0.8^a	DEGLY
		(ii) 0.26 ± 0.03^a	(ii) 2.4 ± 0.3^a	(ii) 0.11 ± 0.02^a	

^a Parameters are for the (i) hydrolysis and (ii) transglycosylation reactions.^b Graphical representation of this data is given *Appendix A*, page 228. Errors were estimated from a non-linear fit by GraFit 4.0 (131).

The pH profiles of the modified enzymes were determined and compared to that of the wild-type enzyme (Figure 2.5). The shapes of the mutant Cex plots are simple bell-shaped profiles similar to that of the wild-type, but are much narrower because the pH profiles are affected on both the acidic and basic limbs. Therefore, the different mutations exhibit effects on the ionization states of both catalytic glutamic acid residues. For the three mutations studied, the calculated pK_a shifts are 0.7 pH units toward a more basic pH for the nucleophilic Glu233 and 0.7–1.5 pH units toward a more acidic pH for the acid/base catalyst Glu127. The profiles were fit using equation 2.1 to provide two pK_a values for each variant, as tabulated in Table 2.3. A role for His80 in the hydrogen-bond network responsible for maintaining the ionization state of the two catalytic residues is indicated by the significant shift in pK_a values of the two catalytic residues in all three mutations.

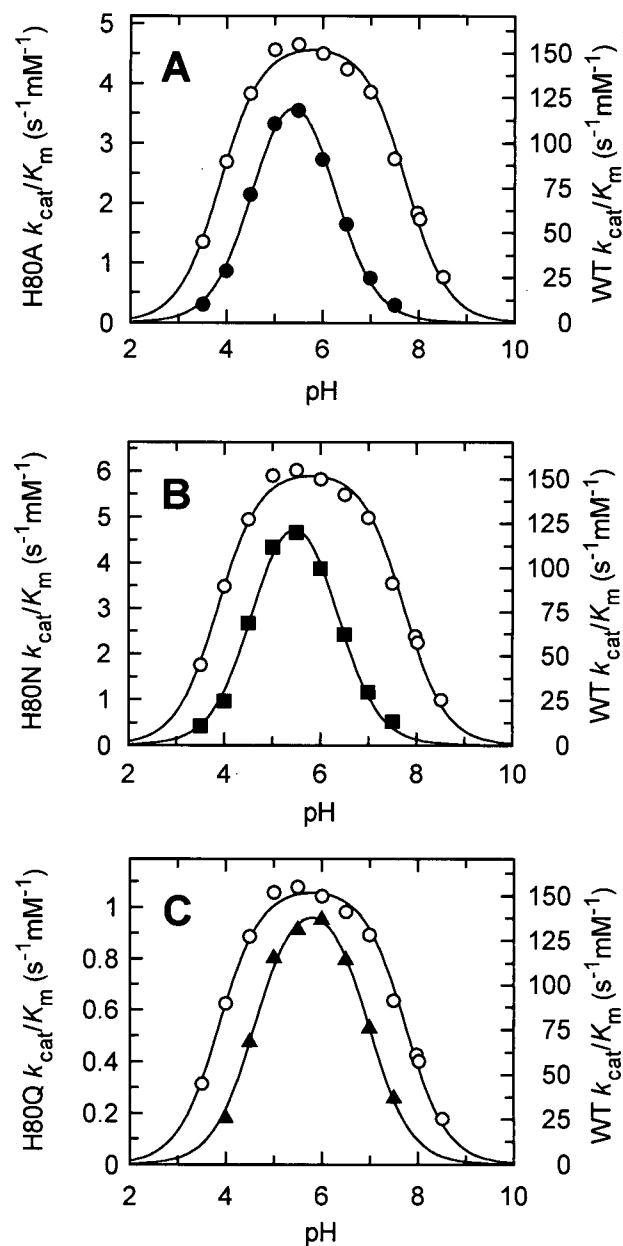


Figure 2.5: pH profiles of wild-type (O) and His80 mutants of Cex. The pH dependence of wild-type Cex was measured using 2,4DNPC where $pK_{a1} = 3.9$ and $pK_{a2} = 7.7$. (A) The H80A (●) mutant enzyme activity was measured using PNPX₂ where $pK_{a1} = 4.6$ and $pK_{a2} = 6.2$. (B) The H80N (■) mutant enzyme activity was measured using PNPX₂ where $pK_{a1} = 4.6$ and $pK_{a2} = 6.3$. (C) The H80Q (▲) mutant enzyme activity was measured using PNPX₂ where $pK_{a1} = 4.6$ and $pK_{a2} = 7.0$

2.2.4.3 Probing the -1 subsite: steady state kinetic analyses of Asn126 and Asn169 mutants

N126A and N169A variants of Cex were previously constructed and purified to apparent homogeneity by Dr. Valerie Notenboom (University of Toronto) to investigate the role of Asn126 and Asn169 residues in the structure and function of Cex. The N169A mutant displays similar kinetic properties to that of native Cex with all substrates tested. The N126A mutant is considerably less active than wild-type Cex (Table 2.8). For both N126A and N169A, deglycosylation is still the rate-determining step in the hydrolysis of the xylobioside substrates. For N126A, the k_{cat} value for the hydrolysis of PNPC decreases sharply, consistent with rate-limiting glycosylation for this substrate.

Table 2.8: Michaelis–Menten parameters for the hydrolysis of aryl glycosides by the *C. fimi* xylanase (Cex) and mutants N126A and N169A.^c

Enzyme	Substrate	Michaelis–Menten Parameters			Rate-Limiting Step (k_{cat}) (DEGLY or GLY)
		k_{cat} (s^{-1})	K_m (mM)	k_{cat}/K_m ($s^{-1} mM^{-1}$)	
Native Cex	2,4DNPC	8.46 ± 0.07	0.068 ± 0.002	124 ± 5	DEGLY
	PNPC	9.24 ± 0.07	0.58 ± 0.01	15.9 ± 0.5	DEGLY
	2,5DNPX ₂	29.9 ± 0.6	0.0145 ± 0.0009	2100 ± 200	DEGLY
	PNPX ₂	32.0 ± 0.4	0.0219 ± 0.0007	1500 ± 70	DEGLY
	ONPX ₂	(i) 38.1 ± 0.8^a	(i) 0.068 ± 0.003^a	(i) 560 ± 40^a	DEGLY
		(ii) 121 ± 8^a	(ii) 1.2 ± 0.1^a	(ii) 100 ± 20^a	
Cex N126A	2,4DNPC	0.49 ± 0.01	0.047 ± 0.002	10.4 ± 0.5	DEGLY
	PNPC	0.052 ± 0.005	12 ± 1	0.0044 ± 0.001	GLY
	2,5DNPX ₂	(i) 1.30 ± 0.01^a	(i) 0.0025 ± 0.0001^a	(i) 520 ± 20^a	DEGLY
		(ii) 2.0 ± 0.1^a	(ii) 0.056 ± 0.008^a	(ii) 36 ± 6^a	
	PNPX ₂	3.5 ± 0.1	7.7 ± 0.2	0.45 ± 0.05	DEGLY
	ONPX ₂	(i) 2.9 ± 0.1^a	(i) 0.39 ± 0.02^a	(i) 7.3 ± 0.5^a	DEGLY
		(ii) 6.9 ± 0.4^a	(ii) 1.6 ± 0.1^a	(ii) 4.4 ± 0.6^a	
Cex N169A	2,4DNPC	2.89 ± 0.03	0.036 ± 0.002	81 ± 4	DEGLY
	PNPC	3.9 ± 0.2	0.59 ± 0.03	6.6 ± 0.5	DEGLY
	2,5DNPX ₂	(i) 19.4 ± 0.3^a	(i) 0.0076 ± 0.0004^a	(i) 2600 ± 200^a	DEGLY
		(ii) 54 ± 4^a	(ii) 0.20 ± 0.03^a	(ii) 270 ± 60^a	
	PNPX ₂	nd ^b	nd ^b	nd ^b	DEGLY
	ONPX ₂	(i) 29 ± 1^a	(i) 0.050 ± 0.006^a	(i) 580 ± 90^a	DEGLY
		(ii) 160 ± 10^a	(ii) 1.2 ± 0.1^a	(ii) 130 ± 20^a	

^a Parameters are for the (i) hydrolysis and (ii) transglycosylation reactions.^b nd indicates that this kinetic parameter was not determined.^c Graphical representation of this data is given *Appendix A*, page 228. Errors were estimated from a non-linear fit by GraFit 4.0 (131).

The pH profiles of the N126A and N169A variants exhibit near wild-type pH profiles (Figure 2.6), although the pH optima are shifted toward a slightly more basic pH. Maximal activity is observed at pH values of 6.4 and 6.1 for the N126A and N169A variants, respectively. The data were fit using equation 2.1 to obtain the pK_a values shown in Table 2.3.

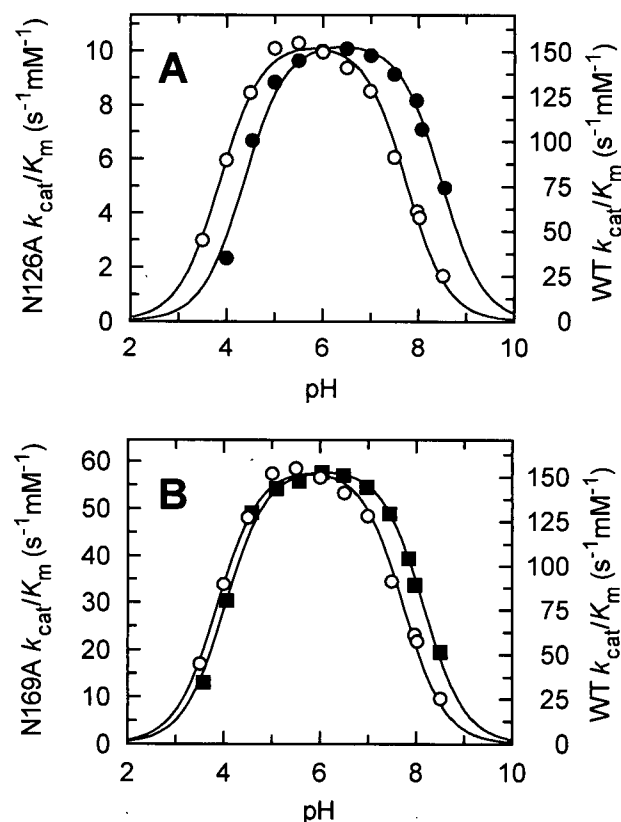


Figure 2.6: pH profiles of wild-type (O) and Asn126 and Asn169 mutants of Cex. The pH dependence of wild-type Cex was measured using 2,4DNPC where $pK_{a1} = 3.9$ and $pK_{a2} = 7.7$. (A) The N126A (●) mutant enzyme activity was measured using 2,4DNPC where $pK_{a1} = 4.4$ and $pK_{a2} = 8.5$. (B) The N169A (■) mutant enzyme activity was measured using 2,4DNPC where $pK_{a1} = 4.0$ and $pK_{a2} = 8.2$.

2.3 Discussion

2.3.1 Effects of mutations on glycosylation and deglycosylation

Changes in the reaction parameters observed for Cex-catalyzed hydrolysis of the cellobiosides and xylobiosides upon mutation of the enzyme can be related to changes in the activation free energy. These values of $\Delta\Delta G^\ddagger$ for each mutation have been calculated

for the glycosylation step (from k_{cat}/K_m values) and for the deglycosylation step k_3 (from k_{cat} values). They are presented in Table 2.9 and summarized in Table 2.10.

As is evident from the values of the rate constants and the free energy changes, the mutations have a significant effect on each of the two steps of Cex catalysis. Further, the magnitude of the effect varies with both the mutation and the step in the reaction.

Table 2.9: Kinetic parameters for the glycosylation and deglycosylation steps of the hydrolysis reaction by variants of Cex.

Enzyme	Substrate	$\frac{k_3^{\text{WT}}}{k_3^{\text{M}}}$	$\frac{(k_{\text{cat}}/K_m)^{\text{WT}}}{(k_{\text{cat}}/K_m)^{\text{M}}}$	$\Delta\Delta G^{\ddagger}_{\text{DEGLY}}$ (kcal mol ⁻¹)	$\Delta\Delta G^{\ddagger}_{\text{GLY}}$ (kcal mol ⁻¹)
Native Cex	2,4DNPC	1	1	0	0
	PNPC	1	1	0	0
	2,5DNPX ₂	1	1	0	0
	PNPX ₂	1	1	0	0
	ONPX ₂	1	1	0	0
Cex E43A	2,4DNPC	1.7 ± 0.02	4.7 ± 0.2	-0.3 ± 0.01	-1.0 ± 0.1
	PNPC	na ^a	160 ± 10	na ^a	-3.1 ± 0.1
	2,5DNPX ₂	1.5 ± 0.02	6.7 ± 0.7	-0.3 ± 0.01	-1.2 ± 0.1
	PNPX ₂	1.2 ± 0.04	290 ± 30	-0.1 ± 0.02	-3.5 ± 0.1
	ONPX ₂	0.8 ± 0.1	19 ± 4	0.1 ± 0.04	-1.8 ± 0.1
Cex N44A	2,4DNPC	0.9 ± 0.01	0.9 ± 0.1	0.1 ± 0.01	0.0 ± 0.1
	PNPC	0.9 ± 0.02	2.7 ± 0.3	0.1 ± 0.01	-0.6 ± 0.1
	2,5DNPX ₂	0.7 ± 0.01	1.8 ± 0.3	0.2 ± 0.01	-0.4 ± 0.1
	PNPX ₂	0.4 ± 0.03	59 ± 10	0.6 ± 0.05	-2.5 ± 0.1
	ONPX ₂	0.5 ± 0.05	4.5 ± 1.1	0.5 ± 0.1	-0.9 ± 0.2
Cex K47A	2,4DNPC	2.0 ± 0.03	77 ± 6	-0.4 ± 0.01	-2.7 ± 0.1
	PNPC	na ^a	23000 ± 5000	na ^a	-6.2 ± 0.1
	2,5DNPX ₂	0.5 ± 0.02	7.0 ± 0.8	0.4 ± 0.02	-1.2 ± 0.1
	PNPX ₂	na ^a	39000 ± 3000	na ^a	-6.5 ± 0.1
	ONPX ₂	na ^a	490 ± 40	na ^a	-3.8 ± 0.1

Enzyme	Substrate	$\frac{k_3^{\text{WT}}}{k_3^{\text{M}}}$	$\frac{(k_{\text{cat}}/K_{\text{m}})^{\text{WT}}}{(k_{\text{cat}}/K_{\text{m}})^{\text{M}}}$	$\Delta\Delta G^\ddagger$ DEGLY (kcal mol ⁻¹)	$\Delta\Delta G^\ddagger$ GLY (kcal mol ⁻¹)
Cex H80A	2,4DNPC	96 ± 4	10 ± 1	-2.8 ± 0.03	-1.4 ± 0.1
	PNPC	na ^a	4300 ± 500	na ^a	-5.2 ± 0.1
	2,5DNPX ₂	120 ± 5	17 ± 3	-2.9 ± 0.03	-1.8 ± 0.1
	PNPX ₂	76 ± 4	2100 ± 200	-2.7 ± 0.03	-4.7 ± 0.1
	ONPX ₂	120 ± 7	66 ± 8	-2.9 ± 0.04	-2.6 ± 0.1
Cex H80N	2,4DNPC	150 ± 10	11 ± 2	-3.1 ± 0.03	-1.5 ± 0.1
	PNPC	230 ± 10	2600 ± 300	-3.4 ± 0.03	-4.9 ± 0.1
	2,5DNPX ₂	250 ± 20	21 ± 3	-3.4 ± 0.05	-1.9 ± 0.1
	PNPX ₂	250 ± 20	1100 ± 300	-3.4 ± 0.05	-4.3 ± 0.1
	ONPX ₂	270 ± 20	64 ± 9	-3.5 ± 0.04	-2.6 ± 0.1
Cex H80Q	2,4DNPC	700 ± 100	20 ± 3	-4.0 ± 0.1	-1.8 ± 0.1
	PNPC	na ^a	7700 ± 1500	na ^a	-5.5 ± 0.1
	2,5DNPX ₂	880 ± 260	38 ± 8	-4.2 ± 0.2	-2.2 ± 0.1
	PNPX ₂	860 ± 230	2400 ± 400	-4.2 ± 0.2	-4.8 ± 0.1
	ONPX ₂	980 ± 250	140 ± 30	-4.2 ± 0.2	-3.1 ± 0.1
Cex N126A	2,4DNPC	17 ± 0.4	12 ± 1	-1.8 ± 0.01	-1.5 ± 0.1
	PNPC	na ^a	3600 ± 800	na ^a	-5.0 ± 0.1
	2,5DNPX ₂	23 ± 0.3	4.0 ± 0.4	-1.9 ± 0.01	-0.8 ± 0.1
	PNPX ₂	9.2 ± 0.3	3200 ± 400	-1.4 ± 0.02	-5.0 ± 0.1
	ONPX ₂	13 ± 1	75 ± 7	-1.6 ± 0.02	-2.7 ± 0.1
Cex N169A	2,4DNPC	2.9 ± 0.1	1.5 ± 0.2	-0.7 ± 0.01	-0.3 ± 0.1
	PNPC	2.4 ± 0.1	2.4 ± 0.3	-0.5 ± 0.03	-0.5 ± 0.1
	2,5DNPX ₂	1.5 ± 0.03	0.8 ± 0.1	-0.3 ± 0.01	0.1 ± 0.1
	PNPX ₂	na ^a	na ^a	na ^a	na ^a
	ONPX ₂	1.3 ± 0.1	1.0 ± 0.2	-0.2 ± 0.02	0.0 ± 0.1

^a na indicates that this parameter is not available.

Table 2.10: Free energy changes at the glycosylation and deglycosylation steps of the hydrolysis reaction by variants of Cex.

Enzyme	$\Delta\Delta G^\ddagger$ DEGLY (kcal mol ⁻¹)		$\Delta\Delta G^\ddagger$ GLY ^b (kcal mol ⁻¹)				
	Cellobiosyl- enzyme	Xylobiosyl- enzyme	2,4DNPC	PNPC	2,5DNPC ₂	PNPC ₂	ONPC ₂
Native Cex	0	0	0	0	0	0	0
Cex E43A	-0.3 ± 0.1	-0.2 ± 0.1	-1.0	-3.1	-1.2	-3.5	-1.8
Cex N44A	0.1 ± 0.1	0.4 ± 0.1	0.0	-0.6	-0.4	-2.5	-0.9
Cex K47A	-0.4 ± 0.1	0.4 ± 0.1	-2.7	-6.2	-1.2	-6.5	-3.8
Cex H80A	-2.8 ± 0.1	-2.9 ± 0.1	-1.4	-5.2	-1.8	-4.7	-2.6
Cex H80N	-3.2 ± 0.1	-3.4 ± 0.1	-1.5	-4.9	-1.9	-4.3	-2.6
Cex H80Q	-4.0 ± 0.2	-4.2 ± 0.2	-1.8	-5.5	-2.2	-4.8	-3.1
Cex N126A	-1.8 ± 0.1	-1.6 ± 0.1	-1.5	-5.0	-0.8	-5.0	-2.7
Cex N169A	-0.6 ± 0.1	-0.3 ± 0.1	-0.3	-0.5	0.1	na ^a	0.0

^a na indicates that this parameter is not available.^b Error estimates for $\Delta\Delta G^\ddagger$ GLY are given in Table 2.9.

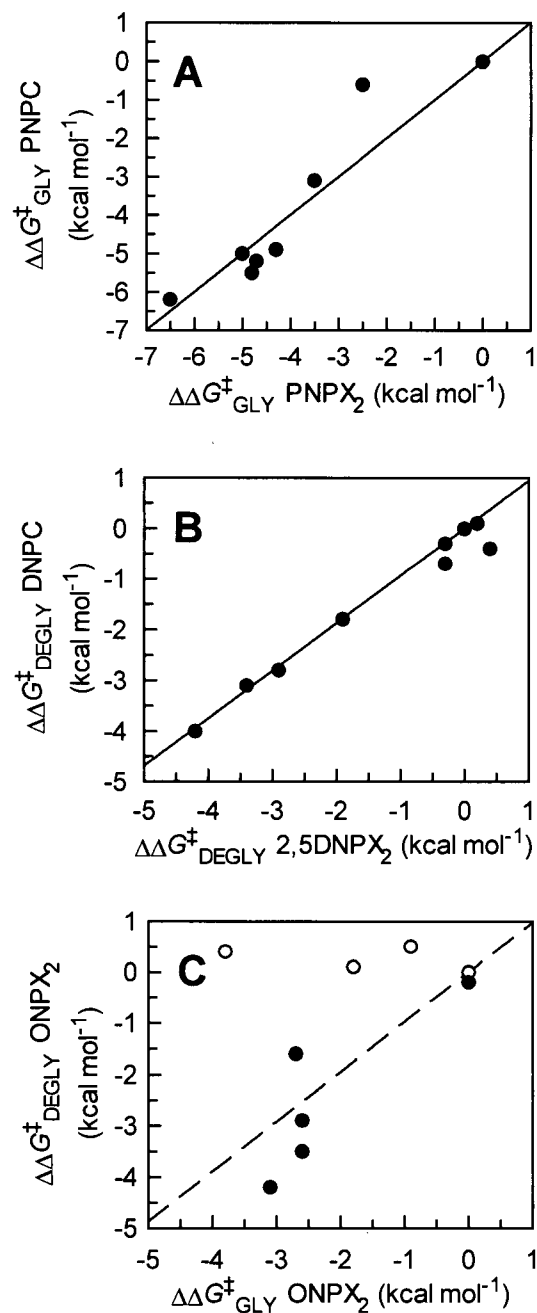


Figure 2.7: (A) Comparison of rate constants for glycosylation of PNPC and PNPX₂ by variants of Cex. A slope of $m = 1.0$ and correlation coefficient of $r = 0.87$ was observed. (B) Comparison of rate constants for deglycosylation of cellobiosyl-enzyme intermediates and xylobiosyl-enzyme intermediates of variants of Cex. A slope of $m = 0.94$ and correlation coefficient of $r = 0.95$ was observed. (C) Comparison of rate constants for glycosylation and deglycosylation reactions for the hydrolysis of ONPX₂ by variants of Cex. Open circles correspond to mutations within the -2 subsite; and closed circles correspond to mutations within the -1 subsite of Cex. A slope of $m = 0.97$ and correlation coefficient of $r = 0.62$ was observed.

The good linear free energy relationship ($r = 0.87$) observed between the rates of *glycosylation* of PNPC and PNPX₂ indicates similarity of transition states for the glycosylation of cellobiosides and xylobiosides by Cex and the series of mutants (Figure 2.7A). An even greater correspondence of transition states for the *deglycosylation* of cellobiosides and xylobiosides, as indicated by the linear free energy relationship ($r = 0.95$), was observed between the rates of deglycosylation of cellobiosides and xylobiosides by Cex and the series of mutants (Figure 2.7B).

Comparison of the rate constants for the *glycosylation* and *deglycosylation* steps should provide insights into the relative amounts of positive charge (oxocarbenium ion character) generated at the two transition states. Such a free energy relationship is presented in Figure 2.7C. This plot has a weak correlation coefficient of $r = 0.62$; the modest correlation coefficient indicating that the mutations affect the two steps of the hydrolysis reaction differently.

2.3.2 A second look at the rate-limiting step in the hydrolysis reaction by Cex and mutants: diffusion-controlled rate constants

Classically, the rate-determining steps in an enzyme-catalyzed reaction have been considered to be those involving chemical conversion of ES to EP complexes or dissociation of products (134). While this situation undoubtedly holds true for many enzymes, there is increasing evidence that for some enzymes the encounter of enzyme and substrate is the rate-determining step, and these enzymes are said to be at least partly diffusion-controlled. Albery and Knowles (135) have remarked that such enzymes have reached the end of their evolutionary kinetic refinement, since further improvements in catalytic efficiency would not be manifested in enhanced rates of reaction. The relevant

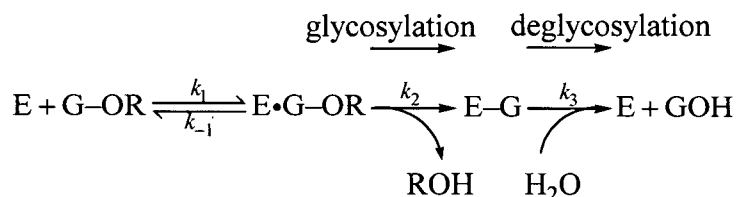
kinetic parameter is the second-order rate constant k_{cat}/K_m , which cannot exceed a diffusion-controlled limiting value that has been estimated to be on the order of $10^8 - 10^{10} \text{ s}^{-1} \text{ M}^{-1}$ for a number of enzyme-substrate complexes (135). The exact value depends in part on the possible contribution of electrostatic forces in the encounter of substrate and enzyme. There is, however, no clear lower limit for k_{cat}/K_m below which an enzyme reaction can no longer be considered to be diffusion controlled, for a number of reasons. For instance, steric constraints can arise from the location of active sites in deep grooves on an enzyme's surface. In addition, catalytically incompetent conformational states of an enzyme can coexist in equilibrium with the native state. The effect of such constraints is a reduction in the diffusion-controlled rate constant. Frequently, the observed association rate constants for enzyme-substrate interactions tend to fall in the range of $10^6 - 10^8 \text{ s}^{-1} \text{ M}^{-1}$ (136).

The rate constants for glycosidases acting on their natural substrates are typically several orders of magnitude below the diffusion-controlled values. Cex, however, is a broad specificity enzyme that hydrolyzes a number of synthetic substrates. For example, the rate constants for the formation of the xylobiosyl-enzyme of Cex, representing the first irreversible step in the reaction, can exceed $2 \times 10^6 \text{ s}^{-1} \text{ M}^{-1}$ (note that k_{cat}/K_m values presented in tables are in units of $\text{s}^{-1} \text{ mM}^{-1}$). This value approaches the diffusion-controlled limiting value and consequently the encounter of enzyme and substrate may be the rate-determining step for this reaction when reactive leaving groups are present.

The observed rate constant for the formation of product is given by

$$k_a = \frac{k_1 k_2}{k_{-1} + k_2} \quad (2.6)$$

where the rate constants k_1 and k_{-1} represent the rate constants for association and dissociation. The well-established kinetic mechanism for Cex-catalyzed reactions is given below.



The deglycosylation step, k_3 , is overall rate determining for synthetic cellobioside and xylobioside substrates with good to moderate leaving groups, while the glycosylation process, k_2 , is limiting for synthetic substrates with poor leaving groups and the natural substrates. The first irreversible step in both cases is glycosylation of the enzyme. Where Michaelis complex formation is at true equilibrium ($k_{-1} \gg k_2$), equation 2.6 reduces to

$$k_a = \frac{k_1 k_2}{k_{-1}} = \frac{k_{\text{cat}}}{K_m} \quad (2.7)$$

Conversely, covalent capture of the glycosyl moiety of the substrate by the enzyme with a rate constant greater than that for dissociation ($k_2 \gg k_{-1}$) leads to

$$\frac{k_{\text{cat}}}{K_m} = k_a \approx k_1 \quad (2.8)$$

Evidence for rate-limiting association was observed for *Agrobacterium* sp. β -glucosidase (21). A biphasic relationship was obtained from the plot of the logarithm of k_{cat}/K_m against the phenol $\text{p}K_a$ of a series of aryl glucosides. It was reasoned that a biphasic relationship in this case could not be due to a change to rate-limiting

deglycosylation at higher reactivities and was most likely due to association of enzyme and substrate becoming rate-limiting with the more reactive substrates. The second-order rate constants ($k_{\text{cat}}/K_{\text{m}}$) for these substrates fell within the range of $2 \times 10^6 - 3 \times 10^7 \text{ s}^{-1} \text{ M}^{-1}$.

It is possible that the rates of glycosylation of Cex and certain variants of Cex by highly reactive substrates approach the diffusion-controlled limits. For instance, the second-order rate constants ($k_{\text{cat}}/K_{\text{m}}$) for 2,5DNPX₂ fall well within the range for which such association has been shown to be rate limiting in other enzyme systems, including *Agrobacterium* sp. β -glucosidase (21) and the almond β -glucosidase (137).

2.3.3 Importance of -2 subsite amino acids Glu43, Asn44, and Lys47

2.3.3.1 Role of Glu43

Data obtained for the aryl β -cellobiosides suggest a change in the rate-limiting step from deglycosylation to glycosylation for the PNPC substrate given the 4-fold decrease in k_{cat} obtained for the substrate relative to 2,4DNPC. Although the activity of the E43A mutant is similar toward 2,4DNPC compared to wild-type Cex, the mutant is significantly less active against PNPC than the unmodified enzyme. The protonation of the glycosidic oxygen may be affected by the E43A mutation. The E43A modification may affect the way cellobiose sits in the active site such that the glycosidic oxygen is not close enough to Glu127 to be protonated. White *et al.* (32) showed that when 2-deoxy-2-fluoro- β -cellobiose was covalently linked to the nucleophile of Cex, Glu43 forms a hydrogen bond with the C-2 hydroxyl of the distal saccharide unit. Consequently, a disruption of this bond in E43A could change the position of cellobioside substrates

within the active site, such that the glycosidic oxygen is no longer in close proximity to Glu127. In contrast, in the glycosylated enzyme the covalent linkage between the nucleophile Glu233 and the anomeric carbon of cellobiose positions the anomeric carbon in close proximity to the water molecule that is deprotonated by Glu127. Thus, the k_{cat} for E43A against 2,4DNPC is similar to native Cex, as protonation of the leaving group is not essential for deglycosylation to occur.

The mutation appears to have a slightly more detrimental effect on the binding of xylobiosides than cellobioside substrates. One possible explanation may be that the mutation generates more room for the accommodation of the C-5' hydroxymethyl moiety at the -2 subsite.

2.3.3.2 Role of Asn44

Crystal studies have shown that Asn44 in Cex forms a hydrogen bond with the hydroxyl at C-3' of the distal xylose of the covalently bound 2-deoxy-2-fluoroxxylobiosyl-enzyme complex (76) and this suggests that it plays an important role in active-site binding (Figure 2.1).

The N44A mutant of Cex exhibited similar properties to the native enzyme. The first-order rate for deglycosylation of the covalent cellobiosyl-enzyme intermediate was 9 s^{-1} for both the N44A mutant and native Cex. Therefore, the mutation presumably affects the transition-state interactions at the transition state for the deglycosylation step to the same extent as the ground-state covalent intermediate complex. Furthermore, $k_{\text{cat}}/K_{\text{m}}$ values for both aryl β -cellobioside substrates remain comparable to those obtained for the wild-type enzyme. Similarly, the rate-determining step for the hydrolysis reaction for the aryl β -xylobioside substrates was deglycosylation. On average, however, the k_{cat}

value increased by 2-fold relative to the native enzyme. The mutation therefore apparently destabilizes ground-state interactions to a greater extent than transition-state interactions for the second step of the hydrolysis reaction. The second-order rate constant k_{cat}/K_m was affected to a greater degree, with at least a 70-fold decrease observed for the PNPX₂ substrate, along with an increased K_m compared with native Cex. Overall, this asparagine residue plays a minimal role in sugar binding at the -2 subsite, and possibly the -3 subsite given that Asn44 is positioned in the distal region of the -2 site. A similar result was obtained against the aryl β -cellobiosides by the equivalent alanine mutant of Asn44 from *C. japonicus* Xyn10A (133).

2.3.3.3 Role of Lys47

The data suggest that Lys47 plays an important role in positioning the substrate into the active site. The K47A mutant retains k_{cat} values that are similar to native Cex against 2,4DNPC and 2,5DNPX₂, although K_m values increase suggesting that the mutation is influencing the glycosylation step. White *et al.* (32) showed that Lys47 in Cex formed hydrogen bonds with both the ring oxygen and C-3 hydroxyl of the distal and proximal glucose molecules of 2-deoxy-2-fluoro- β -cellobiose, respectively, in the glycosyl-enzyme complex. Removal of these hydrogen bonds could significantly alter the position of the substrate at the active site such that the nucleophile, Glu233, is not in close proximity with the anomeric carbon of the proximal sugar at the -1 subsite. Lys47 promotes proper substrate binding by hydrogen-bond donation, and may influence the orientation of the substrate to effect catalysis. However, it is also possible that K47A is having an indirect effect by altering the environment of aromatic residues at the active site of the enzyme. A potential candidate is Trp84, which is only ~ 4 Å from Lys47, and

thus the removal of the charged nitrogen in the Lys47 side chain could enhance the hydrophobic environment of Trp84. This change could alter either the binding of the substrate at the active site or possibly the ionization state of the nucleophile.

2.3.3.4 Role of His80

The active site of the xylanase Cex from *Cellulomonas fimi* contains two histidine residues (His80 and His205) that are almost completely conserved in family 10 glycanases. The structural analysis of the enzyme shows that His80 and His205 are part of an important hydrogen-bond network near the two catalytic residues (Glu127 and Glu233). The three-dimensional structure of Cex also suggests the involvement of His80 in substrate recognition, and shows that His80 is hydrogen bonded to 3-OH group of the proximal saccharide unit and the highly conserved residue Asp123 (Figure 2.1). Co-crystal structures of xylanases from family 10 with xylopentaose (122) and with its 2-fluoro-2-deoxy- β -cellobiosyl intermediate have shown that the equivalent of His80 is hydrogen bonded with the C-3 hydroxyl of the saccharide moiety located in the -1 subsite in either case. The family 10 *S. lividans* Xyn10A contains an equivalent residue, His81 (N ϵ 2) that is hydrogen bonded to Glu236 (O ϵ 1) through a water molecule and is hydrogen bonded through its N δ 1 atom to Asp124 (O δ 2) (138). The corresponding histidine residues in other xylanases of family 10 have also been shown to be involved in maintaining the ionization state of the nucleophile (122, 124).

To study the role of His80 in the structure and function of Cex, three mutations were made at this position. Since hydrogen bonding is involved, His80 was replaced with amino acids that have side chains capable of hydrogen bonding: asparagine (H80N) and glutamine (H80Q). The effects on the catalytic properties of the enzyme could be

due to incorrect positioning of the nucleophile Glu233 in the catalytic site. Another explanation could be that an adequate stabilization of the catalytic intermediate is prevented by reduced interactions between His80 and the proximal sugar group.

The three mutations at position His80 also significantly affect the pH profile of the enzyme (Figure 2.5). For the specific activity profiles, the effects of the three mutations studied affect both the acidic and basic sides, increasing the apparent pK_a by 0.7 pH units toward a more basic pH for the nucleophilic glutamic acid residue and 0.7–1.5 pH units toward a more acid pH for the acid/base catalytic residue (Table 2.3). Therefore, in addition to its role in stabilizing the catalytic intermediate, His80 appears to be a very important residue in the hydrogen-bond network of the active site, and mutation of this residue modifies the interactions necessary to maintain the ionization state of the two catalytic glutamic acid residues of Cex.

In conclusion, the results presented in this study show the importance of His80 for the structure and function of Cex. These residues are involved in a network of hydrogen bonds that are responsible for maintaining the ionization state of the two catalytic residues.

2.3.4 Amino acids that influence the catalytic residues

2.3.4.1 Role of Asn126

An insight into the role of Asn126 can be obtained from the study of White *et al.* (32), who suggested that this residue forms a hydrogen bond with the 2-OH group of the proximal glucose moiety of 2-deoxy-2-fluorocellobiose located at the -1 subsite. Modification of Asn126 to alanine causes a significant decrease in the catalytic activity of

Cex against all the substrates tested. The rate-limiting step of hydrolysis of PNPC by N126A is glycosylation, whereas in the native enzyme deglycosylation is the limiting step in the cleavage of PNPC. These data suggest that Cex N126A is affecting both the efficient protonation of the substrate by Glu127 and the capacity of this residue to mediate subsequent general base catalysis. It is possible that this interaction is important in positioning the glycosidic oxygen in close proximity to Glu127. The N126A mutation may cause an increase in the exposure of certain aromatic residues to a hydrophilic environment, and this subtle modification to the active site could alter the capacity of Glu127 to abstract protons from water. Trp84 is only ~ 3 Å from Asn126, and the removal of the amide component of the Asn126 side chain could increase the hydrophilic environment of the tryptophan residue. Clearly, this is having a greater effect on the glycosylation step of PNPC cleavage, as PNP constitutes a moderate leaving group whereas protonation of 2,4DNP is not required for Cex to cleave 2,4DNPC; hence, the decrease in the rate at which this substrate is glycosylated results in a similar decrease in k_{cat} to PNPC but also an associated increase in K_m .

2.3.4.2 Role of Asn169

Against the aryl β -glycosides, N169A displayed similar k_{cat} and k_{cat}/K_m values as the native enzyme. This suggests that, although highly conserved, Asn169 does not play a pivotal role in the binding of cellobiose or xylobiose in the active site of the enzyme. This is in contrast to the findings of White *et al.* (32) who suggested that the residue forms hydrogen bonds with Asn126 and Glu233 in the structure of the covalently bound 2-deoxy-2-fluoro-cellobiosyl-enzyme intermediate.

The pH profile for the N169A mutant enzyme exhibits a typical bell-shape, providing pK_a values of 4.0 and 8.2. The mutation does not alter the pH dependence of the nucleophilic residue greatly. However, this residue does influence the pK_a value of the acid/base catalytic residue.

2.3.5 Analyses of the pH profiles for Cex variants

The simple pH dependence of *C. fimi* xylanase arises from the critical roles played by two ionizable groups, the nucleophile (Glu233, $pK_a \sim 3.9$) and the acid/base catalyst (Glu127, $pK_a \sim 7.7$), with numerous other ionizable and non-ionizable groups modulating these pK_a 's. The effects of these other groups are brought out in the mutant enzymes where a critical group is removed or perturbed in its properties. In general, residues that contribute positive charges and hydrogen bonds serve to lower the pK_a values of Glu233 and Glu127. In contrast, neighbouring carboxyl groups can either lower or raise the pK_a values of the catalytic glutamic acids depending upon the electrostatic linkage of the ionization constants of the residues involved in the interaction. The pH optimum was shifted from -0.9 to $+0.6$ units by mutating residues within the active site.

Some caution must be applied in interpreting the pH dependence of Michaelis–Menten parameters and assignments of pK_a values (139). Nevertheless, comparison of the effects of pH on wild-type and mutant glycanases is mechanistically relevant and worthy of detailed discussion.

The activity profile of Cex E43A follows apparent pK_a values of 3.7 and 6.9. The Cex E43A mutant is one where a potentially negatively charged residue was removed

from the active site. This resulted in a shift of the pH optimum of E43A from 5.8 to a more acidic value of 5.3. The most notable decrease in the apparent pK_a value was that of the basic limb, corresponding to the ionization of Glu127, by 0.8 pH units from 7.7 to 6.9. This is expected as a negative charge on Glu43 electrostatically destabilizes the conjugate base forms of the catalytic Glu residues, thereby serving to increase their pK_a values relative to that of a neutral residue. This mutation has a greater effect upon the pK_a of Glu127 compared to Glu233, despite Glu43 being closer to Glu233 by 6.7 Å in the crystalline wild-type enzyme.

In the case of Cex N44A, replacement of an Ala for Asn resulted in minimal changes in the pK_a values controlling both limbs of its activity profile ($pK_{a1} = 3.9$ and $pK_{a2} = 8.0$). Removal of hydrogen-bonding residues generally serves to raise the pK_a values of catalytic glutamic acids, as observed.

Removal of a positive charge contributed by Lys47 resulted in a *decrease* in the pH optimum of the enzyme from 5.8 to 4.9. The reduced pK_a observed for Glu127 is *unexpected*, as removal of the positively charged Lys47 should lead to the opposite effect. In general, a positive charge serves to stabilize the conjugate base forms of both catalytic Glu residues, thereby serving to lower their pK_a values relative to neutral residues. There is no obvious explanation for the precise nature by which the mutation leads to a decrease in the pK_a value of Glu127 by a substantial 1.7 units, the largest observed decrease among the series of active-site residue mutants studied. It is possible that the K47A mutation results in localized structural perturbations. The observed shift in the pH optimum of the enzyme likely reflects delicate alterations in the complex hydrogen-bonding network within the active site of Cex.

His80 is positioned approximately 4 Å from Glu233 and 7 Å from Glu127 in the wild-type crystal structure and does not make direct contacts with either catalytic residue. In the structure of the 2F-xylobiosyl-Cex complex (76), however, the Nε2 atom of His80 is observed to make a direct contact with the 3-OH group of the proximal xylose saccharide and a highly conserved interaction is observed between His80 Nδ1 with the Oδ2 atom of Asp123. Mutation of His80 influences the pK_a values of both catalytic residues. Mutation of His80 resulted in an increase in the pK_a of Glu233 from 3.9 to 4.6 for all variants of His80. This is as expected, as the hydrogen bonding properties of His80 stabilize the conjugate base form of Glu233, thereby serving to lower its pK_a value relative to that observed with a neutral residue at this position. Consequently, the increase in the pK_a value of the nucleophile should decrease the pK_a value of the acid/base catalyst due to electrostatic stabilization.

The side chain of Asn126 is positioned such that it can donate a strong hydrogen bond to Asn169, which in turn is involved in a hydrogen-bonding interaction with the carboxyl group of the nucleophile Glu233 (Figure 2.1). When this interaction is removed through mutation of Asn126 to Ala, the pK_a of Glu233 rises by 0.5 units to 4.4. The pH optimum of Cex shifts 0.6 units from 5.8 to 6.4, primarily due to elevation of the apparent pK_a value of Glu127 from 7.7 to 8.5. Asn126 may influence the pK_a of Glu127 since the Nδ2 atom of this asparagine is 4 Å away from Glu127 Oε2.

The Nδ2 atom of Asn169 is involved in a hydrogen-bonding interaction with the Oε2 atom of the carboxyl group of the nucleophile Glu233 (Figure 2.1). When this interaction is removed through mutation of Asn169 to Ala, the pK_a of Glu233 rises by 0.1 units to 4.0. Unexpectedly, the pK_a of Glu127 increases by 0.5 units to a value of 8.2. As

seen for other Cex mutants, the pK_a value Glu127 is more sensitive to changes in the active site than is the pK_a of Glu233. It is clear that the hydrogen bond between Asn169 and Glu233 can serve to lower the pK_a of this nucleophilic residue. However, the mode by which Asn169 lowers the pK_a of Glu127 is less obvious since the N δ 2 atom of this asparagine is >6 Å away from either Glu127 O ϵ 2 or O ϵ 1. The position of the side chain of Asn169 may change with pH such that it can form a hydrogen bond with Glu127. As mentioned previously, however, the ionizations of Glu233 and Glu127 are electrostatically coupled, and via this linkage the changes in the pK_a of one partner can influence the ionization of the other.

In summary, the active site substitutions altered the pH-activity profile of Cex, in terms of both pH optimum and/or apparent pK_a values of the acidic and basic limbs. Any modifications to the local and global environments of Glu233 and Glu127 can result in changes in the pH optima of the enzyme.

2.3.6 Activity of family 10 enzymes

Data presented indicate that binding of substrates to the -2 subsite is important for efficient hydrolysis by Cex of xylobioside and cellobioside substrates. Data presented in various reports (133, 140, 141) show that there are significant differences in the capacity of cellobiose to bind to the active sites of family 10 xylanases. Although the k_{cat} values for hydrolysis of both PNPC and 2,4DNPC by *Cellvibrio japonicus* Xyn10A are similar to those of Cex, the K_m values of Xyn10A were 2 to 3 orders of magnitude higher for the respective substrates, compared to those of *Cellulomonas fimi* xylanase. Furthermore, the rate-limiting steps for the hydrolysis of these two aryl β -cellobiosides

by *CjXyn10A* and *Cex* are glycosylation and deglycosylation, respectively (105, 133). Surprisingly, although the k_{cat} values for aryl β -cellobioside hydrolysis are similar for *Cex* and *Xyn10A*, the *Cellvibrio* enzyme displays virtually no activity against polymeric cellulose substrates, in contrast to *Cex*. The difference in activity against cellulose is likely a reflection of the capacity of the + subsites of *CjXyn10A* and *Cex* to accommodate glucose residues.

The two family 10 xylanases, *C. japonicus* *Xyn10A* and *C. fimi* xylanase *Cex*, hydrolyze aryl β -xylosides and xylobiosides at very different rates also, with $k_{\text{cat}}/K_{\text{m}}$ values for *Cex* being 30–200 times higher than those of *CjXyn10A* (22, 76, 133). Nonetheless, against the natural substrate xylan, the two enzymes have similar activities. In contrast, *Cex* is 20-fold more active against xylo-tetraose X_4 , 10-fold more active against xylo-pentaose X_5 , and 3-fold more active against xylo-triose X_3 than *CjXyn10A* with respect to $k_{\text{cat}}/K_{\text{m}}$ (121). The 30-fold difference between the activities of the two enzymes against 4-nitrophenyl β -xylobioside, compared to the 3-fold difference for X_3 , has been suggested to result from the tighter binding of aryl moieties in the +1 subsite in the substrate binding cleft of *Cex* versus *CjXyn10A*. The efficient formation of a productive complex to the *C. fimi* xylanase results from the tighter binding of the substituted aromatic ring. A fast glycosylation step, with deglycosylation being the rate-determining step in the reaction, leads to a low K_{m} value for catalysis and the accumulation of the glycosyl–enzyme intermediate. In contrast, the glycosyl–enzyme intermediate does not accumulate in *CjXyn10A*, hence the high K_{m} value obtained due to glycosylation being the rate-limiting step in the reaction presumably as a result of the poor binding of the aryl moiety in the substrate binding cleft (121).

The rate-limiting step for hydrolysis of X_3 by both *CjXyn10A* and *Cex* was found to be the glycosylation step (121). However, when the reducing end xylosyl residue of X_3 was substituted by a 4-nitrophenyl group (PNPX₂), the k_{cat}/K_m values increased 10,000- and 1000-fold, respectively, for *CjXyn10A* and *Cex* (121). These significant increases in catalytic efficiency are probably a reflection of the capacity of the substituted phenolic rings to function as excellent leaving groups. Hence, there is little requirement for the glycosidic oxygen to be protonated during the glycosylation step.

2.4 Conclusions

Site-directed mutagenesis studies provided insights into the roles of several residues located in the -2 and -1 subsites of the xylanase from *C. fimi*. The specific activity of these mutant enzymes is affected to various degrees, revealing the importance of these residues for the catalytic function of *Cex*. Furthermore, the pK_a values of the two catalytic residues are affected, demonstrating a role for these highly conserved residues in the hydrogen bond network responsible for maintaining the ionization state of the two catalytic residues.

CHAPTER 3

AN ASSESSMENT OF THE BINDING ENERGY CONTRIBUTION OF HYDROGEN BONDS AT THE TRANSITION STATE USING DEOXYGENATED SUBSTRATES AND SITE-DIRECTED MUTAGENESIS*

* A version of this chapter has been published.

Wicki, J., Schloegl, J., Tarling, C. A., and Withers, S. G. (2007) Recruitment of both uniform and differential binding energy in enzymatic catalysis: xylanases from families 10 and 11. *Biochemistry*, 46: 6996-7005.

3 An Assessment of the Binding Energy Contribution of Hydrogen Bonds at the Transition State Using Deoxygenated Substrates and Site-Directed Mutagenesis

3.1 Introduction

The extraordinary selectivities exhibited by most enzymes for their substrates are necessarily derived from the interactions between the two partners, especially as they are expressed at the transition state. Of these, hydrophobic interactions are thought to contribute the major driving force for association, while hydrogen-bonding interactions and salt-bridge formation are thought to primarily provide the specificity (142). Interactions within a protein–ligand complex play an essential role in enzymatic catalysis and in cell-cell recognition (29, 143–148). Hydrogen-bonding interactions are thought to play a particularly critical role in the recognition of completely buried monosaccharides that contain a large number of hydroxyl groups. Many such protein–ligand interactions have been observed qualitatively from X-ray crystallographic studies of protein–ligand complexes (143, 148–150), while quantification of the contributions of specific hydrogen bonds to a protein–ligand interaction has been obtained through a number of studies using two main approaches (58, 151, 152).

One approach to providing an estimate of the contributions of various hydrogen bonds to binding is by using mutant enzymes in which single residues involved in specific interactions have been modified. In an elegant study by Fersht on a protein–ligand complex of known three-dimensional structure, the side chains involved in hydrogen-bonding interactions with the substrate were systematically removed through site-specific mutagenesis and the affinity of the ligand for each mutant was then

measured (151). More recently, this approach has been applied extensively to the study of glucoamylase (153, 154) and *Bacillus* 1,3-1,4- β -D-glucan 4-glucanohydrolases (155, 156).

Alternatively, another approach to providing an estimate of the magnitude and polarity of a hydrogen bond involves the use of modified substrates in which the individual hydroxyl groups on the sugar moiety have been replaced by hydrogen or by fluorine. This approach has been applied to the study of β -glucosidase from *Aspergillus wentii* (58), glycogen phosphorylase (157, 158), phosphoglucomutase (159), *Escherichia coli* β -galactosidase (27), *Agrobacterium* sp. β -glucosidase (28) and trehalose phosphorylase (160). The replacement of a sugar hydroxyl by hydrogen will remove all hydrogen-bonding interactions at that position, whereas substitution by fluorine will arguably allow hydrogen bonds in which fluorine acts as a hydrogen-bond (proton) acceptor, but not as a donor (Figure 3.1).



Figure 3.1: The hydroxyl can act as a hydrogen-bond donor or acceptor, whereas fluorine can only act as a hydrogen-bond acceptor.

Analysis of changes in binding interactions (K_s , K_i , or in some cases K_m) allows estimation of the contributions to ground-state interactions, whereas analysis of changes in rates (k_{cat}/K_m or k_{cat}) provides insights into transition-state interactions. For instance,

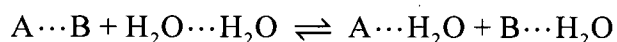
decreases in rate (k_{cat}/K_m) observed for a deoxy sugar might be attributed to the loss of a hydrogen-bonding interaction at that position and allow an estimation of the magnitude of the binding contribution at the transition state. Furthermore, the *type* of binding energy change, whether “differential” or “uniform” in the parlance of Alberty and Knowles (135), may be deduced from examination of kinetic parameters.

An indication of the polarity of a hydrogen bond may be obtained when the rate of hydrolysis for a deoxyfluoro substrate is greater than that of the corresponding deoxy substrate. Thus, if the enzyme acts as the hydrogen-bond donor, the deoxyfluoro substrate may be able to retain some of the binding energy that is lost to the corresponding deoxy sugar substrate, resulting in a higher reaction rate. However, no simple deduction as to the polarity of the interaction at a particular position may be made when a lower rate of hydrolysis is observed for a deoxyfluoro compound versus the corresponding deoxy sugar.

3.1.1 Hydrogen-bonding energetics in water

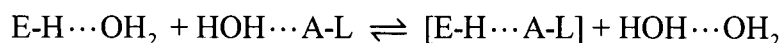
Binding effects arise from the non-covalent interactions that develop between the enzyme and substrate at the transition state for the step in question, thereby stabilizing the transition state and providing catalysis. Hydrogen bonding between ligands and proteins in aqueous solution is a multifaceted process due to the competition of water for the hydrogen-bonding sites (161, 162). The very strong interaction of water with ions, dipoles, and hydrogen-bond acceptors or donors causes a reduction in, or disappearance, of most of the forces that would otherwise cause a strong interaction in a nonpolar solvent or vacuum. When two molecules A and B bind to one another, water has to be

displaced. The net change in energy is the observed binding energy, which measures the affinity of the two molecules for one another in competition with water. The difference between the energy of interaction of two molecules A and B with each other and the energy of interaction with water is small.



In fact, it is the strong energy of interaction of the water molecules with each other, rather than of a direct interaction of solute molecules with each other, that is responsible for the most important non-covalent intermolecular forces in water. It is difficult to pull water molecules apart in order to insert a weakly interacting molecule into the solution because of the large number of hydrogen bonds per unit volume of water. Relatively nonpolar molecules that have a small capacity to form bonds in a vacuum and cannot interact strongly with water are forced out of an aqueous solution and are therefore compelled to interact with each other.

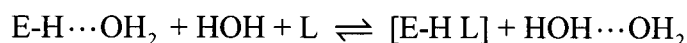
In this study, an overview of the hydrogen-bonding energetics in aqueous solution between enzyme and ligand, and of the ability of fluorine to hydrogen bond is required. A full hydrogen-bond inventory must be performed, as formulated previously by Jencks and Hine (161, 163), in order to understand the role of hydrogen bonding in the energetics of such interactions. A hydrogen-bonding interaction at a single site between a ligand and enzyme in an aqueous medium can be expressed as follows,



where a residue of enzyme **E** acts as a hydrogen-bond donor **H** which pairs with the acceptor **A** of the ligand **L** in the complex. The hydrogen-bonding roles of the enzyme

and the ligand could also be reversed. Although hydrogen-bond geometries may be quite different, both the numbers and types of hydrogen bonds are conserved in the process since there are two hydrogen bonds on each side. Binding energy therefore results partially from enthalpic differences due to different hydrogen-bond geometries but primarily from the increase in entropy associated with the release of water from the active site of the enzyme and the ligand into bulk water.

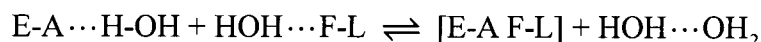
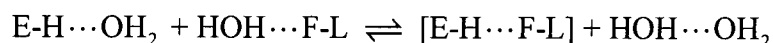
A full loss of the energy of the hydrogen bond does not necessarily result from removal of a hydrogen-bonding group from the ligand **L** since in this case no hydrogen bond would exist between the substrate analogue and water before binding as shown below.



Thus, the energetic difference between the two systems described above will not equal the full hydrogen-bond energy, but rather the difference in strengths of hydrogen bonds formed with the protein and the water. This difference may be rather significant when comparing a hydrogen bond in an evolved enzyme–ligand complex with that formed between a relatively mobile water molecule and a protein residue.

In this study the two cases to be considered involve deoxygenation (OH to H) and deoxyfluorination (OH to F). The former is equivalent to the types of mutations performed by Fersht (151) and will result in complete removal of the hydrogen bond and a space in the complex that might accommodate a water molecule but is likely too small. The substitution of OH to F results in very little size difference, and thereby hampers coincident binding of water. The interaction is far more complex, since the fluorine

could be involved in a hydrogen bond but only as a hydrogen-bond acceptor (*vide infra*). Therefore, one may obtain two situations for the fluoro sugars as shown below.



In the first case the enzyme acts as the hydrogen-bond donor at a particular position and fluorine acts as the hydrogen-bond acceptor, albeit a weak one. In the second case the enzyme accepts a hydrogen bond at a particular position and thus cannot interact favourably with the fluorine. A considerable decrease in affinity should result in this case since there is net loss of a hydrogen bond as the fluorine can still hydrogen bond as acceptor with the water. Thus, the deoxy sugar might have greater affinity than the fluoro sugar in such a situation. The ability of fluorine to act as a hydrogen-bond acceptor has been investigated in a number of studies discussed below.

3.1.2 Hydrogen bonding to fluorine

Fluorine has been documented to be involved in very strong hydrogen bonds. Fluorine is a stronger acceptor than the other halogens (164), but not as strong as oxygens and nitrogens (165). However, in their ionic and metal-bonded forms all the halogens act as considerable proton acceptors. In fact, the strongest known hydrogen bond is that in the $(\text{F}-\text{H}-\text{F})^-$ ion (166). In a large scale analysis by Howard and co-workers (167) of the X-ray data stored in the Cambridge Structural Database (CSD), short contacts of fluorine atoms to acidic hydrogens were discovered and reinforced by theoretical calculations from which half of the binding energy of a hydrogen bond to oxygen was

assigned to fluorine. Furthermore, a survey conducted by Shimoni and Glusker (168) in the CSD revealed that acidic hydrogens prefer to bind to stronger acceptors such as oxygens and nitrogens compared to fluorine atoms. Brammer and co-workers (169) examined the CSD and confirmed the weakness of fluorine hydrogen-bonding interactions, revealing shorter fluorine...donor contacts for $C(sp^3)-F$ structures compared to $C(sp^2)-F$, as previously observed by Howard and co-workers (167). Increased acceptor ability of aliphatic over aryl-bonded fluorine atoms was observed; presumably because the fluorine lone-pairs are in conjugation with the π -orbital system and consequently less able to participate in hydrogen bonding. An exhaustive inspection of the Protein Data Bank (PDB) archive by Carosati and co-workers (170) was carried out to analyze those protein-ligand complexes with fluorines as acceptors and protein NH and OH groups as donors. Statistics were applied to all the PDB complexes whose protein structures had co-crystallized fluorine-containing ligands, and the effect of fluorine hydrogen bonds on the protein-ligand binding was estimated using the program GRID. After protein-ligand complexes were identified as containing geometrically possible hydrogen bonds, the contacts were investigated in detail by measuring the distance $F\cdots D$ and the angle at the donor. Overall, fluorine atoms of ligands were observed in hydrogen-bonding interactions in 18% of the complexes with a fluorine-containing ligand (170).

3.1.3 Electronic effects

Electronic effects have their origin in the considerable differences in electronegativities of these substituents (H, OH, F), and the different effects these will

therefore have on the stability of a positively charged, oxocarbenium ion-like transition state. The magnitudes of these effects will be dependent upon the distance of the substituent from the anomeric center, and will not be a major contributing factor beyond the first sugar ring. The greatest electronic effects are those at the 2-position. For instance, replacement of a hydroxyl group at the 2-position with a hydrogen has been shown to favourably stabilize the oxocarbenium ion-like transition state for glycoside hydrolysis, resulting in substantial rate accelerations. The substitution of fluorine at the 2-position, on the other hand, destabilizes the oxocarbenium transition state. Consequently, 2-deoxyfluoroglycosides, along with the 5-fluoroglycosides, have been successfully used as inactivators to characterize the covalent intermediate in the double-displacement mechanism as discussed previously (31, 41).

Electronic effects were studied by Withers and co-workers (171) for a reaction that proceeds via an oxocarbenium ion-like transition state; that is, the acid-catalyzed hydrolysis of a series of deoxyfluoro-D-glucopyranosyl phosphates. Significant rate decreases were observed from fluorine substitution, with the greatest effect being upon the substitution of the 2-hydroxyl. Corresponding rate increases for a series of deoxy-D-glucopyranosyl phosphates were observed as expected (172). More extensive studies were conducted on the rate constants for the spontaneous hydrolysis of substituted 2,4-dinitrophenyl glycosides, thereby avoiding effects of the substituent on the concentration of the conjugate acid species and its pathway, and these gave similar results (18).

The rate decreases observed for the fluoro sugars in the enzymic reaction are considerably greater than those observed for the corresponding non-enzymatic acid-catalyzed reaction, indicating that the loss of specific binding interactions that normally

contribute to stabilization of the transition state contributes to the rate reductions. The large rate reductions observed, as expressed in decreased k_{cat} and $k_{\text{cat}}/K_{\text{m}}$ values, likely arise from some combination of intrinsic electronic effects and specific binding interactions. Although it is not possible to separate these two effects completely and determine their individual contributions, a reasonable estimate of the relative importance of the two effects can often be obtained, thereby providing useful insights into catalysis.

3.1.4 Objectives

In this study, the specificity constants, $k_{\text{cat}}/K_{\text{m}}$, will be determined for the hydrolysis of a series of deoxy and deoxyfluoro sugar derivatives by the family 10 *C. fimi* xylanase (Cex) and the family 11 *B. circulans* xylanase (Bcx), and these data will be interpreted in terms of active site hydrogen-bonding interactions. The binding energy contributions of individual sugar hydroxyl groups in the enzyme–substrate complexes at the transition state will be calculated using the relationship

$$\Delta\Delta G^\ddagger = -RT \ln \left(\frac{(k_{\text{cat}} / K_{\text{m}})_x}{(k_{\text{cat}} / K_{\text{m}})_y} \right)$$

where x represents either a mutant enzyme or substrate analogue and y the wild-type enzyme or parent substrate. The series of calculated $\Delta\Delta G^\ddagger$ values or apparent binding energy contributions will then be compared to gain new insights into the role of hydrogen binding in catalysis by these two xylanases in particular as well as, more generally, into the molecular basis for remote binding effects upon catalysis. The carbohydrate-binding site of *C. fimi* xylanase will also be analyzed through a mutational analysis to probe the role of protein–carbohydrate interactions defining substrate

specificity. Amino acid residues involved in substrate binding were mutated on the basis of the previously determined X-ray crystal structures of enzyme–substrate complexes. The effects of the mutations of various selected residues on catalysis and binding will be determined by steady state kinetics using a series of chromogenic substrates to assign the individual hydrogen-bond contributions. Comparison of the two methods will provide an evaluation of the validity of the use of such modified substrate analogues and appropriate active-site mutants to probe the role of hydrogen bonding in protein–ligand interactions, as well as an evaluation of the importance of hydrogen bonding in the generation of biological specificity.

3.2 Results and Discussion

3.2.1 Binding energy contributions probed by using substrate analogues

The series of monosubstituted deoxy and deoxyfluoro 4-nitrophenyl β -xylobiosides shown in Figure 3.2 was synthesized by Dr. Johann Schloegl and Dr. Chris A. Tarling, and generously provided for this study. These represent a reasonably full set of substrate analogues for probing the role of hydrogen bonding at each hydroxyl. Unfortunately, despite many attempts, the substrate analogue 4-nitrophenyl 3-deoxy- β -xylobioside (3-deoxy-PNPX₂) could not be synthesized due to its lability (18). Likewise, synthesis of 4-nitrophenyl 2-deoxy- β -xylobioside (2-deoxy-PNPX₂) was not attempted as it was expected to be yet more labile. However, fluorinated analogues were obtained for each position.

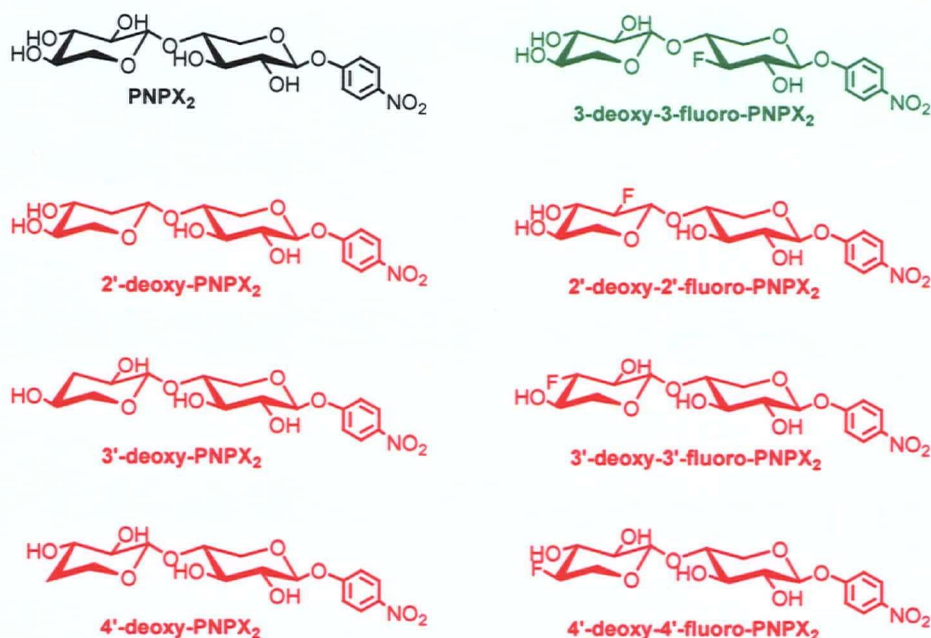


Figure 3.2: Chromogenic synthetic substrates. PNPX₂, 2'-deoxy-PNPX₂, 2'-deoxy-2'-fluoro-PNPX₂, 3'-deoxy-PNPX₂, 3'-deoxy-3'-fluoro-PNPX₂, 4'-deoxy-PNPX₂, and 4'-deoxy-4'-fluoro-PNPX₂ were prepared by Dr. Johann Schloegl. 3'-Deoxy-3'-fluoro-PNPX₂ was prepared by Dr. Chris A. Tarling.

3.2.1.1 Kinetic analysis of family 10 *C. fimi* xylanase

Kinetic parameters (k_{cat} , K_{m} , and $k_{\text{cat}}/K_{\text{m}}$) for hydrolysis of the *p*-nitrophenyl deoxy- and deoxyfluoro- β -xylobiosides by wild-type Cex are presented in Table 3.1. The calculated increase in activation free energy for the glycosylation step associated with each substitution ($\Delta\Delta G^\ddagger$) was calculated from the ratios of the $k_{\text{cat}}/K_{\text{m}}$ values of the parent substrate and the modified analogue according to the equation outlined in the introduction. Values of $k_{\text{cat}}/K_{\text{m}}$ characterize the transition-state interactions between the substrate and the enzyme, since they reflect the activation barrier from free enzyme plus substrate to the transition state for the *glycosylation* step of the reaction.

Table 3.1: Kinetic parameters for the hydrolysis of deoxy/deoxyfluoro analogues by wild-type *C. fimi* xylanase.^d

Sugar Ring	Substrate	Michaelis-Menten Kinetics			Apparent Binding Energy Contribution $\Delta\Delta G^\ddagger$ (kcal mol ⁻¹)
		k_{cat} (s ⁻¹)	K_m (mM)	k_{cat}/K_m (s ⁻¹ mM ⁻¹)	
	PNPX ₂	40 ± 1	0.017 ± 0.001	2300 ± 100	0
Distal	2'H-PNPX ₂	28 ± 4	1.4 ± 0.2	21 ± 5	2.9 ± 0.1
	2'F-PNPX ₂	nd ^c	nd ^c	74 ± 7	2.1 ± 0.1
	3'H-PNPX ₂	47 ± 3	0.42 ± 0.03	110 ± 10	1.9 ± 0.1
	3'F-PNPX ₂	48 ± 2	0.024 ± 0.004	2000 ± 400	0.1 ± 0.1
	4'H-PNPX ₂	32 ± 3	0.034 ± 0.001	930 ± 90	0.6 ± 0.1
	4'F-PNPX ₂	31 ± 3	0.015 ± 0.001	2100 ± 200	0 ± 0.1
Proximal	3F-PNPX ₂ ^a	0.006 ± 0.001	0.96 ± 0.05	0.006 ± 0.001	7.9 ± 0.1
	DNPC ^b	12.9	0.11	117	0
	Inhibitor	k_i (s ⁻¹)	K_i (mM)	k_i/K_i (s ⁻¹ mM ⁻¹)	
	2F-DNPC ^b	0.0011	0.11	0.010	5.8

^a Enzyme kinetics courtesy of Dr. Chris A. Tarling using Mr. David K. Y. Poon's wild-type Cex protein preparation of the catalytic domain.

^b Kinetic parameters taken from Tull and Withers (22).

^c nd indicates that this kinetic parameter was not determined.

^d Graphical representation of this data is given *Appendix A*, page 228. Errors were estimated from a non-linear fit by GraFit 4.0 (131).

In previous kinetic studies on Cex the rate-limiting step in the reaction of Cex with *p*-nitrophenyl xylobioside was confirmed to be the hydrolysis of the xylobiosyl-

enzyme intermediate; that is, the *deglycosylation* step. Indeed the very low K_m value observed is consistent with this conclusion, as it indicates substantial accumulation of the glycosyl–enzyme intermediate. The parameter k_{cat}/K_m reflects the first irreversible step; in this case, formation of the glycosyl–enzyme intermediate. Therefore, by inspecting the effects of each substitution on these two kinetic parameters (k_{cat}/K_m for glycosylation and k_{cat} for deglycosylation) we can gain insights into the importance of the interactions at subsite –2 and –1 on each step in catalysis.

3.2.1.1.1 Distal sugar (–2) interactions

Interestingly, values of k_{cat} remained essentially invariant upon removal of OH groups at subsite –2, where the distal sugar unit binds (Table 3.1). This indicates that the deglycosylation step is insensitive to substitutions on the distal sugar ring. Values of K_m varied up to 90-fold for the different deoxy xylobioside analogues compared to the parent value, while values of k_{cat}/K_m correspondingly suffered up to a 100-fold reduction compared to the parent value determined for PNPX₂. By contrast, distal substitution has very significant effects upon the glycosylation step as shown in the k_{cat}/K_m values, with binding energy contributions from each hydroxyl ranging up to 2.9 kcal mol^{–1}. Since k_{cat}/K_m is the second-order rate constant corresponding to the first irreversible step in the reaction (glycosylation, in this case), it is evident that removal of hydroxyl groups on 4-nitrophenyl β-xylobioside decreases the rate of formation of the glycosyl–enzyme intermediate, but has little effect on rates of its breakdown.

Given the distance of these substitutions from the reaction centre, it is a reasonable assumption that electronic effects on transition-state stabilization are minimized; thus, changes are assigned entirely to hydrogen-binding interactions.

Previous studies of the apparent strengths of hydrogen bonds between enzymes and ligands have suggested that hydrogen bonds between two neutral partners contribute up to about $1.5 \text{ kcal mol}^{-1}$ to overall binding free energy, while those between one neutral and one charged species are worth 3 kcal mol^{-1} or more (27, 151, 152, 157). On that basis, and assuming that lost hydrogen bonding is responsible for the majority of the lost binding energy, this suggests that there are one or more hydrogen bonds at each hydroxyl, probably involving charged partners at the 2'-position, a neutral partner at the 3'-position, and a weak hydrogen bond at the 4'-position of the xylopyranose unit bound in the -2 subsite. For wild-type Cex, values of $\Delta\Delta G^\ddagger$ of 2.9 and $1.9 \text{ kcal mol}^{-1}$ (deoxy analogues) thus identify 2'-OH and 3'-OH in subsite -2 of the second sugar unit as being involved in reasonably strong hydrogen bonds at the transition state for hydrolysis of xylobiosides. As expected, a fairly small $\Delta\Delta G^\ddagger$ value of $0.6 \text{ kcal mol}^{-1}$ contributed by the 4'-OH in subsite -2 is in accord with the enzyme's specificity for xylan polymers which would include a sugar link at this position. This is consistent with the structure of the 2-deoxy-2-fluoroxxylobiosyl-Cex intermediate (76) where it is observed that this OH-group is involved in a hydrogen-bonding interaction with a water molecule.

Interestingly, values of $k_{\text{cat}}/K_{\text{m}}$ for the deoxyfluoro xylobiosides were all greater in comparison to the analogous deoxy substrate, confirming that the enzyme donates a hydrogen bond at the substituted position in each case. Amazingly, replacement by fluorine at C-3' had no significant overall energetic consequences as expressed in the apparent binding energy contribution. This suggests that the fluorine, thus the original 3'-OH, acts as the hydrogen-bond acceptor. Conversely, had the original hydrogen bond been of the opposite polarity, requiring the fluorine to act as a donor, a considerable loss

in transition-state affinity should have resulted. A more detailed interpretation of the data is encumbered by factors such as the slightly smaller overall size of the fluorine (2.74 Å) relative to the oxygen (2.83 Å), the unknown relative hydrogen-bond strengths of fluorine to water and its donor in the active site, and the possible role of the fluorine in promoting other hydrogen-bonding interactions (173).

The deoxygenation at position C-2' results in a larger loss in affinity (2.9 kcal mol⁻¹) relative to that observed for position C-3'. Fluorination can partially reinstate this binding energy, although the fluorosugar still binds 2.1 kcal mol⁻¹ more weakly at the transition state than the parent substrate. A straightforward interpretation of the data implies that the 2'-OH acts as a hydrogen-bond acceptor since the 2'-deoxyfluoro sugar binds slightly better than the 2'-deoxy sugar. Further, an additional hydrogen bond of opposite polarity is suggested in which the sugar hydroxyl acts as the donor given the significant loss in binding energy at the 2'-position. Clearly, this analysis does not eliminate the possibility that sugar hydroxyl groups play dual roles as hydrogen-bond donors and acceptors. Consequently, this method cannot detect the presence of multiple hydrogen-bonding interactions with a particular hydroxyl on the sugar ring. The observed order of hydrogen-bond strength and the role, as donor (D) or acceptor (A), of the sugar hydroxyl at each position in subsite -2 of the second sugar unit is summarized below.

$$2' (D + A) > 3' (A) > 4' (A)$$

The role of the sugar hydroxyl as donor or acceptor at each position is summarized below in Figure 3.3.

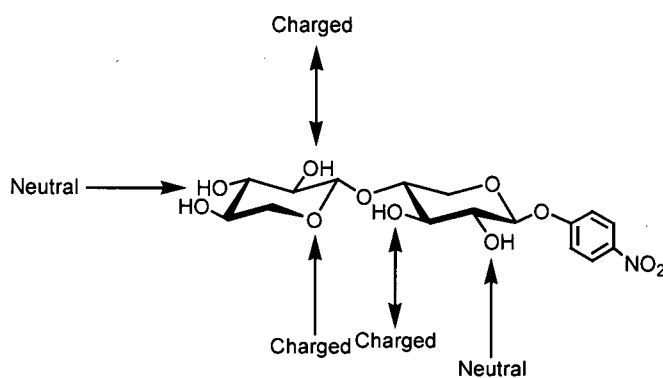


Figure 3.3: Schematic representation of proposed intermolecular hydrogen-bond interactions between 4-nitrophenyl β -xylobioside and Cex based on substrate analogue data, X-ray crystallography and NMR studies.

The polarities of the hydrogen-bonding interactions predicted from the substrate analogue data are indeed consistent with the polarities of the hydrogen bonds observed in the active site of the xylobiosyl-enzyme complex observed by X-ray crystallography (Figure 3.6). A summary of the hydrogen-bonding interactions in the active site of the fluoroxylobiosyl-enzyme complex of Cex is given in Table 3.2.

Table 3.2: Summary of hydrogen-bonding interactions between the xylobiosyl intermediate and protein residues in the active site of the 2-deoxy-2-fluoroxyllobiosyl-enzyme complex of Cex.

Sugar Ring	Atom Involved	Role	Protein Residue	Atom Involved	Role	Distance (± 0.2 Å)
Proximal	2-F	Acceptor	Asn126	N δ 2	Donor	3.3
	3-OH	Donor	His80	N ϵ 2	Acceptor	3.0
	3-OH	Acceptor	Lys47	N ζ	Donor	2.8
Distal	2'-OH	Donor	Glu43	O ϵ 2	Acceptor	2.9
	2'-OH	Acceptor	Trp273	N ϵ 1	Donor	2.9
	3'-OH	Acceptor	Asn44	N δ 2	Donor	3.0
	5'-O	Acceptor	Gln87	N ϵ 2	Donor	3.4
	5'-O	Acceptor	Lys47	N ζ	Donor	3.0

3.2.1.1.2 Proximal sugar (–1) interactions

Unfortunately only a very limited data set is available for xylobioside substrates in which the proximal sugar has been modified, and, as noted earlier, these data are complicated by inductive effects upon transition-state stability. However comparison of the data for 3F-PNPX₂ with that for PNPX₂ reveals that, indeed, both k_{cat} and $k_{\text{cat}}/K_{\text{m}}$ are severely affected, with the transition state for glycosylation being destabilized by a massive 7.9 kcal mol^{–1}, while that for deglycosylation is destabilized by approximately 5.2 kcal mol^{–1}. Part of the rate reduction arises from inductive effects, which can be estimated from spontaneous hydrolysis data. In a study by Namchuk *et al.* (18) on the role of sugar substituents in spontaneous glycoside hydrolysis, the electronic effect of the ring substituent on the principal center of charge development at the transition state was the primary determinant of the rate of hydrolysis of a series of monosubstituted deoxy and deoxyfluoro 2,4-dinitrophenyl β -D-glycopyranosides. The ratios of rates of

spontaneous hydrolysis obtained at the 3-position for F : OH : H substituted glucoses are 0.14 : 1 : 4 respectively; therefore, the inductive effect at the 3-position is relatively small. A straightforward interpretation of the data therefore implies that the 3-OH engages in multiple strong hydrogen-bonding interactions at the transition state, summing to approximately $6.7 \text{ kcal mol}^{-1}$ and $4.0 \text{ kcal mol}^{-1}$ to the glycosylation and deglycosylation steps.

Likewise, but difficult to evaluate, enormous effects upon k_{cat} are seen for substitution of the 2-hydroxyl in the proximal ring by fluorine. Indeed, the substantial decrease in reaction rate due to destabilization of the oxocarbenium ion-like transition state for the enzymatic hydrolysis of glycosides has been the basis for the use of such reagents as mechanism-based inactivators. In fact, 2,4-dinitrophenyl 2-deoxy-2-fluoro-cellobioside was shown to be an excellent time-dependent inactivator for Cex, functioning via the formation and accumulation of a relatively stable 2-deoxy-2-fluoro-cellobiosyl-enzyme intermediate (22). Unfortunately, data are not available to allow direct comparisons of aryl xylobiosides with their 2-deoxy or 2-deoxy-2-fluoro analogues. However, as shown in Table 3.1, inactivation parameters of $k_i = 0.0011 \text{ s}^{-1}$ and $K_i = 0.11 \text{ mM}$ for 2,4-dinitrophenyl 2-deoxy-2-fluoro- β -cellobioside, were obtained by Tull and Withers (22) according to the scheme below:



This scheme is analogous to that of the Michaelis–Menten mechanism. By comparing the inactivation parameter k_i/K_i for the modified “substrate” (2F-DNPC) to the k_{cat}/K_m value obtained for the parent 2,4-dinitrophenyl cellobioside (DNPC), a transition-

state stabilization energy of at least $5.8 \text{ kcal mol}^{-1}$ contributed by the 2-hydroxyl was calculated for the glycosylation step. However, if the fluorine is involved in stabilizing interactions as a hydrogen-bond acceptor, the $\Delta\Delta G^\ddagger$ value obtained will be an underestimate. Effects on the deglycosylation step are much greater. Comparison of k_{cat} for DNPC (reflecting the deglycosylation step) with the reactivation rate constant for the 2-fluorocellobiosyl-enzyme (22) results in a $\Delta\Delta G^\ddagger$ value of $11.3 \text{ kcal mol}^{-1}$, of which part is undoubtedly due to inductive effects. For (non-enzymic) acid-catalyzed hydrolysis, the ratios of rates obtained at the 2-position for F : OH : H substituted glycosides are 0.02 : 1 : 2000 respectively. The $\Delta\Delta G^\ddagger$ as a consequence of fluorination at the 2-position for the non-enzymic reaction is $2.4 \text{ kcal mol}^{-1}$. After applying this correction, a $\Delta\Delta G^\ddagger$ value of approximately 9 kcal mol^{-1} can be conservatively estimated for the contribution of the interactions at the 2-hydroxyl.

3.2.1.2 Kinetic analysis of family 11 *B. circulans* xylanase

Kinetic parameters for the hydrolysis of the deoxy and deoxyfluoro derivatives of 4-nitrophenyl β -xylobioside by wild-type Bcx were determined, and the changes in activation free energy, $\Delta\Delta G^\ddagger$ for the glycosylation step associated with each substitution, are presented in Table 3.3. Values of $k_{\text{cat}}/K_{\text{m}}$ for the modified glycosides are one to three orders of magnitude smaller than those for the parent substrate, PNPX₂. Due to the high K_{m} values exhibited by Bcx for aryl xylobioside substrates, and the scarcity and low solubility of the modified xylobiosides, full Michaelis–Menten kinetic parameters could not be determined. Instead, values of $k_{\text{cat}}/K_{\text{m}}$ for each substrate were determined by the substrate depletion method.

Table 3.3: Kinetic parameters for the hydrolysis of deoxy/deoxyfluoro analogues of PNPX₂ by wild-type *B. circulans* xylanase.

Substrate	Substrate Depletion Kinetics k_{cat}/K_m (s ⁻¹ mM ⁻¹)	Apparent Binding Energy Contribution $\Delta\Delta G^\ddagger$ (kcal mol ⁻¹)
PNPX ₂	0.13 ± 0.01	0
2'H-PNPX ₂	0.0012 ± 0.0001	2.9 ± 0.1
2'F-PNPX ₂	0.0035 ± 0.0004	2.2 ± 0.1
3'H-PNPX ₂	0.0046 ± 0.0005	2.1 ± 0.1
3'F-PNPX ₂	0.050 ± 0.005	0.6 ± 0.1
4'H-PNPX ₂	0.34 ± 0.03	-0.6 ± 0.1
4'F-PNPX ₂	0.41 ± 0.04	-0.7 ± 0.1

The values of $\Delta\Delta G^\ddagger$ for the deoxy sugars listed in Table 3.3 represent estimates of the loss of binding energy at each position at the transition state resulting from removal of the hydroxyl in question, since such substitution has resulted in the observed destabilization of the transition state. Very similar effects to those observed for Cex upon k_{cat}/K_m are seen for Bcx, with $\Delta\Delta G^\ddagger$ values ranging from -0.7 up to 2.9 kcal mol⁻¹ (Table 3.3). Unfortunately, due to the relatively high K_m values exhibited by Bcx and the scarcity of substrate it was not possible to obtain k_{cat} values to probe effects upon the deglycosylation step. The relative order of hydrogen-bond strengths measured for Bcx in the -2 subsite is similar to that observed in the binding of the same substrates to wild-type Cex where position 2' > 3' > 4'. In the case of Bcx, the strongest sum of hydrogen-bond strengths measured in the -2 subsite was that at the 2'-position (2.9 kcal mol⁻¹),

with a slightly weaker interaction measured at the 3'-position ($2.1 \text{ kcal mol}^{-1}$). The interaction at position-4' appears to play little role in substrate binding at the transition state, and even to be slightly destabilizing ($-0.6 \text{ kcal mol}^{-1}$). This result is consistent with this enzyme's specificity for an extended β -1,4-linked polysaccharide substrate xylan (174). In studies of oligosaccharyl fluoride substrates for human pancreatic α -amylase, similar results were obtained. Substrates in which the 4-hydroxyl group at the non-reducing end of the oligosaccharide were methylated were consistently better substrates, presumably because there were no solution-phase hydrogen-bonding partners that would be left unsatisfied at the transition state (175). Although the data obtained for Bcx is less extensive, the same pattern of hydrogen-bond polarities and strengths once again emerges between the crystallographic and the kinetic data.

The interactions between the protein side-chains and the 2-fluoroxyllobioside moiety in the 2F-xylobiosyl-Bcx complex (Figure 3.4) were discussed extensively by Sidhu *et al.* (81). Most notably, the distal xylose residue is maintained in the conventional 4C_1 (chair) conformation and forms hydrogen bonds to Tyr166, Gln7, and Tyr69. The proximal xylose residue is distorted to a ${}^{2,5}B$ (boat) conformation and extensively hydrogen bonds to Tyr69, Glu78, Arg112, and the backbone carbonyl of Pro116.

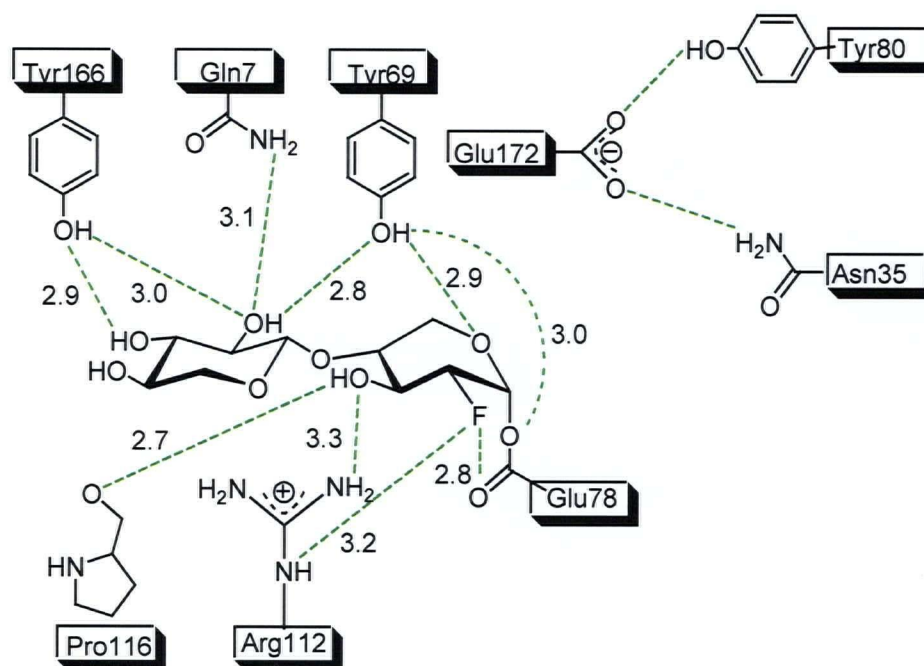


Figure 3.4: Scheme of protein-carbohydrate interactions in the active site region of the 2-fluoroxyllobiosyl-Bcx complex observed by three-dimensional structural analysis (81). Hydrogen-bonding interactions between heteroatoms are in Angstroms.

Interactions with Tyr69 are of particular interest (Figure 3.4). In the structure of the covalent intermediate, the hydroxyl group of Tyr69 donates a hydrogen bond to the O ϵ 2 atom of Glu78 and accepts a hydrogen bond from the 2'-position OH of the distal (nonreducing) xylose ring. This latter hydrogen bond to 2'-OH helps to position the substrate, whereas the former may help orient the nucleophile for the reaction. Furthermore, the phenolic oxygen of Tyr69 also donates a hydrogen bond to the endocyclic oxygen (O-5) of the proximal xylose residue to form a bifurcated hydrogen bond.

Deoxygenation at the 2'-position results in a larger loss in affinity (2.9 kcal mol⁻¹) relative to that observed for the 3'-position (2.1 kcal mol⁻¹). The single hydrogen bond

from Tyr166 to the 3'-position OH of the second xylose moiety therefore appears to provide less transition-state stabilization than those at the 2'-OH. Although fluorination can partially reinstate binding energy at both positions, the 2'-fluorinated compound still binds $2.2 \text{ kcal mol}^{-1}$ more weakly than the parent substrate at the transition state. A simple analysis of the data suggests that the 2'-OH acts as a hydrogen-bond acceptor in at least one interaction since the 2'-deoxyfluoro sugar binds slightly better than the 2'-deoxy sugar. Indeed, structural analysis shows that the 2'-OH plays dual roles as acceptor and donor with Tyr166 and Tyr69, respectively. Furthermore, the hydroxyl at the 3'-position likely acts as a hydrogen-bond acceptor with Tyr166 since the fluorine at C-3' is unable to act as a hydrogen-bond donor and a considerable loss in affinity should result. Accordingly, fluorination at the 3'-position had relatively minor overall energetic consequences as expressed in the apparent binding energy contribution ($0.6 \text{ kcal mol}^{-1}$).

Although the data acquired are limited to interactions that occur in the -2 subsite of the Bcx binding site, significant interactions in the -1 subsite contribute greatly to transition-state stabilization. An important interaction is that involving the O ϵ 1 of Glu78 and the 2-substituent of the proximal sugar. Despite the fact that the interaction between the fluorine and the oxygen in the covalent complex must be destabilizing, the distance between these two atoms is shorter than that seen for the analogous yet stabilizing hydrogen-bonding interaction in the non-covalent complex of Bcx with xylobiose. The shortening of this distance was suggested to be a consequence of the formation of the covalent bond at the anomeric center and the conformational change in the proximal saccharide. Similar interactions in other 2-fluorosugar glycosyl-enzyme complexes (32, 33, 76, 176) have suggested that short, strong hydrogen bonds are formed at this position

in the glycosyl–enzyme intermediate and that this hydrogen bond may be even shorter and stronger at the transition state. This is consistent with the very strong transition-state interactions (typically 5–10 kcal mol⁻¹) measured at the 2-position for a number of glycosidases. Another residue interacting with the 2-position fluorine in the 2F-xylobiosyl–Bcx complex is the highly conserved Arg112. Although an important role has been proposed for the equivalent residue in Cex (Asn126) in hydrogen bonding to the 2-hydroxyl of natural substrate (33), the mutation of Arg112 in Bcx causes a relatively small decrease in catalytic activity (119). Therefore, the most important interaction with the 2-substituent appears to be between the 2-position of the proximal sugar and Oε1 of Glu78.

In summary, these data permit some quantification of the contribution of interactions at each individual hydroxyl group in the –2 subsite to catalysis by Bcx. Atomic resolution crystallographic observation of such interactions would be useful in light of the many studies regarding the fluorosugar–protein interactions where such hydrogen bonding has been cited to explain the high affinity for deoxyfluoro derivatives as compared to deoxy derivatives.

The similarities and differences between Cex and Bcx, two xylanases from distinct families, will be discussed in greater detail in the following section.

Table 3.4: Summary of hydrogen-bonding interactions between the xylobiosyl intermediate and protein residues in the active site of the 2-deoxy-2-fluoroxyllobiosyl-enzyme complex of Bcx (81).

Sugar Ring	Atom Involved	Role ^a	Protein Residue	Atom Involved	Role	Distance (± 0.2 Å)
Proximal	2-F	Acceptor ^b	Glu78	Oε1	Acceptor ^b	2.8
	2-F	Acceptor	Arg112	Nε	Donor	3.2
	3-OH	Acceptor	Arg112	NH ₂	Donor	3.3
	3-OH	Donor	Pro116	O	Acceptor	2.7
	5-O	Acceptor	Tyr69	OH	Donor	2.9
Distal	2'-OH	Acceptor	Gln7	Nε2	Donor	3.1
	2'-OH	Donor	Tyr69	OH	Acceptor	2.8
	2'-OH	Acceptor	Tyr166	OH	Donor	3.0
	3'-OH	Acceptor	Tyr166	OH	Donor	2.9

^a Ligand and protein roles were derived with LPC software (177).

^b The interaction between the fluorine and the oxygen in the covalent complex is destabilizing (81).

3.2.1.3 Comparison of results for two xylanases from distinct families

Kinetic analyses from the previous two sections may be used to reveal information on active site similarities between two unrelated xylanases from two structurally distinct families. Linear free energy relationship (LFER) analysis has been used to show that two highly conserved α -glucan phosphorylases have essentially identical transition-state interactions (178). Similarly, LFER analysis has been used to probe the active site similarities of three enzymes (179) acting on glucose or glucosidic substrates: glucose dehydrogenase (EC 1.1.1.47), glucose oxidase (EC 1.1.3.4), and glucoamylase (EC 3.2.1.3). Despite differences in specificity and structure, the high linear correlation coefficients obtained between $\Delta\Delta G^\ddagger$ values for a series of deoxygenated substrates with these enzymes indicate significant similarity in transition-state

interactions. Similarly, the transition-state binding interactions of Cex and Bcx can be compared using LFER by plotting $\Delta\Delta G^\ddagger$ values for one enzyme versus the corresponding values for another (178, 179). An LFER with slope and correlation coefficient (ρ) close to 1 may suggest two enzymes with very similar active-site transition-state interactions, whereas unrelated enzymes would have very poor correlation coefficients. Therefore, this method reflects how well the binding energetics for different enzymes resemble each other.

The specificity constants, $k_{\text{cat}}/K_{\text{m}}$, determined for Cex and Bcx with the different substrate analogues are given in Table 3.1 and Table 3.3. Changes in activation energy ($\Delta\Delta G^\ddagger$) due to substitution of individual hydroxyl groups are given in Table 3.5. Assuming that removal of the individual hydroxyl groups does not lead to a change in mechanism or rate-limiting step, the measured $\Delta\Delta G^\ddagger$ values reflect changes in hydrogen-bonding interactions. The calculated $\Delta\Delta G^\ddagger$ values for the two enzymes (Table 3.5) show a very similar pattern in the involvement of the substrate hydroxyl groups for transition-state stabilization. The activities of the two enzymes were found to depend heavily on the 2'-OH group, where a change in binding energy of $2.9 \text{ kcal mol}^{-1}$ suggested strong hydrogen bonds between the enzymes and this substrate hydroxyl group. The 3'-OH was involved in weaker interactions, while the 4'-OH had a very small if any role in transition-state binding.

Table 3.5: Binding energy contribution $\Delta\Delta G^\ddagger$ (kcal mol⁻¹) of individual hydroxyl groups in the hydrolysis of PNPX₂ by Cex and Bcx.

Substrate	Cex $\Delta\Delta G^\ddagger$ (kcal mol ⁻¹)	Bcx $\Delta\Delta G^\ddagger$ (kcal mol ⁻¹)
PNPX ₂	0	0
2'H-PNPX ₂	2.9 ± 0.1	2.9 ± 0.1
2'F-PNPX ₂	2.1 ± 0.1	2.2 ± 0.1
3'H-PNPX ₂	1.9 ± 0.1	2.1 ± 0.1
3'F-PNPX ₂	0.1 ± 0.1	0.6 ± 0.1
4'H-PNPX ₂	0.6 ± 0.1	-0.6 ± 0.1
4'F-PNPX ₂	0 ± 0.1	-0.7 ± 0.1

LFER plots of two evolutionarily related phosphorylases were previously reported to have a slope of 1.0 and ρ of 0.999 (178). Cex and Bcx have no overall sequence homology, yet a LFER plot (Figure 3.5) yields a correlation coefficient of 0.92 and a slope of 1.1.

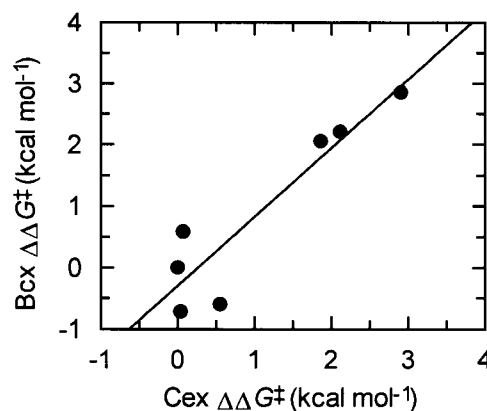


Figure 3.5: Binding energy contribution $\Delta\Delta G^\ddagger$ (kcal mol⁻¹) plot for a series of deoxy- and deoxyfluoro- β -xylobioside analogues with *B. circulans* xylanase (Bcx) and *C. fimi* xylanase (Cex).

Such a strong correlation suggests the two enzymes possess similar transition-state binding interactions, at least those interactions present in the -2 subsite. This result is surprising in light of the differences that exist between these two enzymes. A careful comparison of xylanases in 1988 by Wong *et al.* (94) indicated that these enzymes can be divided into two groups: one consisting of high molecular mass enzymes with low pI values, and the other consisting of low molecular mass enzymes with high pI values. Acidic high molecular mass xylanases (>30 kDa) were found to belong to one family, assigned as glycanase family 10, and basic low molecular mass xylanases, were found to belong to another family, designated as glycanase family 11 (4-6, 120, 180, 181). Family 10 xylanases, such as Cex, show higher affinity for shorter linear β -1,4-xylooligosaccharides than xylanases of family 11, such as Bcx (182). Additionally, enzymes belonging to family 10 exhibit greater catalytic versatility or lower substrate specificity than enzymes of family 11. Significant differences exist in the overall architecture of the substrate binding sites: the substrate binding sites of the family 10

xylanases apparently consist of more shallow clefts versus the substrate binding sites of family 11 enzymes. Three-dimensional analysis of the binding sites of Cex and Bcx in complex with a covalent xylobiopyranosyl residue may be utilized to investigate a basis for the transition-state interactions. In the structure of Cex, a glutamate and tryptophan residue interacts with the 2'-hydroxyl group of the substrate; in Bcx, two tyrosine residues are positioned to hydrogen bond with the 2'-hydroxyl group. An asparagine residue in the -2 subsite of Cex hydrogen bonds with the 3'-hydroxyl group, while a tyrosine residue in Bcx fulfills the same role. Although the properties of the amino acid residues of the two enzymes that interact with the hydroxyl groups are very different, very similar $\Delta\Delta G^\ddagger$ were obtained for both the deoxy and deoxyfluoro derivatives of the xylobioside substrate. The greatest divergence from the observed trend in Figure 3.5 was detected for the 4'-deoxy and 4'-deoxyfluoro derivatives, where it was observed that the 4'-hydroxyl group destabilizes the transition state to a greater extent in Bcx than in Cex. This is consistent with the observation that family 10 xylanases show higher affinity for shorter linear β -1,4-xylooligosaccharides than xylanases of family 11. Further examination and comparison of the "energetic fingerprint" of other glycosidases would be of interest.

In summary, the energetics of transition-state interactions of the active sites of Cex and Bcx have been probed using molecular recognition to indicate key roles for the 2'-OH and 3'-OH groups of the distal xylobiosyl residue. The LFER plot points out similar transition-state interactions despite diverse active-site architectures.

3.2.2 Binding energy contributions probed by using mutant enzymes

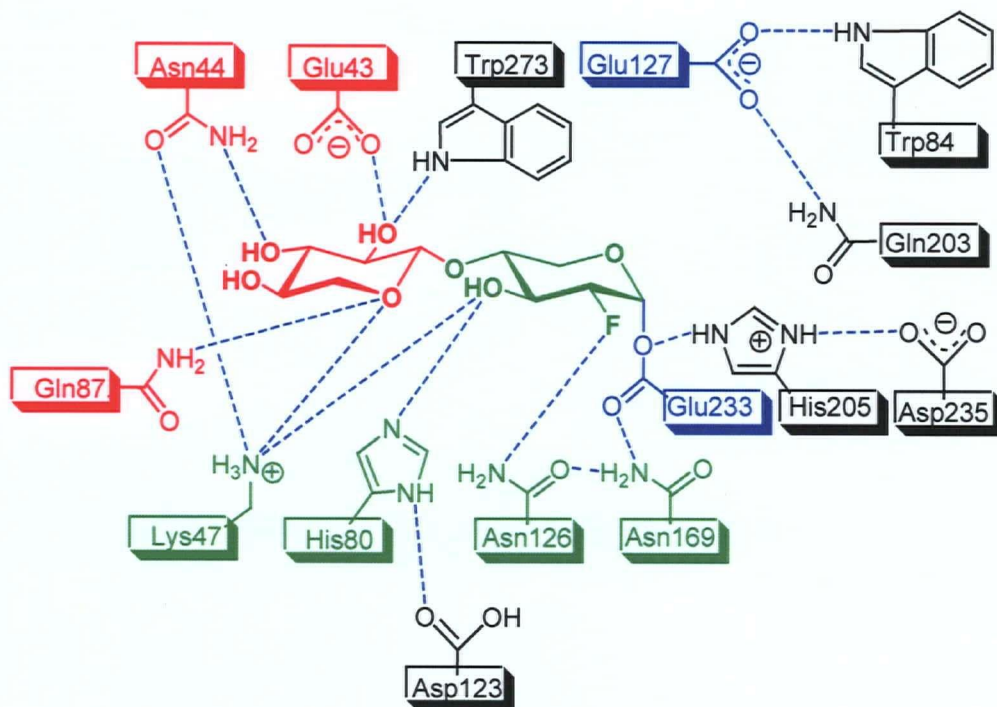


Figure 3.6: Scheme of protein-carbohydrate interactions in the active site region of 2F-xylobiosyl-Cex-cd complex observed by three-dimensional structural analysis (76). Hydrogen-bonding interactions between heteroatoms are in Angstroms. The distance between 2F and the carbonyl oxygen of Glu233 is 2.6 Å (not shown).

Michaelis-Menten kinetic parameters for the hydrolysis of p-nitrophenyl xylobioside by each of the mutants of Cex are presented in Table 3.6. All the mutants were found to be less active than the wild-type enzyme in terms of k_{cat}/K_m values. K_m values are higher than for the wild-type enzyme, consistent with the involvement of the mutated residues in substrate binding. Again, the change in activation energy for the first (glycosylation) step associated with each mutation, calculated from relative k_{cat}/K_m values, is presented. Evaluation of a series of deoxygenated and deoxyfluoro xylobioside substrate analogues with both wild-type and mutant versions of Cex allows an assessment

of the contributions of transition-state stabilizing interactions involving hydrogen-bond donors/acceptors at the sites that are modified by mutagenesis. For mutant Cex, $k_{\text{cat}}/K_{\text{m}}$ values decreased by as much as 5×10^4 -fold relative to wild-type.

3.2.2.1 Design of the mutations

Figure 3.6 shows the putative protein–carbohydrate interactions that are proposed according to the X-ray structure of the glycosyl–enzyme intermediate (32, 33, 76). For subsite –1, the hydrogen-bonding interactions shown might not fully represent those formed at the transition state since ring distortion is expected for the covalently bound xylopyranose unit bearing the glycosidic bond to be hydrolyzed. The protein–carbohydrate contacts observed in the covalent fluoroxylobiosyl–Cex complex involve Lys47, His80 and Asn126, but other interactions may hold if ring distortion occurs upon binding.

Different mutants have been designed to evaluate hydrogen bonding. For hydrogen-bonding residues (Glu, Asn, Lys, His, and Gln), mutation to Ala will remove the interaction, and other mutations such as His → Asn and His → Gln will conserve elements of the functional side-chain group but modify or remove the interaction as a consequence of the larger or shorter side chain. Mutagenesis was performed using the QuikChange system as described in *Materials and Methods* and the mutants of Cex were characterized in *Chapter 2*. The Q87M and N126A mutants were described earlier (76, 183).

3.2.2.2 Subsite -2 interactions

The kinetic parameters determined for hydrolysis of PNPX₂ by the mutants of Cex are given in Table 3.6. When hydrogen bonds that are exclusively formed with the *distal* sugar are destroyed (E43A; N44A; Q87M) the k_{cat} values for hydrolysis of PNPX₂ are essentially unaffected (Table 3.6). However, the effects upon $k_{\text{cat}}/K_{\text{m}}$ are substantial, ranging from 1.0 to 3.7 kcal mol⁻¹. The results indicate that hydrogen bonds formed with the distal sugar are important for the glycosylation transition state, but not for the deglycosylation transition state.

Table 3.6: Kinetic parameters for the hydrolysis of PNPX₂ by wild-type and mutant *C. fimi* xylanase.^a

Subsite	Enzyme	Michaelis-Menten Kinetics			Substrate Depletion Kinetics	Apparent Binding Energy Contribution
		k_{cat} (s ⁻¹)	K_m (mM)	k_{cat}/K_m (s ⁻¹ mM ⁻¹)	k_{cat}/K_m (s ⁻¹ mM ⁻¹)	$\Delta\Delta G^\ddagger$ (kcal mol ⁻¹)
	Native Cex	40 ± 1	0.017 ± 0.001	2300 ± 130	2100	0
-2	Cex E43A	33 ± 3	5 ± 1	6.0 ± 1	5.3	3.7 ± 0.1
	Cex N44A	110 ± 10	4 ± 1	29 ± 6	31	2.7 ± 0.1
	Cex Q87M	58 ± 2	0.12 ± 0.01	480 ± 40	nd ^b	1.0 ± 0.1
-1	Cex K47A	0.43 ± 0.04	10 ± 1	0.045 ± 0.005	0.054	6.7 ± 0.1
	Cex H80A	0.50 ± 0.04	0.59 ± 0.07	0.86 ± 0.12	0.80	4.9 ± 0.1
	Cex H80N	0.15 ± 0.01	0.099 ± 0.003	1.5 ± 0.1	nd ^b	4.5 ± 0.1
	Cex H80Q	0.044 ± 0.002	0.061 ± 0.003	0.72 ± 0.05	nd ^b	5.0 ± 0.1
	Cex N126A	3.5 ± 0.3	8 ± 1	0.45 ± 0.07	0.49	5.3 ± 0.1

^a Graphical representation of this data is given *Appendix A*, page 228. Errors were estimated from a non-linear fit by GraFit 4.0 (131).

^b nd indicates that this kinetic parameter was not determined.

It is of interest to correlate the nature of the enzyme-substrate interactions, as observed crystallographically, with their strengths as, observed kinetically for the glycosylation transition state in this study. The distal sugar at subsite -2 contributes through hydrogen bonding with Glu43, Asn44 and Lys47. Significantly, the strongest interactions with the distal sugar are those at the 2'-position, consistent with a hydrogen bond involving a potentially charged residue (Glu43). Since the 2'-hydroxyl must donate the hydrogen bond to the carboxylate of E43, the loss of almost all the interaction energy

in the 2'-fluorosugar case ($2.1 \text{ kcal mol}^{-1}$) is also understandable, since fluorine cannot donate a hydrogen bond. It could however, still accept a hydrogen bond, if more weakly, from W272, hence the lesser loss of interaction energy than was the case for the 2'-deoxy sugar (167-170). The mutation of Glu43 to Ala decreases k_{cat} only minimally, but results in a 300-fold increase in K_{m} . For the analogous 2'-deoxygenated and 2'-fluorinated substrates, losses of $5.1 \text{ kcal mol}^{-1}$ and $3.4 \text{ kcal mol}^{-1}$ (Table 3.7), respectively, relative to the wild-type enzyme were measured. The additional destabilization due to removal of the 2'-OH group on the distal xylobiose sugar unit may be due to the loss of the interaction between the 2'-hydroxyl and the Trp273 residue worth $1.4 \text{ kcal mol}^{-1}$. Removal of the acidic group may also influence other charged binding side chains contributing to destabilization of the complex.

Table 3.7: Apparent binding energy contribution, $\Delta\Delta G^\ddagger$ (kcal mol⁻¹), of individual substrate hydroxyl groups in the hydrolysis of deoxy/deoxyfluoro analogues of PNPX₂ by wild-type *C. fimi* xylanase and selected mutants

Substrate	Apparent Binding Energy Contribution $\Delta\Delta G^\ddagger$ (kcal mol ⁻¹)		
	E43A	N44A	WT
PNPX ₂	3.7 ± 0.1	2.7 ± 0.1	0
2'H-PNPX ₂	5.1 ± 0.1	nd ^a	2.9 ± 0.1
2'F-PNPX ₂	3.4 ± 0.1	nd ^a	2.1 ± 0.1
3'H-PNPX ₂	nd ^a	3.1 ± 0.1	1.9 ± 0.1
3'F-PNPX ₂	nd ^a	2.7 ± 0.1	0.1 ± 0.1
4'H-PNPX ₂	nd ^a	nd ^a	0.6 ± 0.1
4'F-PNPX ₂	nd ^a	nd ^a	0 ± 0.1

^a nd indicates that this kinetic parameter was not determined.

Asn44 forms a bidentate hydrogen-bond pattern with the xylosyl 3'-OH and the N ζ atom of the Lys47 side chain at subsite -2 in the crystal structure of Cex (76) (Figure 3.6) with a contribution of 2.7 kcal mol⁻¹ to transition-state stabilization (Table 3.7). For the analogous 3'-deoxygenated and 3'-fluorinated substrates, losses of 3.1 kcal mol⁻¹ and 2.7 kcal mol⁻¹, respectively, relative to the wild-type enzyme were measured (Table 3.7). An apparent binding energy contribution of 1.9 kcal mol⁻¹ measured for the 3'-OH group (Table 3.1) indicates that the additional loss of interaction energy caused by mutation at Asn44 may be due to the disruption of the interaction of the amide carbonyl with the charged K47. No significant hydrogen-bonding interactions are seen at the 4'-position of

the distal sugar since further sugar residues are normally appended at this site in the intact xylan substrate. Again, consistently, the deoxy and deoxyfluorosugars are turned over at essentially the same rates as the parent species.

3.2.2.3 Subsite -1 interactions

A different model emerges when considering hydrogen bonds formed with the *proximal* sugar. In all mutants in which side chains interacting with the proximal sugar are modified (K47A; H80A; H80N; H80Q; N126A), values of both k_{cat} and $k_{\text{cat}}/K_{\text{m}}$ drop (Table 3.6). The largest effect is upon $k_{\text{cat}}/K_{\text{m}}$, with $\Delta\Delta G^\ddagger$ values ranging from 4.5-6.7 kcal mol⁻¹.

The particularly important transition-state hydrogen-bonding interactions at the 3-position of the proximal sugar arise from a pair of charged hydrogen-bonding interactions. The 3-OH engages in strong hydrogen-bonding interactions with a positively charged Lys47 residue, recently unequivocally shown to be charged by ¹⁵N-NMR analysis of the trapped intermediate (184), and His80, also recently shown by ¹⁵N-NMR to be present in its charged, conjugate acid form in the free enzyme, but to lose its proton upon formation of the glycosyl-enzyme intermediate (185). Mutation of His80 to Ala introduces 4.9 kcal mol⁻¹ (Table 3.6) overall destabilization with PNPX₂, which includes the elimination of the hydrogen bond between the carboxylate function of Asp123 and the 3-OH of the proximal xylose residue. Mutating the side chain to Asn or Gln has approximately the same effect. This effect, too large for a single hydrogen-bonding interaction, probably indicates an additional role of His80 in transition-state stabilization. Mutation of Lys47 to Ala introduces 6.7 kcal mol⁻¹ (Table 3.7) overall destabilization with PNPX₂, which includes the elimination of a hydrogen bond between

the endocyclic oxygen and the O δ 1 atom of Asn44 at subsite -2, as well as the 3-hydroxyl group at subsite -1 (worth only 1.9 kcal mol⁻¹). This substantial effect results from removal of a positively charged side chain that will likely influence other side chains interacting through a hydrogen-bond network and/or influence the p*K*_a of neighbouring charged groups. Again, mutation of either of these residues is seen to have drastic effects on rates, as would be expected when a charged hydrogen-bonding network such as this is destroyed.

Finally, removal of interactions at the 2-position of the proximal sugar either by mutation (N126A: $\Delta\Delta G^\ddagger = 5.3$ kcal mol⁻¹) or via fluorine substitution ($\Delta\Delta G^\ddagger = 5.8$ kcal mol⁻¹) slows the glycosylation step enormously. Interactions at this position of the saccharide are important for transition-state stabilization in a number of glycosidases, providing up to 10 kcal mol⁻¹ stabilization (27, 28), but the identity of the amino acid residues involved is not clearly established. However, the principal transition-state interaction at OH-2 is thought to be that with the carbonyl oxygen of the nucleophile (E233). The loss of transition-state stabilization due to the mutation of Asn126 to Ala may also result from the loss of a hydrogen bond from Asn126 to Asn169, which in turn aids in positioning Glu233.

3.2.3 Uniform and differential binding interactions

Interactions with the distal (-2) sugar contribute significantly to $k_{\text{cat}}/K_{\text{m}}$ (up to 3.7 kcal mol⁻¹), thus to the formation of the glycosyl-enzyme intermediate, but not to k_{cat} , thus to the hydrolysis of the glycosyl-enzyme. Interactions with the proximal (-1) sugar are much more substantial, contributing up to 6.7 kcal mol⁻¹ to both $k_{\text{cat}}/K_{\text{m}}$ and k_{cat} . The

implication of these results, as is illustrated in Figure 3.7, is that interactions with the distal sugar maintain similar magnitudes in the transition states for glycosylation and deglycosylation, *as well as* in the intervening glycosyl–enzyme intermediate. These interactions can thus be referred to as “uniform binding interactions” in the parlance of Alberty and Knowles (135, 136). They form in the first Michaelis complex, and are maintained with equal strength in all the intervening states along the reaction coordinate. Such interactions serve to improve $k_{\text{cat}}/K_{\text{m}}$, but have no positive effect whatsoever upon k_{cat} . By contrast, interactions with the proximal sugar are considerably stronger at the two transition states than in the intermediate, and thus fall into the category of “differential binding interactions” of Alberty and Knowles (135, 136). Interactions of this class are harder to recruit as they must necessarily exploit the bonding arrangements and charge distributions present at the transition state that differ from those in the ground state in order to achieve this selectivity.

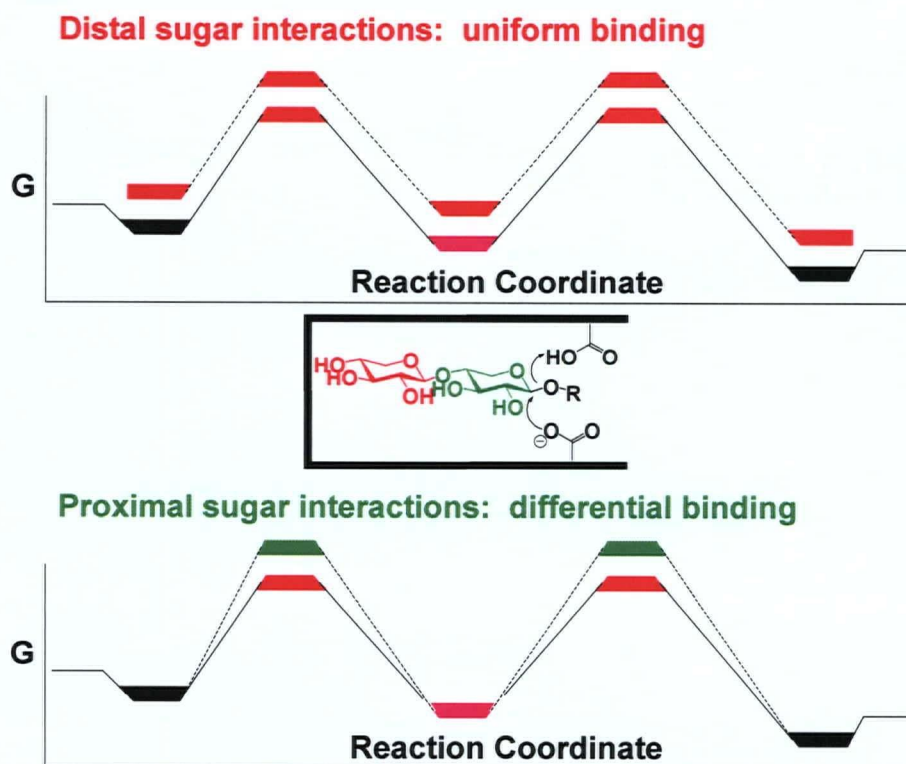


Figure 3.7: Reaction coordinate diagram showing the consequences of modifications to the (a) distal sugar and (b) proximal sugar.

These observations may be explained by the substantial conformational rearrangement that occurs in the *proximal* sugar to accommodate the planar oxocarbenium ion centre formed at the transition state, most likely via a 4H_3 half-chair conformation in the case of Cex (186). Interactions will be optimal at this transition-state conformation. By contrast, no conformational changes are expected at the *distal* sugar. It therefore appears that Cex recruits both uniform binding interactions (at the distal sugar) and differential binding interactions (at the proximal sugar) in effecting catalysis on oligosaccharides.

Interestingly, some clues of this behaviour had been suggested earlier, in a study of the mechanisms of hydrolysis of aryl cellobiosides and aryl glucosides by Cex (22). The rate-limiting step for aryl glucosides was the glycosylation step, while that for aryl cellobiosides was deglycosylation, as revealed by Brønsted plot analyses. Therefore, the presence of an extra glucose moiety appears to selectively accelerate the glycosylation step, consistent with the reaction coordinate diagrams in Figure 3.7A. Uniform lowering of the energy levels of the two transition states and the intermediate will change the rate-limiting step from glycosylation to deglycosylation. Furthermore, examination of the slopes of the two Brønsted plots derived from $k_{\text{cat}}/K_{\text{m}}$ values, which reveal the charge development on the aglycone oxygen at the glycosylation transition state in each case, provide further insight. A slope of -1 for the *glucosides* indicated full negative charge development, while a slope of -0.3 for the *cellobiosides* revealed less charge development when both subsites were occupied. This likely results from a greater degree of nucleophilic pre-association by the nucleophile (Glu233) and/or a greater extent of proton donation from the acid catalyst (Glu127). The finding of slightly lower α -deuterium kinetic isotope effects measured for the cellobiosides is consistent with greater pre-association as at least one of the contributing factors.

3.3 Conclusions

Molecular recognition using substrate analogues has successfully been used to identify and quantify interactions between various functional groups and modified sugar substrates in Cex and Bcx. While hydrogen bonds at the 2'- and 3'-positions of the distal saccharide aid in stabilizing the oxocarbenium ion-like transition state for glycosylation,

the strongest stabilization energies were those measured for hydroxyl groups of the proximal saccharide in subsite -1 of Cex. This is in accord with the mechanism for Cex and Bcx, where no distortion of the distal sugar ring occurs, whereas considerable distortion is expected for the proximal sugar unit. Furthermore, a remarkably good agreement on the contributions of specific hydrogen bonding interactions to catalysis by two different xylanases was demonstrated using two different approaches. Kinetic analyses with a series of 8 mutants of Cex, in which active-site residues interacting with the substrate were mutated, yielded complementary insights on the role of amino acid residues in the binding cleft and the magnitude of protein-substrate interactions. Interaction strengths measured were consistent with the nature of the hydrogen bonds involved: charged or neutral. In those enzyme variants where the ionization properties at the active site were potentially altered (i.e., the mutations of Glu43 and Lys47), evidence of disturbances of hydrogen-bonding interactions with hydroxyl groups at subsite -2 and -1 were observed. The change in pK_a values resulting from the change in local charge may account for these disturbances. The strongest bond energies were measured in subsite -1, suggesting that these interactions are critical for substrate binding and bond hydrolysis. Particularly important was the revelation that both 'uniform' and 'differential' binding interactions are recruited in the active site of a single enzyme.

CHAPTER 4

INQUIRY INTO THE TRANSITION-STATE ANALOGY OF A SERIES OF IMINOSUGAR INHIBITORS FOR A XYLANASE*

* A version of this chapter has been published.

Wicki, J., Williams, S. J., and Withers, S. G. (2007) Transition-state mimicry by glycosidase inhibitors: a critical kinetic analysis. *Journal of the American Chemical Society*, 129: 4530-4531.

4 Inquiry Into the Transition-State Analogy of a Series of Iminosugar Inhibitors for a Xylanase

4.1 Introduction

Transition-state analogues have proved to be an extremely important class of enzyme inhibitors, not only as therapeutic agents, but also as probes of the enzyme mechanism itself. Before applying this investigative tool to discern pertinent fundamental features of the transition state, an enzyme inhibitor must be determined to be a transition-state mimic rather than a fortuitously binding inhibitor. Therefore, the criteria used for designating enzyme inhibitors as transition-state analogues will be reviewed in this section.

4.1.1 Transition-state theory

Transition states are the balance point of catalysis where bonds are partially made and/or broken. The potential energy surface in a typical chemical reaction consists of two distinct regions corresponding to the reactant(s) and product(s) that are separated by an energy barrier at a saddle point on the surface. A common representation of the reaction kinetics passing through the activation barrier is given by the reaction coordinate diagram (Figure 4.1).

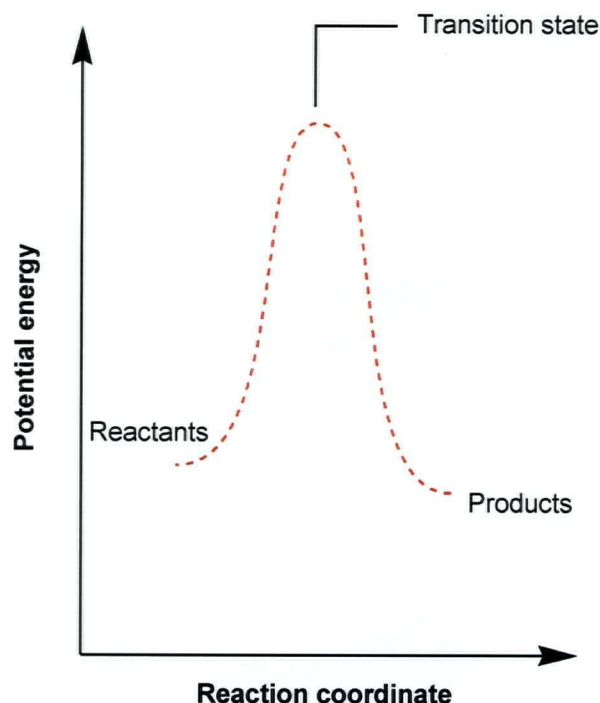


Figure 4.1: A reaction profile. The horizontal axis is the reaction coordinate and the vertical axis is the potential or Gibbs free energy. The transition state corresponds to the maximum of the Gibbs free energy.

The structure represented by this saddle point is the *activated complex* although the term *transition state* is often applied. Transition-state theory originated in the 1930s with the work of Eyring (187). The theory makes two basic assumptions: (1) that there is a thermodynamic equilibrium between the transition state and the state of reactants, and (2) that the rate of a chemical reaction is proportional to the concentration of the particle(s) in the high-energy transition state. These assumptions lead to the Eyring equation for the rate constant k of a chemical reaction (Equation 4.1).

$$k = \kappa \frac{k_b T}{h} e^{-\Delta G^\ddagger / RT} \quad (4.1)$$

In this equation κ is the transmission coefficient which defines the fraction of the molecules that go to the product state when they have reached the transition state, k_b is Boltzmann's constant, h is Plank's constant, T is the absolute temperature, and ΔG^\ddagger is the Gibbs free energy of activation. This is the difference between the Gibbs energy of the transition state and the Gibbs energy of the reactants.

In fact, the Eyring equation provides theoretical validation of the empirically derived relationship by Arrhenius, which states that:

$$k = Ae^{-\Delta E_a/RT} \quad (4.2)$$

where A is the pre-exponential factor, E_a is the activation energy of the reaction, R is the gas constant, and T is the absolute temperature.

4.1.2 Enzyme catalysis

Enzymes accelerate chemical reactions by stabilizing the transition-state structure of the substrate relative to that of the ground state, and often involve alternative pathways from that of the non-catalyzed reaction (29, 188-194). Four common mechanisms by which an enzyme might be expected to bring about rate acceleration include approximation of the reactants, covalent catalysis, general acid/base catalysis, and the induction of distortion or strain in the substrate, the enzyme, or both. Utilizing these mechanisms enzymes lower the energy of the transition state, thereby allowing a greater population of the starting material to attain the energy needed to overcome the activation energy and proceed to product.

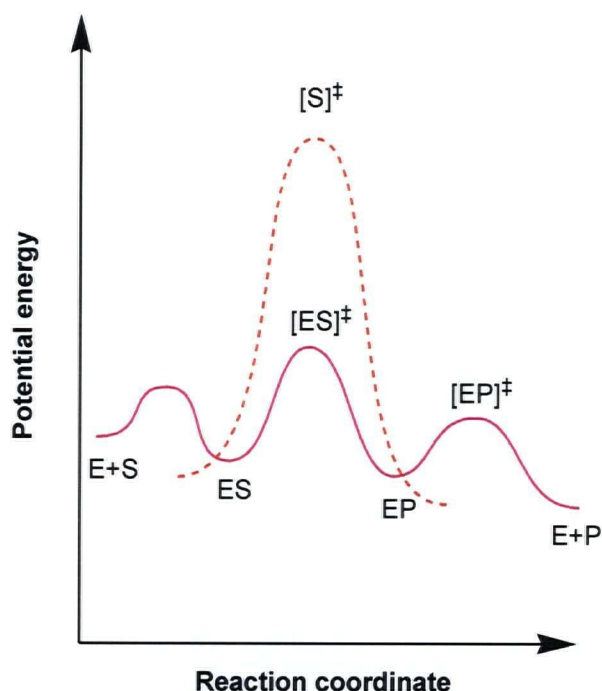


Figure 4.2: Reaction coordinate diagram to show how an enzyme can increase the rate of reaction of a bound substrate by stabilizing the transition state.

Transition-state theory as applied to enzymatic catalysis provides an approach to understanding enzymatic catalysis in terms of the factors that determine the strength of binding of ligands to proteins. The prediction that the transition state should bind to the enzyme much more tightly than does the substrate is supported by experimental results with stable analogues of transition states (29, 188-194). Transition-state analogues have great potential for use in understanding enzymatic catalysis and are discussed in greater detail in the following section.

4.1.3 Experimental approaches to enzymatic transition-state structure

4.1.3.1 KIE to determine TS structure

Kinetic isotope effects (KIE) permit experimental access to the TS structure and are perhaps the only way to obtain detailed TS information. The defining features of enzymatic transition states (bond-lengths, bond-angles and molecular electrostatic potential surfaces) can be approached experimentally by the measurement of intrinsic kinetic isotope effects (195, 196). The theory and application of isotope effects to establish TS structures for enzymatic reactions is well documented elsewhere (192, 197-199). KIE analysis of transition-state structures has not been widely investigated compared to structural techniques that measure stable states (NMR and crystallography) because its application requires thorough knowledge of each enzymatic catalytic mechanism. Nevertheless, transition-state structures derived from kinetic isotope effect analysis have provided an atomic outline for the design of transition-state analogues (188, 196, 198, 199).

Protein structural similarity has not been a strong predictor of transition-state structure. For example, the catalytic sites of human and bovine purine nucleoside phosphorylases are identical within the error of X-ray diffraction experiments, yet the transition states differ considerably (200). Thymidine phosphorylase, another ribosyltransferase, was predicted from structural and computational analysis to have a dissociative transition state, but kinetic isotope effect analysis established a near-classical S_N2 transition state (201, 202).

4.1.3.2 Computational approaches to the transition state

Ab initio computations of enzymatic transition states starting from crystal structure models have become increasingly accessible as computational power has increased together with better atomic models from crystallographic starting points (203-205). Use of quantum-mechanical and molecular-mechanical (QM/MM) allows the calculation of reaction trajectories, thereby providing transition-state structures and energies of reaction.

Quantum-mechanical and molecular-mechanical (QM/MM) separation of enzymes into catalytic site and the non-catalytic regions permits inclusion of both dynamic and electronic/electrostatic components to transition state formation. Transition states located by ab initio searches of this type have found agreement with experimental intrinsic KIE measurements in some cases, but not in others (206). A major barrier for computational approaches to enzymatic transition states is the structural model for the starting point. Computational chemistry can simulate dynamic motion for periods of only a few nanoseconds (10^{-9} s), while catalysis occurs on the scale of milliseconds (10^{-3} s). On the nanoseconds scale, covalent bond equilibration occurs and local motion can be optimized (e.g., amino acid side chain torsion angles) but there can be no significant loop, domain or group movements of the type that are well known to convert Michaelis complexes to the transition state. Thus computational approaches to the transition state from these enzymatic ground state complexes are only approximations of actual transition states. They are unlikely to return robust predictions of the transition state unless the close approach of enzymatic groups to the substrate that constitute the transition state interactions can be reproduced. This requirement is best met when the starting point for

computational chemistry is a high-resolution crystal structure of an enzyme with a transition-state analogue bound at the catalytic site. The significance of experimental KIEs as the basis for computational approaches to enzymatic transition states cannot be overemphasized.

4.1.3.3 TS analogues

Transition-state analogue inhibitors are designed from the hypothesis that chemically stable analogues that mimic geometric and molecular electrostatic features of the transition state will be bound to the enzyme tighter than the substrate by a factor equal to the ratio of enzymatic and non-catalytic processes (188, 207). Transition-state analogues with nearly irreversible binding can hypothetically be designed for enzymes with typical catalytic rate enhancements (10^{10} to 10^{15}). However, the dissociation constants (K_i) for transition-state analogues designed to date fall short of attaining the affinity calculated for the transition states, since the actual enzymatic transition state has non-equilibrium bond lengths and charges that cannot be accurately copied in chemically stable molecules.

Nevertheless, dissociation constants in the picomolar range are not uncommon (208, 209). For instance, zebularine binds to cytidine deaminase with an estimated K_i value of 1.2×10^{-12} M (210). Analogues in the femtomolar range (10^{-15} M) have also been designed. Recently, Singh *et al.* tested inhibitors of *Escherichia coli* 5'-methylthioadenosine/S-adenosylhomocysteine nucleosidase (MTAN) (211). The most powerful inhibitor was 5'-*p*-Cl-phenylthio-DADMe-immucillin-A with a K_i value of 47 fM (47×10^{-15} M), representing one of the most powerful non-covalent inhibitors reported for any enzyme.

The specific arrangements of many transition-state analogue inhibitors within the active sites of enzymes have been determined by X-ray crystallography (212, 213). These structures have provided insight into the interactions that might be responsible for transition-state stabilization. For instance, a number of transition-state analogue designs have incorporated geometric differences between ground and transition states (194, 214-218). The orientation of hydrogen bonds between enzyme and substrate in the transition state may be investigated using transition-state analogue inhibitors with a defined conformation and orientation of the functional groups. The electronic characteristics of charged intermediates have also been exploited. Nevertheless, many questions remain concerning the details of TSA binding and the origin of the high binding affinities observed.

4.1.4 Criteria for transition-state analogy

Many potent inhibitors are known to bind in a very different manner than the transition state; therefore, the observation of binding affinity that is greater than that of the ground state is not sufficient proof of transition-state analogy. While the structural analogy between inhibitor and transition state has been investigated in a limited number of studies (194, 219), a number of more rigorous criteria have been suggested to characterize transition-state analogy. These criteria, discussed below, include (a) strong inhibition, (b) slow inhibition, (c) free energy relationships (d) thermodynamic parameters, and (e) pH profiles.

4.1.4.1 Strong inhibition

Although a good transition-state analogue must necessarily be a strong inhibitor, a strong inhibitor does not have to be a transition-state analogue. In fact, a strong inhibitor may not even bind to the active site. Therefore, one cannot classify an inhibitor as a transition-state analogue based solely on strong inhibition.

4.1.4.2 Slow inhibition

Two basic kinetic mechanisms (Figure 4.3) have been described to account for the slow-binding inhibition of enzyme-catalyzed reactions (220, 221). One mechanism involves the slow interaction of an inhibitor with enzyme (mechanism A), while the other involves the rapid formation of an enzyme-inhibitor complex that undergoes a slow conformational change (mechanism B). Mechanism A assumes that the formation of an EI complex is a single slow step and that the magnitude of $k_3[I]$ is quite small relative to the rate constants, $k_1[S]$ and k_2 for the conversion of substrate to product (136). Mechanism B, which is more general, assumes the rapid formation of an EI complex that then undergoes a slow conformational change to an EI* complex. Again, all other steps, and in particular $k_3[I]$ and k_{-3} , are assumed to be fast relative to k_4 and k_{-4} .

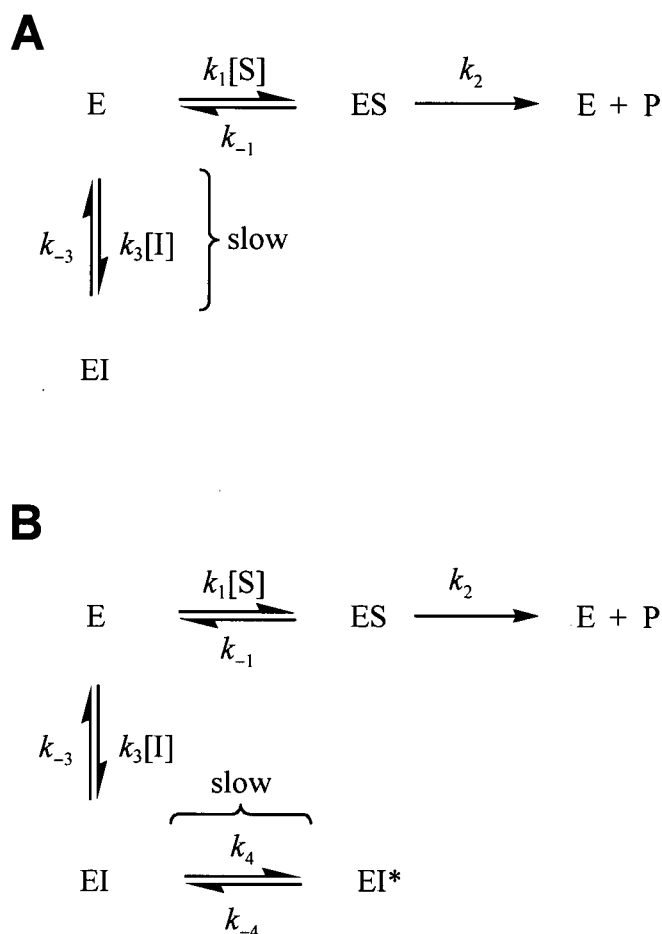


Figure 4.3: Two potential mechanisms for slow-binding inhibition.

Slow-binding inhibition has been suggested as a criterion for transition-state analogy based on the following hypothesis. Some enzymes are in a conformation that binds the substrate in a ground-state conformation, but then undergo a conformational change in order to bind the transition state better. TSA inhibitors can only bind to the conformationally changed enzyme, and the slow-binding behaviour is associated with the time spent for the enzyme to change conformation (222).

However, in most cases, slow binding is an inevitable consequence of the low concentrations of tight-binding inhibitor used to determine its K_i (193, 223). When working with very low inhibitor concentrations that are comparable with the concentration of enzyme, the enzyme-inhibitor complex is present at concentrations comparable with that of the unbound enzyme; changes in experimental conditions change appreciably as a result when working with slow-binding inhibitors. Also, when working with low concentrations of inhibitor and enzyme, the rates for the bimolecular process are necessarily low. Association is a slower event if the concentrations of both inhibitor and enzyme are low and the two ligands have to find each other in solution (the probability of collision is low).

For the condition that $[I] \gg [E]_0$, the rate equations for mechanisms A and B are readily derived and it has been possible to distinguish between these mechanisms by analysis of the time courses of the reactions as a function of initial substrate and inhibitor concentrations. It has also been possible to analyze data corresponding to mechanisms A and B when the inhibition constant of a tight-binding inhibitor is of similar magnitude to the enzyme concentration by performing experiments at elevated enzyme concentrations (221). Also, methods that take substrate depletion into account have been described for analysing experiments in which the initial substrate concentration is below K_m (224).

The slow-binding component may be eliminated if the enzyme and inhibitor are pre-incubated and the reaction started by addition of substrate (225). Nevertheless, slow onset inhibition is too poorly understood a process to be a safe criterion. Alternatively, it may be more appropriate to apply "fast-binding" behaviour as a criterion for "substrate analogy" rather than the reverse.

4.1.4.3 Free energy relationships

Rigorous criteria have been proposed by Wolfenden (226) and by Thompson (227) to address the question of whether a particular glycosidase inhibitor is a transition-state analogue or simply a fortuitously binding inhibitor. Alterations in inhibitor/substrate structure or enzyme active site should produce parallel effects on inhibitor binding (reflected in K_i) to those seen on transition-state stabilization, as inferred from the inverse second order rate constant K_m/k_{cat} . Therefore, as a consequence of the thermodynamic cycle of Figure 4.4, a correlation between the inhibitor K_i value and the substrate K_m/k_{cat} value is indicative of transition state analogy, as derived below. Similarly, a correlation of inhibitor K_i versus substrate K_m values provides evidence of ground state analogy. This approach has been reviewed by Mader and Bartlett (194). Such alterations can be achieved through modification of the ligands *or* of the protein.

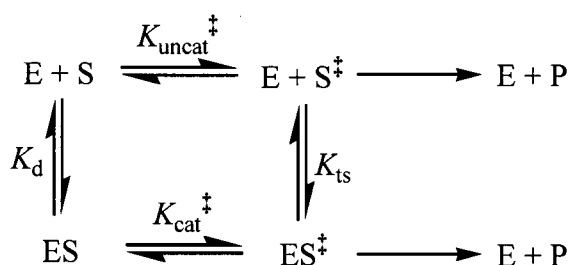


Figure 4.4: Thermodynamic box illustrating the relationship between ground-state and transition-state binding. The designations E, S, and P refer to enzyme, substrate in the ground state form, and product, respectively, while S^\ddagger represents the transition state structure.

Equation 4.3 relates the dissociation constant K_S and the hypothetical dissociation constant K_{ts} to the pseudo equilibrium constants $K_{\text{uncat}}^\ddagger$ for the uncatalyzed reaction and K_{cat}^\ddagger for the enzyme-catalyzed reaction. Using a variation of the Eyring equation

($k = \kappa \nu K^\ddagger$) with the assumption that the transmission coefficient κ and the frequency of the normal mode oscillation ν are equivalent for the uncatalyzed and catalyzed reactions, the hypothetical dissociation constant for the transition-state structure, K_{ts} , may be related to the substrate dissociation constant, K_S , by the ratio of the uncatalyzed and catalyzed rate constants, k_{uncat} and k_{cat} , as shown in equation 4.4. The transition-state structure is bound to an enzyme with an increase in affinity over the ground state that is proportional to the increase in the rate constant for the catalyzed over the uncatalyzed reaction. This transition-state analogy was first recognized by Pauling (147) in 1946 and later implemented by Lienhard (228) and Wolfenden (190) to provide a basis for the design of tight binding enzyme inhibitors.

$$\frac{K_{ts}}{K_{\text{uncat}}^\ddagger} = \frac{K_S}{K_{\text{cat}}^\ddagger} \quad (4.3)$$

$$K_{ts} = \left(\frac{k_{\text{uncat}}}{k_{\text{cat}}} \right) K_S \quad (4.4)$$

As no inhibitor will be a perfect mimic of the transition state, the relationship between K_i and K_{ts} may be obtained by introducing a proportionality constant (d).

$$K_i = dK_{ts} = dK_S \left(\frac{k_{\text{uncat}}}{k_{\text{cat}}} \right) \quad (4.5)$$

Equation 4.6 may be derived by rewriting equation 4.5 in logarithmic form and separating the proportionality constant d and the uncatalyzed rate constant k_{uncat} (equating K_S/k_{cat} with K_m/k_{cat}).

$$\log K_i = \log \left(\frac{K_m}{k_{\text{cat}}} \right) + \log dk_{\text{uncat}} \quad (4.6)$$

Through the relationship $\Delta G^0 = -RT \ln K$, the plot of $\log K_i$ against $\log(K_m/k_{\text{cat}})$ is directly proportional to the free energies of binding for the inhibitor and transition state since the proportionality constant d along with the unmeasurable k_{uncat} become part of the constant $\log dk_{\text{uncat}}$. A slope of 1 in the correlation of equation 4.6 means that structural changes produce the same effects on binding of the inhibitor and the binding of the substrate transition state. Likewise, ground-state analogy can be sought through a correlation between $\log K_i$ and $\log K_m$, assuming $K_m \approx K_s$.

One approach to obtain a correlation involves the synthesis of a series of modified substrates and identically modified inhibitors, followed by a kinetic evaluation with the wild-type enzyme, along with measurement of K_i values for the inhibitors. Previous correlations of this type have shown that a series of phosphorus-containing peptide inhibitors are transition-state analogues for thermolysin (229, 230), carboxypeptidase A (231), pepsin (232), and a collagenase (233). Similarly, nojiritetrazoles were shown by this method to be true transition-state analogues for a range of glycosidases (234). Most recently, this approach has been applied to investigate the binding of two known potent inhibitors to human *O*-GlcNAcase; a family 84 glycosidase (235).

Another approach involves generating a series of mutant enzymes, and then measurement of k_{cat}/K_m and K_i values with each mutant for a single substrate and transition state analogue inhibitor, respectively. The latter approach has been applied to rat carboxypeptidase A (236), glucoamylase (237), and cyclodextrin glycosyltransferase (238).

A linear relationship will only gauge the degree to which the varied part of the inhibitor or enzyme structure mimics the corresponding region of the transition state, and therefore depends on the substrates and inhibitors binding in the same fashion across the series (194). The tightness of the correlation may in fact provide an indication of the degree to which the binding geometries and electronic nature of the inhibitor and transition state remain constant. However, parts of the inhibitor that are not varied, may not resemble the transition state. For example, a study by Vasella's and Withers' groups found a linear relationship between $\ln(k_{\text{cat}}/K_m)$ for hydrolysis of 4-nitrophenyl glycoside by a series of different mannosidases, glucosidases, and galactosidases and the $\ln(K_i)$ value for *gluco*- and *manno*-tetrazole (234). Surprisingly, despite the use of different substrates and different enzymes, a linear correlation was obtained. However, the only varied part of the inhibitor was the 2-hydroxyl group and no variation in the charge of the inhibitor was made. The only conclusion that can be drawn from this correlation is that the 2-hydroxyl group interacts with the protein active site in the same manner that it does in the transition state. These results do not reveal anything about the transition-state mimicry of any other part of the molecule. Similar free energy relationship studies have been made for other glycosidase inhibitors (238, 239).

4.1.4.4 Thermodynamic parameters

Wolfenden suggested that the binding of true transition-state mimics should be driven by enthalpy (207, 240). A comparison of the temperature dependences of uncatalyzed single-substrate and hydrolytic reactions with those of the corresponding enzyme reactions showed that these enzymes invariably lower the reaction's enthalpy of activation substantially, by an amount that tends to determine the effectiveness of the

enzyme as a catalyst, while the entropy of activation of a reaction changes only to a modest extent. In laboratory experiments (240), spontaneous uncatalyzed reactions were shown to be much more sensitive to temperature than generally assumed. For enzyme reactions, k_{cat} is less temperature-sensitive. As a result of this tendency, the corresponding rate enhancements ($k_{\text{cat}}/k_{\text{non}}$) increase with decreasing temperature, and enzyme affinities for transition-state analogue inhibitors are expected to increase with decreasing temperature, more sharply than do enzyme affinities for the corresponding substrates in the ground state. This sharp temperature dependence of K_i provides a new criterion for testing potential transition state analogue inhibitors.

4.1.4.5 pH profiles

It has been proposed that a transition-state mimic should be a true analogue of the transition state if the pH dependence of inhibition correlates with the pH dependence of k_{cat}/K_m of the enzyme (194). However, an incredibly complex expression for the pH dependence of inhibition occurs if the inhibitor is ionisable since the pH dependence of K_i depends upon the pH dependence of the free enzyme, free inhibitor *and* the enzyme/inhibitor complex (139). In this type of analysis, the pH dependence of catalysis will include the pH dependence of free enzyme and something mimicking the enzyme/inhibitor complex, but, by definition, will not include the pH dependence of the *free* inhibitor. Therefore, the pH dependence of catalysis should mimic the pH dependence of inhibition for a transition-state analogue if the inhibitor is non-ionisable. Nevertheless, this criterion has been used to disqualify inhibitors whose binding profile as a function of pH did not correlate with that of catalysis (241-243), which occurred when the inhibitor changed charge over the observed pH range. Nevertheless, the inhibitor

could still be a transition-state analogue, albeit an imperfect one, at one pH and not another.

4.1.5 Inhibitors of glycoside hydrolysis

The best small molecule inhibitors currently available for glycosidases (219, 244) have K_i values of just 10^{-9} to 10^{-10} M. Transition states for glycoside hydrolysis feature extensive sp^2 hybridization and partial positive charge (predominantly along the bond between the anomeric carbon and endocyclic oxygen) and likely involve pyranoside distortion to half-chair (4H_3 or 3H_4 or their closely related envelope form) or boat ($^{2,5}B$ or $B^{2,5}$) conformations (63). In the design of transition-state analogues of glycoside hydrolysis, much of the focus has been on mimicking these features. Most designs focusing on geometry have tried to create inhibitors that are in a half-chair conformation. It should be noted, however, that the most substantial evidence for this conformation comes from measurement of kinetic isotope effects that show various degrees of sp^2 -character at the anomeric carbon of the transition state (245).

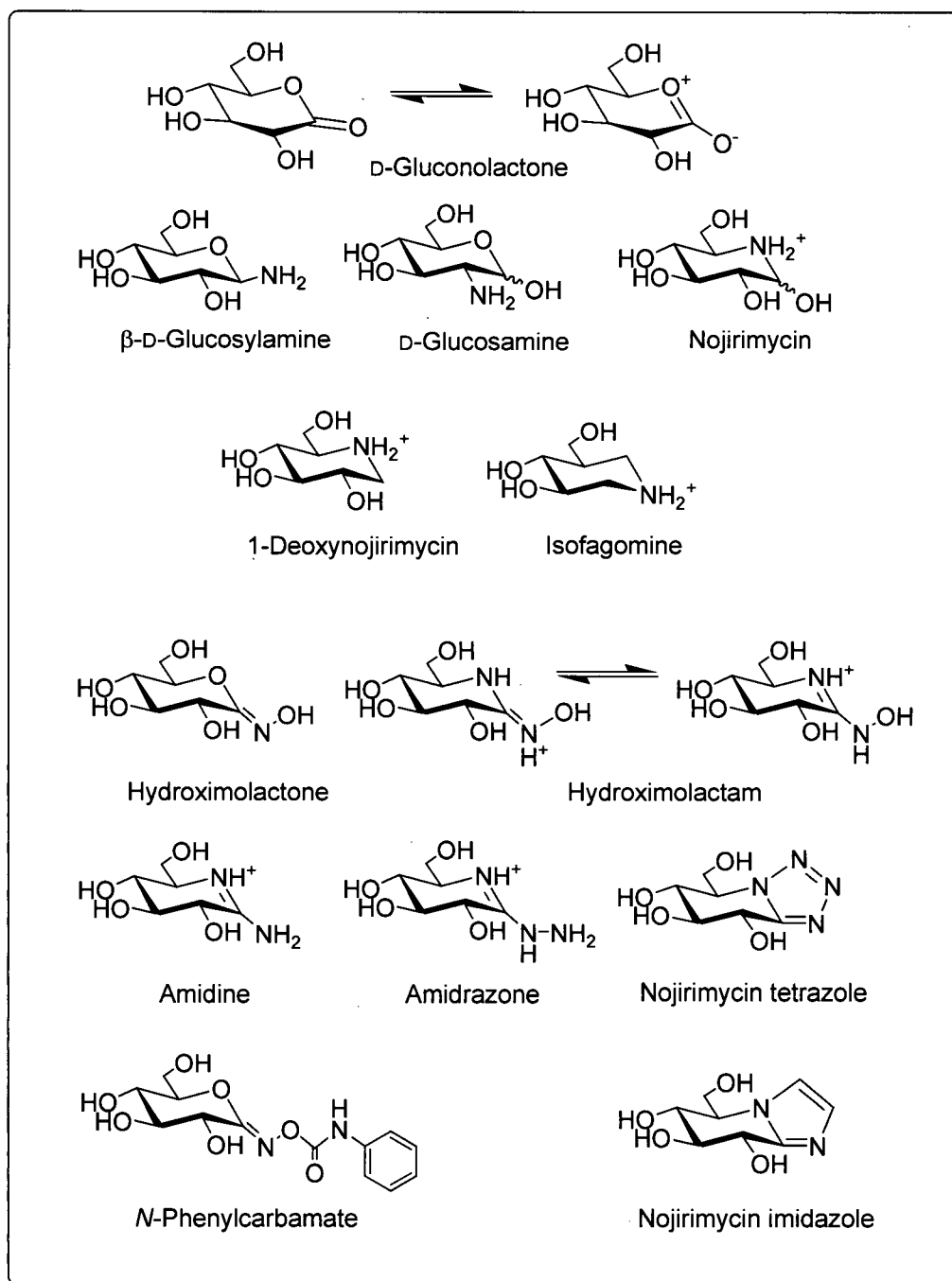


Figure 4.5: Structures of some naturally occurring and synthetic glycosidase inhibitors in the *gluco*-configuration.

Some of the first tight-binding glycosidase inhibitors investigated were the glyconolactones, depicted in Figure 4.5 in the *gluco*-configuration (246). These were argued to function as transition-state analogue inhibitors by virtue of the resemblance to the oxocarbenium ion. Unfortunately, their usefulness has been limited by their instability. Another class of naturally occurring glycosidase inhibitors are that of the glycosylamines and glycosamines, as shown in Figure 4.5. The good inhibition in these cases is attributed to the presence of a protonated (or protonatable) amine moiety, which was proposed to interact electrostatically with the carboxylate groups at the active site. Nojirimycin was discovered as an isolate from *Streptomyces* by Ishida *et al.* (247), and resembles glucose very closely, differing only by the presence of an endocyclic nitrogen rather than oxygen. Subsequently, 1-deoxynojirimycin was obtained by Inouye *et al.* (248) by reduction of nojirimycin. Over three decades a large number of naturally occurring or synthesized hydroxylated piperidines, pyrrolidines and other related structures have been reported and tested.

Particularly noteworthy are the isofagomines, which incorporate a nitrogen atom in place of C1 (249). Isofagomine was the first azasugar prepared with nitrogen in the pseudo-anomeric position (250, 251), and because of the close resemblance between this azasugar and the natural product fagomine, the compound was named isofagomine. The 2-hydroxy group had been omitted for stability reasons. Isofagomine is a potent inhibitor of β -glucosidases, while α -glucosidase inhibition is moderate. The onset of inhibition of isofagomine with sweet almond β -glucosidase was found to be slow, and the binding was found to be driven by a large increase in entropy in contrast to the binding of deoxynojirimycin, which was found to bind due to a decrease in enthalpy (252).

Attempts to develop stable analogues of glyconolactones have resulted in compounds such as the hydroximolactones, hydroximolactams and the *N*-phenylcarbamates (Figure 4.5). These compounds have a flattened chair conformation and an sp^2 -hybridized anomeric carbon. The *gluco*-, *manno*-, and *galacto*-derivatives of hydroximolactams have been made, and have been characterized as broad spectra inhibitors of glycosidases (253-256). The most stable tautomer of the *gluco*-hydroximolactam has an exocyclic double bond. This has been shown, both in the solid state and in solution, by X-ray, ^1H NMR, and by ^{15}N NMR of the ^{15}N -labeled isotopomers (257, 258). Thus, the double bond was not endocyclic as assumed by Tong *et al.* but exocyclic (257). The location of the double bond is important because it has a large effect on the conformation of the compound and also on the interpretation of the inhibitory properties.

An approach to mimic both the flattened chair conformation and the positive charge of the assumed transition state was begun in 1991 by Vasella's group (259). They tried to mimic the conformation and charge of the transition state by synthesizing compounds that consisted of an azasugar fused with heterocycles such as tetrazoles, triazoles, or imidazoles (19). In this way it was possible to make a series of compounds which mimicked the transition state in the desired manner and which had a wide range of pK_a values (260). Furthermore, another benefit was that the azoles were expected to be more stable than the amidines and amidine derivatives that were already known. It should also be pointed out that imidazole itself and derivatives of L-histidine also have turned out to be moderate to strong inhibitors of different glycosidases (261).

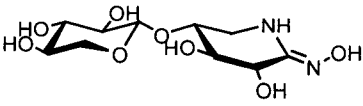
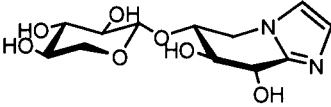
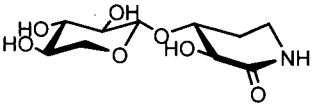
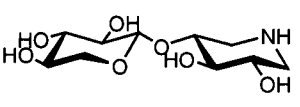
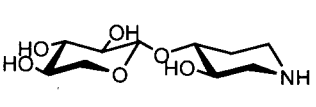
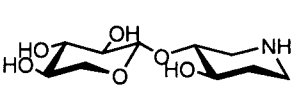
Subsequently, Tatsuta's group also synthesized compounds of this class (262, 263). Some of the most powerful glycosidase inhibitors contain imidazole moieties (260, 264), and are more selective than the amidines and their derivatives.

The azoles are not only interesting because of their strong inhibitory properties, but also have provided a better understanding of the enzymatic mechanism of the hydrolysis of glycosides (19). In 1996 Heightman *et al.* noticed that the moderate to strong β -glycosidase inhibitors all had a heteroatom (N or O) at the glycosidic position and that similar compounds which did not have a heteroatom in this position were weak inhibitors; therefore, they suggested that there is an important interaction with the enzyme at this position (265). Assuming that the inhibitors are bound in the same way in the enzyme as the substrate, it is reasonable to propose that the enzyme-inhibitor interaction is an interaction between the catalytic acid and the heteroatom, thus mimicking the protonation of the glycosidic oxygen at the substrate. It should also be possible to determine whether a glycosidase is a *syn*- or *anti*-protonator by investigating the inhibitory properties of a series of carefully selected compounds. For example, the imidazoles, which contain a heteroatom at the glycosidic position, would be expected to be selective *anti*-protonators because the orientation of the lone pair at the glycosidic nitrogen should allow it to interact with the catalytic acid only in this type of enzymes.

4.1.6 Inhibitors of Cex

Xylobio-derived inhibitors have been made and investigated by the Withers group as inhibitors (Table 4.1) of two different xylanases, namely, the retaining enzymes Cex and Bcx.

Table 4.1: Inhibition constants (K_i) for Cex and Bcx with various xylobio-derived iminosugars.

	Compound	pK_a	Cex (μM)	Bcx (μM)
1		4.9 ± 0.1	0.37^a	1400^a
2		5.9 ± 0.1	0.15^a	520^a
3		< -5	0.34^b	9000^b
4		6.9 ± 0.1	5.8^a	1500^a
5		8.8 ± 0.2	0.13^a	1100^a
6		nd ^c	110^a	3100^a

^a Data taken from Williams *et al.* (52).
^b Data taken from Williams *et al.* (183).
^c nd indicates that this parameter was not determined.

The inhibitor **5** was an inhibitor of Cex in the nanomolar region ($K_i = 0.13 \mu M$) and as such the strongest inhibitor of this enzyme yet described. All the inhibitors studied were poor inhibitors of Bcx with inhibition constants ranging from 520 to 9000 μM . This low activity against the family 11 xylanase was explained by the enzyme being a *syn*-protonator that favors boat conformers in the enzyme-catalyzed transition state, while Cex was believed to prefer a half-chair conformation.

Structures of all the above-mentioned *xylobio*-derived azasugars, except **6**, complexed in the Cex active site were determined by X-ray crystallography (51). It was shown that, as expected, all inhibitors were bound in the -2 and -1 subsites. It was further revealed that for deoxynojirimycin analogue **4** together with the isofagomine **5**, the azasugar moiety adopted a 4C_1 conformation. Even though *xylobio*-isofagomine **5** is a very potent inhibitor of Cex, it demonstrated only a few contacts with the enzyme. The most important interaction was proposed to be between the protonated anomeric nitrogen and the oxygen of the catalytic nucleophile. Because of the small number of enzyme/inhibitor interactions and the conformation of the isofagomine, its strong binding was proposed to be fortuitous (51). Deoxynojirimycin analogue **4** binds 830 times better than xylobiose, although no direct interactions were observed to the azasugar's nitrogen atom. Two water molecules, however, were found to form hydrogen bonds to the basic center, one of which forms a hydrogen bond back to the enzyme (51).

4.1.7 Aims of this study

The primary aim of the work to be presented in this chapter is to discern the important features that mimic the transition state of a model family 10 xylanase (Cex). Since very little is known about the structure of the transition state, insights from our study of Cex could provide a starting point towards a greater understanding of the nature of interactions that can potentially occur between the enzyme and the substrate during the course of the catalytic reaction.

To investigate this aspect of the enzyme, the kinetic parameters for inhibition of four classes of potential transition-state analogue inhibitors will be examined.

Discernment between the crucial features of a transition-state analogue will be achieved through a series of inhibition studies with five inhibitors and a series of mutants of Cex. Linear free energy relationship plots will be constructed to show whether the inhibitors are indeed transition-state analogues. Additionally, the pH dependence of inhibition will be investigated. The information gained from these studies will provide insight about the enzyme-substrate interactions at the transition state of the Cex-catalyzed hydrolysis reaction. An understanding of the transition state is a valuable asset, for it will greatly aid in the design of compounds in the quest for highly potent inhibitors and specific therapeutic drugs.

4.2 Results and Discussion

The binding of several different active site mutants of *Cellulomonas fimi* xylanase to a series of iminosugar inhibitors (1-5) has been investigated through measurement of K_i values. The mutations represent several key amino acid positions, most of which are believed to play important roles in ground-state and transition-state binding interactions of Cex. Michaelis-Menten parameters (k_{cat} , K_m , and k_{cat}/K_m) were determined for each mutant enzyme with *o*-nitrophenyl xylobioside (ONPX₂) and are reported in Chapter 2. The structural changes within these mutant enzymes give rise to k_{cat}/K_m values varying by about three orders of magnitude. Such a wide variation in k_{cat}/K_m values is valuable for establishing a meaningful correlation with K_i values for the inhibitors in order to gain insight into the nature of the strong inhibition afforded by these nitrogen-containing compounds.

4.2.1 Inhibition of Cex mutants by iminosugar inhibitors

Inhibition constants for a series of iminosugar inhibitors were measured with a series of Cex mutants, and these are presented in Table 4.2. For the wild-type enzyme and the N169A mutant, the K_i values were determined from a full analysis using a range of substrate and inhibitor concentrations as is shown for the inhibition of Cex N169A by *xylobio*-imidazole **2** in Figure 4.7. Inhibition was strictly competitive in all cases.

In all other cases, K_i values were determined from data obtained at a series of inhibitor concentrations using a fixed concentration of substrate as described under *Materials and Methods*.

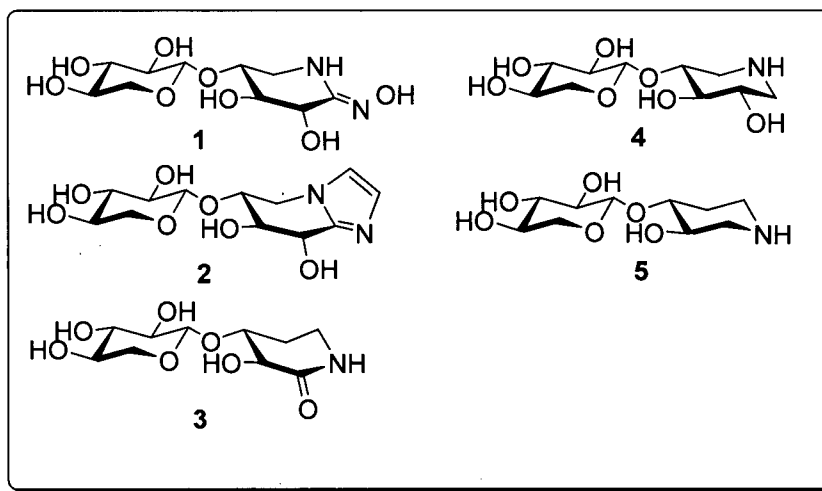


Figure 4.6: Structures of the 5 iminosugars studied.

Table 4.2: Inhibition constants (K_i) for *C. fimi* xylanase and mutants with various xylobio-derived iminosugars.^c

Enzyme	Xylobiose-based inhibitor				
	Lactam Oxime	Imidazole	Isofagomine Lactam	Deoxy-nojirimycin	Isofagomine
	1	2	3	4	5
	(μ M)	(μ M)	(μ M)	(μ M)	(μ M)
Wild-Type	0.37 ^a	0.15 ^a	0.34 ^b	5.8 ^a	0.13 ^a
Glu43Ala	110	22	96	2100	45
Asn44Ala	23	8.9	24	180	7.1
Lys47Ala	2300	1000	2300	6600	870
His80Ala	140	43	1000	800	5.9
His80Asn	350	87	340	370	13
His80Gln	1300	350	340	590	6.7
Gln87Met	4.9	1.1	2.1	18	0.39
Gln87Tyr	16	6.4	11	62	1.2
Asn126Ala	1300 ^b	200 ^b	2000 ^b	4800 ^b	1.6 ^b
Glu127Ala	13	99	28	660	35
Asn169Ala	2.1	0.41	1.5	17	0.12

^a Data taken from Williams *et al.* (52).

^b Data taken from Williams *et al.* (183).

^c Graphical representation of this data is given *Appendix A*, page 269. A relative error of 10% is estimated for the inhibition constants (K_i).

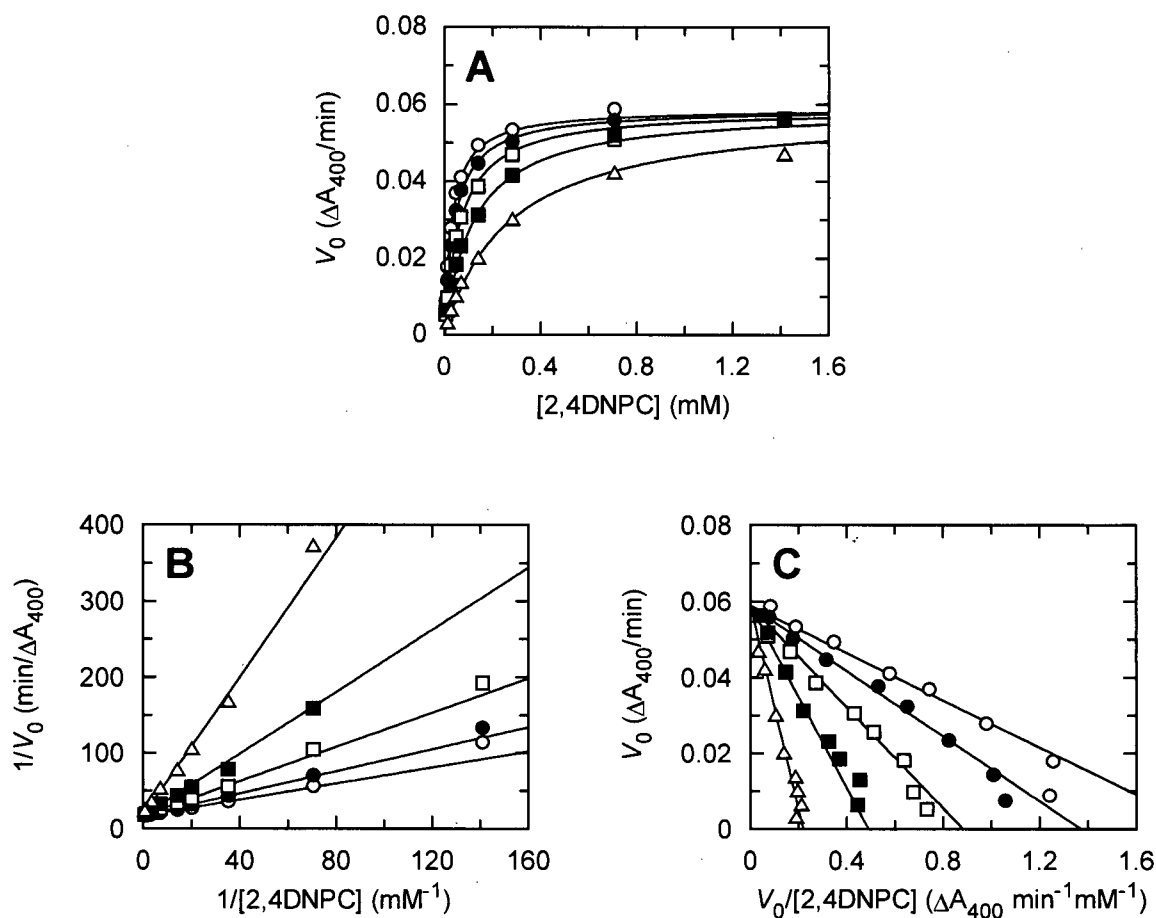


Figure 4.7: Inhibition of Cex N169A by *xylobio*-imidazole at varying concentrations of 2,4DNPC. Plot A is the Michaelis-Menten plot, plot B is the Lineweaver-Burk plot, and plot C is the Eadie-Hofstee plot. The concentrations of *xylobio*-imidazole were 0 (\circ), 0.123 (\bullet), 0.370 (\square), 0.925 (\blacksquare), and 2.47 μM (\triangle).

The mutant enzymes bind to all inhibitors, but less tightly than does wild-type Cex, with widely varying K_i values. For example, for *xylobio*-imidazole, affinities ranging from a K_i of 160 nM for wild-type Cex to 1.0 mM for Cex K47A were measured. This large loss of affinity upon removal of the Lys47 side chain is again consistent with the key role played by this residue.

4.2.2 How good a transition-state analogue is the inhibitor?

A rigorous approach to establish transition-state analogy of the series of iminosugar inhibitors for Cex-catalyzed xylanase hydrolysis has been to use free energy correlations between inhibitor binding and transition-state stabilization (194, 229). A strong correlation with a slope of 1 reveals the inhibitor is a transition-state analogue. Any slope greater or smaller than this may indicate a lesser degree of mimicry. It is not, however, clear that a slope of 1.0 is *required* to indicate any degree of mimicry as has been suggested (194), a conclusion that was developed on the assumption of direct proportionality of rate constants and equilibrium constants themselves (188, 228). Conversely, scattered plots that have weak correlations suggest the inhibitor is a poor transition-state analogue or a fortuitously binding inhibitor (266). Furthermore, strong correlations having a slope of 1 between $\log(K_i)$ of the inhibitor and $\log(K_s)$ values for binding of the substrate reveal ground-state analogy. For enzymes with a rapid-equilibrium substrate binding step, $\log(K_m)$ may be used, or alternatively $\log(K_i)$ for a known ground-state analogue may also be used.

It is useful to review previous LFER studies on glycosidases with similar classes of inhibitor. The first published study of a correlation in glycosidases between substrate and inhibitor specificity, as a probe of transition-state mimicry, was that on the *gluco*- and *manno*-nojirimycin tetrazoles with a series of glucosidases and mannosidases (234). In this study a pair of substrates and inhibitors was studied with the corresponding pair of glycosidases from a variety of sources. A plot of $\log(K_m/k_{cat})$ for each of these substrates versus the $\log(K_i)$ value for the tetrazole inhibitor of the corresponding configuration was linear with a slope of 0.96 and a correlation coefficient of 0.9. The plot of $\log(K_m)$ for the

substrate versus $\log(K_i)$ for the corresponding tetrazole was a scatter plot with a correlation coefficient of 0.2. The tetrazoles were therefore classified as transition-state analogues.

It is noteworthy that in two studies to check the transition-state analogy of acarbose, correlations of $\log(K_i)$ versus $\log(K_m/k_{cat})$ have yielded slopes other than 1 (237, 238). The approach followed in both cases involved the generation of a series of mutants of the enzyme in question, then measurement of kinetic parameters for the hydrolysis of a defined substrate by each of these mutants. The inhibition of each of these mutants by acarbose was then investigated, and K_i values determined. The first such study was performed with the family 15 *Aspergillus niger* glucoamylase using maltose as substrate. The plot was linear with a slope of 0.38 and a correlation coefficient of 0.88, indicating some degree of transition-state mimicry. A second study of acarbose as a transition-state analogue was performed on the retaining family 13 cyclodextrin glycosyltransferase from *Bacillus circulans*. Values of k_{cat} , K_m and k_{cat}/K_m were determined for the reaction of both α -glucosyl fluoride and α -maltotriosyl fluoride with each of 8 mutants and with the wild-type enzyme. In addition, K_i values were measured for the inhibition of each mutant by acarbose. A plot of $\log(K_m/k_{cat})$ for α -glucosyl fluoride versus the $\log(K_i)$ value acarbose was linear with a slope of 2.2 and a correlation coefficient of 0.98. Interesting, acarbose functions as a transition-state analogue for both an inverting α -glucosidase and retaining α -glucosyl transferase.

Although castanospermine and deoxynojirimycin are good competitive inhibitors of *Agrobacterium* sp. β -glucosidase with K_i values of 2.8 and 12 μ M respectively (21, 28), plots of $\log(K_m/k_{cat})$ versus $\log(K_i)$ for these inhibitors failed to show any significant

correlation. Despite their high affinity binding, neither of these classes of compound was found to function as a transition-state analogue, but rather appeared to act as a fortuitous inhibitor.

In the present study, plots of $\log(k_{\text{cat}}/K_{\text{m}})$ for the Cex-catalyzed hydrolysis of ONPX₂ versus $\log(1/K_{\text{i}})$ for the inhibitors in Figure 4.8 were constructed. Excellent correlations ($r = 0.96\text{--}0.97$) were observed with slopes close to 1 for the sp²-hybridized inhibitors (compounds 1–3), clearly indicating a substantial degree of mimicry (Figure 4.8, plots A, B, and C). Changes in binding interactions with the inhibitors (compounds 1–3) therefore correlate quite well with changes in transition-state binding interactions with substrate.

Somewhat weaker correlations were seen for 4 and 5, with correlation coefficients of 0.89 and 0.77, respectively (Figure 4.8, plots D and E). The poorer correlations observed for the sp³-hybridized inhibitors (compounds 4 and 5) clearly indicate that both inhibitors have some properties of a transition-state analogue, presumably their charge, but are not as good analogues as the sp²-hybridized inhibitors (compounds 1–3). The poorer correlation observed for the isofagomine 5 over the deoxynojirimycin 4 might be attributed to the absence of a 2-hydroxyl, which interacts with the nucleophile and Asn126, and has been shown to contribute greatly to transition-state stabilization in β -glycosidases (17). The inferior correlation relative to the deoxynojirimycin may also reflect the poorer mimicry of transition-state charge distribution. Indeed, this conclusion of poorer transition-state mimicry by 5 is consistent with the findings of Davies *et al.* (218), who detected a large entropic contribution in a calorimetric study of binding of (+)-isofagomine to *Thermotoga maritima* family 1 β -glycosidase (TmGH1). The binding

of deoxynojirimycin, on the other hand, was largely driven by a large, favourable, enthalpic contribution, consistent with Wolfenden's suggestion that the binding of true transition-state analogues should be driven by enthalpy (240).

Correlations with K_m values were not possible, as K_m is not the true dissociation constant of the enzyme-substrate complex, but rather represents the overall dissociation constant of all enzyme-bound species. In the case of Cex and the series of mutants, deglycosylation, resulting in accumulation of the glycosyl-enzyme intermediate, was shown to be the rate-limiting step in the hydrolysis of aryl xylobiosides (*Chapter 2*). Correlations probing for ground-state analogy were therefore not possible.

Nevertheless, interesting patterns emerge when comparing the results of this study to those mentioned above. It seems apparent that the sp^2 -hybridized class of inhibitor, including tetrazoles, acarbose, and inhibitors 1–3, function as transition-state analogues. On the other hand, weak correlations observed for the sp^3 -hybridized class of inhibitor, in particular deoxynojirimycin and isofagomine, seem to suggest that these two inhibitors are ground-state analogues or adventitious binders to the enzymes studied (21, 28, 237, 266).

Surprisingly, recent studies have shown that the sp^2 -hybridized 'PUGNAc' inhibitor is a poor mimic for the family 84 glycosidase *O*-GlcNAcase, which utilizes substrate-assisted catalysis. NAG-thiazoline, which possesses an sp^3 -hybridized anomeric centre, is a better transition-state mimic in this case (235).

The future design of sp^2 - and sp^3 -hybridized classes of compounds as glycosidase inhibitors should be undertaken with these findings under consideration.

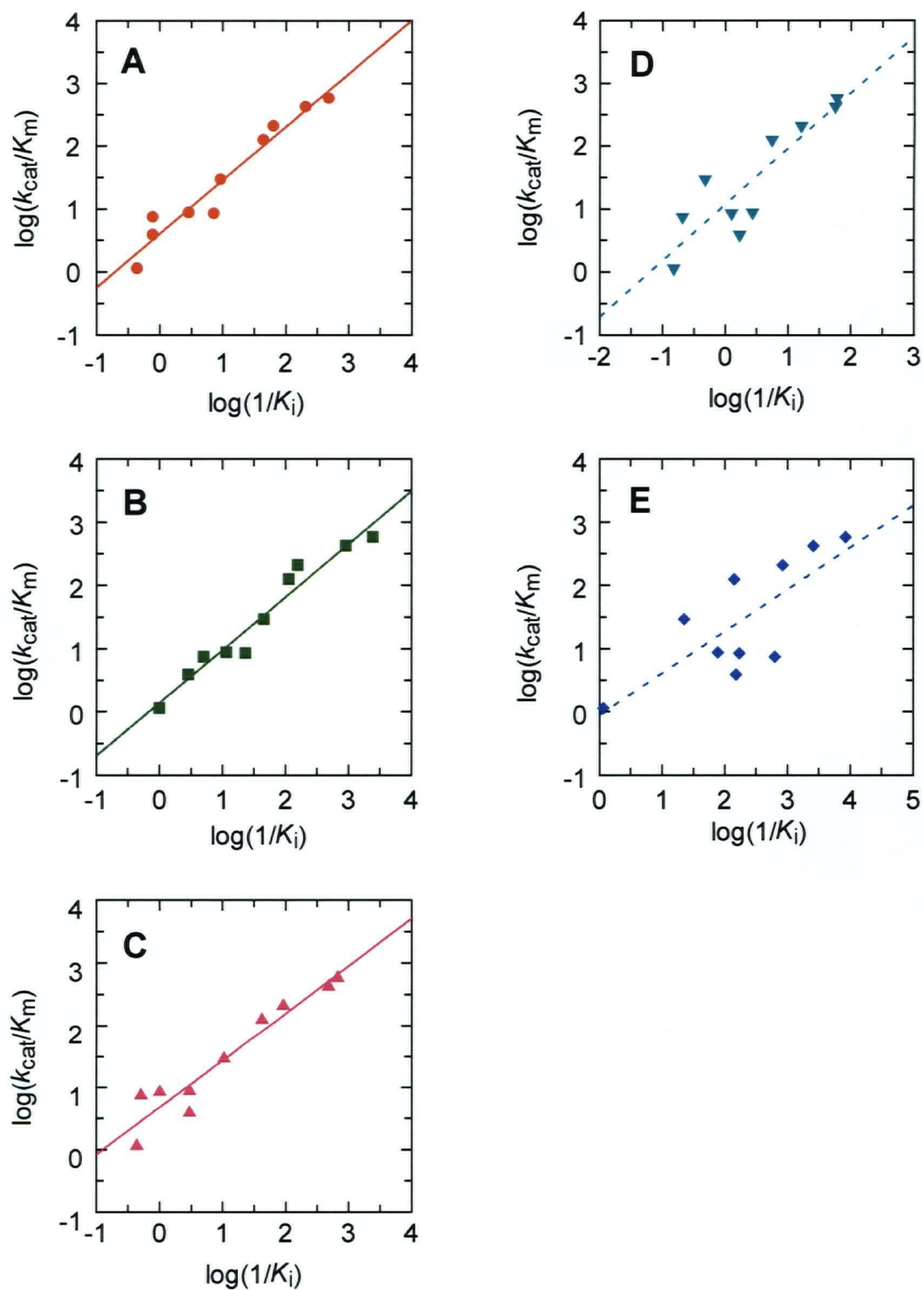


Figure 4.8: Transition state analogy plots for *C. fimi* xylanase Cex. Comparison between k_{cat}/K_m for ONPX₂ and inhibitor K_i values for *xylobio*-derived (A) lactam oxime 1; (B) imidazole 2; (C) isifagomine lactam 3; (D) deoxynojirimycin 4; and (E) isifagomine 5.

4.2.3 The pK_a values of *xylobio*-derived inhibitors

The pK_a values of the conjugate acid forms of *xylobio*-derived iminosugar inhibitors were determined by potentiometric titration (see Figure 4.9) and the results are summarized in Table 4.3. Determination of the pK_a values of the azasugar inhibitors is important in order to gain insight into the inhibition of these compounds.

Potentiometric titration of the acidic form of *gluco*-lactam oxime revealed a pK_a value of 5.6 (254), although a lower value of 4.8 for the lactam oxime has been reported as well (257). The *xylobio*-lactam oxime used in this study yielded a pK_a value of 4.9. Furthermore, the pK_a of the *xylobio* analogue of imidazole was measured to be 5.9, close to that reported for the *gluco* and *cellobio* analogue (pK_a 6.1) (219).

The pK_a of deoxynojirimycin and its *marino* and *galacto* analogues were reported (267) to be 6.3, 7.2, and 7.1, respectively. The *xylobio*-derived analogue yielded a pK_a value of 6.9. The pK_a of the protonated forms of isofagomine and its *galacto* analogue were measured to be 8.4 (250) and 8.8 (268), respectively (269). The *xylobio*-derived analogue used for this study yielded a pK_a value of 8.8.

The pK_a of the *xylobio*-isofagomine lactam was not measured, but is likely well below -5, as amides are very strong bases (conjugated acid pK_a between -6 and -10).

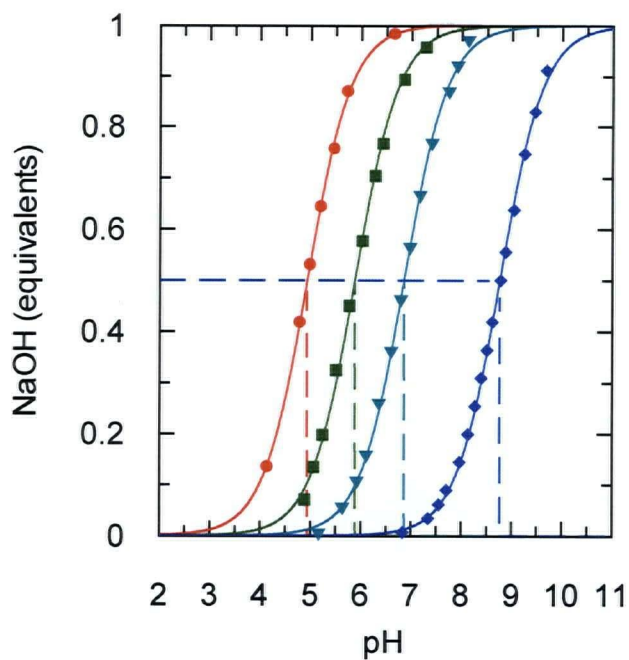
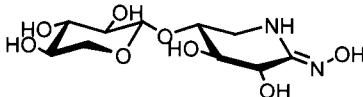
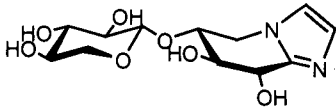
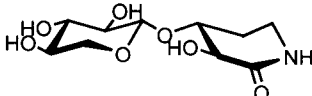
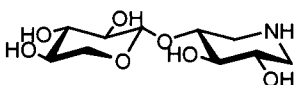
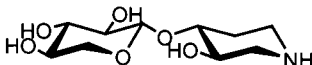


Figure 4.9: Titration curves for the conjugate acid forms of the *xylobio*-derived lactam oxime (●), imidazole (■), deoxynojirimycin (▼), and isofagomine (◆). *Note:* amides are strong bases (conjugated acid pK_a between -6 and -10); therefore, the pK_a of the *xylobio*-isofagomine lactam is likely well below -5 .

Table 4.3: *Xylobio*-derived inhibitor pK_a values of the conjugate acid.

<i>Xylobio</i> -derived Inhibitor	pK_a
	4.9 ± 0.1
	5.9 ± 0.1
	< -5
	6.9 ± 0.1
	8.8 ± 0.2

At the pH at which inhibition constants (K_i) were obtained (pH 7.0), the sp^2 -hybridized *xylobio* analogues of the lactam oxime **1**, imidazole **2** and isofagomine lactam **3** are likely to be in their neutral, unprotonated form. The sp^3 -hybridized *xylobio* analogue of the deoxynojirimycin **4** is half-protonated in solution, while the isofagomine **5** is in its charged, protonated form.

4.2.4 The pH dependence of the binding of *xylobio*-derived inhibitors

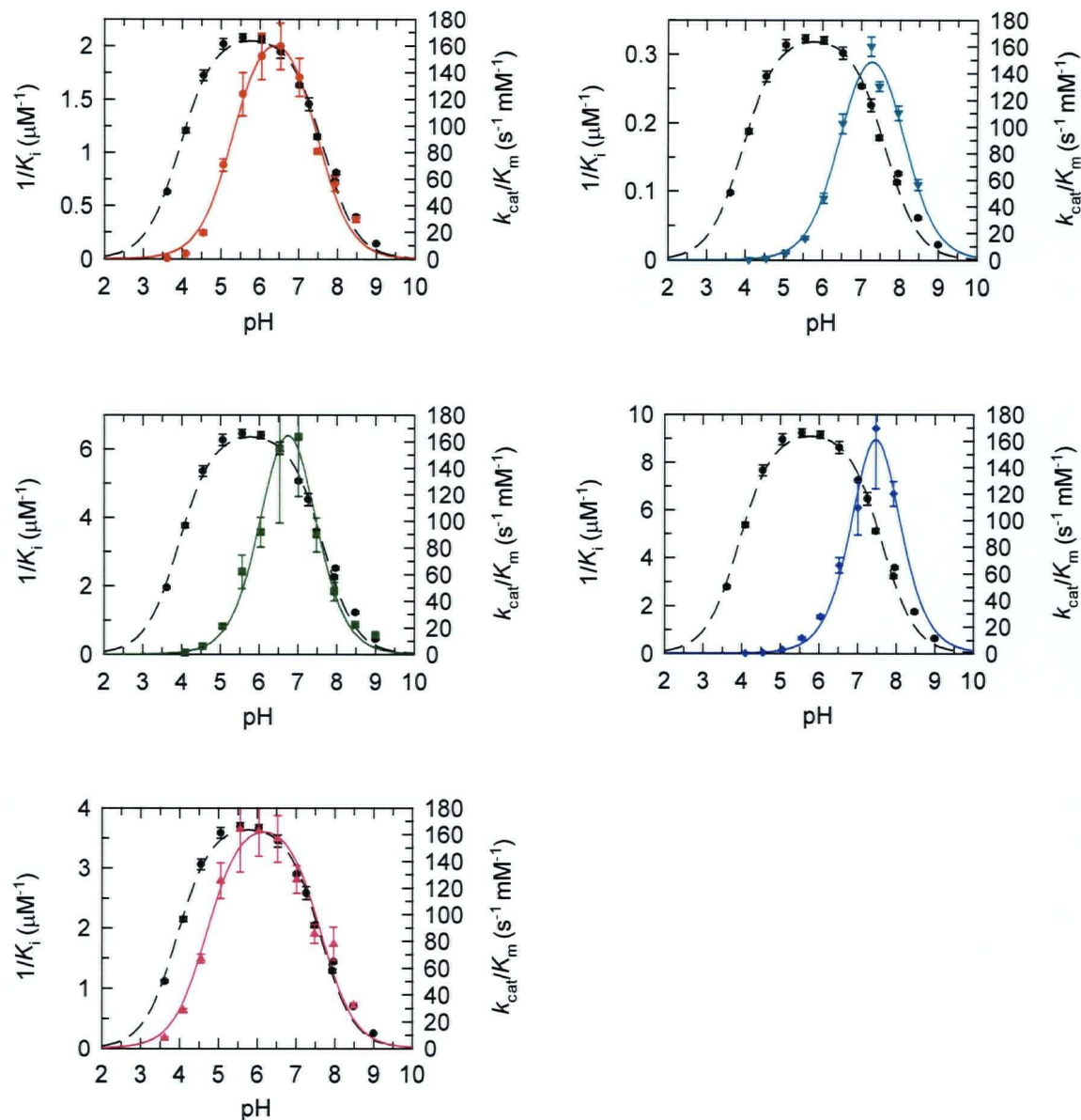
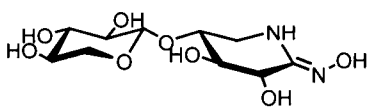
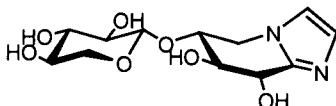
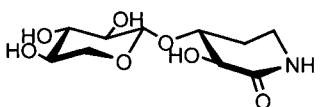
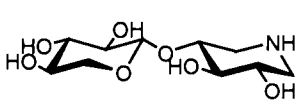
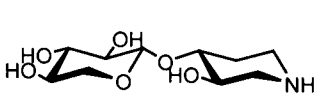


Figure 4.10: pH dependence of $k_{\text{cat}}/K_{\text{m}}$ for Cex (●), $1/K_{\text{i}}$ for *xylobio*-derived lactam oxime pK_{a} 4.9 (●), imidazole pK_{a} 5.9 (■), isofagomine lactam $\text{pK}_{\text{a}} < -5$ (▲), deoxynojirimycin pK_{a} 6.9 (▼), and isofagomine pK_{a} 8.8 (◆). Fits to “bell-shaped” profiles are shown for $k_{\text{cat}}/K_{\text{m}}$ (dashed line) and $1/K_{\text{i}}$ (coloured solid lines).

Table 4.4: Parameters determined from the pH profile for the binding of *xylobio*-derived inhibitors to wild-type Cex.

<i>Xylobio</i> -derived inhibitor	K_i at pH 7.0 (μM)	$\text{p}K_{a1}$	$\text{p}K_{a2}$	pH of optimum inhibition/ activity
	0.59 ± 0.06	5.3 ± 0.1	7.5 ± 0.1	6.4 ± 0.2
	0.16 ± 0.04	6.2 ± 0.1	7.3 ± 0.1	6.7 ± 0.2
	0.36 ± 0.03	4.7 ± 0.1	7.6 ± 0.1	6.2 ± 0.2
	3.2 ± 0.1	6.5 ± 0.1	8.0 ± 0.1	7.3 ± 0.2
	0.16 ± 0.03	7.2 ± 0.2	\sim	7.5 ± 0.2
WT Cex	\sim	3.9 ± 0.04	7.6 ± 0.04	5.8 ± 0.1

4.2.4.1 *Xylobio*-derived lactam oxime, imidazole, and isofagomine lactam

The pH profile of k_{cat}/K_m for Cex is bell-shaped with an optimum at 5.8, and acidic and basic limbs of $\text{p}K_a$ 3.9 and 7.6 (Figure 4.10). As with other related systems (109, 115, 270, 271), this pH profile most likely represents titration of the nucleophile and acid/base, respectively.

The pH dependence of $1/K_i$ for **1–3** are similarly bell-shaped, with slight alkaline shifts relative to catalysis (Figure 4.10). The pH optimum for inhibition of **2** is around 6.7, with acidic and basic limb pK_a values of 6.2 and 7.3, respectively. The simplest explanation of the pH profiles is that the acidic limb is likely to reflect protonation of the inhibitor (which has a solution pK_a of 5.9) and the basic limb protonation of the acid/base residue. This suggests that at the pH optimum for Cex activity, **2** is bound in a predominantly protonated form, as experimentally observed with the *cellobio*-derived form of **2** in complex with a family 5 endoglucanase using atomic resolution X-ray data (272).

The pH optimum for inhibition by **1** is around pH 6.4, with acidic and basic limb pK_a values of 5.3 and 7.5, respectively. The basic limb is likely to reflect the protonation of the acid/base residue, and the acidic limb is likely to reflect protonation of the inhibitor (**1** has a solution pK_a of 4.9). This suggests that at the pH optimum for Cex activity, **1** is bound in a predominantly *unprotonated* form.

The pH optimum for inhibition by **3** is around pH 6.2, with acidic and basic limb pK_a values of 4.7 and 7.6, respectively. The titration profile for compound **3** is interesting to interpret in that the protonation state of the compound is *unlikely* to change (since **3** has a solution pK_a of < -5 , and will remain unprotonated throughout the pH range of enzyme activity). Therefore, the acidic limb is likely to reflect protonation of the nucleophile whose pK_a has increased approximately 0.8 units from a pK_a value of 3.9. The basic limb is likely to reflect the protonation of the acid/base residue, whose pK_a remains unchanged.

As has been pointed out by others, the interpretation of pH profiles of inhibition is notoriously difficult since they are a combination of the events surrounding the free enzyme, the inhibitor and the enzyme–inhibitor complex (139).

4.2.4.2 *Xylobio*-derived deoxynojirimycin and isofagomine

Cex is inhibited by **4** and **5** with K_i values of 3.2 μM and 160 nM at pH 7.0,, respectively. The pH optimum for inhibition of **4** is around 7.3, with acidic and basic limb $\text{p}K_a$ values of 6.5 and 8.0, respectively. The pH dependence of $1/K_i$ of **5** gives an acidic limb of $\text{p}K_a$ 7.2, although the basic limb could not be determined with accuracy because the alkaline shift in pH dependence did not allow for sufficient data points to be collected. Consistent with other studies of inhibition by **5**, maximal binding occurs at high pH where the enzyme has lost significant activity (218, 271, 273). This has been interpreted in other studies as the protonated inhibitor optimally binding to an enzyme with a deprotonated acid/base and deprotonated nucleophilic residues (218, 271). In light of X-ray crystallographic data of *cellobio*-derived **5**, the alkaline shift of the acidic limb may simply indicate that a protonated inhibitor cannot bind tightly to an enzyme in which the acid/base catalytic residue is also protonated (271).

In previous studies, deoxynojirimycin and its derivatives have yielded acid and basic limbs for $1/K_i$ that are difficult to interpret. In a study by Gloster *et al.* (273), a pH dependence of $1/K_i$ for **4** with *S. lividans* xylanase gave acidic and basic limbs of $\text{p}K_a$ 6.6 and 7.8. The atomic resolution structure of **4** in complex with the xylanase from *S. lividans* Xyn10A suggested unusual $\text{p}K_a$ changes of the enzyme's active-site residues upon binding (273). Given that the $\text{p}K_a$ value for **4** is 6.9 (Table 4.3) and the pH of crystallization was 5.8, it was expected that the inhibitor would be present in the active

site of the enzyme in protonated form. At pH 5.8, the nucleophile was protonated when *xylobio*-deoxynojirimycin was bound to *S/Xyn10A* (273). One interpretation of the pH profile that was suggested was that the drop of $1/K_i$ with an acidic limb of 6.6 reflected the titration of the nucleophile whose pK_a had increased approximately 2 units from a pK_a value of 4.1 (273). A similar interpretation was suggested for the pH profile of inhibition for **5**. Indeed, NMR spectrometry has been used to demonstrate significant ligand-dependent shifts in pK_a values for catalytic residues within the active sites of glycosidases (115).

As with the inhibition of other glycosidases (241, 243, 271) by iminosugars, the inhibition of Cex as a function of pH does not correlate with the pH dependence of k_{cat}/K_m of the enzyme. Optimal inhibition occurs at pH values where the acid/base of the enzyme becomes partially or fully ionized and catalysis is reduced or absent. Indeed, optimal inhibition occurs at pH values where the enzyme displays reduced activity.

4.3 Conclusion: Transition-state mimics or fortuitous binders?

By definition, a "transition-state mimic" is never perfect and will not capture all of the binding energy available in an enzyme active site for the reaction transition state. In assessing a transition-state analogue, one must consider what enzyme-inhibitor interactions are relevant to transition-state binding, as well as what interactions are absent in the analysis. Atomic structural analyses of inhibitor complexes with Cex have identified important interactions with active-site residues in the enzyme (51, 183). In this study, the correlation of K_i with k_{cat}/K_m in linear free energy relationships (LFERs) (194)

has provided a mathematically rigorous means of investigating transition-state mimicry (207, 240).

Certainly, the sp^3 -hybridized inhibitors, deoxynojirimycin and isofagomine, achieve some resemblance to the enzyme-catalyzed transition state. In fact, the sp^3 -hybridized isofagomine was the most potent inhibitor despite it being the poorest transition-state mimic studied, demonstrating that powerful inhibition can be obtained with partial resemblance to the transition state. Nevertheless, the sp^2 -hybridized inhibitors (lactam oxime, imidazole, and isofagomine lactam) exhibited a higher degree of transition-state mimicry as assessed by the stronger correlations obtained in the transition-state analogy plots.

The finding that sp^2 -hybridized inhibitors are true transition state analogues, while sp^3 -hybridized inhibitors are not, indicates that true transition-state mimicry demands sp^2 hybridization at the anomeric centre, at least for the enzyme studied. Attempts to take advantage of the 10^{16} -fold affinity increases available to transition-state analogues should therefore focus upon maintaining an sp^2 geometry at the anomeric centre.

CHAPTER 5

MATERIALS AND METHODS

5 Materials and Methods

5.1 Molecular Biology

5.1.1 Reagents, enzymes, and bacterial strains

Growth media components were obtained from Sigma. Plasmid-containing strains were grown in Luria Broth containing 100 µg/mL ampicillin or 50 µg/mL kanamycin. *Pwo* DNA polymerase and deoxynucleoside triphosphates were obtained from Roche. *Pfu* DNA polymerase was from Promega. Restriction endonucleases and T4 DNA ligase were from New England BioLabs unless otherwise indicated. *Escherichia coli* One Shot™ TOP10 competent cells (F^- *mcrA* Δ (*mrr-hsdRMS-mcrBC*) ϕ 80*lacZ* Δ M15 Δ *lacX74* *deoR* *recA1* *araD139* Δ (*ara-leu*)7697 *galU* *galK* *rpsL* *endA1* *nupG*) and the Zero Blunt™ PCR Cloning Kit were from Invitrogen. The QuikChange™ Site-Directed Mutagenesis Kit and Epicurian Coli® XL1-Blue electroporation-competent cells (*recA1* *endA1* *gyrA96* *thi-1* *hsdR17* *supE44* *relA1* *lac* [*F'* *proAB* *lacI*^f Δ M15 Tn10 (Tet^r)] were from Stratagene. PCR DNA fragment purification and plasmid purification kits were from Qiagen or Promega.

5.1.2 Oligonucleotides

Synthesis of oligonucleotide primers (Table 5.1) and DNA sequencing was performed by the Nucleic Acids and Peptide Services (NAPS) Unit at the University of British Columbia (Vancouver, Canada).

Table 5.1: Primers used in the mutagenesis of *C. fimi* xylanase.

Name	Oligonucleotide Sequence	Important Characteristics
QEf	5'-GTC GGG TTC <u>GAG</u> TCG CAC CTC ATC GTC GGC CAG <u>GTA</u> CCG GGC GAC-3'	Forward Q203E mutagenic primer with engineered <i>Kpn</i> I restriction site.
QEr	5'-GTC GCC CGG <u>TAC</u> CTG GCC GAC GAT GAG GTG CGA <u>CTC</u> GAA CCC GAC-3'	Reverse Q203E mutagenic primer with engineered <i>Kpn</i> I restriction site.
QAf	5'-GTC GGG TTC <u>GCG</u> TCG CAC CTC ATC GTC GGC CAG <u>GTA</u> CCG GGC GAC-3'	Forward Q203A mutagenic primer with engineered <i>Kpn</i> I restriction site.
QAr	5'-GTC GCC CGG <u>TAC</u> CTG GCC GAC GAT GAG GTG CGA <u>GCG</u> GAA CCC GAC-3'	Reverse Q203A mutagenic primer with engineered <i>Kpn</i> I restriction site.
DAf	5'-GTG CGC ATC ACC GAG <u>CTA</u> <u>GCC</u> ATC CGC ATG CGG ACG-3'	Forward D235A mutagenic primer with engineered <i>Nhe</i> I restriction site.
DAr	5'-CGT CCG CAT GCG GAT <u>GGC</u> <u>TAG</u> CTC GGT GAT GCG CAC-3'	Reverse D235A mutagenic primer with engineered <i>Nhe</i> I restriction site.
HAf	5'-GCC GAC ACC <u>GGT</u> AAG GAG CTG TAC GGC <u>GCC</u> ACG CTC G -3'	Forward H80A mutagenic primer with engineered <i>Age</i> I restriction site.
HAr	5'- C GAG CGT <u>GGC</u> GCC GTA CAG CTC CTT <u>ACC</u> GGT GTC GGC-3'	Reverse H80A mutagenic primer with engineered <i>Age</i> I restriction site.
HNf	5'-GCC GAC ACC <u>GGT</u> AAG GAG CTG TAC GGC <u>AAC</u> ACG CTC G -3'	Forward H80N mutagenic primer with engineered <i>Age</i> I restriction site.
HNr	5'- C GAG CGT <u>GTT</u> GCC GTA CAG CTC CTT <u>ACC</u> GGT GTC GGC-3'	Reverse H80N mutagenic primer with engineered <i>Age</i> I restriction site.
HQf	5'-GCC GAC ACC <u>GGT</u> AAG GAG CTG TAC GGC <u>CAG</u> ACG CTC G -3'	Forward H80Q mutagenic primer with engineered <i>Age</i> I restriction site.
HQr	5'- C GAG CGT <u>CTG</u> GCC GTA CAG CTC CTT <u>ACC</u> GGT GTC GGC-3'	Reverse H80Q mutagenic primer with engineered <i>Age</i> I restriction site.
KAf	5'-GTC GTC GCC GAG AAT <u>GCG</u> ATG <u>GCG</u> TGG GAC GCC ACC-3'	Forward K47A mutagenic primer with engineered <i>Bsm</i> I restriction site.

Name	Oligonucleotide Sequence	Important Characteristics
KAr	5'-GGT GGC GTC CCA <u>CGC</u> CAT CGC <u>ATT</u> CTC GGC GAC GAC-3'	Reverse K47A mutagenic primer with engineered <i>Bsm</i> I restriction site.
NAf	5'-GAC AGC <u>GAA</u> TTC AAC CTC GTC GTC GCC GAG <u>GCC</u> GCG ATG AAG-3'	Forward N44A mutagenic primer with engineered <i>Eco</i> RI restriction site.
NAr	5'-CTT CAT CGC <u>GGC</u> CTC GGC GAC GAC GAG GTT GAA <u>TTC</u> GCT GTC-3'	Reverse N44A mutagenic primer with engineered <i>Eco</i> RI restriction site.
EAf	5'- C CTC GTC GTC GCC <u>GCG</u> AAT <u>GCG</u> ATG AAG TGG GAC-3'	Forward E43A mutagenic primer with engineered <i>Bsm</i> I restriction site.
EAr	5'-GTC CCA CTT CAT CGC <u>ATT</u> <u>CGC</u> GGC GAC GAC GAG G -3'	Reverse E43A mutagenic primer with engineered <i>Bsm</i> I restriction site.
FP1	5'-TCG CCC GGG GAT CCT AGG ACC ACG CCC GCA CCC GGC CAC-3'	Forward flanking primer.
FP2	5'-CGA CTC GCC CGA CAG GGG GAT GGG CGT GAA CCC GAT CGC-3'	Reverse flanking primer.
SP1	5'-GTG TGG AAT TGT GAG CGG-3'	Sequencing primer.
SP2	5'-GTC GCC GAC CAC TTC GAG-3'	Sequencing primer.

Note: Mutated residues are underlined. Mutated amino acid codons are in **bold**. Restriction sites are in *italics*.

5.1.3 Site-directed mutagenesis by linear amplification

The genes encoding for *cex* D235A, H80A, H80N, H80Q, K47A, N44A, and E43A were linearly amplified following the protocol outlined in Stratagene's QuikChange™ Site-Directed Mutagenesis Kit (Figure 5.1).

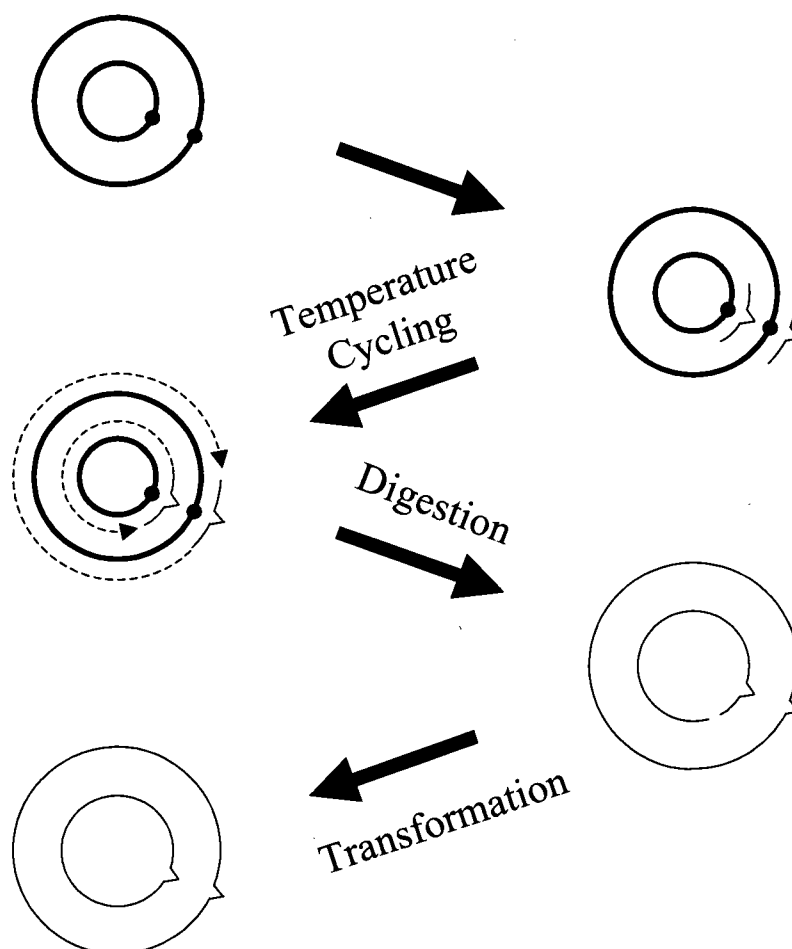


Figure 5.1: Introducing mutations by the QuikChange™ Site-Directed Mutagenesis method. A supercoiled dsDNA vector with an insert of interest (—●—) and two synthetic oligonucleotide primers (—^—) containing the desired mutation are mixed. The oligonucleotide primers, each complementary to opposite strands of the vector, are extended during temperature cycling using *Pfu* DNA polymerase to generate mutated plasmid containing staggered nicks. Following temperature cycling, the methylated, nonmutated parental DNA template is digested with *Dpn* I. The circular, nicked dsDNA is transformed into XL1-Blue supercompetent cells. After transformation, the nicks in the mutated plasmid are repaired by the XL1-Blue supercompetent cells.

The reaction mixture contained 150 ng oligonucleotide primers, 250 μ M each of the four deoxynucleoside triphosphates, and 50 ng of plasmid pUC12-1.1*cex*(PTIS) in 50 μ L of *Pfu* DNA polymerase reaction buffer containing 8% DMSO. Plasmid pUC12-1.1*cex*(PTIS) contains the 1.4 kb *cex* gene (274). The reaction was initiated by

adding 4 U of *Pfu* DNA polymerase (Promega). After heating the reaction mixture to 95°C for 30 s, sixteen cycles (30 s at 95°C, 1 min at 55°C, and 9 min at 68°C) were performed in a thermal cycler (GeneAmp® PCR System 2400, Perkin Elmer). Agarose gel electrophoresis confirmed the presence of sufficient amplification product. The parental supercoiled dsDNA was digested with 20 U *Dpn* I restriction enzyme at 37°C for 1 hour. Epicurian Coli® XL1-Blue electroporation-competent cells (Stratagene) were subsequently transformed with 1 µL of the *Dpn* I treated DNA from the amplification reaction using the BioRad GenePulser® II and 0.1 cm cuvettes under the following conditions: 1.8 kV, 25 µF, 200 Ω. The cells were plated on LB agar plates containing 100 µg/mL ampicillin and incubated at 37°C overnight. Single colonies were selected and grown overnight in LB media containing 100 µg/mL ampicillin. Plasmid DNA was isolated using the QIAprep® Spin Miniprep Kit from Qiagen or the Wizard® Plus Minipreps DNA Purification System from Promega. Plasmid DNA was stored in water at -20°C. Restriction endonuclease mapping revealed positive clones, which were subsequently sequenced to verify the correct mutations. The cloned products were subsequently transformed into electrocompetent *E. coli* JM101 cells using the BioRad GenePulser® II and 0.2 cm cuvettes under the following conditions: 2.5 kV, 25 µF, 400 Ω. Cells were selected by the ampicillin resistance conferred by pUC12-1.1 on LB_{amp} agar plates. Single colonies were selected and grown overnight in LB_{amp} for long-term storage in 10% DMSO at -70°C.

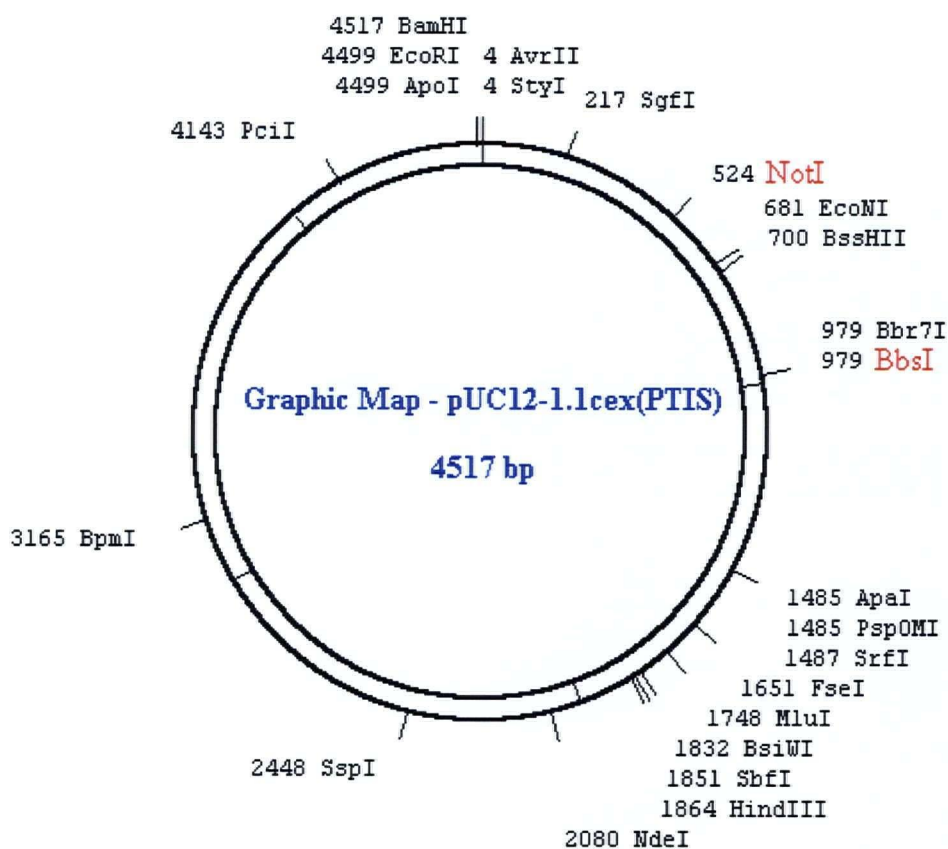


Figure 5.2: Restriction map of pUC12-1.1cex(PTIS).

5.1.4 Site-directed mutagenesis by PCR

A connecting PCR mutagenic strategy outlined in Figure 5.3 was used to introduce the desired Q203A and Q203E mutations and a silent mutation that would introduce a unique *Kpn* I restriction site into plasmid pUC12-1.1cex(PTIS).

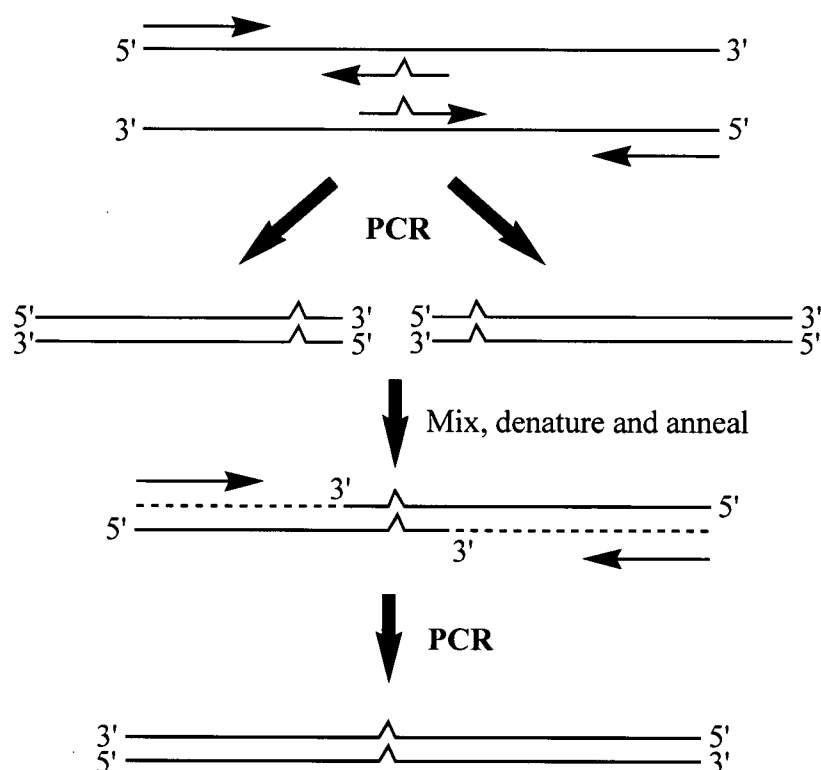


Figure 5.3: Introducing mutations by in vitro overlap-extension PCR. Two PCRs are performed to produce two fragments that carry overlapping sequences. These two fragments are then mixed, denatured, and annealed to obtain mutant DNAs in a further PCR.

Two separate PCRs were performed using pUC12-1.1*cex*(PTIS) as the template and either an outside-forward flanking primer and inside-reverse mutagenic primer, or inside-forward mutagenic primer and outside-reverse flanking primer, to produce two DNA fragments that carry overlapping sequences and intended mutations. The PCR reaction mixtures contained 30 ng pUC12-1.1*cex*(PTIS), 150 ng oligonucleotide primers and 250 μ M each of the four deoxynucleoside triphosphates in 50 μ L *Pwo* polymerase buffer containing 8% DMSO. After heating to 95°C for two minutes, the PCR reaction was initiated by adding 5 U of *Pwo* DNA polymerase (Roche). Fifteen PCR cycles (30 s at 95°C, 30 s at 65°C less 1°C per cycle, and 1.5 min at 72°C) followed by 20 PCR cycles

(30 s at 95°C, 30 s at 55°C, and 1.5 min plus 5 s per cycle at 72°C) and a final extension for 5 minutes at 72°C were performed in a thermal cycler (GeneAmp® PCR System 2400, Perkin Elmer). Agarose gel electrophoresis of the PCR reaction mixture revealed two DNA fragments of 780 bp and 1100 bp that were isolated using the QIAEX II DNA Extraction Kit according to the manufacturer's protocol (Qiagen). These two fragments were mixed and heated to 95°C for two minutes. After adding 5 U of *Pwo* DNA polymerase (Roche), 20 PCR cycles were performed to extend the fragments. Fifteen PCR cycles (30 s at 95°C, 30 s at 60°C less 1°C per cycle, and 1.5 min at 72°C) followed by 20 PCR cycles (30 s at 95°C, 30 s at 48°C, and 1.5 min plus 5 s per cycle at 72°C) and a final extension for 5 minutes at 72°C were performed in a thermal cycler (GeneAmp® PCR System 2400, Perkin Elmer). Agarose gel electrophoresis of the PCR reaction mixture failed to reveal the expected 1845 bp fragment. An alternative strategy described below was attempted.

The resulting two fragments (1.2 µg) from the first PCR were digested with 30 U *Kpn* I restriction endonuclease. Following purification of the digested PCR products using the QIAquick™ PCR Purification Kit, a ligation was performed using 4 U T4 DNA ligase (Invitrogen) for 1 hour at 16°C. Subsequently, a blunt-end ligation into vector pCR®-Blunt was performed using the Zero Blunt™ PCR Cloning Kit from Invitrogen. *E. coli* One Shot™ TOP10 competent cells (Invitrogen) were then transformed with the ligation mixture. The cells were plated on LB agar plates containing 50 µg/mL kanamycin and incubated at 37°C overnight. Single colonies were selected and grown overnight at 37°C in LB media containing 50 µg/mL kanamycin. Plasmid DNA was isolated using the QIAprep® Spin Miniprep Kit from Qiagen or the Wizard® Plus

Minipreps DNA Purification System from Promega. Restriction endonuclease mapping revealed positive clones, which were subsequently sequenced to verify the correct mutations.

5.1.5 Overexpression and purification by active-site mutants of Cex

The *E. coli* JM101 transformants from the previously prepared DMSO stocks were selected on LB_{amp} (100 µg/mL) agar plates. A single colony was picked and grown for 6 hours in 3 mL of LB_{amp}, and this culture was subsequently used to inoculate 1 L of TYP_{amp}. After the culture grew to an OD₆₀₀ of 2-3 at 30-37°C, 0.2 mM isopropyl β-D-thiogalactoside (IPTG) was added to induce protein expression and grown for an additional 4 hours at 25°C. Overexpression of the enzyme was monitored by sampling of both induced and non-induced cells using SDS-polyacrylamide gel electrophoresis. Induced cells were then harvested by centrifugation at 5000 rpm for 20 minutes at 4°C. A cell extract was prepared using BugBuster™ Protein Extraction Reagent. The cell pellet from a 1 L culture was resuspended in 50 mL of BugBuster reagent at room temperature and 50 µL of Benzonase. EDTA was added to 0.5 mM and PMSF to 1.0 mM. The mixture was incubated with shaking for 10-20 minutes. Following removal of the insoluble cell debris by centrifugation at 16,000 × g for 20 minutes at 4°C, the soluble cell extract was added to 450 mL of 500 mM NaCl in 50 mM sodium phosphate buffer (pH 7.0). EDTA and PMSF were added to 0.5 mM.

Cex was purified from the clarified cell extract by affinity chromatography on cellulose. Approximately 25 g of CF1 cellulose (Sigma) was gently stirred with distilled water, allowed to settle, and the “cellofines” were decanted. The cellulose was packed

into an XK50/20 column (Pharmacia), yielding a column volume of approximately 150 mL. The column was attached to an FPLC system (Pharmacia) and equilibrated with 5 column volumes of 500 mM NaCl in 50 mM sodium phosphate buffer (pH 7.0) at a flow rate of 5 mL/min. The soluble cell extract from the 1 L cell culture was applied to the column at a flow rate of 5 mL/min. The column was washed with 2 column volumes of 500 mM NaCl in 50 mM sodium phosphate buffer (pH 7.0) followed by 1 column volume of 50 mM sodium phosphate buffer (pH 7.0) at a flow rate of 5 mL/min. Cex protein was eluted with 2.5 column volumes of distilled H₂O at a flow rate of 5 mL/min. The absorbance of the eluate was measured continuously at 280 nm, and appropriate fractions were pooled and passed through a 0.22 μ m filter (Millipore).

The protein sample was further purified on a 5 mL HiTrap Mono Q HP column attached to an FPLC system (Pharmacia). The column was washed with 5 column volumes of 20 mM Tris-HCl buffer (pH 7.5), 5 column volumes of 20 mM Tris-HCl buffer containing 1 M NaCl (pH 7.5), and then 10 column volumes of 20 mM Tris-HCl buffer (pH 7.5) at a flow rate of 5 mL/min. The protein sample was adjusted to pH 8.0 with 20 mM Tris-HCl and applied onto the HiTrap Mono Q HP column at a flow rate of 5 mL/min. The column was washed with 4 column volumes of 20 mM Tris-HCl buffer (pH 7.5). Cex protein was eluted from the anion-exchange column with a linear NaCl gradient from 0 to 500 mM in a buffer containing 20 mM Tris-HCl (pH 7.5). Fractions (8 mL) were collected at a flow rate of 5.0 mL/min and analyzed using SDS-polyacrylamide gel electrophoresis on a Mini-PROTEAN II apparatus (BioRad). Protein bands were visualized by staining with Coomassie Blue. Fractions containing pure enzyme were pooled and stored at 4°C. If necessary, the enzyme was concentrated to at

least 2.0 mg/mL using a Centriprep concentrator (30 kDa cutoff) from Amicon. Final protein concentration was calculated from measured absorbance 280 nm using the previously determined extinction coefficient for Cex ($\epsilon_{280} = 1.61 \text{ mL mg}^{-1} \text{ cm}^{-1}$).

5.1.6 Protein mass determination

The molecular weights of purified Cex and Cex mutants were determined by ion spray mass spectrometry. Mass spectra were recorded on a PE-Sciex API 300 triple-quadrupole mass spectrometer (Sciex, Thornhill, Ontario, Canada) equipped with an ion spray ion source by Mr. Shouming He. Enzyme samples (10 μg) were injected into the mass spectrometer to generate the spectra. The masses of the generated mutants were confirmed by comparison between the expected molecular weights and those provided by the spectra.

5.2 Enzyme Kinetics

5.2.1 General materials and procedures

All buffer chemicals and other reagents were obtained from Sigma or Aldrich Chemical Companies unless otherwise noted. The following compounds were prepared and generously provided by co-workers in this laboratory. Xylobiosyl lactam oxime, xylobiosyl deoxynojirimycin, xylobiosyl isofagomine, and xylobiosyl isofagomine lactam were synthesized by Dr. Spencer J. Williams while xylobiosyl imidazole was prepared by Dr. Roland Hoos. 4-Nitrophenyl β -xylobioside, 4-nitrophenyl 2'-deoxy- β -xylobioside, 4-nitrophenyl 2'-deoxy-2'-fluoro- β -xylobioside, 4-nitrophenyl 3'-deoxy-

β -xylobioside, 4-nitrophenyl 3'-deoxy-3'-fluoro- β -xylobioside, 4-nitrophenyl 4'-deoxy- β -xylobioside, and 4-nitrophenyl 4'-deoxy-4'-fluoro- β -xylobioside were prepared by Dr. Johann Schloegl. 2,4-Dinitrophenyl β -D-cellobioside and 4-nitrophenyl β -D-cellobioside were synthesized by Lloyd Mackenzie while 2,5-dinitrophenyl β -xylobioside and 2-nitrophenyl β -xylobioside were prepared by Dr. Lothar Ziser.

All absorbance measurements were recorded on a Unicam UV4 UV/Vis spectrophotometer equipped with a circulating water bath.

5.2.2 Steady state kinetics

Michaelis-Menten parameters for aryl glycosides were determined by continuous measurement of the release of the substituted phenol product using a Unicam UV4 spectrophotometer as described previously (21). Reactions were monitored at appropriate wavelengths using the extinction coefficients given in Table 5.5. Phenol pK_a values used were those reported in Kempton and Withers (21). The buffer used for Cex was 50 mM sodium phosphate buffer, pH 7.00, containing 0.1% w/v bovine serum albumin (BSA) at 37°C. The kinetic studies for Bcx were performed at 40°C in 20 mM MES, pH 6.00, containing 50 mM NaCl and 0.1% w/v BSA. Concentrations of aryl glycosides were confirmed by total hydrolysis of the glycoside and determination of the final concentration of phenol released. Initial rates of enzyme-catalyzed hydrolysis of aryl glycosides were determined by incubating solutions of the appropriate substrate concentrations in 1 cm cuvettes within the spectrophotometer until thermally equilibrated. Reactions were initiated by the addition of enzyme, and the release of phenol product was monitored at the appropriate wavelength. In order to ensure linear

kinetics and to obtain a sufficient absorbance change for accurate calculation of the rates, the concentration of enzyme added and the length of time that the reaction was monitored was selected such that less than 10% of the total substrate was converted to product.

Enzyme-catalyzed hydrolysis for each substrate was measured at 8 to 10 different substrate concentrations ranging from about $0.1 K_m$ to $7 K_m$, where practical. Values for K_m and k_{cat} were determined from the initial rates of hydrolysis (V_0) versus substrate concentration by non-linear regression analysis using the computer program GraFit 4.0 (131). In cases where significant transglycosylation was observed a non-linear regression was performed on data from 0.1 to approximately 2 times K_m . The values of k_{cat} and K_m so obtained were then compared to those determined from linear regression of the reciprocal data as plotted according to Lineweaver-Burke. In almost all cases the kinetic constants K_m , V_{max} , and k_{cat} were calculated from a fit to the Michaelis-Menten equation. For those mutants with very high K_m values, thus for which saturation behavior could not be observed, an accurate value of k_{cat}/K_m was obtained from the slope of the Lineweaver-Burk plot, and very approximate estimates of the individual parameters were obtained from the intercepts.

In addition, the second-order rate constants (k_{cat}/K_m) were determined from progress curves at low substrate concentrations as described in section 5.2.4 on page 192. The individual contribution of each substrate hydroxyl group to transition-state stabilization with the wild-type enzyme was determined from the relation $\Delta\Delta G^\ddagger = -RT \ln \left((k_{cat}/K_m)_x / (k_{cat}/K_m)_y \right)$, where x represents a substrate analogue or mutant enzyme and y the parent substrate or wild-type enzyme.

5.2.3 pH stability studies

Enzyme stabilities over the assay time of the pH dependence studies were examined by incubating enzyme in 50 mM sodium phosphate buffer containing 0.1% w/v BSA at extreme pH values of 3.5, 4.0 and 10.0. The components of the pH incubation mixture are given in Table 5.2.

Table 5.2: pH Incubation mixture for enzyme stability studies.

Enzyme	Total Assay Volume (μL)	BSA Volume (μL)	Enzyme Volume (μL)	Buffer Volume (μL)	Stock [E] (mg/mL)
WT	300	30	10	260	2.00
E43A	200	20	10	170	2.48
N44A	500	50	10	440	3.00
K47A	200	20	20	160	1.91
H80A	100	10	20	70	1.46
H80N	100	10	20	70	1.49
H80Q	100	10	20	70	1.19
Q87M	300	30	10	260	2.13
Q87Y	300	30	10	260	2.18
N169A	300	30	20	250	2.58
N126A	100	10	20	70	2.90

At various time intervals, aliquots of the mixture were removed and injected into another preincubated solution of 2,4DNPC in 50 mM sodium phosphate buffer (pH 7.00) containing 0.1% w/v BSA (Table 5.3). The half-lives were determined by nonlinear analysis of the residual activity as a function of time of incubation. In all cases, no more than 10% enzyme death had occurred over a period of 1 hour. Subsequent determinations of k_{cat} and K_m were then only made at pH values at which the enzyme was stable (>95% activity retained) over a 5 minute period.

Table 5.3: Standard assay conditions for enzyme stability.

Enzyme	Total Assay Volume (μL)	[2,4DNPC] (mM)	Enzyme Volume (μL)	Final [E] (mg/mL)
WT	800	0.076	10	8.33×10^{-04}
E43A	800	0.22	10	1.55×10^{-03}
N44A	800	0.076	10	7.50×10^{-04}
K47A	800	0.55	20	4.78×10^{-03}
H80A	200	0.022	20	2.92×10^{-02}
H80N	200	0.022	20	2.98×10^{-02}
H80Q	200	0.022	20	2.38×10^{-02}
Q87M	800	0.055	10	8.88×10^{-04}
Q87Y	800	0.11	10	9.08×10^{-04}
N169A	800	0.055	10	2.15×10^{-03}
N126A	800	0.055	20	1.45×10^{-02}

5.2.4 pH dependence studies

The dependence of k_{cat}/K_m on pH for wild-type Cex and mutants was determined as follows. Appropriate substrate at a concentration of less than less than $1/5 K_m$ in the appropriate buffer containing 0.1% w/v BSA and 150 mM NaCl was incubated at 37°C until thermally equilibrated (Table 5.4). Following the addition of 10 μL enzyme, the release of 2,4-dinitrophenolate was monitored by following the absorbance at 400 nm until substrate depletion was observed. The change in absorbance with respect to time was fitted to a first-order rate equation using the program GraFit that yielded pseudo first-order rate constants at each pH value. At low substrate concentrations, the reaction rates are given by the equation:

$$V = \left(\frac{k_{\text{cat}}}{K_m} \right) [E]_0 [S]$$

Thus, pseudo first-order rate constants measured correspond to $[E]_0 \left(\frac{k_{\text{cat}}}{K_m} \right)$, from which k_{cat}/K_m is easily obtained. The pH of each reaction mixture was measured after completion of reaction to ensure that the pH had not fluctuated during the reaction.

Table 5.4: Standard assay conditions for pH profiles.

Enzyme	Substrate	Assay [S] (mM)	Total Assay Volume (μL)	Assay [E] (mM)
WT	2,4DNPC	0.0109	800	5.24×10^{-05}
E43A	2,4DNPC	0.0109	800	6.50×10^{-04}
N44A	2,4DNPC	0.0109	800	7.86×10^{-05}
K47A	2,5DNPX ₂	0.0422	800	5.01×10^{-05}
H80A	PNPX ₂	0.0586	200	1.48×10^{-03}
H80N	PNPX ₂	0.0293	200	1.51×10^{-03}
H80Q	PNPX ₂	0.0293	200	1.20×10^{-03}

5.2.5 Kinetics of inhibition

K_i values for inhibitors were determined by estimating an approximate K_i value by using a “range-finding” assay at a fixed substrate concentration with a range of inhibitor concentrations (6-10), which encompassed the K_i value ultimately determined, generally from 0.3 to 3 K_i . The observed rates were plotted in the form of a Dixon plot and the K_i value was determined (assuming competitive inhibition) by an intersection of this line with a horizontal line drawn through $1/V_{\text{max}}$. All reactions were performed at 37°C in 50 mM sodium phosphate buffer (pH 7.00) containing 0.1% w/v BSA. A full K_i determination was then carried out at a series of six different substrate concentrations bracketing the K_i value with each of five inhibitor concentrations bracketing the

approximate K_i value. The nonlinear regression analysis program GraFit 4.0 (131) was used for fitting of all such data.

The pH dependence for inhibition was determined via the substrate depletion method, with substrate present at less than $1/5 K_m$. The inhibition constant of the enzyme-inhibitor complex, K_i , was calculated from the effect of the inhibitor on the ratio of the two steady-state parameters:

$$\left(\frac{K_m}{k_{cat}} \right)_{app} = \left(\frac{K_m}{k_{cat}} \right) \left(1 + \frac{[I]}{K_i} \right)$$

At each pH, appropriate substrate at a concentration of less than $1/5 K_m$ in the appropriate buffer containing 0.1% w/v BSA and 150 mM NaCl and a range of inhibitor concentrations was incubated at 37°C. The reaction was initiated upon addition of enzyme, and the substrate was depleted to obtain k_{obs} . The parameter K_m/k_{cat} was determined conveniently under first-order conditions ($[S] \ll K_m$). The first-order rate

constants $\left(\frac{k_{cat}}{K_m} \right)_{app}$ were evaluated graphically from a plot of absorbance versus time.

The absorbance was monitored at a wavelength that gave a convenient absorbance change. The K_i value was obtained from plot of $\left(\frac{K_m}{k_{cat}} \right)_{app}$ versus $[I]$. To obtain a pH dependence for inhibition, $1/K_i$ versus pH was plotted.

5.2.6 pK_a determinations for inhibitors

All pH determinations were carried out using a Radiometer PHM 82 pH meter equipped with an Orion 8103 Ross pH electrode. Dilute solutions of the inhibitors were prepared in deionized water at room temperature. The amine solution (100 μ L) was acidified by addition of 2-3 μ L of HCl. The solution was then back-titrated by addition of 1 μ L aliquots of NaOH using a micrometer burette (Gilmont[®] Instruments). The pH after each addition was recorded and fit to a pH titration curve using GraFit 4.0 (131).

5.2.7 Determination of extinction coefficients

Extinction coefficients (ϵ) were measured at 37°C at pH 7.00 in 50 mM sodium phosphate buffer. Phenols and glycosides were dried *in vacuo*, weighed, and dissolved in a known volume of buffer. Absorbance values were taken at an appropriate wavelength for five different concentrations of substrate. Extinction coefficients were determined from Beer's Law:

$$\epsilon = \frac{A}{c \times l}$$

where A is the absorbance at a particular wavelength, c is the concentration of solution (mM) and l is the cell pathlength (1 cm).

To convert the observed rate of change of absorbance ($\Delta A/\text{min}$) to rate of phenol release (mM/min), the extinction coefficient difference ($\Delta\epsilon$) between the phenol and the glycoside was used:

$$V_0 = \frac{\Delta A / \text{min}}{\Delta \epsilon}$$

It should be noted that $\epsilon_{\text{glycoside}}$ values were negligible.

Table 5.5: Extinction coefficients of substituted phenols at 37°C in sodium phosphate buffer, pH 7.00.

Phenol Substituent	Wavelength Monitored (nm)	ϵ_{phenol} ($\text{mM}^{-1}\text{cm}^{-1}$)	$\epsilon_{\text{glycoside}}$ ($\text{mM}^{-1}\text{cm}^{-1}$)	$\Delta \epsilon$ ($\text{mM}^{-1}\text{cm}^{-1}$)
2,4-Dinitro	400	11.40	0.00	11.40
2,5-Dinitro	440	4.10	0.00	4.10
4-Nitro	400	9.42	0.00	9.42
2-Nitro	400	2.36	0.00	2.36

REFERENCES

References

1. Wolfenden, R., Lu, X., and Young, G. (1998) Spontaneous hydrolysis of glycosides. *J. Am. Chem. Soc.* 120, 6814-6815.
2. Davies, G. J., Wilson, K. S., and Henrissat, B. (1997) Nomenclature for sugar-binding subsites in glycosyl hydrolases. *Biochem. J.* 321, 557-559.
3. Henrissat, B., Callebaut, I., Fabrega, S., Lehn, P., Mornon, J.-P., and Davies, G. (1995) Conserved catalytic machinery and the prediction of a common fold for several families of glycosyl hydrolases. *Proc. Natl. Acad. Sci. USA.* 92, 7090-7094.
4. Henrissat, B., and Bairoch, A. (1996) Updating the sequence-based classification of glycosyl hydrolases. *Biochem. J.* 316, 695-696.
5. Henrissat, B., and Davies, G. (1997) Structural and sequence-based classification of glycoside hydrolases. *Curr. Opin. Struct. Biol.* 7, 637-644.
6. Davies, G. J., Gloster, T. M., and Henrissat, B. (2005) Recent structural insights into the expanding world of carbohydrate-active enzymes. *Curr. Opin. Struct. Biol.* 15, 637-645.
7. Sinnott, M. L. (1990) Catalytic mechanism of enzymic glycosyl transfer. *Chem. Rev.* 90, 1171-1202.
8. Koshland, D. E. (1953) Stereochemistry and mechanism of enzymatic reactions. *Biol. Rev.* 28, 416-436.
9. McCarter, J. D., and Withers, S. G. (1994) Mechanisms of enzymatic glycoside hydrolysis. *Curr. Opin. Struct. Biol.* 4, 885-892.
10. Zechel, D. L., and Withers, S. G. (1999) Glycosyl transferase mechanisms, in *Comprehensive Natural Products Chemistry* (Poulter, C. D., Ed.) ed., pp 279-314, Pergamon, Amsterdam.
11. Mark, B. L., Vocadlo, D. J., Knapp, S., Triggs-Raine, B. L., Withers, S. G., and James, M. N. G. (2001) Crystallographic evidence for substrate-assisted catalysis in a bacterial β -hexosaminidase. *J. Biol. Chem.* 276, 10330-10337.

12. Markovic-Housley, Z., Miglierini, G., Soldatova, L., Rizkallah, P. J., Müller, U., and Schirmer, T. (2000) Crystal structure of hyaluronidase, a major allergen of bee venom. *Structure*. 8, 1025-1035.
13. Rye, C. S., and Withers, S. G. (2000) Glycosidase mechanisms. *Curr. Opin. Chem. Biol.* 4, 573-589.
14. Zechel, D. L., and Withers, S. G. (2001) Dissection of nucleophilic and acid-base catalysis in glycosidases. *Curr. Opin. Chem. Biol.* 5, 643-649.
15. Vasella, A., Davies, G. J., and Böhm, M. (2002) Glycosidase mechanisms. *Curr. Opin. Chem. Biol.* 6, 619-629.
16. Withers, S. G. (2001) Mechanisms of glycosyl transferases and hydrolases. *Carbohydr. Polym.* 44, 325-337.
17. Zechel, D. L., and Withers, S. G. (2000) Glycosidase mechanisms: anatomy of a finely tuned catalyst. *Acc. Chem. Res.* 33, 11-18.
18. Namchuk, M. N., McCarter, J. D., Becalski, A., Andrews, T., and Withers, S. G. (2000) The role of sugar substituents in glycoside hydrolysis. *J. Am. Chem. Soc.* 122, 1270-1277.
19. Heightman, T. D., and Vasella, A. T. (1999) Recent insights into inhibition, structure, and mechanism of configuration-retaining glycosidases. *Angew. Chem. Int. Ed.* 38, 750-770.
20. Sinnott, M. L., and Withers, S. G. (1974) The β -galactosidase-catalysed hydrolyses of β -D-galactopyranosyl pyridium salts. Rate-limiting generation of an enzyme-bound galactopyranosyl cation in a process dependent only on aglycone acidity. *Biochem. J.* 143, 751-762.
21. Kempton, J. B., and Withers, S. G. (1992) Mechanism of *Agrobacterium* β -glucosidase: kinetic studies. *Biochemistry*. 31, 9961-9969.
22. Tull, D., and Withers, S. G. (1994) Mechanisms of cellulases and xylanases: a detailed kinetic study of the exo- β -1,4-glycanase from *Cellulomonas fimi*. *Biochemistry*. 33, 6363-6370.
23. Sinnott, M. L. (1978) Ions, ion-pairs and catalysis by the *lacZ* β -galactosidase of *Escherichia coli*. *FEBS Lett.* 94, 1-9.

24. Huang, X., Surry, C., Hiebert, T., and Bennet, A. J. (1995) Hydrolysis of (2-deoxy- β -D-glucopyranosyl)pyridinium salts. *J. Am. Chem. Soc.* 117, 10614-10621.
25. Withers, S., Rupitz, K., and Street, I. (1988) 2-Deoxy-2-fluoro-D-glycosyl fluorides. A new class of specific mechanism-based glycosidase inhibitors. *J. Biol. Chem.* 263, 7929-7932.
26. Withers, S. G., and Street, I. P. (1988) Identification of a covalent α -D-glucopyranosyl enzyme intermediate formed on a β -glucosidase. *J. Am. Chem. Soc.* 110, 8551-8553.
27. McCarter, J. D., Adam, M. J., and Withers, S. G. (1992) Binding energy and catalysis. Fluorinated and deoxygenated glycosides as mechanistic probes of *Escherichia coli* (*lacZ*) β -galactosidase. *Biochem. J.* 286, 721-727.
28. Namchuk, M. N., and Withers, S. G. (1995) Mechanism of *Agrobacterium* β -glucosidase: kinetic analysis of the role of noncovalent enzyme/substrate interactions. *Biochemistry.* 34, 16194-16202.
29. Wolfenden, R., and Kati, W. M. (1991) Testing the limits of protein-ligand binding discrimination with transition-state analogue inhibitors. *Acc. Chem. Res.* 24, 209-215.
30. Braun, C., Brayer, G. D., and Withers, S. G. (1995) Mechanism-based inhibition of yeast α -glucosidase and human pancreatic α -amylase by a new class of inhibitors: 2-deoxy-2,2-difluoro- α -glycosides. *J. Biol. Chem.* 270, 26778-26781.
31. McCarter, J. D., and Withers, S. G. (1996) 5-Fluoro glycosidases: a new class of mechanism-based inhibitors of both α - and β -glucosidases. *J. Am. Chem. Soc.* 118, 241-242.
32. White, A., Tull, D., Johns, K., Withers, S. G., and Rose, D. R. (1996) Crystallographic observation of a covalent catalytic intermediate in a β -glycosidase. *Nat. Struct. Biol.* 3, 149-154.

33. Notenboom, V., Birsan, C., Nitz, M., Rose, D. R., Warren, R. A. J., and Withers, S. G. (1998) Insights into transition state stabilization of the β -1,4-glycosidase Cex by covalent intermediate accumulation in active site mutants. *Nat. Struct. Biol.* 5, 812-818.
34. Vocadlo, D. J., Davies, G. J., Laine, R., and Withers, S. G. (2001) Catalysis by hen egg-white lysozyme proceeds via a covalent intermediate. *Nature* 412, 835-838.
35. Tull, D., Miao, S., Withers, S. G., and Aebersold, R. (1995) Identification of derivatized peptides without radiolabels: tandem mass spectrometric localization of the tagged active-site nucleophiles of two cellulases and a β -glucosidase. *Anal. Biochem.* 224, 509-514.
36. Miao, S., Ziser, L., Aebersold, R., and Withers, S. G. (1994) Identification of glutamic acid 78 as the active site nucleophile in *Bacillus subtilis* xylanase using electrospray tandem mass spectrometry. *Biochemistry* 33, 7027-7032.
37. Miao, S., McCarter, J. D., Grace, M. E., Grabowski, G. A., Aebersold, R., and Withers, S. G. (1994) Identification of Glu340 as the active-site nucleophile in human glucocerebrosidase by use of electrospray tandem mass spectrometry. *J. Biol. Chem.* 269, 10975-10978.
38. Wicki, J., Rose, D. R., and Withers, S. G. (2002) Trapping covalent intermediates on β -glycosidases. *Methods Enzymol.* 354, 84-105.
39. Mosi, R. M., and Withers, S. G. (2002) Trapping of α -glycosidase intermediates. *Methods Enzymol.* 354, 64-84.
40. Withers, S. G., and Aebersold, R. (1995) Approaches to labeling and identification of active site residues in glycosidases. *Protein Sci.* 4, 361-372.
41. Street, I. P., Kempton, J. B., and Withers, S. G. (1992) Inactivation of a β -glucosidase through the accumulation of a stable 2-deoxy-2-fluoro- α -D-glucopyranosyl-enzyme intermediate: a detailed investigation. *Biochemistry* 31, 9970-9978.
42. Kuroki, R., Weaver, L. H., and Matthews, B. W. (1999) Structural basis of the conversion of the T4 lysozyme into a transglycosidase by reengineering the active site. *Proc. Natl. Acad. Sci. USA* 96, 8949-8954.

43. Gebler, J. C., Trimbur, D. E., Warren, R. A. J., Aebersold, R., Namchuk, M., and Withers, S. G. (1995) Substrate-induced inactivation of a crippled β -glucosidase mutant: identification of the labeled amino acid and mutagenic analysis of its role. *Biochemistry*. 34, 14547-14553.
44. Lawson, S. L., Wakarchuk, W. W., and Withers, S. G. (1996) Effects of both shortening and lengthening the active site nucleophile of *Bacillus circulans* xylanase on catalytic activity. *Biochemistry*. 35, 10110-10118.
45. Wang, Q., Graham, R. W., Trimbur, D., Warren, R. A. J., and Withers, S. G. (1994) Changing enzymatic reaction mechanisms by mutagenesis: conversion of a retaining glucosidase to an inverting enzyme. *J. Am. Chem. Soc.* 116, 11594-11595.
46. Zechel, D. L., Reid, S. P., Nashiru, O., Mayer, C., Stoll, D., Jakeman, D. L., Warren, R. A. J., and Withers, S. G. (2001) Enzymatic synthesis of carbon-fluorine bonds. *J. Am. Chem. Soc.* 123, 4350-4351.
47. Mackenzie, L. F., Wang, Q., Warren, R. A. J., and Withers, S. G. (1998) Glycosynthases: mutant glycosidases for oligosaccharide synthesis. *J. Am. Chem. Soc.* 120, 5583-5584.
48. Faijes, M., Fairweather, J. K., Driguez, H., and Planas, A. (2001) Oligosaccharide synthesis by coupled *endo*-glycosynthases of different specificity: a straightforward preparation of two mixed-linkage hexasaccharide substrates of 1,3/1,4- β -glucanases. *Chemistry*. 7, 4651-4655.
49. Fort, S., Boyer, V., Greffe, L., Davies, G. J., Moroz, O., Christiansen, L., Schülein, M., Cottaz, S., and Driguez, H. (2000) Highly efficient synthesis of β (1 \rightarrow 4)-oligo- and -polysaccharides using mutant cellulases. *J. Am. Chem. Soc.* 122, 5429-5437.
50. Trincone, A., Perugino, G., Rossi, M., and Moracci, M. (2000) A novel thermophilic glycosynthase that affects branching glycosylation. *Bioorg. Med. Chem. Lett.* 10, 365-368.

51. Notenboom, V., Williams, S. J., Hoos, R., Withers, S. G., and Rose, D. R. (2000) Detailed structural analysis of glycosidase/inhibitor interactions: complexes of Cex from *Cellulomonas fimi* with xylobiose-derived aza-sugars. *Biochemistry*. 39, 11553-11563.
52. Williams, S. J., Hoos, R., and Withers, S. G. (2000) Nanomolar versus millimolar inhibition by xylobiose-derived azasugars: significant differences between two structurally distinct xylanases. *J. Am. Chem. Soc.* 122, 2223-2235.
53. Wang, Q., Trimbur, D., Graham, R., Warren, R. A. J., and Withers, S. G. (1995) Identification of the acid/base catalyst in *Agrobacterium faecalis* β -glucosidase by kinetic analysis of mutants. *Biochemistry*. 34, 14554-14562.
54. Lawson, S. L., Wakarchuk, W. W., and Withers, S. G. (1997) Positioning the acid/base catalyst in a glycosidase: studies with *Bacillus circulans* xylanase. *Biochemistry*. 36, 2257-2265.
55. Wang, Q., and Withers, S. G. (1995) Substrate-assisted catalysis in glycosidases. *J. Am. Chem. Soc.* 117, 10137-10138.
56. Fierobe, H.-P., Mirgorodskaya, E., McGuire, K. A., Roepstorff, P., Svensson, B., and Clarke, A. J. (1998) Restoration of catalytic activity beyond wild-type level in glucoamylase from *Aspergillus awamori* by oxidation of the Glu400 \rightarrow Cys catalytic-base mutant to cysteinesulfinic acid. *Biochemistry*. 37, 3743-3752.
57. Fierobe, H.-P., Clarke, A. J., Tull, D., and Svensson, B. (1998) Enzymatic properties of the cysteinesulfinic acid derivative of the catalytic-base mutant Glu400 \rightarrow Cys of glucoamylase from *Aspergillus awamori*. *Biochemistry*. 37, 3753-3759.
58. Roeser, K. R., and Legler, G. (1981) Role of sugar hydroxyl groups in glycoside hydrolysis. Cleavage mechanism of deoxyglucosides and related substrates by β -glucosidase A3 from *Aspergillus wentii*. *Biochim. Biophys. Acta*. 657, 321-333.

59. Wentworth, D. F., and Wolfenden, R. (1974) Slow binding of D-galactal, a "reversible" inhibitor of bacterial β -galactosidase. *Biochemistry*. 13, 4715-4720.
60. Cleland, W. W., Frey, P. A., and Gerlt, J. A. (1998) The low barrier hydrogen bond in enzymatic catalysis. *J. Biol. Chem.* 273, 25529-25532.
61. Davies, G. J., Sinnott, M. L., and Withers, S. G. (1997) *Reactions of electrophilic carbon, phosphorus and sulfur*, in Comprehensive Biological Catalysis (Sinnott, M. L., Ed.) Vol. 1, Academic Press, London.
62. IUPAC-IUB (1980) *Eur. J. Biochem.* 111, 295-298.
63. Davies, G. J., Ducros, V. M., Varrot, A., and Zechel, D. L. (2003) Mapping the conformational itinerary of β -glycosidases by X-ray crystallography. *Biochem. Soc. Trans.* 31, 523-527.
64. Blake, C. C. F., Johnson, L. N., Mair, G. A., North, A. C. T., Phillips, D. C., and Sarma, V. R. (1967) Crystallographic studies of the activity of hen egg-white lysozyme. *Proc. R. Soc. Lond. Ser. B Biol. Sci.* 167, 378-388.
65. Ford, L. O., Johnson, L. N., Machin, P. A., Phillips, D. C., and Tjian, R. (1974) Crystal structure of a lysozyme-tetrasaccharide lactone complex. *J. Mol. Biol.* 88, 349-371.
66. Hadfield, A. T., Harvey, D. J., Archer, D. B., MacKenzie, D. A., Jeenes, D. J., Radford, S. E., Lowe, G., Dobson, C. M., and Johnson, L. N. (1994) Crystal structure of the mutant D52S hen egg white lysozyme with an oligosaccharide product. *J. Mol. Biol.* 243, 856-872.
67. Strynadka, N. C., and James, M. N. (1991) Lysozyme revisited: crystallographic evidence for distortion of an *N*-acetylmuramic acid residue bound in site D. *J. Mol. Biol.* 220, 401-424.
68. Kuroki, R., Weaver, L. H., and Matthews, B. W. (1993) A covalent enzyme-substrate intermediate with saccharide distortion in a mutant T4 lysozyme. *Science*. 262, 2030-2033.
69. Varrot, A., Schülein, M., and Davies, G. J. (2000) Insights into ligand-induced conformational change in Cel5A from *Bacillus agaradhaerens* revealed by a catalytically active crystal form. *J. Mol. Biol.* 297, 819-828.

70. Davies, G. J., Mackenzie, L., Varrot, A., Dauter, M., Brzozowski, A. M., Schülein, M., and Withers, S. G. (1998) Snapshots along an enzymatic reaction coordinate: analysis of a retaining β -glycoside hydrolase. *Biochemistry*. 37, 11707-11713.
71. Sulzenbacher, G., Driguez, H., Henrissat, B., Schülein, M., and Davies, G. J. (1996) Structure of the *Fusarium oxysporum* endoglucanase I with a nonhydrolyzable substrate analogue: substrate distortion gives rise to the preferred axial orientation for the leaving group. *Biochemistry*. 35, 15280-15287.
72. Sulzenbacher, G., Schülein, M., and Davies, G. J. (1997) Structure of the endoglucanase I from *Fusarium oxysporum*: native, cellobiose, and 3,4-epoxybutyl β -D-cellobioside-inhibited forms, at 2.3 Å resolution. *Biochemistry*. 36, 5902-5911.
73. Tews, I., Perrakis, A., Oppenheim, A., Dauter, Z., Wilson, K. S., and Vorgias, C. E. (1996) Bacterial chitinase structure provides insight into catalytic mechanism and the basis of Tay-Sachs disease. *Nat. Struct. Biol.* 3, 638-648.
74. Juers, D. H., Heightman, T. D., Vasella, A., McCarter, J. D., Mackenzie, L., Withers, S. G., and Matthews, B. W. (2001) A structural view of the action of *Escherichia coli* (*lacZ*) β -galactosidase. *Biochemistry*. 40, 14781-14794.
75. Sulzenbacher, G., Mackenzie, L. F., Wilson, K. S., Withers, S. G., Dupont, C., and Davies, G. J. (1999) The crystal structure of a 2-fluorocellotriosyl complex of the *Streptomyces lividans* endoglucanase CelB2 at 1.2 Å resolution. *Biochemistry*. 38, 4826-4833.
76. Notenboom, V., Birsan, C., Warren, R. A. J., Withers, S. G., and Rose, D. R. (1998) Exploring the cellulose/xylan specificity of the β -1,4-glycanase Cex from *Cellulomonas fimi* through crystallography and mutation. *Biochemistry*. 37, 4751-4758.

77. Mackenzie, L. F., Sulzenbacher, G., Divne, C., Jones, T. A., Wöldike, H. F., Schülein, M., Withers, S. G., and Davies, G. J. (1998) Crystal structure of the family 7 endoglucanase I (Cel7B) from *Humicola insolens* at 2.2 Å resolution and identification of the catalytic nucleophile by trapping of the covalent glycosyl-enzyme intermediate. *Biochem. J.* 335, 409-416.
78. Stoddart, J. F. (1971) *Stereochemistry of Carbohydrates*, in Stereochemistry of Carbohydrates John Wiley and Sons, New York.
79. Sabini, E., Sulzenbacher, G., Dauter, M., Dauter, Z., Jørgensen, P. L., Schülein, M., Dupont, C., Davies, G. J., and Wilson, K. S. (1999) Catalysis and specificity in enzymatic glycoside hydrolysis: a $2,5B$ conformation for the glycosyl-enzyme intermediate revealed by the structure of the *Bacillus agaradhaerens* family 11 xylanase. *Chem. Biol.* 6, 483-492.
80. Sabini, E., Wilson, K. S., Danielsen, S., Schülein, M., and Davies, G. J. (2001) Oligosaccharide binding to family 11 xylanases: both covalent intermediate and mutant product complexes display $2,5B$ conformations at the active center. *Acta Crystallogr. Sect. D Biol. Cryst.* 57, 1344-1347.
81. Sidhu, G., Withers, S. G., Nguyen, N. T., McIntosh, L. P., Ziser, L., and Brayer, G. D. (1999) Sugar ring distortion in the glycosyl-enzyme intermediate of a family G/11 xylanase. *Biochemistry.* 38, 5346-5354.
82. Ducros, V. M., Zechel, D. L., Murshudov, G. N., Gilbert, H. J., Szabó, L., Stoll, D., Withers, S. G., and Davies, G. J. (2002) Substrate distortion by a β -mannanase: snapshots of the Michaelis and covalent-intermediate complexes suggest a $B_{2,5}$ conformation for the transition state. *Angew. Chem. Int. Ed. Engl.* 41, 2824-2827.
83. Numao, S., Kuntz, D. A., Withers, S. G., and Rose, D. R. (2003) Insights into the mechanism of *Drosophila melanogaster* Golgi α -mannosidase II through the structural analysis of covalent reaction intermediates. *J. Biol. Chem.* 278, 48074-48083.
84. Deslongchamps, P. (1983) *Stereoelectric Effects in Organic Chemistry*, in Organic Chemistry Pergamon Press, Oxford.

85. Kirby, A. J. (1984) Stereoelectronic effects on acetal hydrolysis. *Acc. Chem. Res.* 17, 305-311.
86. Kulkarni, N., Shendye, A., and Rao, M. (1999) Molecular and biotechnological aspects of xylanases. *FEMS Microbiol. Rev.* 23, 411-456.
87. Subramaniyan, S., and Prema, P. (2002) Biotechnology of microbial xylanases: enzymology, molecular biology, and application. *Crit. Rev. Biotechnol.* 22, 33-64.
88. Cleemput, G., Hessing, M., Oort, M. v., Deconynck, M., and Delcour, J. A. (1997) Purification and characterization of a β -D-xylosidase and an endo-xylanase from wheat flour. *Plant Physiol.* 113, 377-386.
89. Shallom, D., and Shoham, Y. (2003) Microbial hemicellulases. *Curr. Opin. Microbiol.* 6, 219-228.
90. Beg, Q. K., Kapoor, M., Mahajan, L., and Hoondal, G. S. (2001) Microbial xylanases and their industrial applications: a review. *Appl. Microbiol. Biotechnol.* 56, 326-338.
91. Bissoon, S., Christov, L., and Singh, S. (2002) Bleach boosting effects of purified xylanase from *Thermomyces lanuginosus* SSBP on bagasse pulp. *Process Biochem.* 37, 567-572.
92. Malathi, V., and Devegowda, G. (2001) In vitro evaluation of nonstarch polysaccharide digestibility of feed ingredients by enzymes. *Poult. Sci.* 80, 302-305.
93. Mathlouthi, N., Saulnier, L., Quemener, B., and Larbier, M. (2002) Xylanase, β -glucanase, and other side enzymatic activities have greater effects on the viscosity of several feedstuffs than xylanase and β -glucanase used alone or in combination. *J. Agric. Food Chem.* 50, 5121-5127.
94. Wong, K. K., Tan, L. U., and Saddler, J. N. (1988) Multiplicity of β -1,4-xylanase in microorganisms: functions and applications. *Microbiol. Rev.* 52, 305-317.
95. Lynd, L. R., Cushman, J. H., Nichols, R. J., and Wyman, C. E. (1991) Fuel ethanol from cellulosic biomass. *Science.* 251, 1318-1323.

96. Harbak, L., and Thygesen, H. V. (2002) Safety evaluation of a xylanase expressed in *Bacillus subtilis*. *Food Chem. Toxicol.* 40, 1-8.
97. Courtin, C. M., Roelants, A., and Delcour, J. A. (1999) Fractionation-reconstitution experiments provide insight into the role of endoxylanases in bread-making. *J. Agric. Food Chem.* 47, 1870-1877.
98. Ingelbrecht, J. A., Verwimp, T., and Delcour, J. A. (2000) Endoxylanases in durum wheat semolina processing: solubilization of arabinoxylans, action of endogenous inhibitors, and effects on rheological properties. *J. Agric. Food Chem.* 48, 2017-2022.
99. Figueroa-Espinoza, M. C., Poulsen, C., S  , J. B., Zargahi, M. R., and Rouau, X. (2002) Enzymatic solubilization of arabinoxylans from isolated rye pentosans and rye flour by different *endo*-xylanases and other hydrolyzing enzymes. Effect of a fungal laccase on the flour extracts oxidative gelation. *J. Agric. Food Chem.* 50, 6473-6484.
100. Mielenz, J. R. (2001) Ethanol production from biomass: technology and commercialization status. *Curr. Opin. Microbiol.* 4, 324-329.
101. Galbe, M., and Zacchi, G. (2002) A review of the production of ethanol from softwood. *Appl. Microbiol. Biotechnol.* 59, 618-628.
102. Chandrakant, P., and Bisaria, V. S. (1998) Simultaneous bioconversion of cellulose and hemicellulose to ethanol. *Crit. Rev. Biotechnol.* 18, 295-331.
103. Sommer, P., Georgieva, T., and Ahring, B. K. (2004) Potential for using thermophilic anaerobic bacteria for bioethanol production from hemicellulose. *Biochem. Soc. Trans.* 32, 283-289.
104. O'Neill, G. P., Goh, S. H., Warren, R. A. J., Kilburn, D. G., and R. C. Miller, J. (1986) Structure of the gene encoding the exoglucanase of *Cellulomonas fimi*. *Gene.* 44, 325-330.
105. MacLeod, A. M., Lindhorst, T., Withers, S. G., and Warren, R. A. J. (1994) The acid/base catalyst in the exoglucanase/xylanase from *Cellulomonas fimi* is glutamic acid 127: evidence from detailed kinetic studies of mutants. *Biochemistry.* 33, 6371-6376.

106. Gilkes, N. R., Henrissat, B., Kilburn, D. G., R. C. Miller, J., and Warren, R. A. J. (1991) Domains in microbial β -1,4-glycanases: sequence conservation, function, and enzyme families. *Microbiol. Rev.* 55, 303-315.
107. Withers, S. G., Dombroski, D., Berven, L. A., Kilburn, D. G., Jr, R. C. M., Warren, R. A., and Gilkes, N. R. (1986) Direct ^1H n.m.r. determination of the stereochemical course of hydrolyses catalysed by glucanase components of the cellulase complex. *Biochem. Biophys. Res. Commun.* 139, 487-494.
108. Tull, D., Withers, S. G., Gilkes, N. R., Kilburn, D. G., Warren, A. J., and Aebersold, R. (1991) Glutamic acid 274 is the nucleophile in the active site of a "retaining" exoglucanase from *Cellulomonas fimi*. *J. Biol. Chem.* 266, 15621-15625.
109. MacLeod, A. M., Tull, D., Rupitz, K., Warren, R. A. J., and Withers, S. G. (1996) Mechanistic consequences of mutation of active site carboxylates in a retaining β -1,4-glycanase from *Cellulomonas fimi*. *Biochemistry.* 35, 13165-13172.
110. Tull, D., Burgoyne, D. L., Chow, D. T., Withers, S. G., and Aebersold, R. (1996) A mass spectrometry-based approach for probing enzyme active sites: identification of Glu 127 in *Cellulomonas fimi* exoglycanase as the residue modified by *N*-bromoacetyl cellobiosylamine. *Anal. Biochem.* 234, 119-125.
111. Ziser, L., Setyawati, I., and Withers, S. G. (1995) Syntheses and testing of substrates and mechanism-based inactivators for xylanases. *Carbohydr. Res.* 274, 137-153.
112. White, A., Withers, S. G., Gilkes, N. R., and Rose, D. R. (1994) Crystal structure of the catalytic domain of the β -1,4-glycanase Cex from *Cellulomonas fimi*. *Biochemistry.* 33, 12546-12552.
113. Sung, W. L., Luk, C. K., Zahab, D. M., and Wakarchuk, W. (1993) Overexpression of the *Bacillus subtilis* and *circulans* xylanases in *Escherichia coli*. *Protein Expr. Purif.* 4, 200-206.

114. Birsan, C., Johnson, P., Joshi, M., MacLeod, A., McIntosh, L., Monem, V., Nitz, M., Rose, D. R., Tull, D., Wakarchuk, W. W., Wang, Q., Warren, R. A., White, A., and Withers, S. G. (1998) Mechanisms of cellulases and xylanases. *Biochem. Soc. Trans.* 26, 156-160.
115. McIntosh, L. P., Hand, G., Johnson, P. E., Joshi, M. D., Körner, M., Plesniak, L. A., Ziser, L., Wakarchuk, W. W., and Withers, S. G. (1996) The pK_a of the general acid/base carboxyl group of a glycosidase cycles during catalysis: a ^{13}C -NMR study of *Bacillus circulans* xylanase. *Biochemistry*. 35, 9958-9966.
116. Joshi, M. D., Hedberg, A., and McIntosh, L. P. (1997) Complete measurement of the pK_a values of the carboxyl and imidazole groups in *Bacillus circulans* xylanase. *Protein Sci.* 6, 2667-2670.
117. Plesniak, L. A., Connelly, G. P., Wakarchuk, W. W., and McIntosh, L. P. (1996) Characterization of a buried neutral histidine residue in *Bacillus circulans* xylanase: NMR assignments, pH titration, and hydrogen exchange. *Protein Sci.* 5, 2319-2328.
118. Joshi, M. D., Sidhu, G., Pot, I., Brayer, G. D., Withers, S. G., and McIntosh, L. P. (2000) Hydrogen bonding and catalysis: a novel explanation for how a single amino acid substitution can change the pH optimum of a glycosidase. *J. Mol. Biol.* 299, 255-279.
119. Wakarchuk, W. W., Campbell, R. L., Sung, W. L., Davoodi, J., and Yaguchi, M. (1994) Mutational and crystallographic analyses of the active site residues of the *Bacillus circulans* xylanase. *Protein Sci.* 3, 467-475.
120. Davies, G., and Henrissat, B. (1995) Structures and mechanisms of glycosyl hydrolases. *Structure*. 3, 853-859.
121. Charnock, S. J., Spurway, T. D., Xie, H., Beylot, M.-H., Virden, R., Warren, R. A. J., Hazlewood, G. P., and Gilbert, H. J. (1998) The topology of the substrate binding clefts of glycosyl hydrolase family 10 xylanases are not conserved. *J. Biol. Chem.* 273, 32187-32199.

122. Harris, G. W., Jenkins, J. A., Connerton, I., Cummings, N., Leggio, L. L., Scott, M., Hazlewood, G. P., Laurie, J. I., Gilbert, H. J., and Pickersgill, R. W. (1994) Structure of the catalytic core of the family F xylanase from *Pseudomonas fluorescens* and identification of the xylopentaose-binding sites. *Structure*. 2, 1107-1116.
123. Derewenda, U., Swenson, L., Green, R., Wei, Y., Morosoli, R., Shareck, F., Kluepfel, D., and Derewenda, Z. S. (1994) Crystal structure, at 2.6-Å resolution, of the *Streptomyces lividans* xylanase A, a member of the F family of β -1,4-D-glycanases. *J. Biol. Chem.* 269, 20811-20814.
124. Dominguez, R., Souchon, H., Spinelli, S., Dauter, Z., Wilson, K. S., Chauvaux, S., Beguin, P., and Alzari, P. M. (1995) A common protein fold and similar active site in two distinct families of β -glycanases. *Nat. Struct. Biol.* 2, 569-576.
125. Pell, G., Szabo, L., Charnock, S. J., Xie, H., Gloster, T. M., Davies, G. J., and Gilbert, H. J. (2004) Structural and biochemical analysis of *Cellvibrio japonicus* xylanase 10C: how variation in substrate-binding cleft influences the catalytic profile of family GH-10 xylanases. *J. Biol. Chem.* 279, 11777-11788.
126. Ducros, V., Charnock, S. J., Derewenda, U., Derewenda, Z. S., Dauter, Z., Dupont, C., Shareck, F., Morosoli, R., Kluepfel, D., and Davies, G. J. (2000) Substrate specificity in glycoside hydrolase family 10. Structural and kinetic analysis of the *Streptomyces lividans* xylanase 10A. *J. Biol. Chem.* 275, 23020-23026.
127. Xie, H., Flint, J., Vardakou, M., Lakey, J. H., Lewis, R. J., Gilbert, H. J., and Dumon, C. (2006) Probing the structural basis for the difference in thermostability displayed by family 10 xylanases. *J. Mol. Biol.* 360, 157-167.
128. Vardakou, M., Flint, J., Christakopoulos, P., Lewis, R. J., Gilbert, H. J., and Murray, J. W. (2005) A family 10 *Thermoascus aurantiacus* xylanase utilizes arabinose decorations of xylan as significant substrate specificity determinants. *J. Mol. Biol.* 352, 1060-1067.

129. Payan, F., Leone, P., Porciero, S., Furniss, C., Tahir, T., Williamson, G., Durand, A., Manzanares, P., Gilbert, H. J., Juge, N., and Roussel, A. (2004) The dual nature of the wheat xylanase protein inhibitor XIP-I: structural basis for the inhibition of family 10 and family 11 xylanases. *J. Biol. Chem.* 279, 36029-36037.
130. Renard, M., and Fersht, A. R. (1973) Anomalous pH dependence of k_{cat}/K_M in enzyme reactions. Rate constants for the association of chymotrypsin with substrates. *Biochemistry.* 12, 4713-4718.
131. Leatherbarrow, R. J. (1989) Erithacus Software Limited,
132. Gilkes, N. R., Langsford, M. L., Kilburn, D. G., Robert C. Miller, J., and Warren, R. A. J. (1984) Mode of action and substrate specificities of cellulases from cloned bacterial genes. *J. Biol. Chem.* 259, 10455-10459.
133. Charnock, S. J., Lakey, J. H., Virden, R., Hughes, N., Sinnott, M. L., Hazlewood, G. P., Pickersgill, R., and Gilbert, H. J. (1997) Key residues in subsite F play a critical role in the activity of *Pseudomonas fluorescens* subspecies *cellulosa* xylanase A against xylooligosaccharides but not against highly polymeric substrates such as xylan. *J. Biol. Chem.* 272, 2942-2951.
134. Cleland, W. W. (1975) What limits the rate of an enzyme-catalyzed reaction? *Acc. Chem. Res.* 8, 145-151.
135. Albery, W. J., and Knowles, J. R. (1976) Evolution of enzyme function and the development of catalytic efficiency. *Biochemistry.* 15, 5631-5640.
136. Fersht, A. (1999) *Structure and mechanism in protein science: a guide to enzyme catalysis and protein folding*, in W. H. Freeman and Company, New York.
137. Dale, M. P., Kopfler, W. P., Chait, I., and Byers, L. D. (1986) β -Glucosidase: substrate, solvent, and viscosity variation as probes of the rate-limiting steps. *Biochemistry.* 25, 2522-2529.
138. Moreau, A., Roberge, M., Manin, C., Shareck, F., Kluepfel, D., and Morosoli, R. (1994) Identification of two acidic residues involved in the catalysis of xylanase A from *Streptomyces lividans*. *Biochem. J.* 302, 291-295.

139. Knowles, J. R. (1976) The intrinsic pK_a -values of functional groups in enzymes: improper deductions from the pH-dependence of steady-state parameters. *Crit. Rev. Biochem.* 4, 165-173.
140. Biely, P., Kratky, Z., and Vršanská, M. (1981) Substrate-binding site of endo-1,4- β -xylanase of the yeast *Cryptococcus albidus*. *Eur. J. Biochem.* 119, 559-564.
141. Moreau, A., Shareck, F., Kluepfel, D., and Morosoli, R. (1994) Alteration of the cleavage mode and of the transglycosylation reactions of the xylanase A of *Streptomyces lividans* 1326 by site-directed mutagenesis of the Asn173 residue. *Eur. J. Biochem.* 219, 261-266.
142. Fersht, A. R. (1984) Basis of biological specificity. *Trends Biochem. Sci.* 9, 145-147.
143. Bourne, Y., Tilbeurgh, H. v., and Cambillau, C. (1993) Protein-carbohydrate interactions. *Curr. Opin. Struct. Biol.* 3, 681-686.
144. Bundle, D. R., and Young, N. M. (1992) Carbohydrate-protein interactions in antibodies and lectins. *Curr. Opin. Struct. Biol.* 2, 666-673.
145. Quijcho, F. A. (1993) Probing the atomic interactions between proteins and carbohydrates. *Biochem. Soc. Trans.* 21, 442-448.
146. Vyas, N. K. (1991) Atomic features of protein-carbohydrate interactions. *Curr. Opin. Struct. Biol.* 1, 732-740.
147. Pauling, L. (1946) *Chem. Eng. News.* 24, 1375.
148. Williams, S. J., and Davies, G. J. (2001) Protein-carbohydrate interactions: learning lessons from nature. *Trends Biotechnol.* 19, 356-362.
149. Gloster, T. M., Roberts, S., Dücros, V. M.-A., Perugino, G., Rossi, M., Hoos, R., Moracci, M., Vasella, A., and Davies, G. J. (2004) Structural studies of the β -glycosidase from *Sulfolobus solfataricus* in complex with covalently and noncovalently bound inhibitors. *Biochemistry.* 43, 6101-6109.
150. Varrot, A., and Davies, G. J. (2003) Direct experimental observation of the hydrogen-bonding network of a glycosidase along its reaction coordinate revealed by atomic resolution analyses of endoglucanase Cel5A. *Acta Crystallogr. D Biol. Crystallogr.* 59, 447-452.

151. Fersht, A. R., Shi, J. P., Knill-Jones, J., Lowe, D. M., Wilkinson, A. J., Blow, D. M., Brick, P., Carter, P., Waye, M. M. Y., and Winter, G. (1985) Hydrogen bonding and biological specificity analysed by protein engineering. *Nature*. 314, 235-238.
152. Fersht, A. R. (1987) Dissection of the structure and activity of the tyrosyl-tRNA synthetase by site-directed mutagenesis. *Biochemistry*. 26, 8031-8037.
153. Sierks, M. R., and Svensson, B. (2000) Energetic and mechanistic studies of glucoamylase using molecular recognition of maltose OH groups coupled with site-directed mutagenesis. *Biochemistry*. 39, 8585-8592.
154. Frandsen, T. P., Stoffer, B. B., Palcic, M. M., Hof, S., and Svensson, B. (1996) Structure and energetics of the glucoamylase-isomaltose transition-state complex probed by using modeling and deoxygenated substrates coupled with site-directed mutagenesis. *J. Mol. Biol.* 263, 79-89.
155. Piotukh, K., Serra, V., Borriss, R., and Planas, A. (1999) Protein-carbohydrate interactions defining substrate specificity in *Bacillus* 1,3-1,4- β -D-glucan 4-glucanohydrolases as dissected by mutational analysis. *Biochemistry*. 38, 16092-16104.
156. Gaiser, O. J., Piotukh, K., Ponnuswamy, M. N., Planas, A., Borriss, R., and Heinemann, U. (2006) Structural basis for the substrate specificity of a *Bacillus* 1,3-1,4- β -glucanase. *J. Mol. Biol.* 357, 1211-1225.
157. Street, I. P., Armstrong, C. R., and Withers, S. G. (1986) Hydrogen bonding and specificity. Fluorodeoxy sugars as probes of hydrogen bonding in the glycogen phosphorylase-glucose complex. *Biochemistry*. 25, 6021-6027.
158. Street, I. P., Rupitz, K., and Withers, S. G. (1989) Fluorinated and deoxygenated substrates as probes of transition-state structure in glycogen phosphorylase. *Biochemistry*. 28, 1581-1587.
159. Percival, M. D., and Withers, S. G. (1992) Binding energy and catalysis: deoxyfluoro sugars as probes of hydrogen bonding in phosphoglucomutase. *Biochemistry*. 31, 498-505.

160. Eis, C., and Nidetzky, B. (2002) Substrate-binding recognition and specificity of trehalose phosphorylase from *Schizophyllum commune* examined in steady-state kinetic studies with deoxy and deoxyfluoro substrate analogues and inhibitors. *Biochem. J.* 363, 335-340.
161. Jencks, W. P. (1969) *Catalysis in Chemistry and Enzymology*, in *Catalysis in Chemistry and Enzymology* McGraw-Hill, New York.
162. Klotz, I. M., and Franzen, J. S. (1962) Hydrogen bonds between model peptide groups in solution. *J. Am. Chem. Soc.* 84, 3461-3466.
163. Hine, J. (1972) Structural effects on rates and equilibria. Hydrogen-bonded intermediates and stepwise mechanisms for proton-exchange reactions between oxygen atoms in hydroxylic solvents. *J. Am. Chem. Soc.* 94, 5766-5771.
164. West, R., Powell, D. L., Whatley, L. S., Lee, M. K. T., and Schleyer, P. v. R. (1962) The relative strengths of alkyl halides as proton acceptor groups in hydrogen bonding. *J. Am. Chem. Soc.* 84, 3221-3222.
165. Murray-Rust, P., Stallings, W. C., Monti, C. T., Preston, R. K., and Glusker, J. P. (1983) Intermolecular interactions of the carbon-fluorine bond: the crystallographic environment of fluorinated carboxylic acids and related structures. *J. Am. Chem. Soc.* 105, 3206-3214.
166. Harrell, S. A., and McDaniel, D. H. (1964) Strong hydrogen bonds. II. The hydrogen difluoride ion. *J. Am. Chem. Soc.* 86, 4497-4497.
167. Howard, J. A. K., Hoy, V. J., O'Hagan, D., and Smith, G. T. (1996) How good is fluorine as a hydrogen bond acceptor? *Tetrahedron.* 52, 12613-12622.
168. Shimoni, L., and Glusker, J. P. (1994) The geometry of intermolecular interactions in some crystalline fluorine-containing organic compounds. *Struct. Chem.* 5, 383-397.
169. Brammer, L., Bruton, E. A., and Sherwood, P. (2001) Understanding the behavior of halogens as hydrogen bond acceptors. *Cryst. Growth Des.* 1, 277-290.

170. Carosati, E., Sciabola, S., and Cruciani, G. (2004) Hydrogen bonding interactions of covalently bonded fluorine atoms: from crystallographic data to a new angular function in the GRID force field. *J. Med. Chem.* 47, 5114-5125.
171. Withers, S. G., MacLennan, D. J., and Street, I. P. (1986) The synthesis and hydrolysis of a series of deoxyfluoro-D-glucopyranosyl phosphates. *Carbohydr. Res.* 154, 127-144.
172. Withers, S. G., Percival, M. D., and Street, I. P. (1989) The synthesis and hydrolysis of a series of deoxy- and deoxyfluoro- α -D- "glucopyranosyl" phosphates. *Carbohydr. Res.* 173, 43-66.
173. Withers, S. G., Street, I. P., and Rettig, S. J. (1986) The preferred conformation of 2-fluoro-2-deoxy β -D-mannopyranosyl fluoride. An X-ray crystallographic and 2-dimensional proton nuclear magnetic resonance study. *Can. J. Chem.* 64, 232-236.
174. Törrönen, A., and Rouvinen, J. (1997) Structural and functional properties of low molecular weight endo-1,4- β -xylanases. *J. Biotechnol.* 57, 137-149.
175. Damager, I., Numao, S., Chen, H., Brayer, G. D., and Withers, S. G. (2004) Synthesis and characterisation of novel chromogenic substrates for human pancreatic α -amylase. *Carbohydr. Res.* 339, 1727-1737.
176. Burmeister, W. P., Cottaz, S., Driguez, H., Iori, R., Palmieri, S., and Henrissat, B. (1997) The crystal structures of *Sinapis alba* myrosinase and a covalent glycosyl-enzyme intermediate provide insights into the substrate recognition and active-site machinery of an S-glycosidase. *Structure.* 5, 663-675.
177. Sobolev, V., Sorokine, A., Prilusky, J., Abola, E. E., and Edelman, M. (1999) Automated analysis of interatomic contacts in proteins. *Bioinformatics.* 15, 327-332.
178. Withers, S. G., and Rupitz, K. (1990) Measurement of active-site homology between potato and rabbit muscle α -glucan phosphorylases through use of a linear free energy relationship. *Biochemistry.* 29, 6405-6409.

179. Sierks, M. R., Bock, K., Refn, S., and Svensson, B. (1992) Active site similarities of glucose dehydrogenase, glucose oxidase, and glucoamylase probed by deoxygenated substrates. *Biochemistry*. 31, 8972-8977.
180. Henrissat, B. (1991) A classification of glycosyl hydrolases based on amino acid sequence similarities. *Biochem. J.* 280, 309-316.
181. Henrissat, B., and Bairoch, A. (1993) New families in the classification of glycosyl hydrolases based on amino acid sequence similarities. *Biochem. J.* 293, 781-788.
182. Biely, P., Vršanská, M., Tenkanen, M., and Kluepfel, D. (1997) Endo- β -1,4-xylanase families: differences in catalytic properties. *J. Biotech.* 57, 151-166.
183. Williams, S. J., Notenboom, V., Wicki, J., Rose, D. R., and Withers, S. G. (2000) A new, simple, high-affinity glycosidase inhibitor: analysis of binding through X-ray crystallography, mutagenesis, and kinetic analysis. *J. Am. Chem. Soc.* 122, 4229-4230.
184. Poon, D. K. Y., Schubert, M., Au, J., Okon, M., Withers, S. G., and McIntosh, L. P. (2006) Unambiguous determination of the ionization state of a glycoside hydrolase active site lysine by ^1H - ^{15}N heteronuclear correlation spectroscopy. *J. Am. Chem. Soc.* 128, 15388-15389.
185. Schubert, M., Poon, D. K. Y., Wicki, J., Tarling, C. A., Kwan, E. M., Nielsen, J. E., Withers, S. G., and McIntosh, L. P. (2007) Probing electrostatic interactions along the reaction pathway of a glycoside hydrolase: histidine characterization by NMR spectroscopy. *Biochemistry*. submitted,
186. Money, V. A., Smith, N. L., Scaffidi, A., Stick, R. V., Gilbert, H. J., and Davies, G. J. (2006) Substrate distortion by a lichenase highlights the different conformational itineraries harnessed by related glycoside hydrolases. *Angew. Chem. Int. Ed.* 45, 5136-5140.
187. Eyring, H. (1935) The activated complex and the absolute rate of chemical reactions. *Chem. Rev.* 17, 65-77.
188. Wolfenden, R. (1969) Transition state analogues for enzyme catalysis. *Nature*. 223, 704-705.

189. Wolfenden, R. (1972) Analog approaches to the structure of the transition state in enzyme reactions. *Acc. Chem. Res.* 5, 10-18.
190. Wolfenden, R. (1976) Transition-state analog inhibitors and enzyme catalysis. *Annu. Rev. Biophys. Bioeng.* 5, 271-306.
191. Radzicka, A., and Wolfenden, R. (1995) Transition-state and multisubstrate analog inhibitors. *Methods Enzymol.* 249, 284-312.
192. Schramm, V. L. (1998) Enzymatic transition states and transition state analog design. *Annu. Rev. Biochem.* 67, 693-720.
193. Morrison, J. F., and Walsh, C. T. (1988) The behavior and significance of slow-binding enzyme inhibitors. *Adv. Enzymol. Relat. Area Mol. Biol.* 61, 201-301.
194. Mader, M. M., and Bartlett, P. A. (1997) Binding energy and catalysis: the implications for transition-state analogs and catalytic antibodies. *Chem. Rev.* 97, 1281-1302.
195. Schramm, V. L. (2003) Enzymatic transition state poise and transition state analogues. *Acc. Chem. Res.* 36, 588-596.
196. Schramm, V. L. (2005) Enzymatic transition states: thermodynamics, dynamics and analogue design. *Arch. Biochem. Biophys.* 433, 13-26.
197. Cleland, W. W. (1995) Isotope effects: determination of enzyme transition state structure. *Meth. Enzymol.* 249, 341-373.
198. Schramm, V. L. (1999) Enzymatic transition-state analysis and transition-state analogs. *Methods Enzymol.* 308, 301-355.
199. Berti, P. J. (1999) Determining transition states from kinetic isotope effects. *Methods Enzymol.* 308, 355-397.
200. Lewandowicz, A., and Schramm, V. L. (2004) Transition state analysis for human and *Plasmodium falciparum* purine nucleoside phosphorylases. *Biochemistry.* 43, 1458-1468.

201. Mendieta, J., Martín-Santamaría, S., Priego, E.-M., Balzarini, J., Camarasa, M.-J., Pérez-Pérez, M.-J., and Gago, F. (2004) Role of histidine-85 in the catalytic mechanism of thymidine phosphorylase as assessed by targeted molecular dynamics simulations and quantum mechanical calculations. *Biochemistry*. 43, 405-414.
202. Birck, M. R., and Schramm, V. L. (2004) Nucleophilic participation in the transition state for human thymidine phosphorylase. *J. Am. Chem. Soc.* 126, 2447-2453.
203. Garcia-Viloca, M., Gao, J., Karplus, M., and Truhlar, D. G. (2004) How enzymes work: analysis by modern rate theory and computer simulations. *Science*. 303, 186-195.
204. Gao, J., Ma, S., Major, D. T., Nam, K., Pu, J., and Truhlar, D. G. (2006) Mechanisms and free energies of enzymatic reactions. *Chem. Rev.* 106, 3188-3209.
205. Bruice, T. C. (2006) Computational approaches: reaction trajectories, structures, and atomic motions. Enzyme reactions and proficiency. *Chem. Rev.* 106, 3119-3139.
206. Garcia-Viloca, M., Truhlar, D. G., and Gao, J. (2003) Reaction-path energetics and kinetics of the hydride transfer reaction catalyzed by dihydrofolate reductase. *Biochemistry*. 42, 13558-13575.
207. Wolfenden, R., and Snider, M. J. (2001) The depth of chemical time and the power of enzymes as catalysts. *Acc. Chem. Res.* 34, 938-945.
208. Lewandowicz, A., Ringia, E. A. T., Ting, L.-M., Kim, K., Tyler, P. C., Evans, G. B., Zubkova, O. V., Mee, S., Painter, G. F., Lenz, D. H., Furneaux, R. H., and Schramm, V. L. (2005) Energetic mapping of transition state analogue interactions with human and *Plasmodium falciparum* purine nucleoside phosphorylases. *J. Biol. Chem.* 280, 30320-30328.
209. Singh, V., Shi, W., Evans, G. B., Tyler, P. C., Furneaux, R. H., Almo, S. C., and Schramm, V. L. (2004) Picomolar transition state analogue inhibitors of human 5'-methylthioadenosine phosphorylase and X-ray structure with MT-immucillin-A. *Biochemistry*. 43, 9-18.

210. Guo, H., Rao, N., Xu, Q., and Guo, H. (2005) Origin of tight binding of a near-perfect transition-state analogue by cytidine deaminase: implications for enzyme catalysis. *J. Am. Chem. Soc.* 127, 3191-3197.
211. Singh, V., Evans, G. B., Lenz, D. H., Mason, J. M., Clinch, K., Mee, S., Painter, G. F., Tyler, P. C., Furneaux, R. H., Lee, J. E., Howell, P. L., and Schramm, V. L. (2005) Femtomolar transition state analogue inhibitors of 5'-methylthioadenosine/*S*-adenosylhomocysteine nucleosidase from *Escherichia coli*. *J. Biol. Chem.* 280, 18265-18273.
212. Lolis, E., and Petsko, G. A. (1990) Transition-state analogs in protein crystallography: probes of the structural source of enzyme catalysis. *Annu. Rev. Biochem.* 59, 597-630.
213. Kirby, A. J. (1994) Crystallographic approaches to transition state structures, in *Advances in Physical Organic Chemistry*, Vol 29 ed., pp 87-183, Academic Press Ltd, London.
214. Wolfenden, R. (1999) Conformational aspects of inhibitor design: enzyme-substrate interactions in the transition state. *Bioorg. Med. Chem.* 7, 647-652.
215. Gloster, T. M., Macdonald, J. M., Tarling, C. A., Stick, R. V., Withers, S. G., and Davies, G. J. (2004) Structural, thermodynamic, and kinetic analyses of tetrahydrooxazine-derived inhibitors bound to β -glucosidases. *J. Biol. Chem.* 279, 49236-49242.
216. Gloster, T. M., Madsen, R., and Davies, G. J. (2006) Dissection of conformationally restricted inhibitors binding to a β -glucosidase. *Chembiochem.* 7, 738-742.
217. Gloster, T. M., Roberts, S., Perugino, G., Rossi, M., Moracci, M., Panday, N., Terinek, M., Vasella, A., and Davies, G. J. (2006) Structural, kinetic, and thermodynamic analysis of glucoimidazole-derived glycosidase inhibitors. *Biochemistry.* 45, 11879-11884.

218. Zechel, D. L., Boraston, A. B., Gloster, T., Boraston, C. M., Macdonald, J. M., Tilbrook, D. M. G., Stick, R. V., and Davies, G. J. (2003) Iminosugar glycosidase inhibitors: structural and thermodynamic dissection of the binding of isofagomine and 1-deoxynojirimycin to β -glucosidases. *J. Am. Chem. Soc.* 125, 14313-14323.
219. Lillielund, V. H., Jensen, H. H., Liang, X. F., and Bols, M. (2002) Recent developments of transition-state analogue glycosidase inhibitors of non-natural product origin. *Chem. Rev.* 102, 515-553.
220. Cha, S. (1975) Tight-binding inhibitors: kinetic behavior. *Biochem. Pharmacol.* 24, 2177-2185.
221. Perdicakis, B., Montgomery, H. J., Guillemette, J. G., and Jervis, E. (2005) Analysis of slow-binding enzyme inhibitors at elevated enzyme concentrations. *Anal. Biochem.* 337, 211-223.
222. Legler, G. (1999) in *Iminosugars as glycosidase inhibitors* (Stütz, A., Ed.) ed., pp 31-67, Wiley-VCH, Weinheim.
223. Bartlett, P. A., and Marlowe, C. K. (1987) Possible role for water dissociation in the slow binding of phosphorus-containing transition-state-analogue inhibitors of thermolysin. *Biochemistry.* 26, 8553-8561.
224. Waley, S. G. (1993) The kinetics of slow-binding and slow, tight-binding inhibition: the effects of substrate depletion. *Biochem. J.* 294, 195-200.
225. Frieden, C., Kurz, L. C., and Gilbert, H. R. (1980) Adenosine deaminase and adenylyate deaminase: comparative kinetic studies with transition state and ground state analog inhibitors. *Biochemistry.* 19, 5303-5309.
226. Westerik, J. O. C., and Wolfenden, R. (1972) Aldehydes as inhibitors of papain. *J. Biol. Chem.* 247, 8195-8197.
227. Thompson, R. C. (1973) Use of peptide aldehydes to generate transition-state analogs of elastase. *Biochemistry.* 12, 47-51.
228. Lienhard, G. E. (1973) *Science.* 180, 149-154.
229. Bartlett, P. A., and Marlowe, C. K. (1983) Phosphonamidates as transition-state analogue inhibitors of thermolysin. *Biochemistry.* 22, 4618-4624.

230. Morgan, B. P., Scholtz, J. M., Ballinger, M. D., Zipkin, I. D., and Bartlett, P. A. (1991) Differential binding energy: a detailed evaluation of the influence of hydrogen-bonding and hydrophobic groups on the inhibition of thermolysin by phosphorus-containing inhibitors. *J. Am. Chem. Soc.* *113*, 297-307.
231. Hanson, J. E., Kaplan, A. P., and Bartlett, P. A. (1989) Phosphonate analogues of carboxypeptidase A substrates are potent transition-state analogue inhibitors. *Biochemistry.* *28*, 6294-6305.
232. Bartlett, P. A., and Giangiordano, M. A. (1996) Transition state analogy of phosphonic acid peptide inhibitors of pepsin. *J. Org. Chem.* *61*, 3433-3438.
233. Mookhtiar, K. A., Grobelny, D., Galaray, R. E., and Wart, H. E. V. (1988) Ketone-substrate analogues of *Clostridium histolyticum* collagenases: tight-binding transition-state analogue inhibitors. *Biochemistry.* *27*, 4299-4304.
234. Ermert, P., Vasella, A., Weber, M., Rupitz, K., and Withers, S. G. (1993) Configurationally selective transition state analogue inhibitors of glycosidases. A study with nojiritetrazoles, a new class of glycosidase inhibitors. *Carbohydr. Res.* *250*, 113-128.
235. Whitworth, G. E., Macauley, M. S., Stubbs, K. A., Dennis, R. J., Taylor, E. J., Davies, G. J., Greig, I. R., and Vocadlo, D. J. (2007) Analysis of PUGNAc and NAG-thiazoline as transition state analogues for human O-GlcNAcase: mechanistic and structural insights into inhibitor selectivity and transition state poise. *J. Am. Chem. Soc.* *129*, 635-644.
236. Phillips, M. A., Kaplan, A. P., Rutter, W. J., and Bartlett, P. A. (1992) Transition-state characterization: a new approach combining inhibitor analogues and variation in enzyme structure. *Biochemistry.* *31*, 959-963.
237. Berland, C. R., Sigurskjold, B. W., Stoffer, B., Frandsen, T. P., and Svensson, B. (1995) Thermodynamics of inhibitor binding to mutant forms of glucoamylase from *Aspergillus niger* determined by isothermal titration calorimetry. *Biochemistry.* *34*, 10153-10161.

238. Mosi, R., Sham, H., Uitdehaag, J. C. M., Ruiterkamp, R., Dijkstra, B. W., and Withers, S. G. (1998) Reassessment of acarbose as a transition state analogue inhibitor of cyclodextrin glycosyltransferase. *Biochemistry*. 37, 17192-17198.
239. Withers, S. G., Namchuk, M., and Mosi, R. (1999) Iminosugars as glycosidase inhibitors: nojirimycin and beyond, in *Iminosugars as glycosidase inhibitors: nojirimycin and beyond* (Stütz, A. E., Ed.) ed., pp 188-206, Wiley-VCH, Weinheim.
240. Wolfenden, R., Snider, M., Ridgway, C., and Miller, B. (1999) The temperature dependence of enzyme rate enhancements. *J. Am. Chem. Soc.* 121, 7419-7420.
241. Dale, M. P., Ensley, H. E., Kern, K., Sastry, K. A. R., and Byers, L. D. (1985) Reversible inhibitors of β -glucosidase. *Biochemistry*. 24, 3530-3539.
242. Hartman, F. C., LaMuraglia, G. M., Tomozawa, Y., and Wolfenden, R. (1975) The influence of pH on the interaction of inhibitors with triosephosphate isomerase and determination of the pK_a of the active-site carboxyl group. *Biochemistry*. 14, 5274-5279.
243. Axamawaty, M. T., Fleet, G. W., Hannah, K. A., Namgoong, S. K., and Sinnott, M. L. (1990) Inhibition of the α -L-arabinofuranosidase III of *Monilinia fructigena* by 1,4-dideoxy-1,4-imino-L-threitol and 1,4-dideoxy-1,4-imino-L-arabinitol. *Biochem. J.* 266, 245-249.
244. Asano, N. (2003) Glycosidase inhibitors: update and perspectives on practical use. *Glycobiology*. 13, 93R-104R.
245. Lee, J. K., Bain, A. D., and Berti, P. J. (2004) Probing the transition states of four glucoside hydrolyses with ^{13}C kinetic isotope effects measured at natural abundance by NMR spectroscopy. *J. Am. Chem. Soc.* 126, 3769-3776.
246. Conchie, J., and Levvy, G. A. (1957) Inhibition of glycosidases by aldonolactones of corresponding configuration. *Biochem. J.* 57, 389-395.
247. Ishida, N., Kumagai, K., Niida, T., Tsuruoka, T., and Yumato, H. (1967) *J. Antibiot.* 20, 66-71.
248. Inouye, S., Tsuruoka, T., Ito, T., and Niida, T. (1968) Structure and synthesis of nojirimycin. *Tetrahedron*. 24, 2125-2144.

249. Kajimoto, T., Liu, K. K. C., Pederson, R. L., Zhong, Z., Ichikawa, Y., Porco, J. A., and Wong, C. H. (1991) Enzyme-catalyzed aldol condensation for asymmetric synthesis of azasugars: synthesis, evaluation, and modeling of glycosidase inhibitors. *J. Amer. Chem. Soc.* **113**, 6187-6196.
250. Jespersen, T. M., Dong, W., Sierks, M. R., Skrydstrup, T., Lundt, I., and Bols, M. (1994) Isofagomine, a potent, new glycosidase inhibitor. *Angew. Chem., Int. Ed. Engl.* **33**, 1778-1779.
251. Jespersen, T. M., Bols, M., Sierks, M. R., and Skrydstrup, T. (1994) Synthesis of isofagomine, a novel glycosidase inhibitor. *Tetrahedron.* **50**, 13449-13460.
252. Bülow, A., Plesner, I. W., and Bols, M. (2000) A large difference in the thermodynamics of binding of isofagomine and 1-deoxynojirimycin to β -glucosidase. *J. Am. Chem. Soc.* **122**, 8567-8568.
253. Ganem, B., and Papandreou, G. (1991) Mimicking the glucosidase transition state: shape/charge considerations. *J. Am. Chem. Soc.* **113**, 8984-8985.
254. Papandreou, G., Tong, M. K., and Ganem, B. (1993) Amidine, amidrazone, and amidoxime derivatives of monosaccharide aldonolactams: synthesis and evaluation as glycosidase inhibitors. *J. Am. Chem. Soc.* **115**, 11682-11690.
255. Vonhoff, S., Heightman, T. D., and Vasella, A. (1998) Inhibition of glycosidases by lactam oximes: influence of the aglycon in disaccharide analogues. *Helv. Chim. Acta.* **81**, 1710-1725.
256. Hoos, R., Vasella, A., Rupitz, K., and Withers, S. G. (1997) D-Glyconhydroximolactams strongly inhibit α -glycosidases. *Carbohydr. Res.* **298**, 291-298.
257. Hoos, R., Naughton, A. B., Thiel, W., Vasella, A., Weber, W., Rupitz, K., and Withers, S. G. (1993) D-Gluconhydroximo-1,5-lactam and related N-arylcarbamates - theoretical calculations, structure, synthesis, and inhibitory effect on β -glucosidases. *Helv. Chim. Acta.* **76**, 2666-2686.
258. Tong, M. K., Papandreou, G., and Ganem, B. (1990) Potent, broad-spectrum inhibition of glycosidases by an amidine derivative of D-glucose. *J. Am. Chem. Soc.* **112**, 6137-6139.

259. Ermert, P., and Vasella, A. (1991) Synthesis of a glucose-derived tetrazole as a new β -glucosidase inhibitor - a new synthesis of 1-deoxynojirimycin. *Helv. Chim. Acta.* 74, 2043-2053.
260. Panday, N., and Vasella, A. (1999) Synthesis of glucose- and mannose-derived N-acetylamino imidazopyridines and their evaluation as inhibitors of glycosidases. *Synthesis. SP*, 1459-1468.
261. Field, R. A., Haines, A. H., Chrystal, E. J., and Luszniak, M. C. (1991) Histidines, histamines and imidazoles as glycosidase inhibitors. *Biochem. J.* 274, 885-889.
262. Tatsuta, K., Miura, S., Ohta, S., and Gunji, H. (1995) Syntheses and glycosidase inhibiting activities of nagstatin analogs. *J. Antibiot. (Tokyo).* 48, 286-288.
263. Tatsuta, K., Ikeda, Y., and Miura, S. (1996) Synthesis and glycosidase inhibitory activities of nagstatin triazole analogs. *J. Antibiot. (Tokyo).* 49, 836-838.
264. Panday, N., Canac, Y., and Vasella, A. (2000) Very strong inhibition of glucosidases by C(2)-substituted tetrahydroimidazopyridines. *Helv. Chim. Acta.* 83, 58-79.
265. Heightman, T. D., Locatelli, M., and Vasella, A. (1996) Synthesis of fused triazoles as probes for the active site of retaining β -glycosidases: From which direction is the glycoside protonated? *Helv. Chim. Acta.* 79, 2190-2200.
266. Stütz, A. E. (1999) *Iminosugars as glycosidase inhibitors: nojirimycin and beyond*, in *Iminosugars as glycosidase inhibitors: nojirimycin and beyond* (Stütz, A. E., Ed.) Vol. Wiley-VCH, Weinheim.
267. Legler, G., and Pohl, S. (1986) Synthesis of 5-amino-5-deoxy-D-galactopyranose and 1,5-dideoxy-1,5-imino-D-galactitol, and their inhibition of α - and β -D-galactosidases. *Carbohydr. Res.* 155, 119-129.
268. Ichikawa, Y., and Igarashi, Y. (1995) An extremely potent inhibitor for β -galactosidase. *Tetrahedron Lett.* 36, 4585-4586.

269. Jensen, H. H., Lyngbye, L., and Bols, M. (2001) A free-energy relationship between the rate of acidic hydrolysis of glycosides and the pK_a of isofagomines. *Angew. Chem. Int. Ed.* 40, 3447-3449.
270. Vocadlo, D. J., Wicki, J., Rupitz, K., and Withers, S. G. (2002) A case for reverse protonation: identification of Glu160 as an acid/base catalyst in *Thermoanaerobacterium saccharolyticum* β -xylosidase and detailed kinetic analysis of a site-directed mutant. *Biochemistry.* 41, 9736-9746.
271. Varrot, A., Tarling, C. A., Macdonald, J. M., Stick, R. V., Zechel, D. L., Withers, S. G., and Davies, G. J. (2003) Direct observation of the protonation state of an imino sugar glycosidase inhibitor upon binding. *J. Am. Chem. Soc.* 125, 7496-7497.
272. Varrot, A., Schülein, M., Pipelier, M., Vasella, A., and Davies, G. J. (1999) Lateral protonation of a glycosidase inhibitor - structure of the *Bacillus agaradhaerens* Cel5A in complex with a cellobiose-derived imidazole at 0.97 Å resolution. *J. Am. Chem. Soc.* 121, 2621-2622.
273. Gloster, T. M., Williams, S. J., Roberts, S., Tarling, C. A., Wicki, J., Withers, S. G., and Davies, G. J. (2004) Atomic resolution analyses of the binding of xylobiose-derived deoxynojirimycin and isofagomine to xylanase Xyn10A. *Chem. Commun.* 16, 1794-1795.
274. O'Neill, G. P., Kilburn, D. G., Warren, R. A. J., and Robert C. Miller, J. (1986) Overproduction from a cellulase gene with a high guanosine-plus-cytosine content in *Escherichia coli*. *Appl. Environ. Microbiol.* 52, 737-743.

APPENDIX A

GRAPHICAL REPRESENTATION OF KINETIC DATA

A GRAPHICAL REPRESENTATION OF DATA

A.1 Steady State Kinetics for the Hydrolysis of Xylobiosides or Cellobiosides

A.1.1 Native Cex

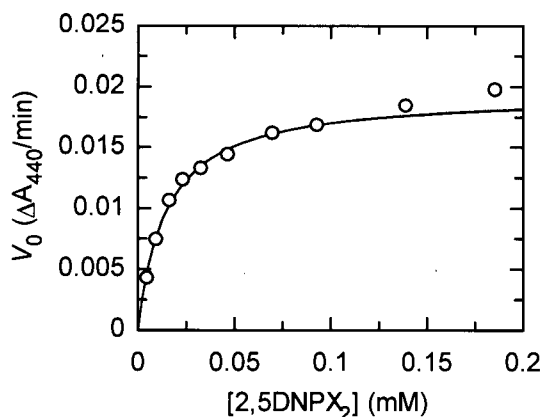


Figure A.1: Michaelis-Menten plot for the hydrolysis of 2,5DNPX₂ catalyzed by wild-type Cex.

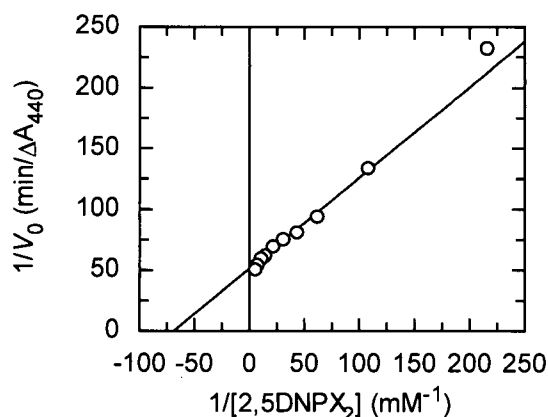


Figure A.2: Lineweaver-Burk plot for the hydrolysis of 2,5DNPX₂ catalyzed by wild-type Cex.

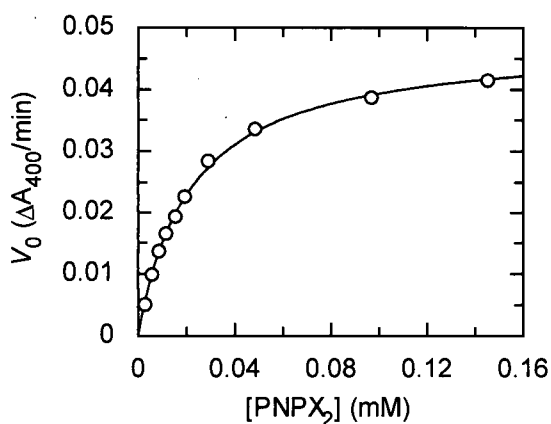


Figure A.3: Michaelis-Menten plot for the hydrolysis of PNPX₂ catalyzed by wild-type Cex.

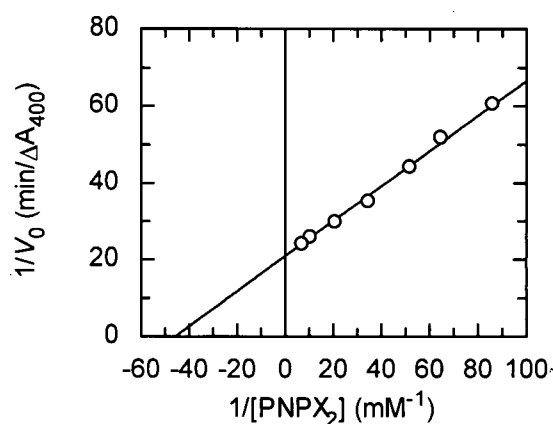


Figure A.4: Lineweaver-Burk plot for the hydrolysis of PNPX₂ catalyzed by wild-type Cex.

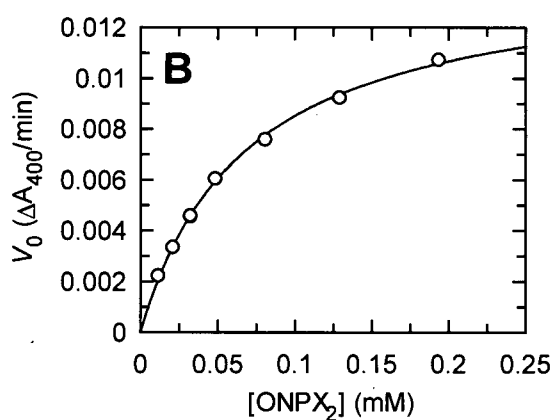
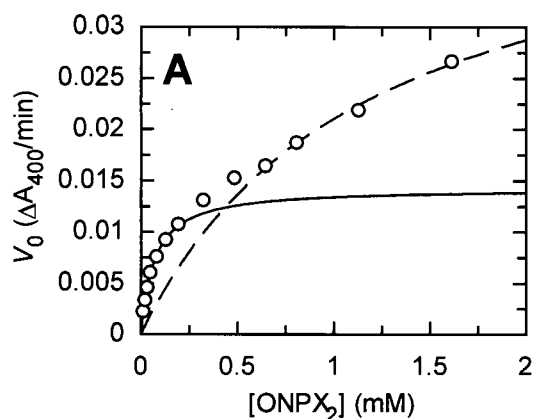


Figure A.5. Michaelis–Menten plot for the hydrolysis of ONPX_2 catalyzed by wild-type Cex. Plot A shows all data points with a solid line drawn through the points that represent the hydrolysis reaction and a dashed line through those that represent the transglycosylation reaction. Plot B shows the Michaelis–Menten plot for the hydrolysis reaction.

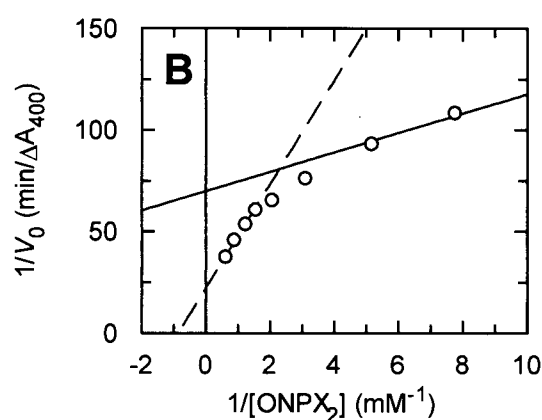
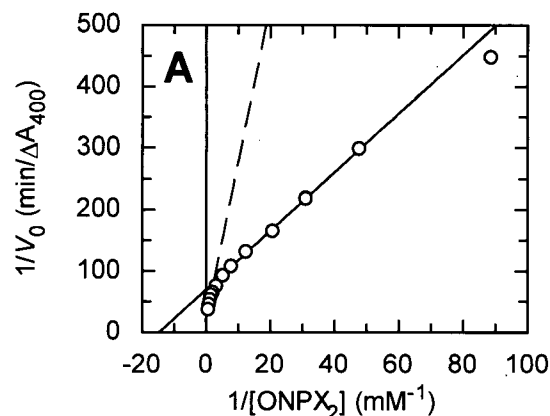


Figure A.6. Lineweaver–Burk plot for the hydrolysis of ONPX_2 catalyzed by wild-type Cex. The solid line represents the hydrolysis reaction and the dashed line represents the transglycosylation reactions. Plot A shows all data points. Plot B magnifies data points obtained for the transglycosylation reaction.

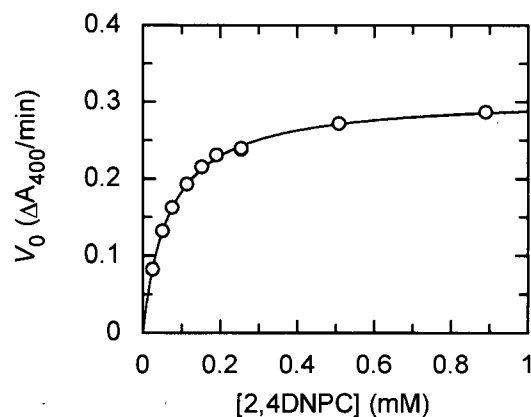


Figure A.7: Michaelis-Menten plot for the hydrolysis of 2,4DNPC catalyzed by wild-type Cex.

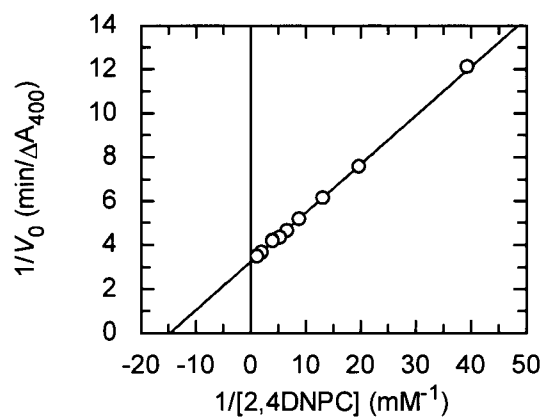


Figure A.8: Lineweaver-Burk plot for the hydrolysis of 2,4DNPC catalyzed by wild-type Cex.

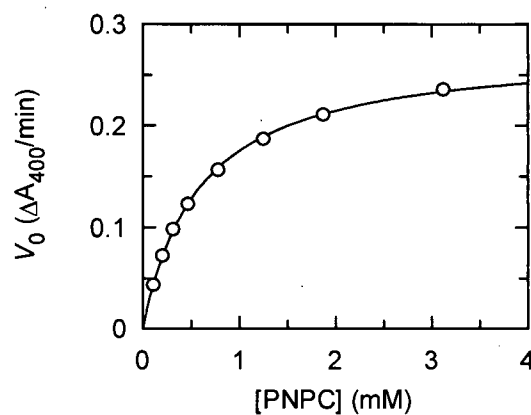


Figure A.9: Michaelis-Menten plot for the hydrolysis of PNPC catalyzed by wild-type Cex.

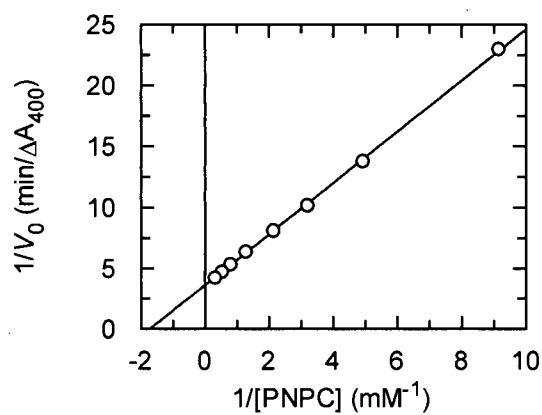


Figure A.10: Lineweaver-Burk plot for the hydrolysis of PNPC catalyzed by wild-type Cex.

A.1.2 Cex E43A

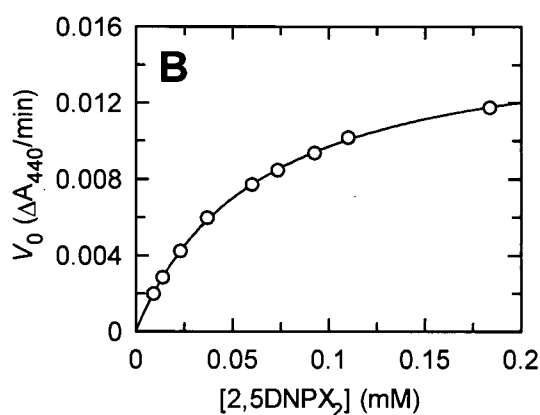
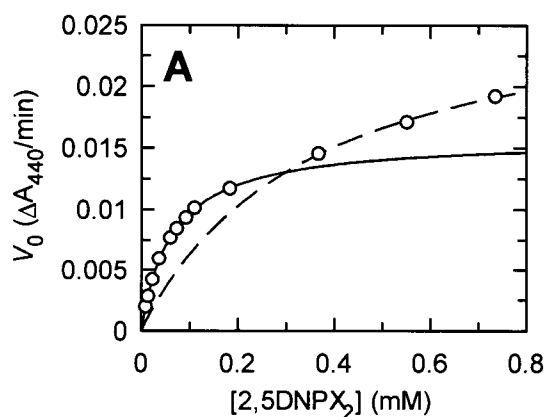


Figure A.11: Michaelis-Menten plot for the hydrolysis of 2,5DNPX₂ catalyzed by Cex E43A. Plot A shows all data points with a solid line drawn through the points that represent the hydrolysis reaction and a dashed line through those that represent the transglycosylation reaction. Plot B shows the Michaelis-Menten plot for the hydrolysis reaction.

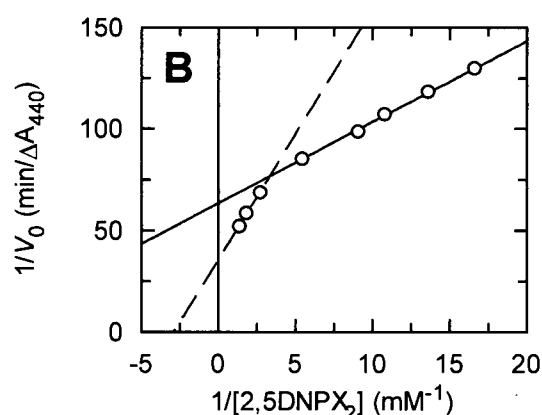
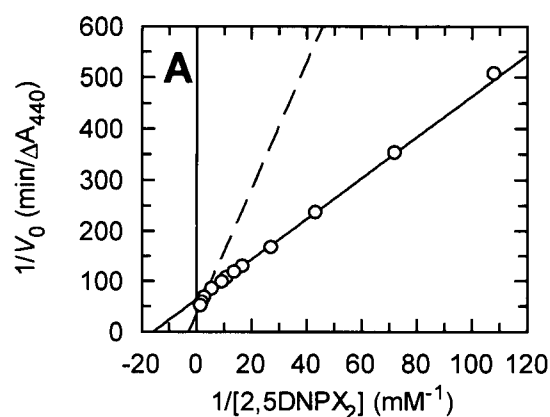


Figure A.12: Lineweaver-Burk plot for the hydrolysis of 2,5DNPX₂ catalyzed by Cex E43A. The solid line represents the hydrolysis reaction and the dashed line represents the transglycosylation reactions. Plot A shows all data points. Plot B magnifies data points obtained for the transglycosylation reaction.

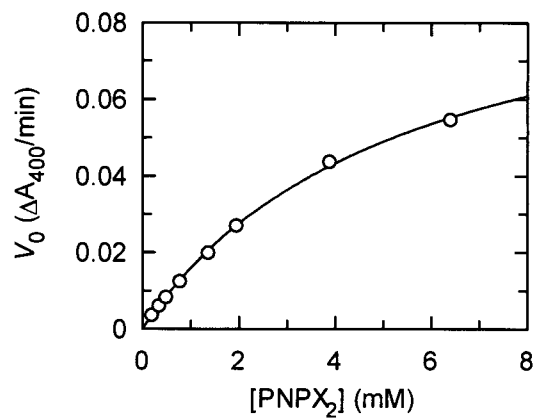


Figure A.13: Michaelis–Menten plot for the hydrolysis of PNPX_2 catalyzed by Cex E43A.

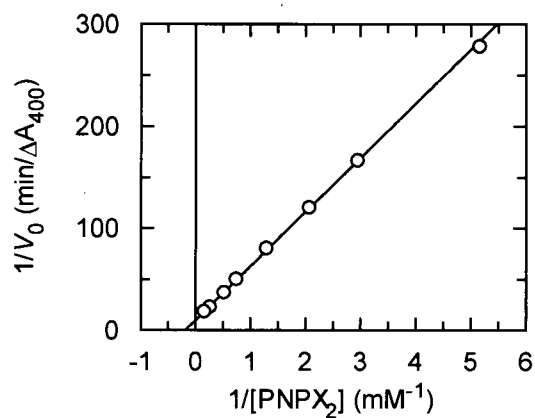


Figure A.14: Lineweaver–Burk plot for the hydrolysis of PNPX_2 catalyzed by Cex E43A.

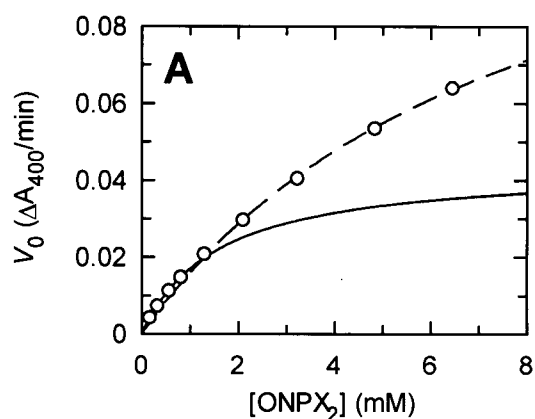


Figure A.15: Michaelis-Menten plot for the hydrolysis of ONPX_2 catalyzed by Cex E43A. Plot A shows all data points with a solid line drawn through the points that represent the hydrolysis reaction and a dashed line through those that represent the transglycosylation reaction. Plot B shows the Michaelis-Menten plot for the hydrolysis reaction.

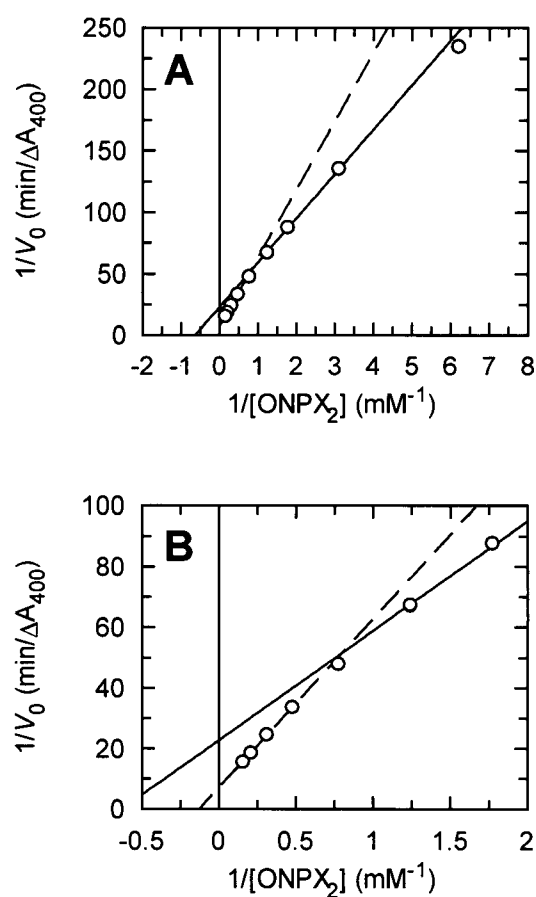


Figure A.16: Lineweaver-Burk plot for the hydrolysis of ONPX_2 catalyzed by Cex E43A. The solid line represents the hydrolysis reaction and the dashed line represents the transglycosylation reactions. Plot A shows all data points. Plot B magnifies data points obtained for the transglycosylation reaction.

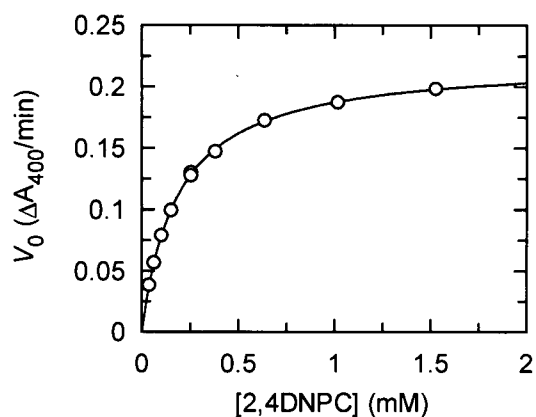


Figure A.17: Michaelis-Menten plot for the hydrolysis of 2,4DNPC catalyzed by Cex E43A.

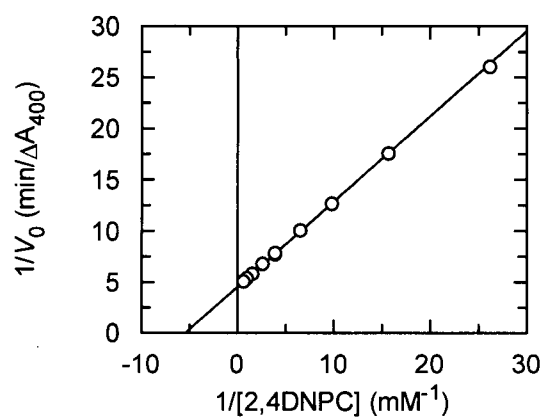


Figure A.18: Lineweaver-Burk plot for the hydrolysis of 2,4DNPC catalyzed by Cex E43A.

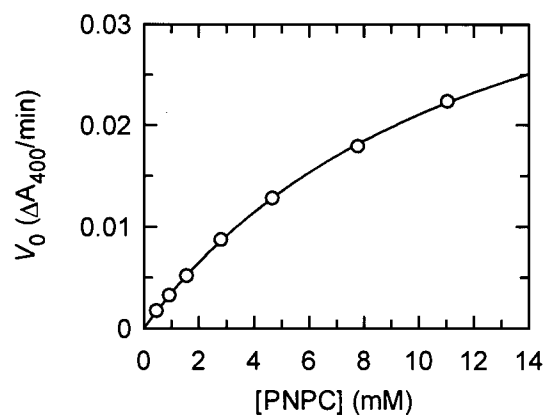


Figure A.19: Michaelis-Menten plot for the hydrolysis of PNPC catalyzed by Cex E43A.

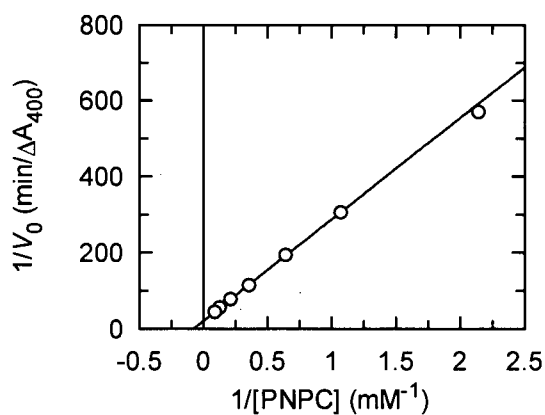


Figure A.20: Lineweaver-Burk plot for the hydrolysis of PNPC catalyzed by Cex E43A.

A.1.3 Cex N44A

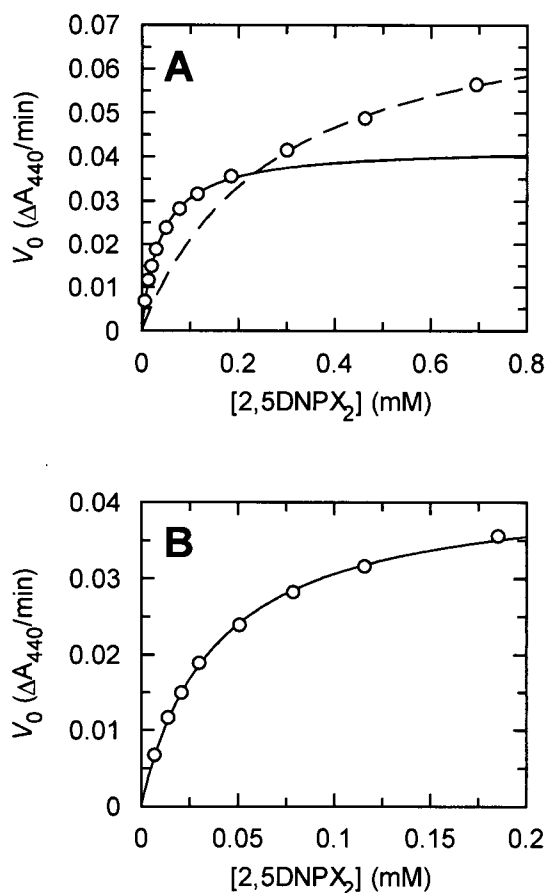


Figure A.21: Michaelis–Menten plot for the hydrolysis of 2,5DNPX₂ catalyzed by Cex N44A. Plot A shows all data points with a solid line drawn through the points that represent the hydrolysis reaction and a dashed line through those that represent the transglycosylation reaction. Plot B shows the Michaelis–Menten plot for the hydrolysis reaction.

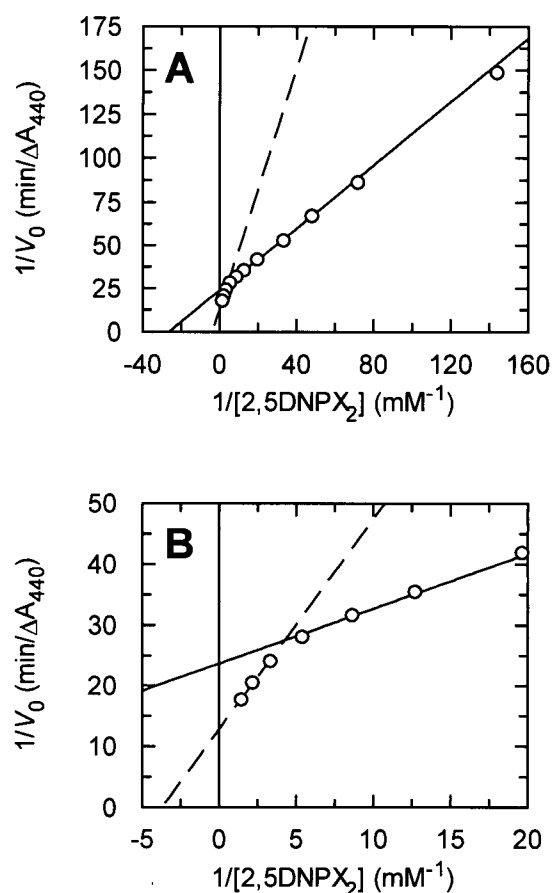


Figure A.22: Lineweaver–Burk plot for the hydrolysis of 2,5DNPX₂ catalyzed by Cex N44A. The solid line represents the hydrolysis reaction and the dashed line represents the transglycosylation reactions. Plot A shows all data points. Plot B magnifies data points obtained for the transglycosylation reaction.

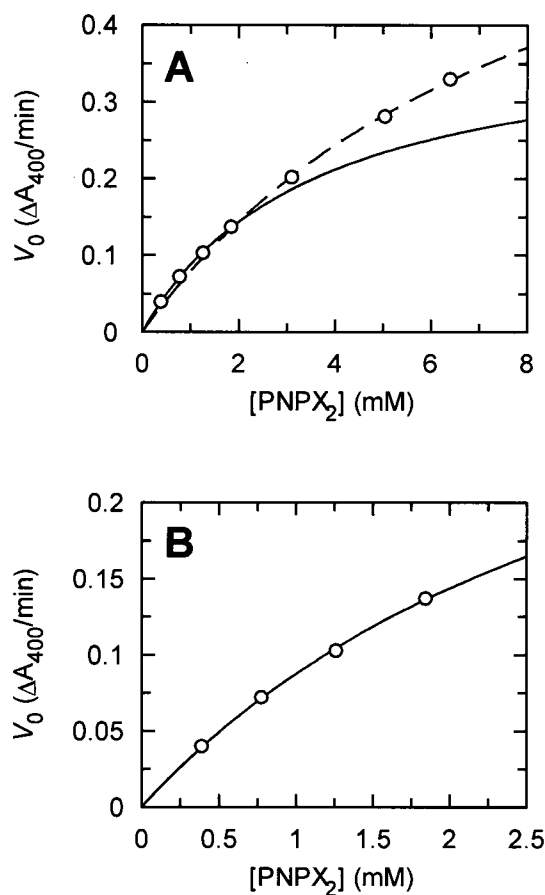


Figure A.23: Michaelis-Menten plot for the hydrolysis of PNPX₂ catalyzed by Cex N44A. Plot A shows all data points with a solid line drawn through the points that represent the hydrolysis reaction and a dashed line through those that represent the transglycosylation reaction. Plot B shows the Michaelis-Menten plot for the hydrolysis reaction.

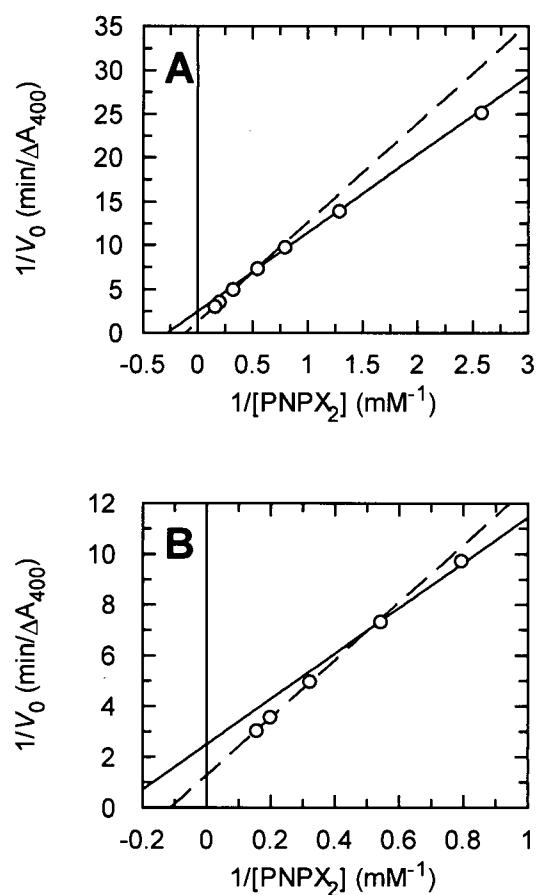


Figure A.24: Lineweaver-Burk plot for the hydrolysis of PNPX₂ catalyzed by Cex N44A. The solid line represents the hydrolysis reaction and the dashed line represents the transglycosylation reactions. Plot A shows all data points. Plot B magnifies data points obtained for the transglycosylation reaction.

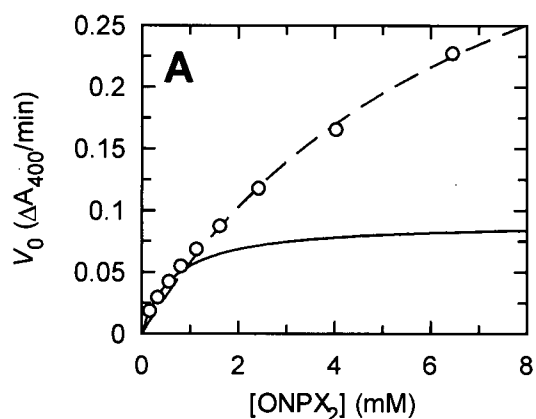


Figure A.25: Michaelis-Menten plot for the hydrolysis of ONPX_2 catalyzed by Cex N44A. Plot A shows all data points with a solid line drawn through the points that represent the hydrolysis reaction and a dashed line through those that represent the transglycosylation reaction. Plot B shows the Michaelis-Menten plot for the hydrolysis reaction.

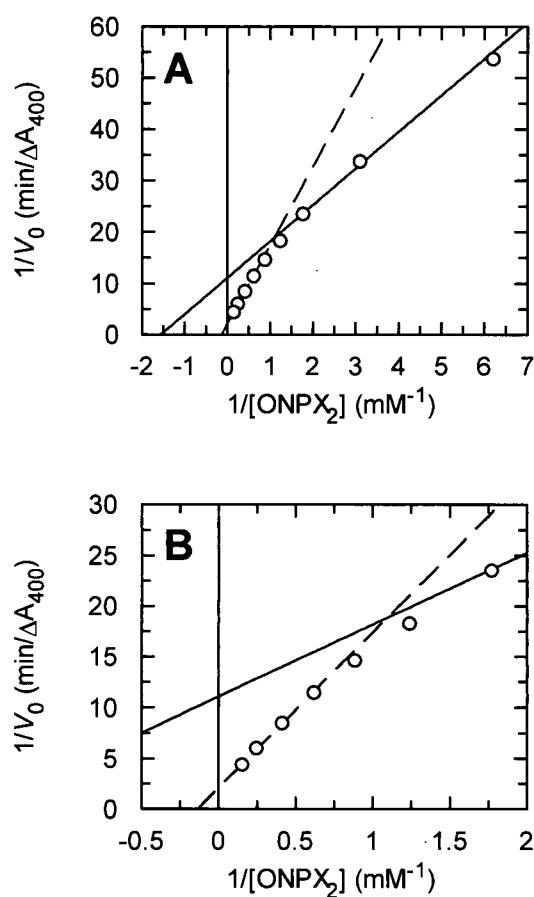


Figure A.26: Lineweaver-Burk plot for the hydrolysis of ONPX_2 catalyzed by Cex N44A. The solid line represents the hydrolysis reaction and the dashed line represents the transglycosylation reactions. Plot A shows all data points. Plot B magnifies data points obtained for the transglycosylation reaction.

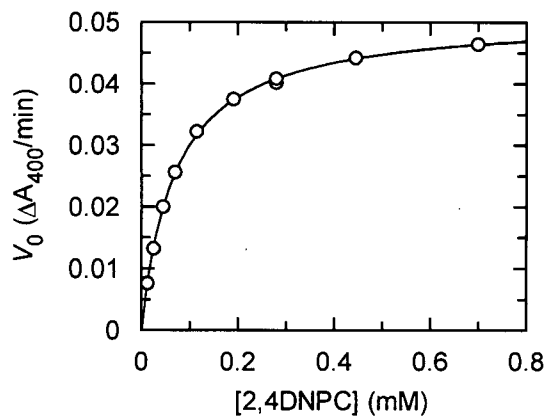


Figure A.27: Michaelis-Menten plot for the hydrolysis of 2,4DNPC catalyzed by Cex N44A.

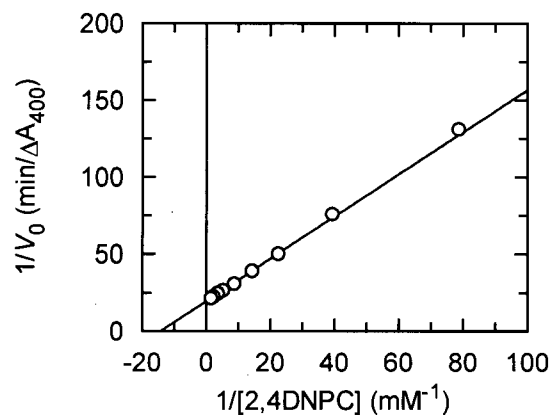


Figure A.28: Lineweaver-Burk plot for the hydrolysis of 2,4DNPC catalyzed by Cex N44A.

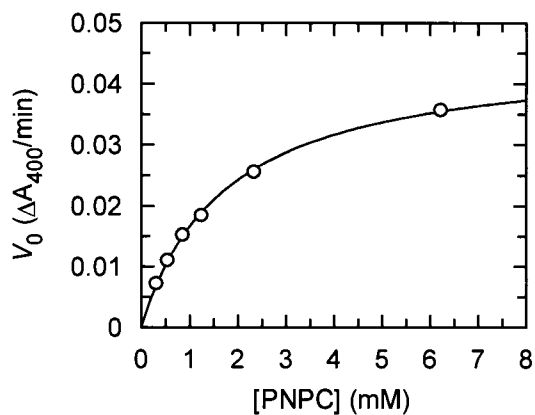


Figure A.29: Michaelis-Menten plot for the hydrolysis of PNPC catalyzed by Cex N44A.

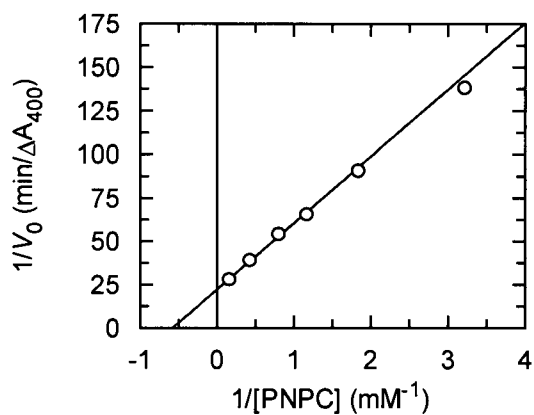


Figure A.30: Lineweaver-Burk plot for the hydrolysis of PNPC catalyzed by Cex N44A.

A.1.4 Cex K47A

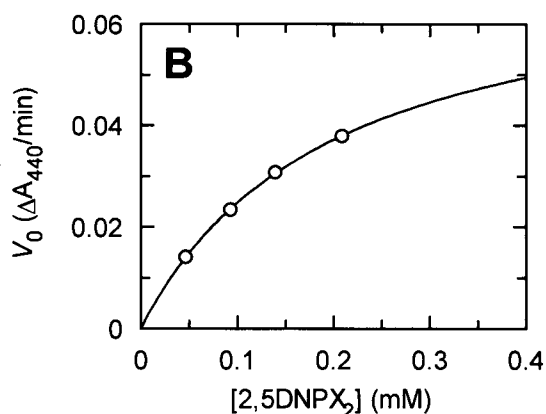
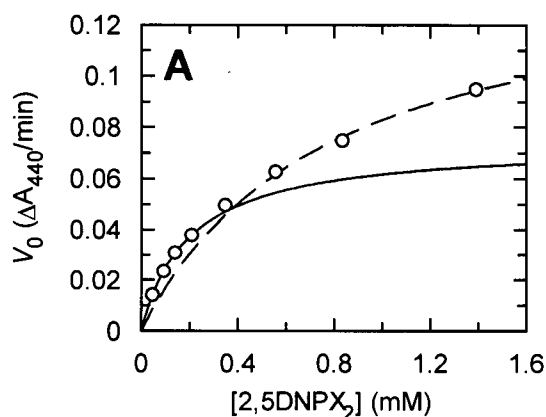


Figure A.31: Michaelis–Menten plot for the hydrolysis of 2,5DNPX₂ catalyzed by Cex K47A. Plot A shows all data points with a solid line drawn through the points that represent the hydrolysis reaction and a dashed line through those that represent the transglycosylation reaction. Plot B shows the Michaelis–Menten plot for the hydrolysis reaction.

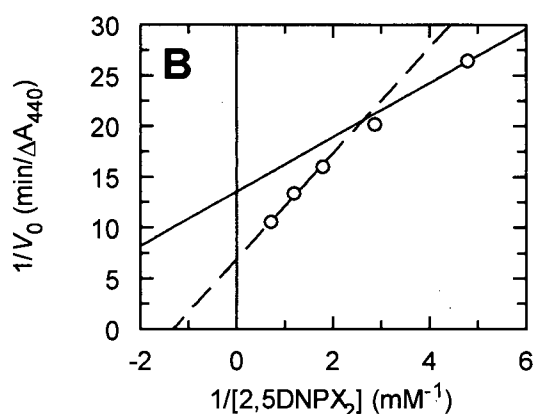
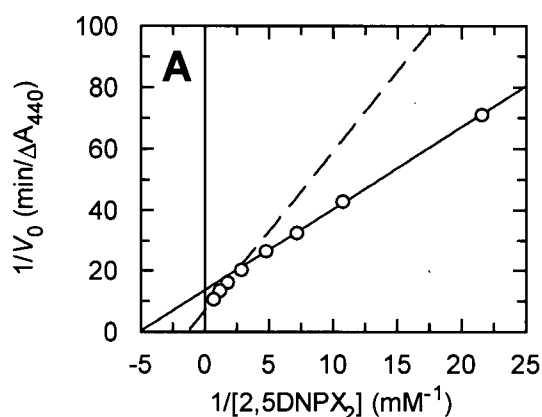


Figure A.32: Lineweaver–Burk plot for the hydrolysis of 2,5DNPX₂ catalyzed by Cex K47A. The solid line represents the hydrolysis reaction and the dashed line represents the transglycosylation reactions. Plot A shows all data points. Plot B magnifies data points obtained for the transglycosylation reaction.

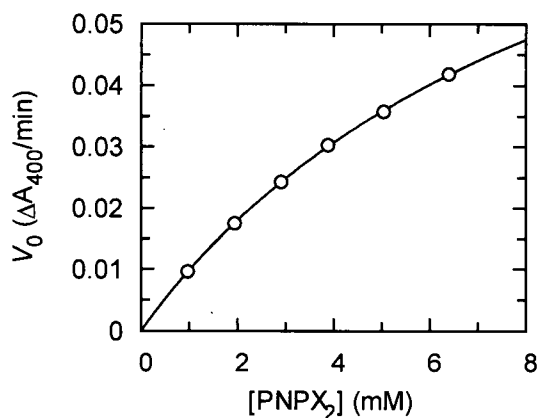


Figure A.33: Michaelis-Menten plot for the hydrolysis of PNPX_2 catalyzed by Cex K47A.

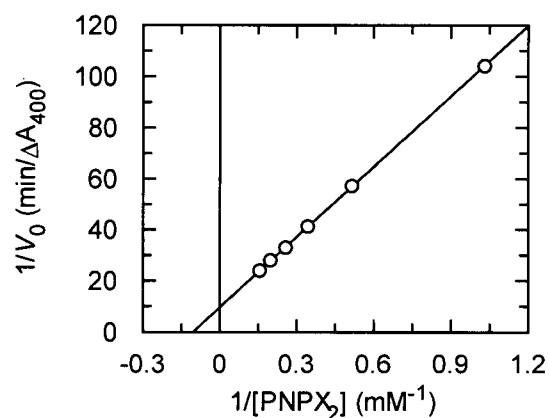


Figure A.34: Lineweaver-Burk plot for the hydrolysis of PNPX_2 catalyzed by Cex K47A.

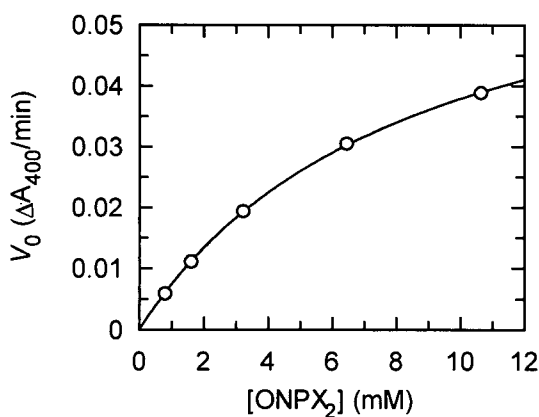


Figure A.35: Michaelis-Menten plot for the hydrolysis of ONPX_2 catalyzed by Cex K47A.

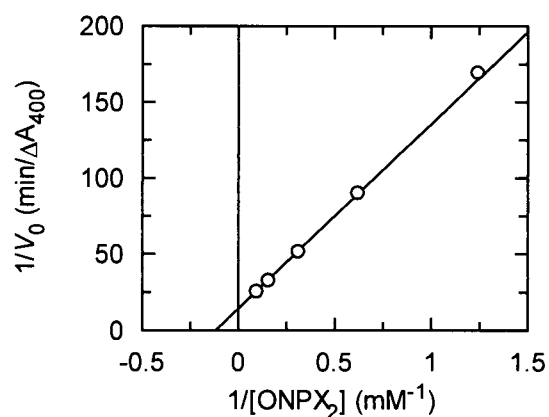


Figure A.36: Lineweaver-Burk plot for the hydrolysis of ONPX_2 catalyzed by Cex K47A.

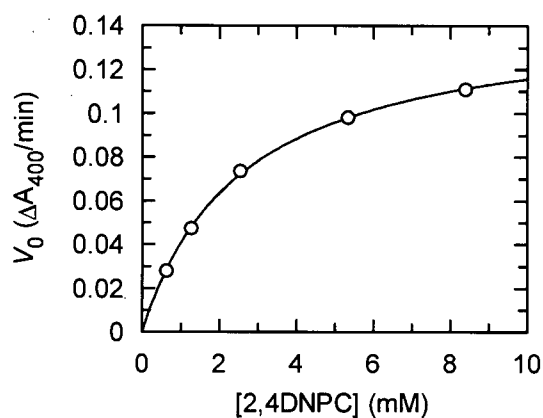


Figure A.37: Michaelis-Menten plot for the hydrolysis of 2,4DNPC catalyzed by Cex K47A.

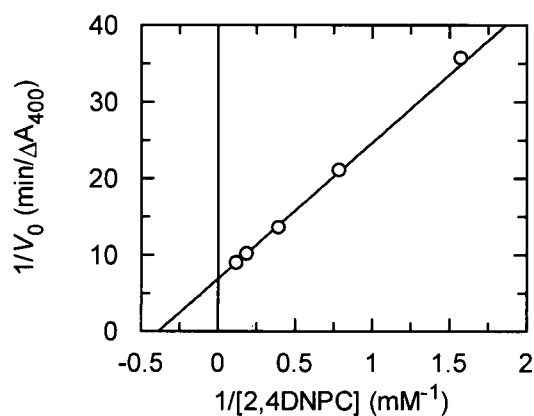


Figure A.38: Lineweaver-Burk plot for the hydrolysis of 2,4DNPC catalyzed by Cex K47A.

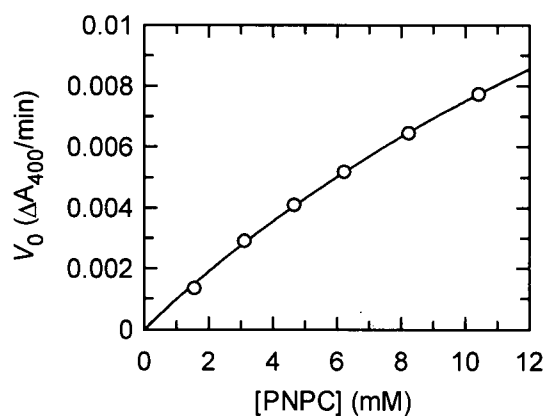


Figure A.39: Michaelis-Menten plot for the hydrolysis of PNPC catalyzed by Cex K47A.

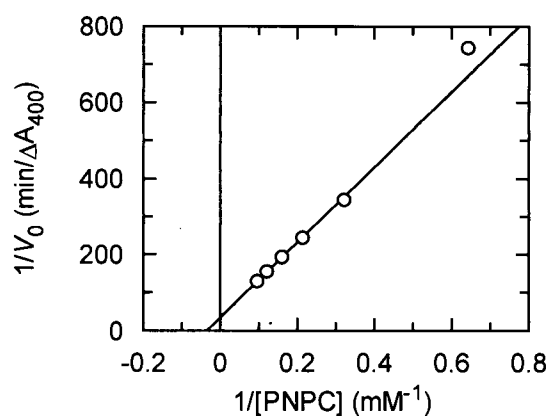


Figure A.40: Lineweaver-Burk plot for the hydrolysis of PNPC catalyzed by Cex K47A.

A.1.5 Cex H80A

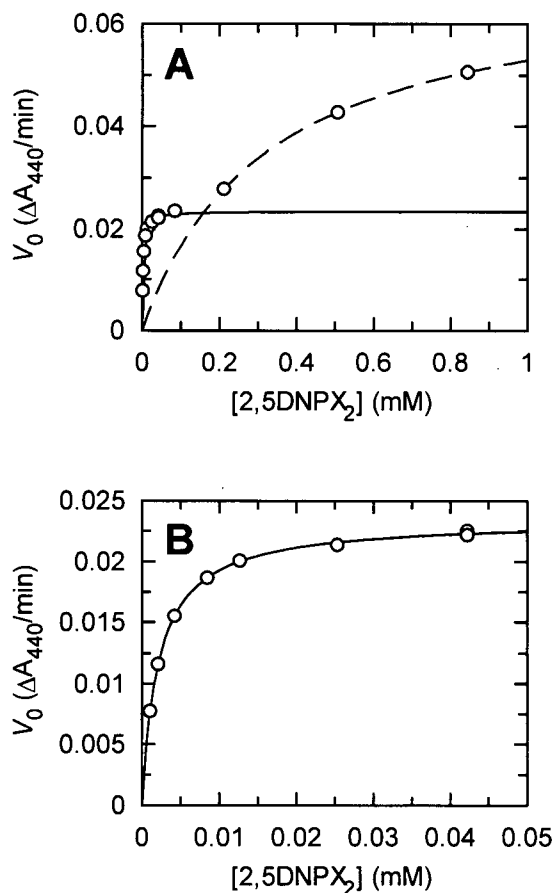


Figure A.41: Michaelis-Menten plot for the hydrolysis of 2,5DNPX₂ catalyzed by Cex H80A. Plot A shows all data points with a solid line drawn through the points that represent the hydrolysis reaction and a dashed line through those that represent the transglycosylation reaction. Plot B shows the Michaelis-Menten plot for the hydrolysis reaction.

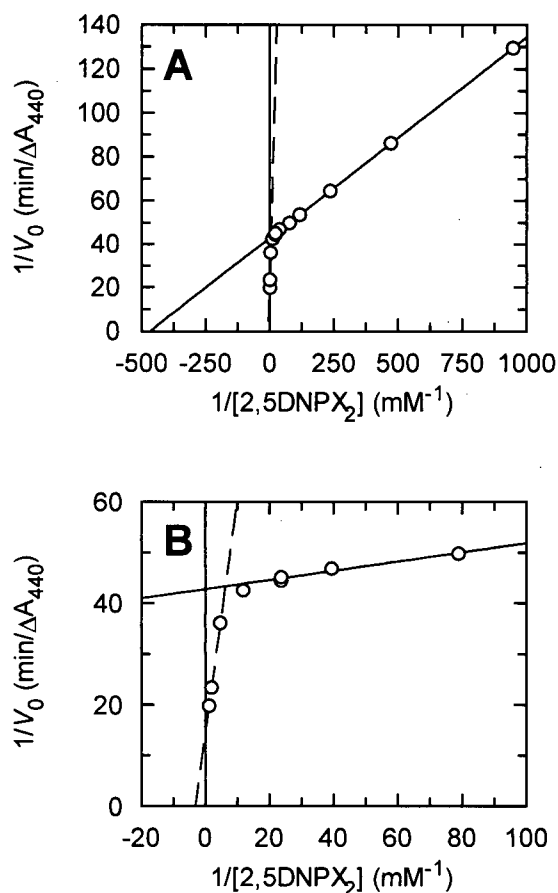


Figure A.42: Lineweaver-Burk plot for the hydrolysis of 2,5DNPX₂ catalyzed by Cex H80A. The solid line represents the hydrolysis reaction and the dashed line represents the transglycosylation reactions. Plot A shows all data points. Plot B magnifies data points obtained for the transglycosylation reaction.

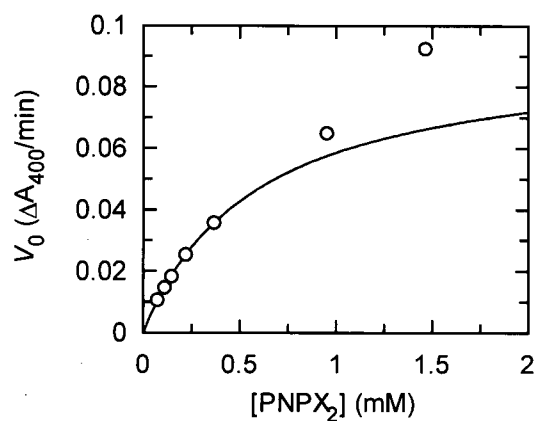


Figure A.43: Michaelis–Menten plot for the hydrolysis of PNPX_2 catalyzed by Cex H80A.

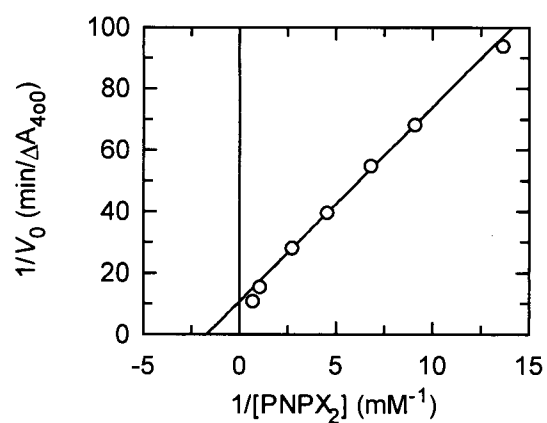


Figure A.44: Lineweaver–Burk plot for the hydrolysis of PNPX_2 catalyzed by Cex H80A.

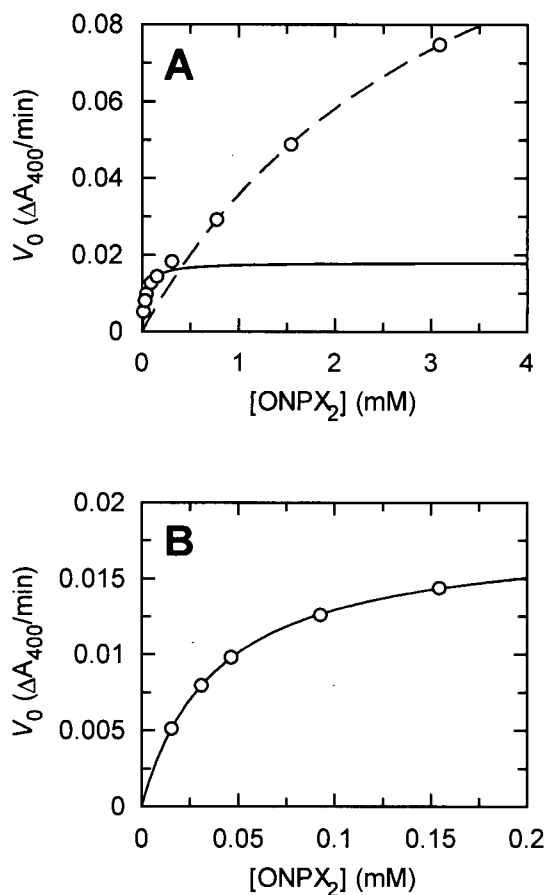


Figure A.45: Michaelis-Menten plot for the hydrolysis of ONPX_2 catalyzed by Cex H80A. Plot A shows all data points with a solid line drawn through the points that represent the hydrolysis reaction and a dashed line through those that represent the transglycosylation reaction. Plot B shows the Michaelis-Menten plot for the hydrolysis reaction.

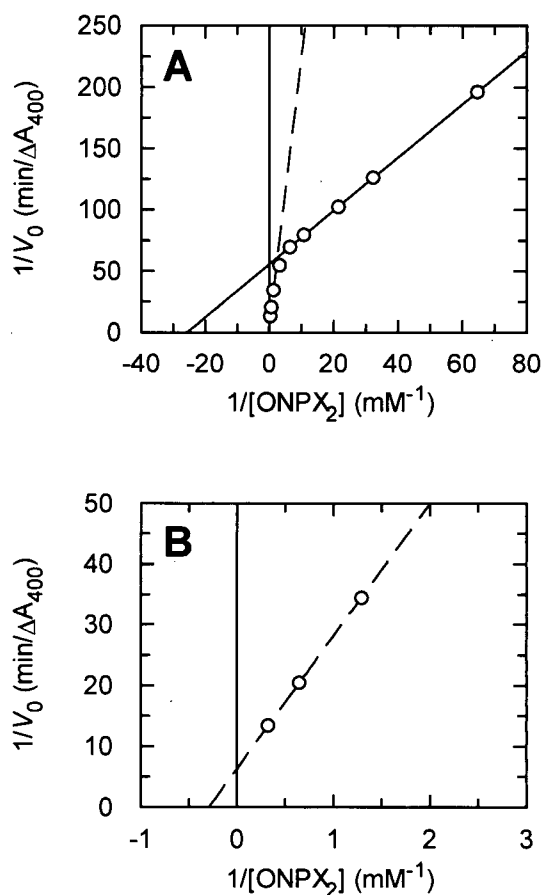


Figure A.46: Lineweaver-Burk plot for the hydrolysis of ONPX_2 catalyzed by Cex H80A. The solid line represents the hydrolysis reaction and the dashed line represents the transglycosylation reactions. Plot A shows all data points. Plot B magnifies data points obtained for the transglycosylation reaction.

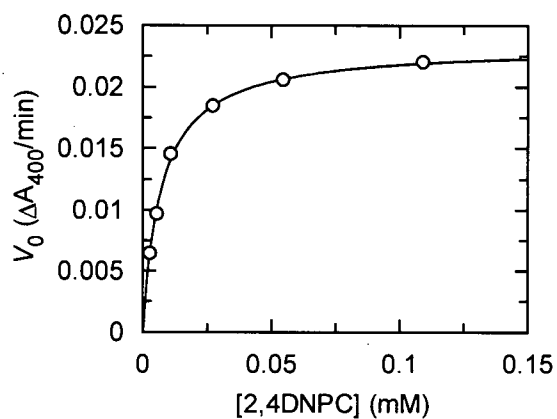


Figure A.47: Michaelis–Menten plot for the hydrolysis of 2,4DNPC catalyzed by Cex H80A.

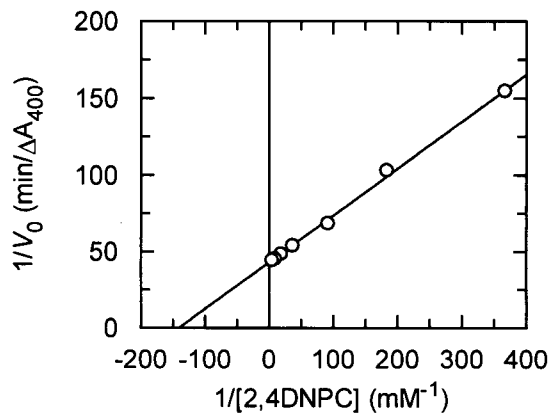


Figure A.48: Lineweaver–Burk plot for the hydrolysis of 2,4DNPC catalyzed by Cex H80A.

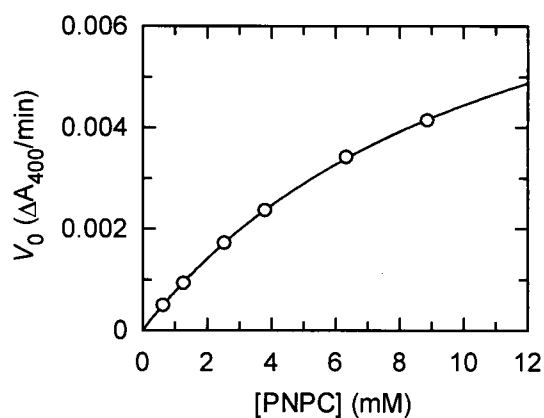


Figure A.49: Michaelis–Menten plot for the hydrolysis of PNPC catalyzed by Cex H80A.

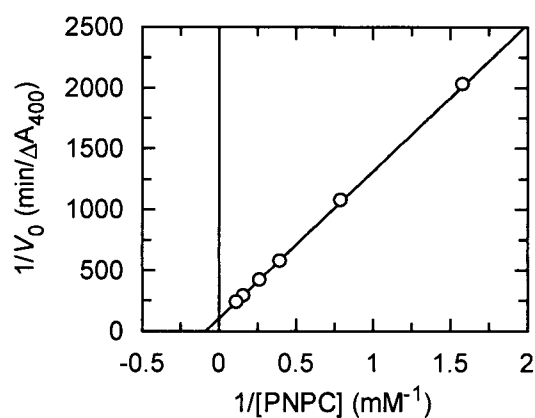


Figure A.50: Lineweaver–Burk plot for the hydrolysis of PNPC catalyzed by Cex H80A.

A.1.6 Cex H80N

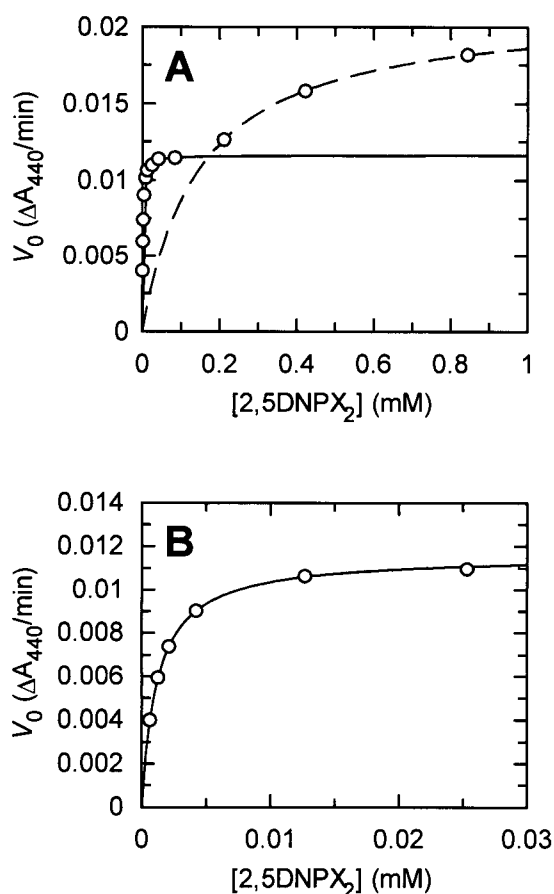


Figure A.51: Michaelis–Menten plot for the hydrolysis of 2,5DNPX₂ catalyzed by Cex H80N. Plot A shows all data points with a solid line drawn through the points that represent the hydrolysis reaction and a dashed line through those that represent the transglycosylation reaction. Plot B shows the Michaelis–Menten plot for the hydrolysis reaction.

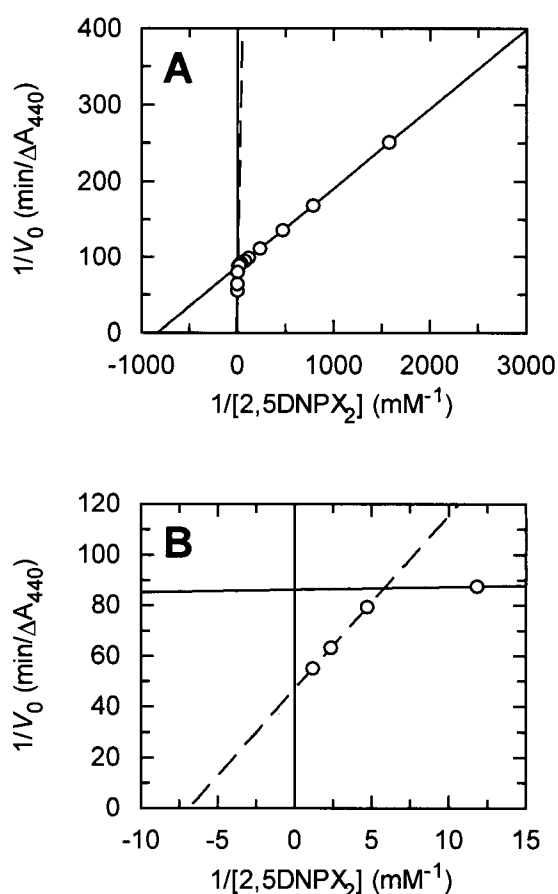


Figure A.52: Lineweaver–Burk plot for the hydrolysis of 2,5DNPX₂ catalyzed by Cex H80N. The solid line represents the hydrolysis reaction and the dashed line represents the transglycosylation reactions. Plot A shows all data points. Plot B magnifies data points obtained for the transglycosylation reaction.

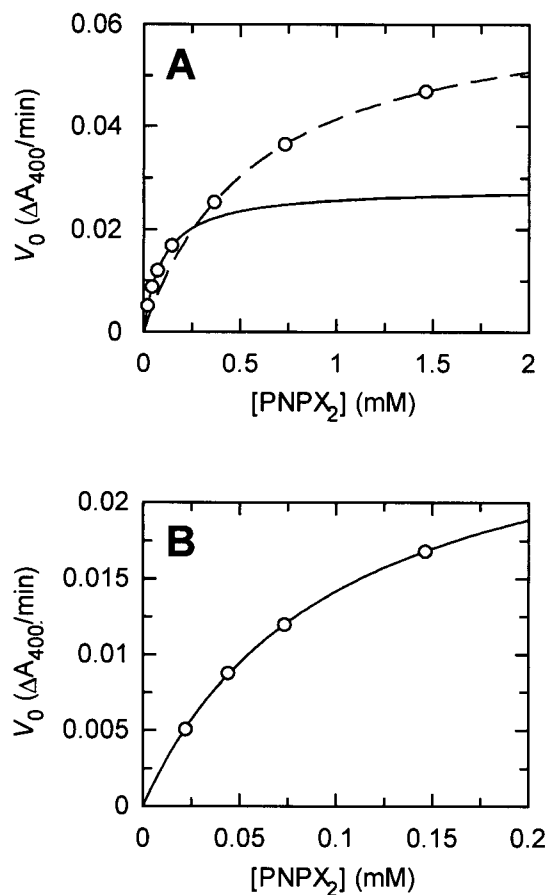


Figure A.53: Michaelis-Menten plot for the hydrolysis of PNPX₂ catalyzed by Cex H80N. Plot A shows all data points with a solid line drawn through the points that represent the hydrolysis reaction and a dashed line through those that represent the transglycosylation reaction. Plot B shows the Michaelis-Menten plot for the hydrolysis reaction.

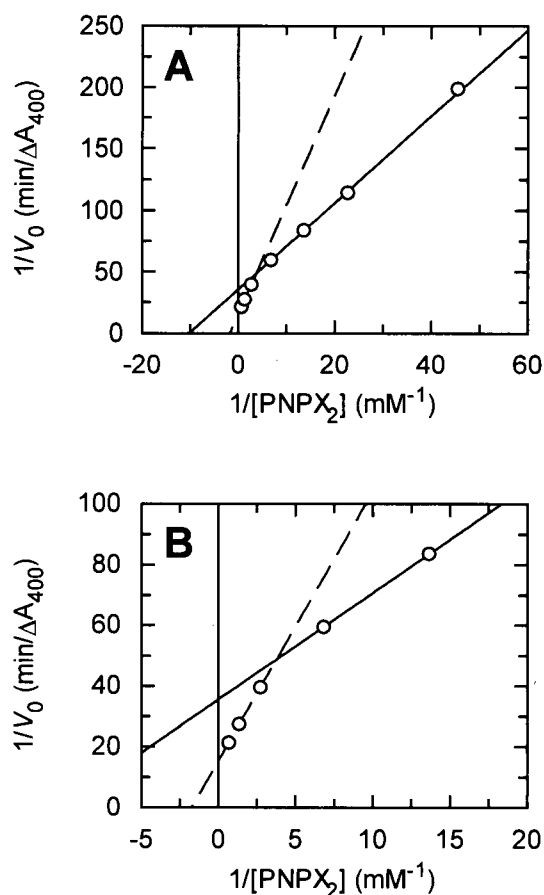


Figure A.54: Lineweaver-Burk plot for the hydrolysis of PNPX₂ catalyzed by Cex H80N. The solid line represents the hydrolysis reaction and the dashed line represents the transglycosylation reactions. Plot A shows all data points. Plot B magnifies data points obtained for the transglycosylation reaction.

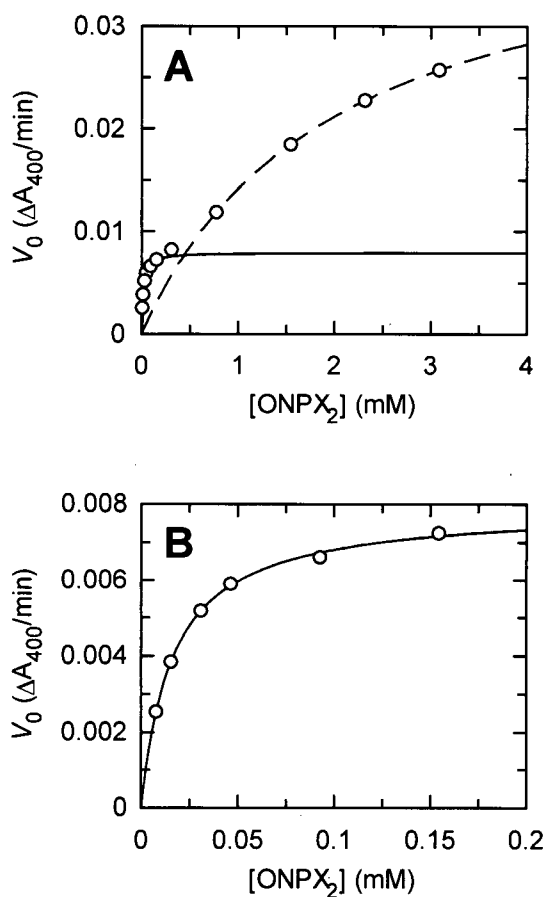


Figure A.55: Michaelis-Menten plot for the hydrolysis of ONPX₂ catalyzed by Cex H80N. Plot A shows all data points with a solid line drawn through the points that represent the hydrolysis reaction and a dashed line through those that represent the transglycosylation reaction. Plot B shows the Michaelis-Menten plot for the hydrolysis reaction.

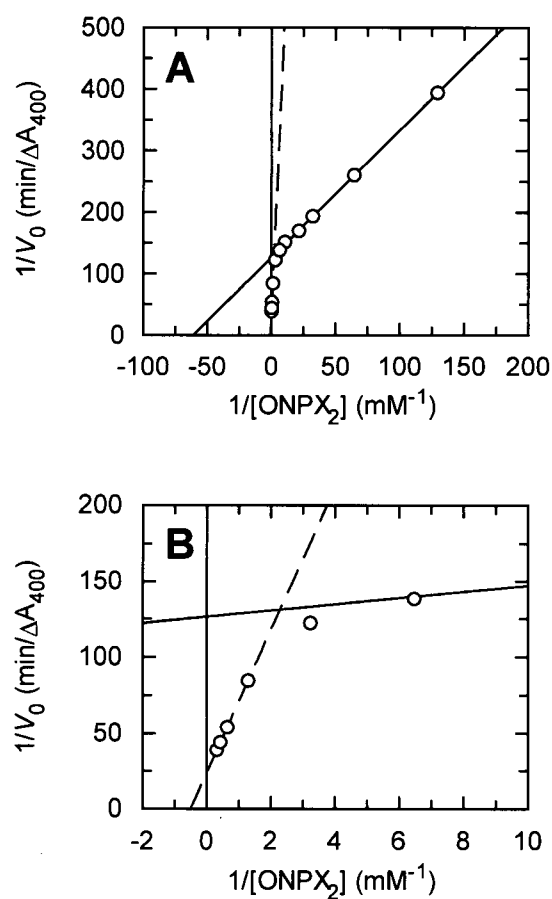


Figure A.56: Lineweaver-Burk plot for the hydrolysis of ONPX₂ catalyzed by Cex H80N. The solid line represents the hydrolysis reaction and the dashed line represents the transglycosylation reactions. Plot A shows all data points. Plot B magnifies data points obtained for the transglycosylation reaction.

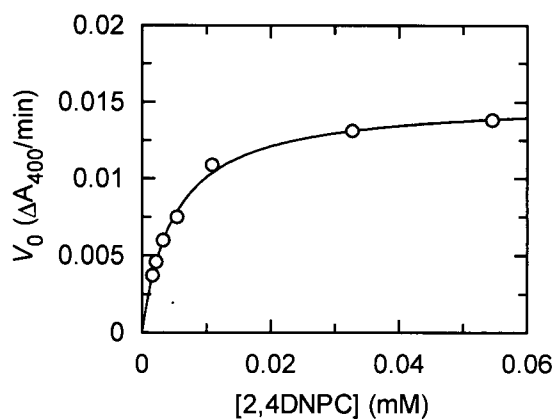


Figure A.57: Michaelis-Menten plot for the hydrolysis of 2,4DNPC catalyzed by Cex H80N.

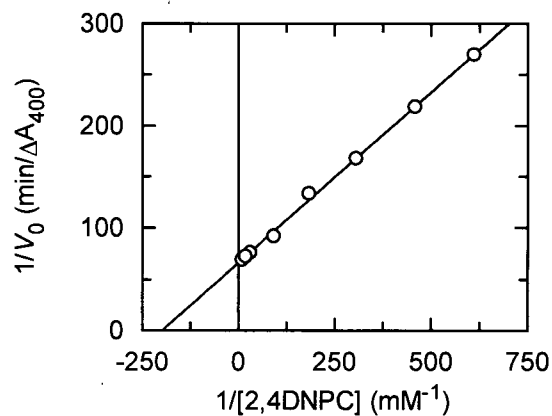


Figure A.58: Lineweaver-Burk plot for the hydrolysis of 2,4DNPC catalyzed by Cex H80N.

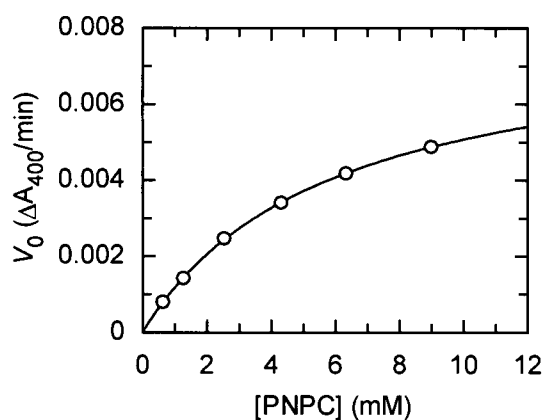


Figure A.59: Michaelis-Menten plot for the hydrolysis of PNPC catalyzed by Cex H80N.

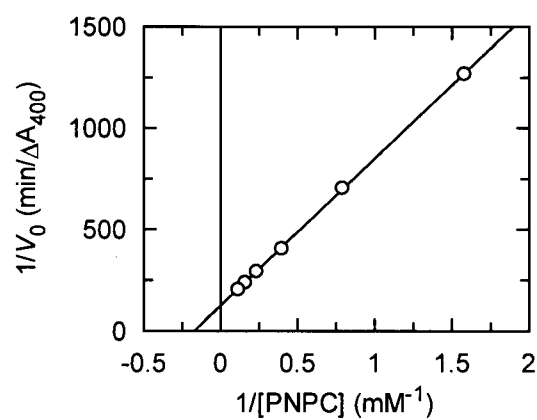


Figure A.60: Lineweaver-Burk plot for the hydrolysis of PNPC catalyzed by Cex H80N.

A.1.7 Cex H80Q

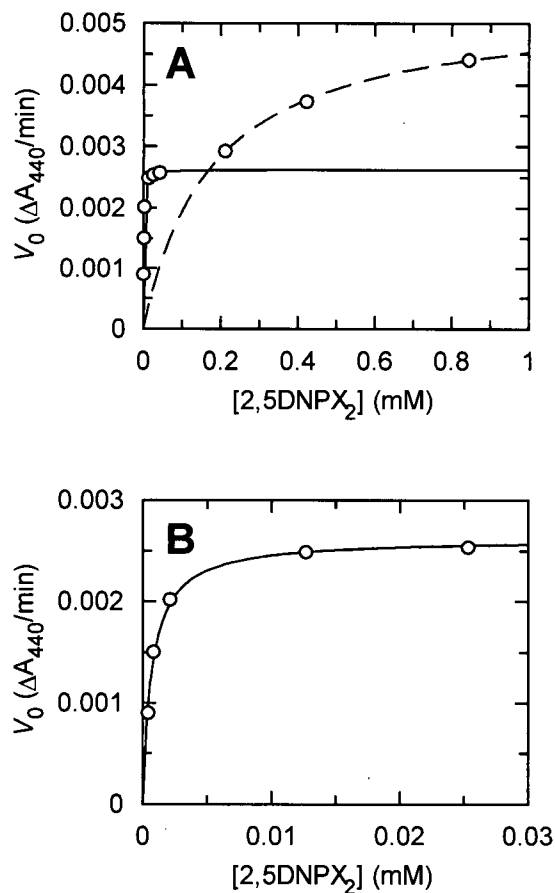


Figure A.61: Michaelis-Menten plot for the hydrolysis of 2,5DNPX₂ catalyzed by Cex H80Q. Plot A shows all data points with a solid line drawn through the points that represent the hydrolysis reaction and a dashed line through those that represent the transglycosylation reaction. Plot B shows the Michaelis-Menten plot for the hydrolysis reaction.

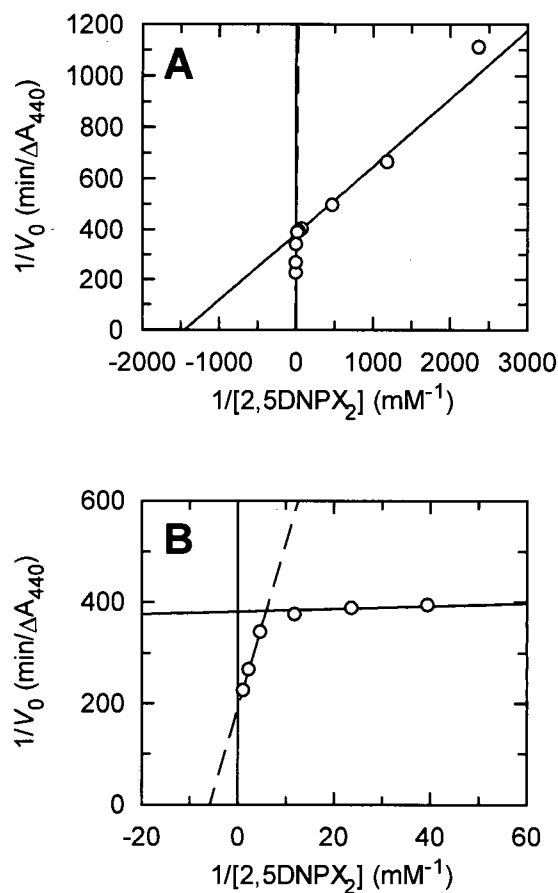


Figure A.62: Lineweaver-Burk plot for the hydrolysis of 2,5DNPX₂ catalyzed by Cex H80Q. The solid line represents the hydrolysis reaction and the dashed line represents the transglycosylation reactions. Plot A shows all data points. Plot B magnifies data points obtained for the transglycosylation reaction.

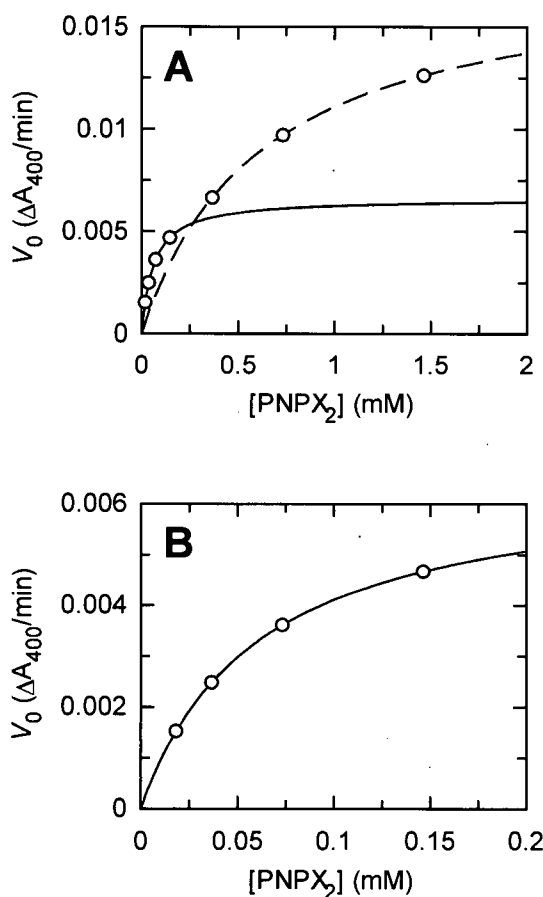


Figure A.63: Michaelis-Menten plot for the hydrolysis of PNPX_2 catalyzed by Cex H80Q. Plot A shows all data points with a solid line drawn through the points that represent the hydrolysis reaction and a dashed line through those that represent the transglycosylation reaction. Plot B shows the Michaelis-Menten plot for the hydrolysis reaction.

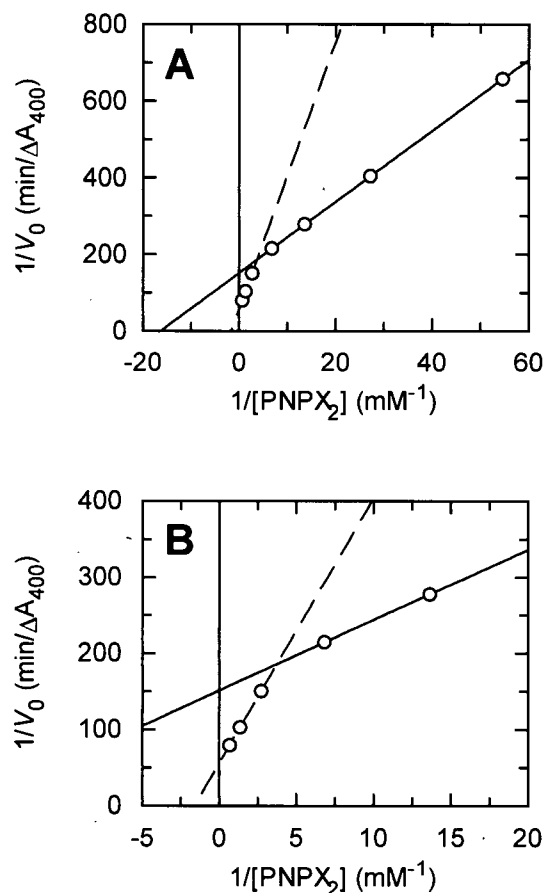


Figure A.64: Lineweaver-Burk plot for the hydrolysis of PNPX_2 catalyzed by Cex H80Q. The solid line represents the hydrolysis reaction and the dashed line represents the transglycosylation reactions. Plot A shows all data points. Plot B magnifies data points obtained for the transglycosylation reaction.

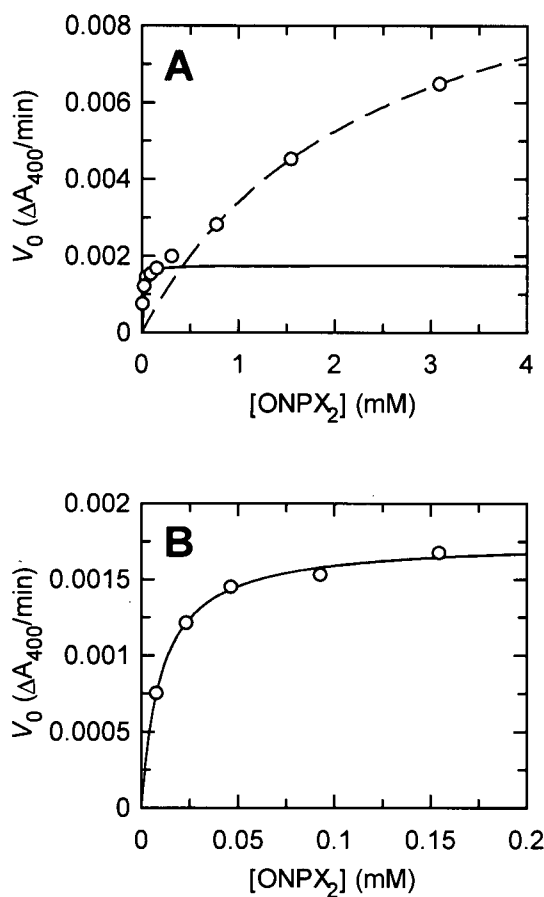


Figure A.65: Michaelis-Menten plot for the hydrolysis of ONPX_2 catalyzed by Cex H80Q. Plot A shows all data points with a solid line drawn through the points that represent the hydrolysis reaction and a dashed line through those that represent the transglycosylation reaction. Plot B shows the Michaelis-Menten plot for the hydrolysis reaction.

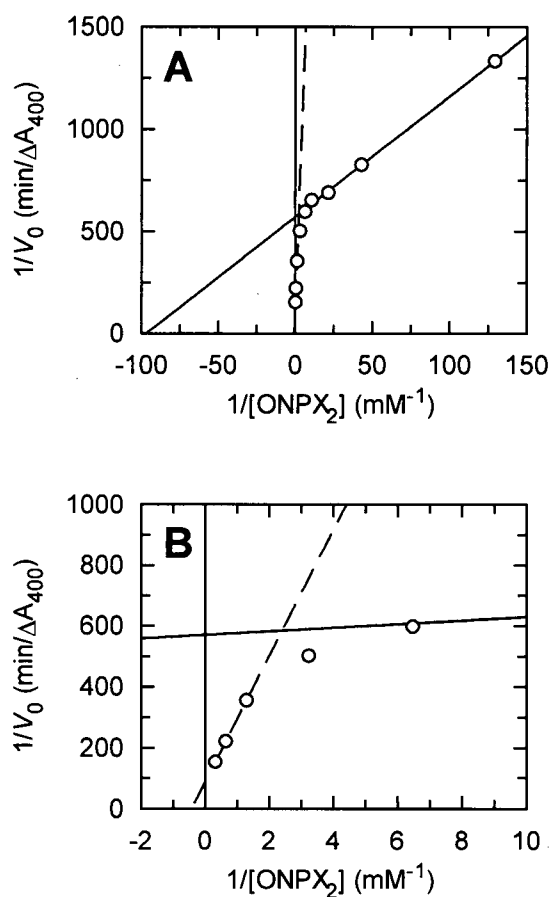


Figure A.66: Lineweaver-Burk plot for the hydrolysis of ONPX_2 catalyzed by Cex H80Q. The solid line represents the hydrolysis reaction and the dashed line represents the transglycosylation reactions. Plot A shows all data points. Plot B magnifies data points obtained for the transglycosylation reaction.

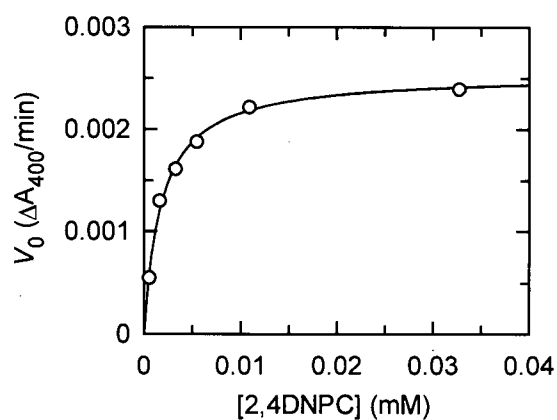


Figure A.67: Michaelis-Menten plot for the hydrolysis of 2,4DNPC catalyzed by Cex H80Q.

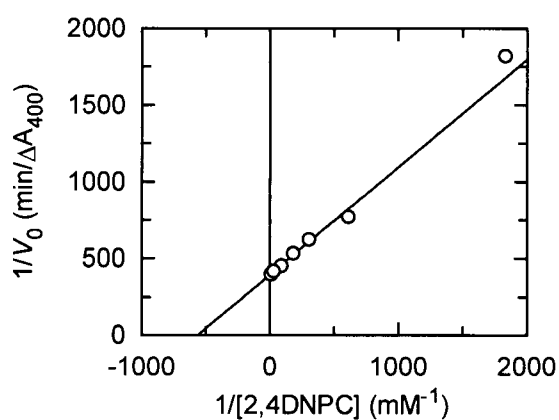


Figure A.68: Lineweaver-Burk plot for the hydrolysis of 2,4DNPC catalyzed by Cex H80Q.

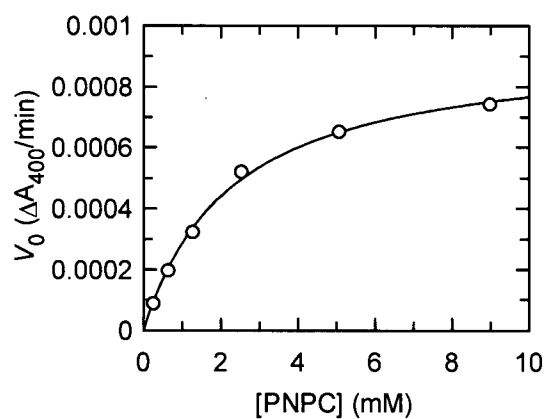


Figure A.69: Michaelis-Menten plot for the hydrolysis of PNPC catalyzed by Cex H80Q.

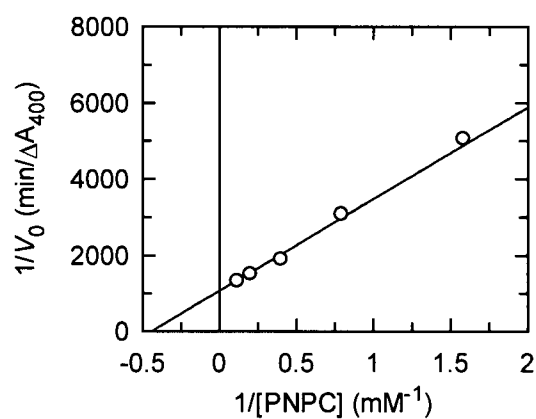


Figure A.70: Lineweaver-Burk plot for the hydrolysis of PNPC catalyzed by Cex H80Q.

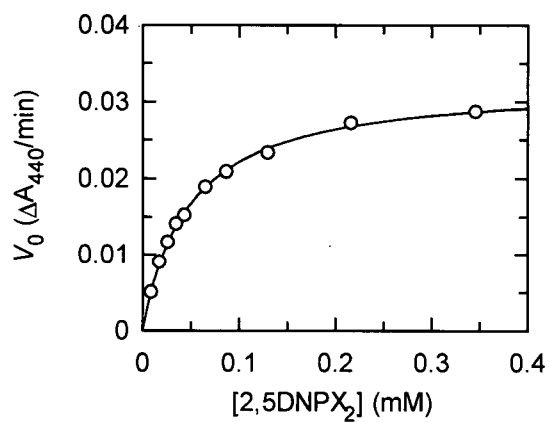
A.1.8 Cex Q87M

Figure A.71: Michaelis–Menten plot for the hydrolysis of 2,5DNPX₂ catalyzed by Cex Q87M.

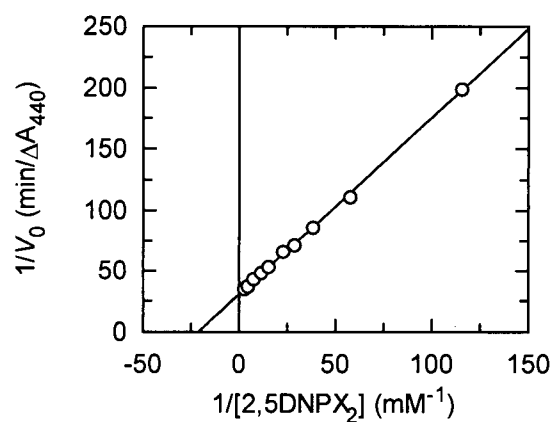


Figure A.72: Lineweaver–Burk plot for the hydrolysis of 2,5DNPX₂ catalyzed by Cex Q87M.

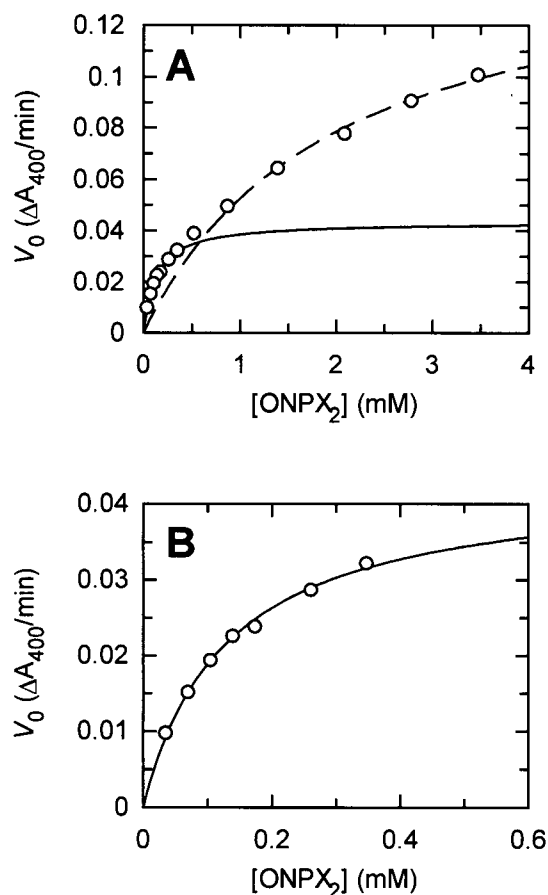


Figure A.73: Michaelis-Menten plot for the hydrolysis of ONPX₂ catalyzed by Cex Q87M. Plot A shows all data points with a solid line drawn through the points that represent the hydrolysis reaction and a dashed line through those that represent the transglycosylation reaction. Plot B shows the Michaelis-Menten plot for the hydrolysis reaction.

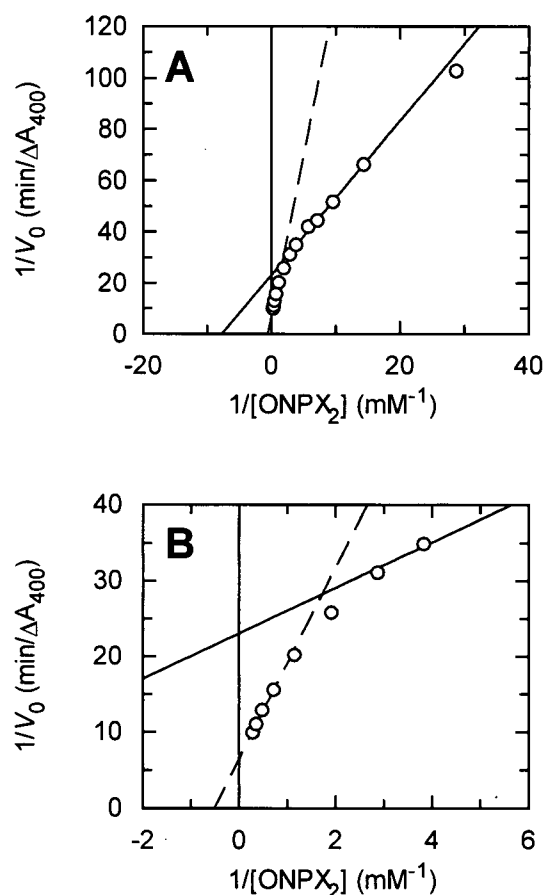


Figure A.74: Lineweaver-Burk plot for the hydrolysis of ONPX₂ catalyzed by Cex Q87M. The solid line represents the hydrolysis reaction and the dashed line represents the transglycosylation reactions. Plot A shows all data points. Plot B magnifies data points obtained for the transglycosylation reaction.

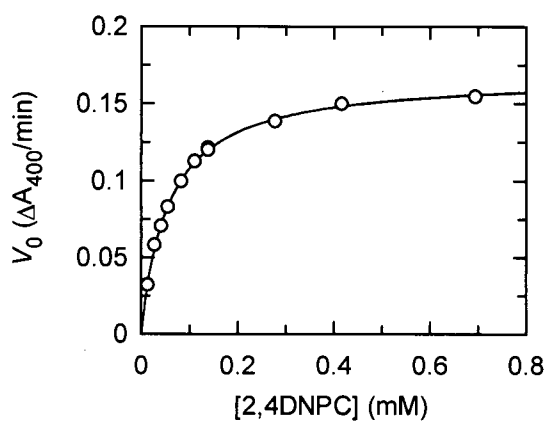


Figure A.75: Michaelis-Menten plot for the hydrolysis of 2,4DNPC catalyzed by Cex Q87M.

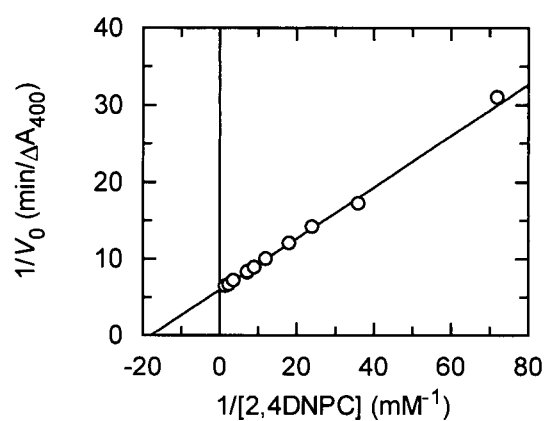


Figure A.76: Lineweaver-Burk plot for the hydrolysis of 2,4DNPC catalyzed by Cex Q87M.

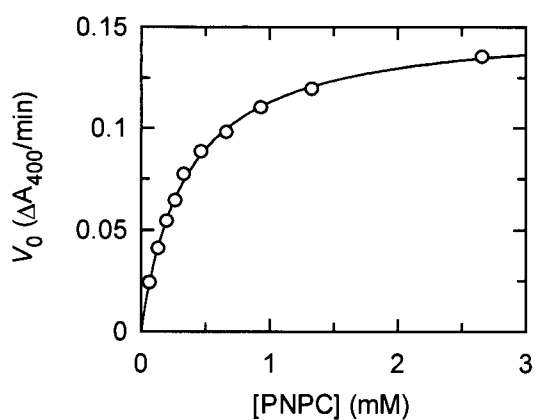


Figure A.77: Michaelis-Menten plot for the hydrolysis of PNPC catalyzed by Cex Q87M.

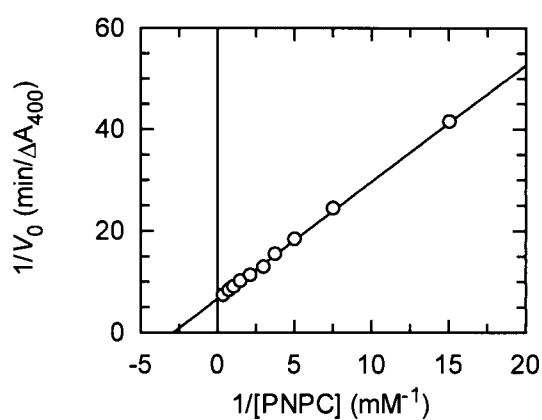


Figure A.78: Lineweaver-Burk plot for the hydrolysis of PNPC catalyzed by Cex Q87M.

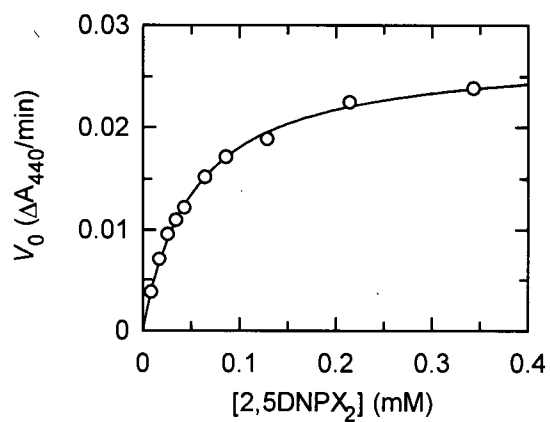
A.1.9 Cex Q87Y

Figure A.79: Michaelis–Menten plot for the hydrolysis of 2,5DNPX₂ catalyzed by Cex Q87Y.

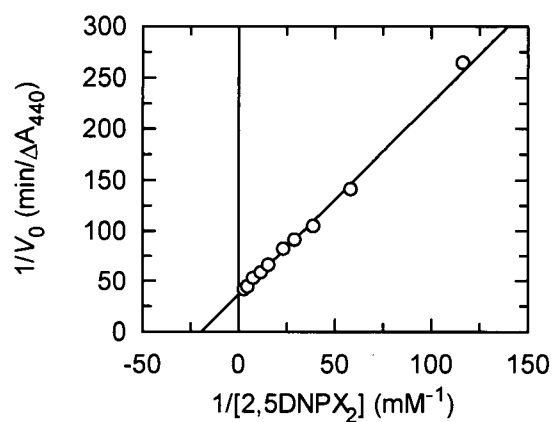


Figure A.80: Lineweaver–Burk plot for the hydrolysis of 2,5DNPX₂ catalyzed by Cex Q87Y.

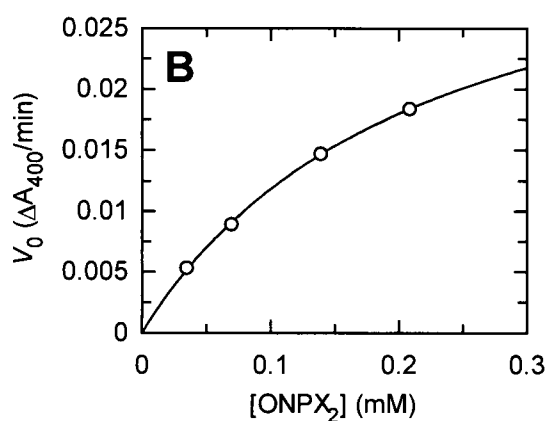
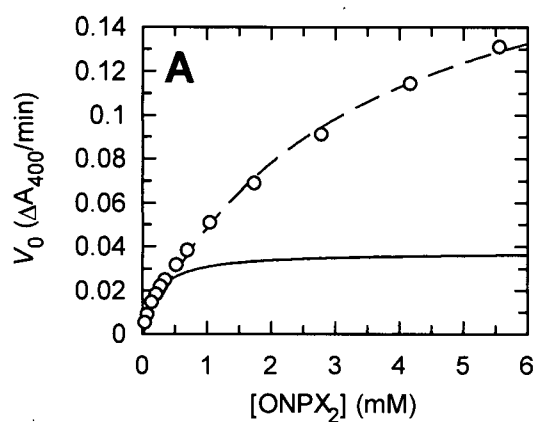


Figure A.81: Michaelis-Menten plot for the hydrolysis of ONPX₂ catalyzed by Cex Q87Y. Plot A shows all data points with a solid line drawn through the points that represent the hydrolysis reaction and a dashed line through those that represent the transglycosylation reaction. Plot B shows the Michaelis-Menten plot for the hydrolysis reaction.

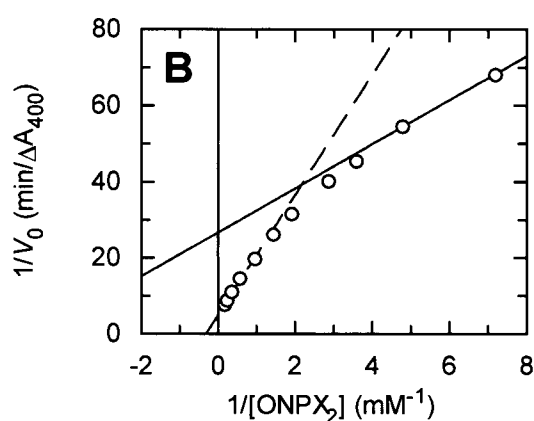
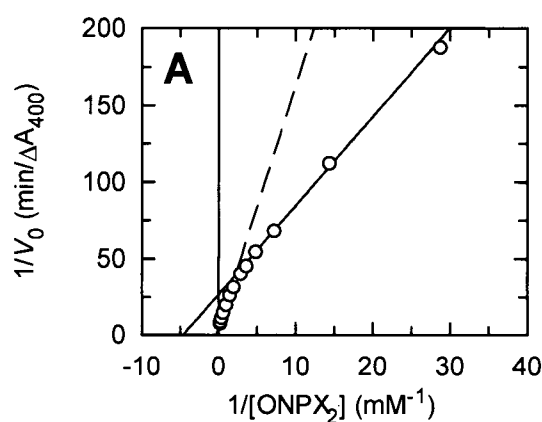


Figure A.82: Lineweaver-Burk plot for the hydrolysis of ONPX₂ catalyzed by Cex Q87Y. The solid line represents the hydrolysis reaction and the dashed line represents the transglycosylation reactions. Plot A shows all data points. Plot B magnifies data points obtained for the transglycosylation reaction.

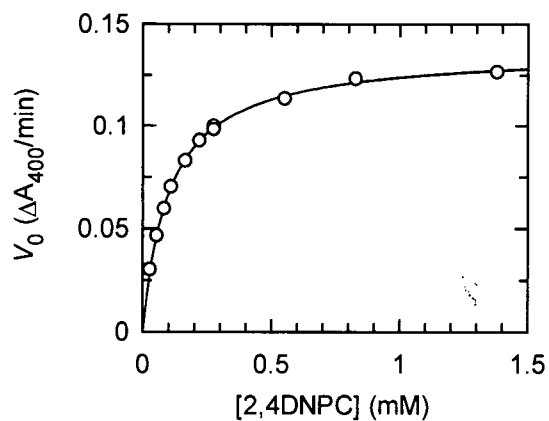


Figure A.83: Michaelis–Menten plot for the hydrolysis of 2,4DNPC catalyzed by Cex Q87Y.

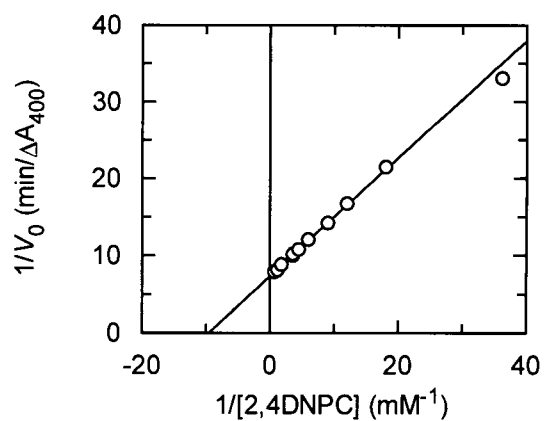


Figure A.84: Lineweaver–Burk plot for the hydrolysis of 2,4DNPC catalyzed by Cex Q87Y.

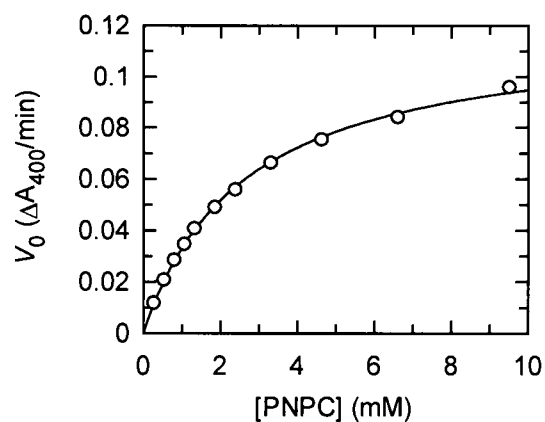


Figure A.85: Michaelis–Menten plot for the hydrolysis of PNPC catalyzed by Cex Q87Y.

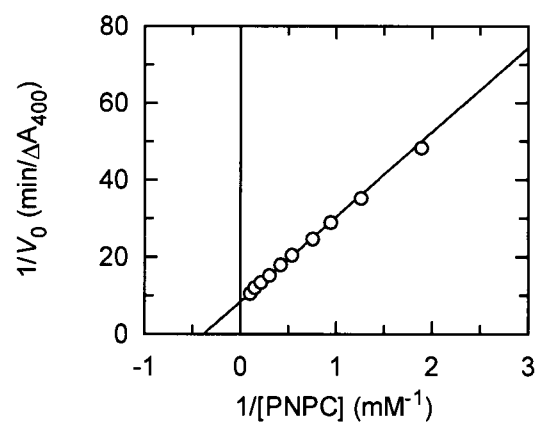


Figure A.86: Lineweaver–Burk plot for the hydrolysis of PNPC catalyzed by Cex Q87Y.

A.1.10Cex N126A

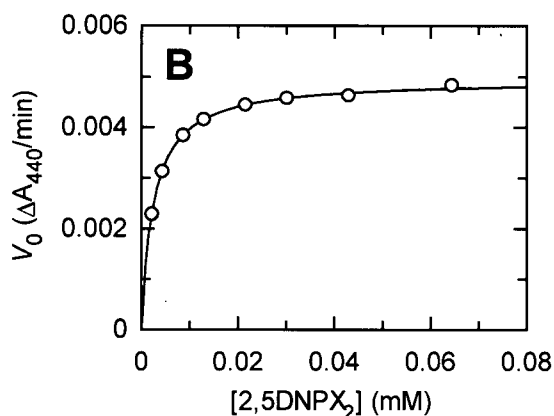
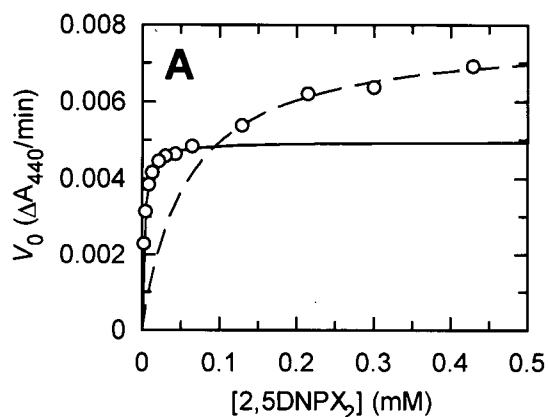


Figure A.87: Michaelis-Menten plot for the hydrolysis of 2,5DNPX₂ catalyzed by Cex N126A. Plot A shows all data points with a solid line drawn through the points that represent the hydrolysis reaction and a dashed line through those that represent the transglycosylation reaction. Plot B shows the Michaelis-Menten plot for the hydrolysis reaction.

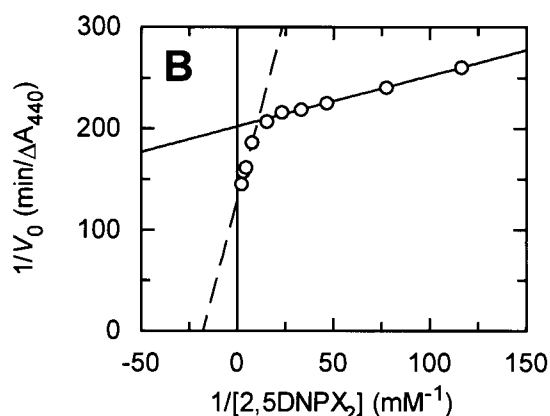
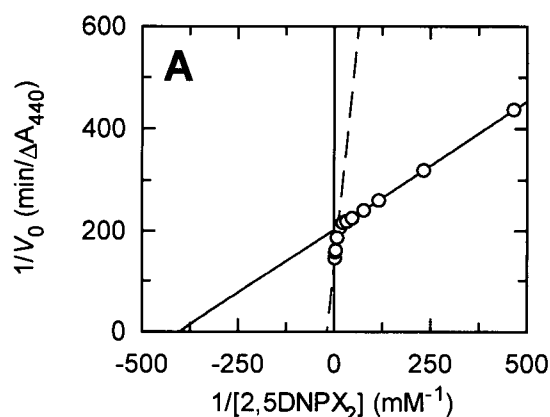


Figure A.88: Lineweaver-Burk plot for the hydrolysis of 2,5DNPX₂ catalyzed by Cex N126A. The solid line represents the hydrolysis reaction and the dashed line represents the transglycosylation reactions. Plot A shows all data points. Plot B magnifies data points obtained for the transglycosylation reaction.

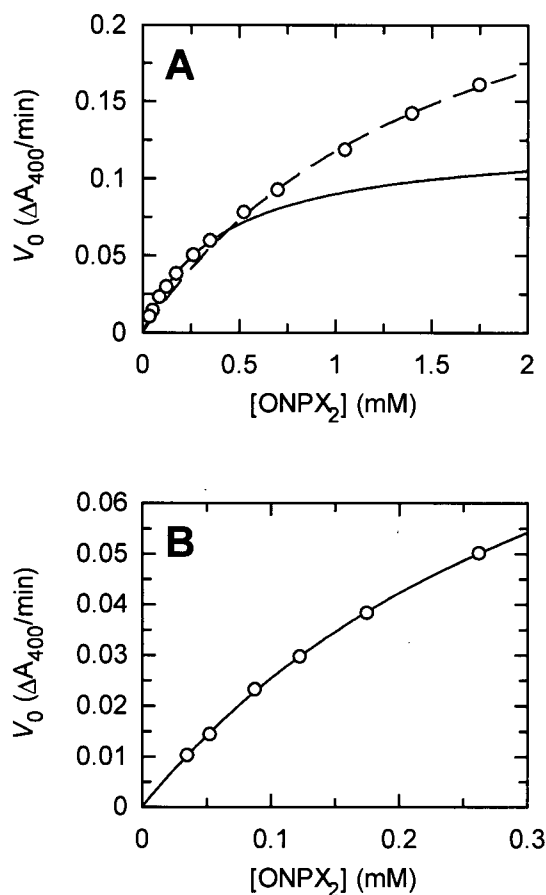


Figure A.89: Michaelis-Menten plot for the hydrolysis of ONPX₂ catalyzed by Cex N126A. Plot A shows all data points with a solid line drawn through the points that represent the hydrolysis reaction and a dashed line through those that represent the transglycosylation reaction. Plot B shows the Michaelis-Menten plot for the hydrolysis reaction.

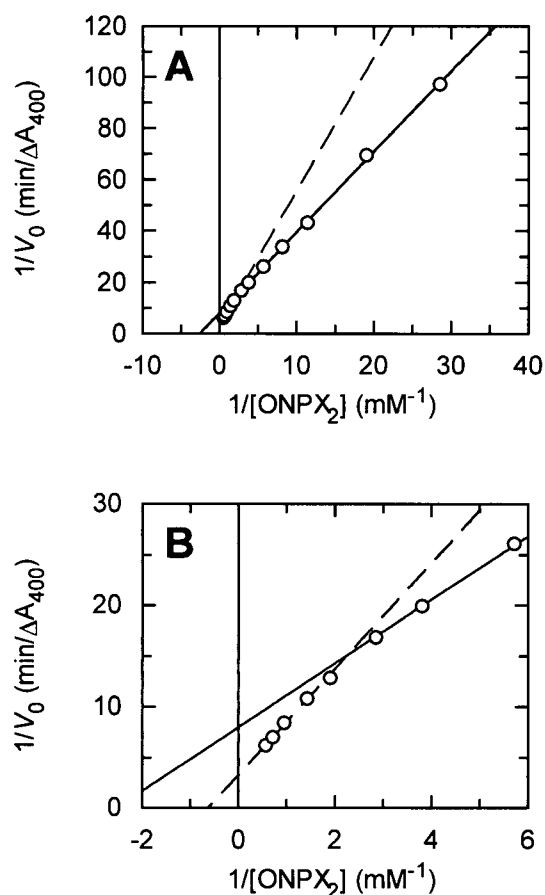


Figure A.90: Lineweaver-Burk plot for the hydrolysis of ONPX₂ catalyzed by Cex N126A. The solid line represents the hydrolysis reaction and the dashed line represents the transglycosylation reactions. Plot A shows all data points. Plot B magnifies data points obtained for the transglycosylation reaction.

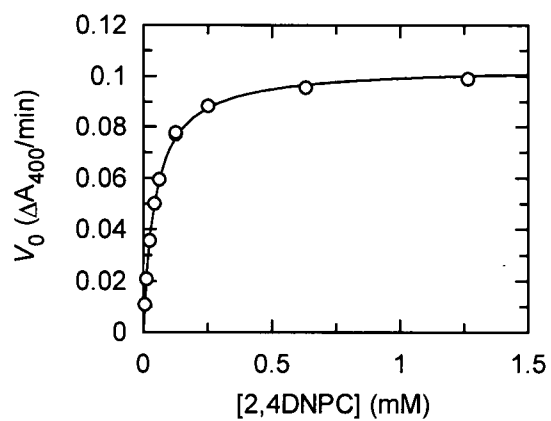


Figure A.91: Michaelis-Menten plot for the hydrolysis of 2,4DNPC catalyzed by Cex N126A.

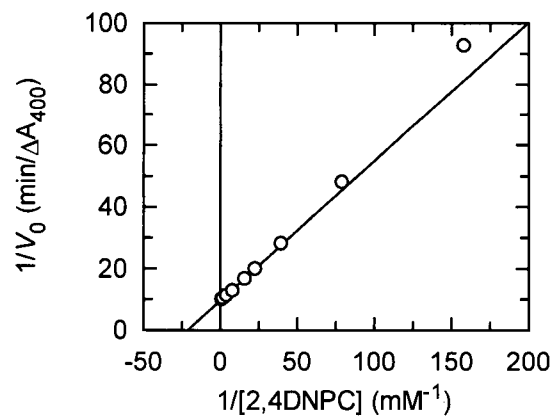


Figure A.92: Lineweaver-Burk plot for the hydrolysis of 2,4DNPC catalyzed by Cex N126A.

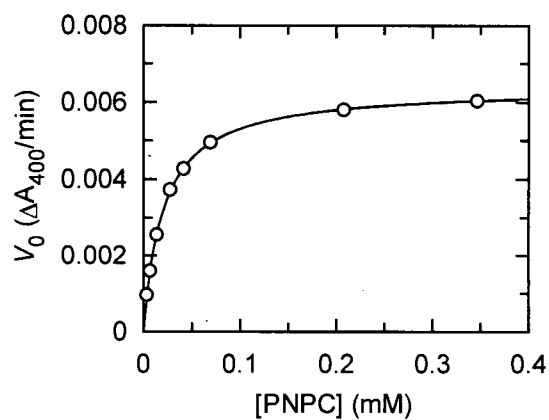
A.1.11 Cex E127A

Figure A.93: Michaelis-Menten plot for the hydrolysis of PNPC catalyzed by Cex E127A.

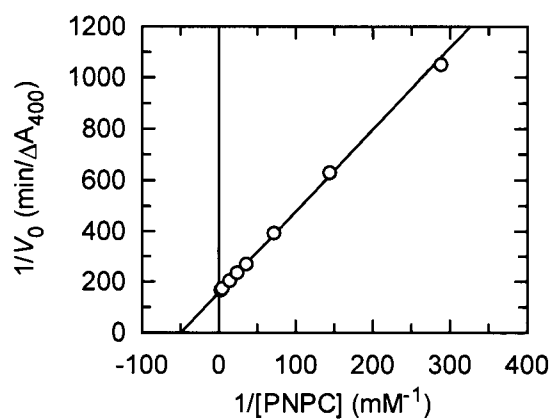


Figure A.94: Lineweaver-Burk plot for the hydrolysis of PNPC catalyzed by Cex E127A.

A.1.12Cex N169A

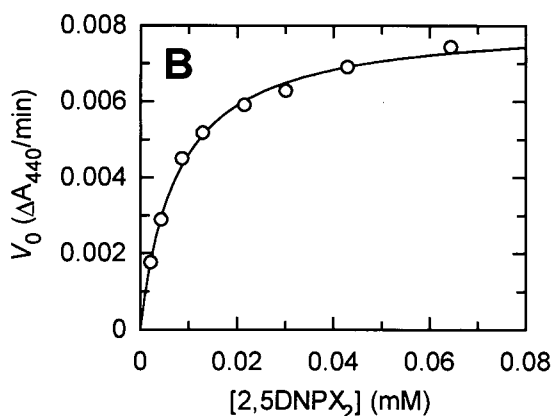
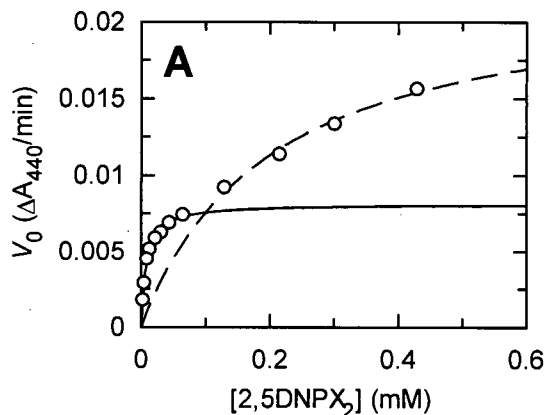


Figure A.95: Michaelis-Menten plot for the hydrolysis of 2,5DNPX₂ catalyzed by Cex N169A. Plot A shows all data points with a solid line drawn through the points that represent the hydrolysis reaction and a dashed line through those that represent the transglycosylation reaction. Plot B shows the Michaelis-Menten plot for the hydrolysis reaction.

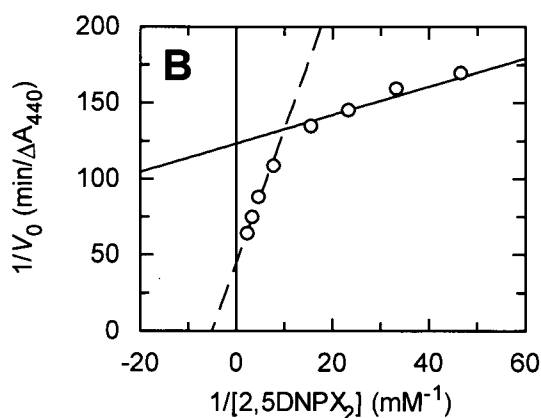
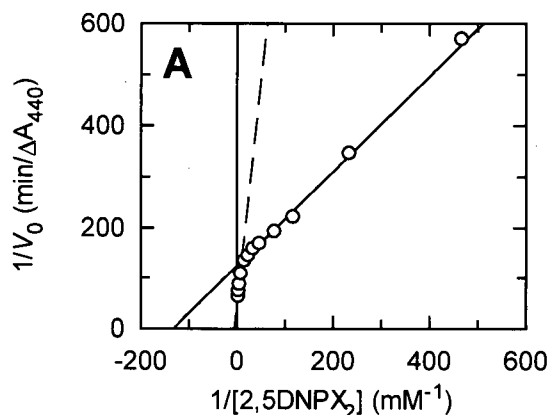


Figure A.96: Lineweaver-Burk plot for the hydrolysis of 2,5DNPX₂ catalyzed by Cex N169A. The solid line represents the hydrolysis reaction and the dashed line represents the transglycosylation reactions. Plot A shows all data points. Plot B magnifies data points obtained for the transglycosylation reaction.

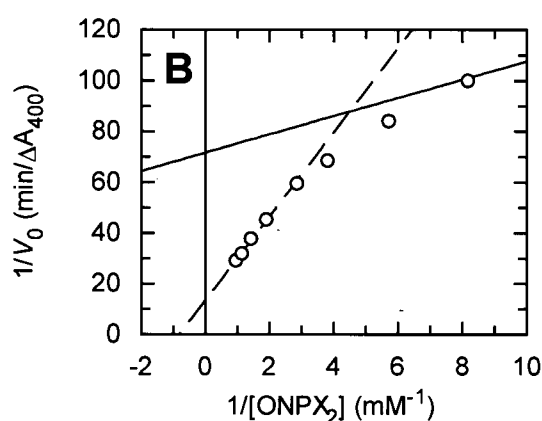
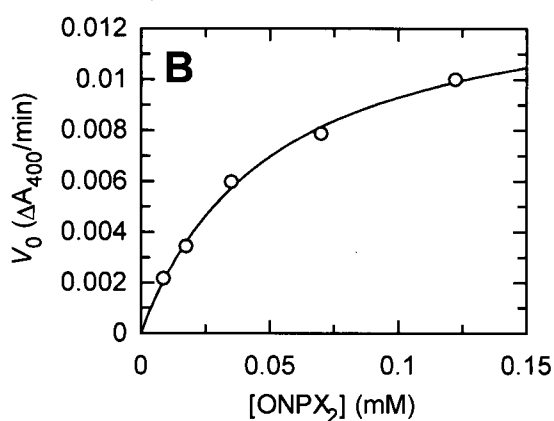
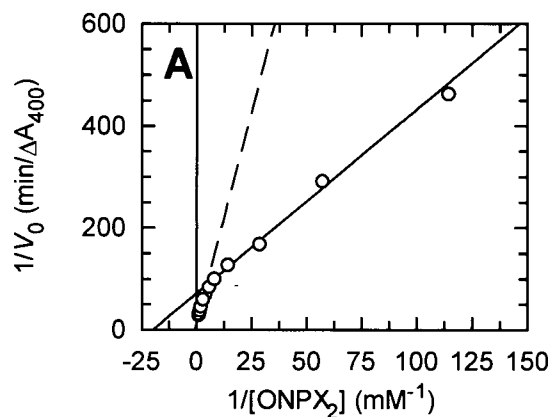
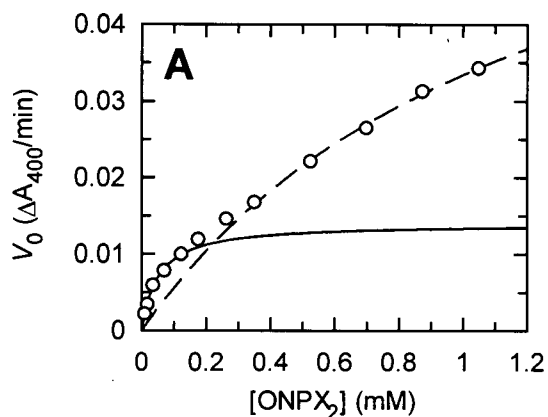


Figure A.97: Michaelis-Menten plot for the hydrolysis of ONPX_2 catalyzed by Cex N169A. Plot A shows all data points with a solid line drawn through the points that represent the hydrolysis reaction and a dashed line through those that represent the transglycosylation reaction. Plot B shows the Michaelis-Menten plot for the hydrolysis reaction.

Figure A.98: Lineweaver-Burk plot for the hydrolysis of ONPX_2 catalyzed by Cex N169A. The solid line represents the hydrolysis reaction and the dashed line represents the transglycosylation reactions. Plot A shows all data points. Plot B magnifies data points obtained for the transglycosylation reaction.

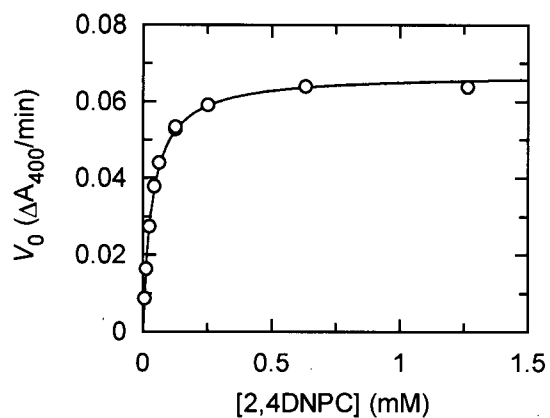


Figure A.99: Michaelis–Menten plot for the hydrolysis of 2,4DNPC catalyzed by Cex N169A.

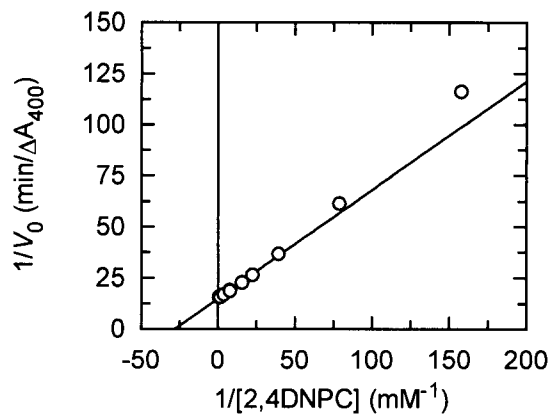


Figure A.100: Lineweaver–Burk plot for the hydrolysis of 2,4DNPC catalyzed by Cex N169A.

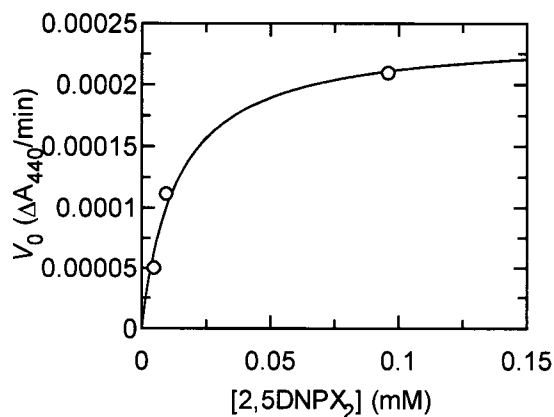
A.1.13 Cex H205N

Figure A.101: Michaelis-Menten plot for the hydrolysis of 2,5DNPX₂ catalyzed by Cex H205N.

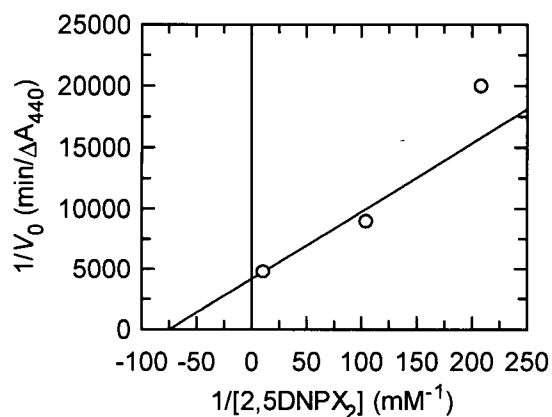


Figure A.102: Lineweaver-Burk plot for the hydrolysis of 2,5DNPX₂ catalyzed by Cex H205N.

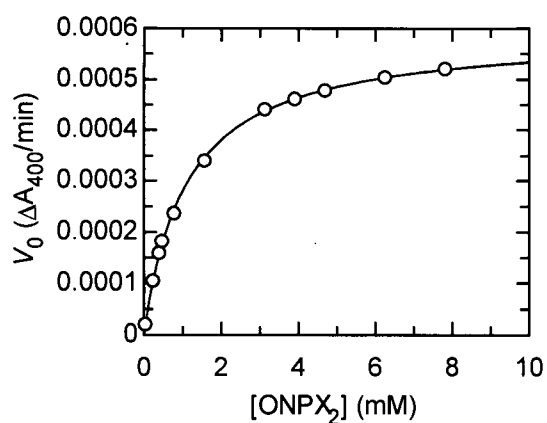


Figure A.103: Michaelis-Menten plot for the hydrolysis of ONPX₂ catalyzed by Cex H205N.

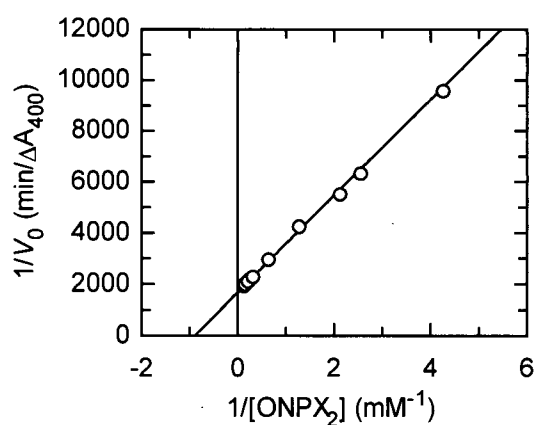


Figure A.104: Lineweaver-Burk plot for the hydrolysis of ONPX₂ catalyzed by Cex H205N.

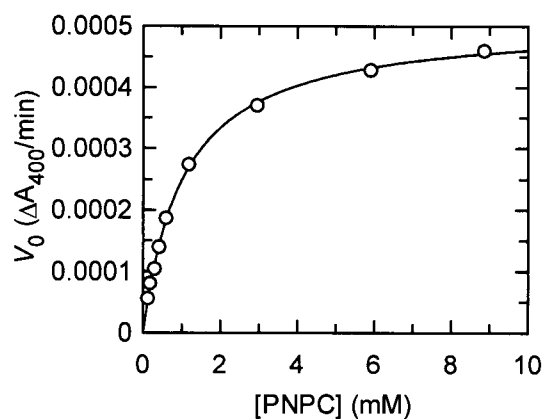


Figure A.105: Michaelis-Menten plot for the hydrolysis of PNPC catalyzed by Cex H205N.

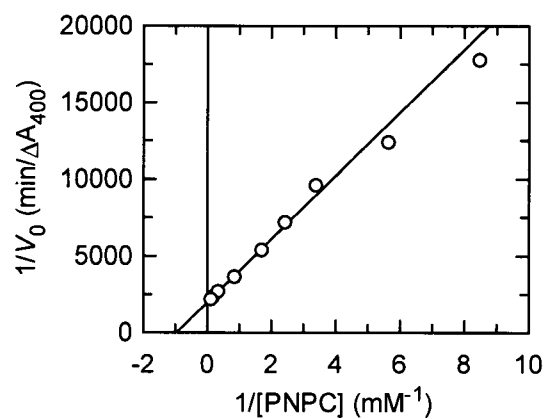


Figure A.106: Lineweaver-Burk plot for the hydrolysis of PNPC catalyzed by Cex H205N.

A.2 Steady State Kinetics for Inhibition by Imino Sugar Inhibitors

A.2.1 Cex E43A

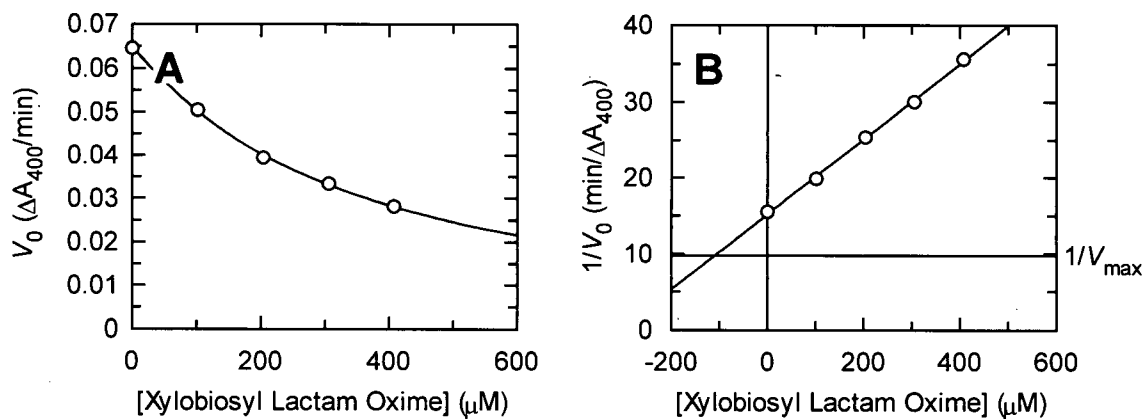


Figure A.107: Inhibition of Cex E43A by Xylobiosyl Lactam Oxime.

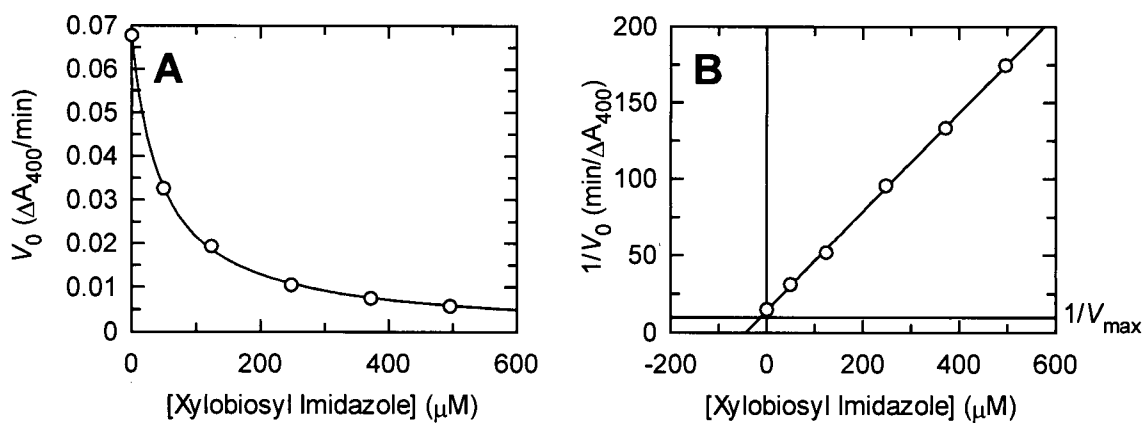


Figure A.108: Inhibition of Cex E43A by Xylobiosyl Imidazole.

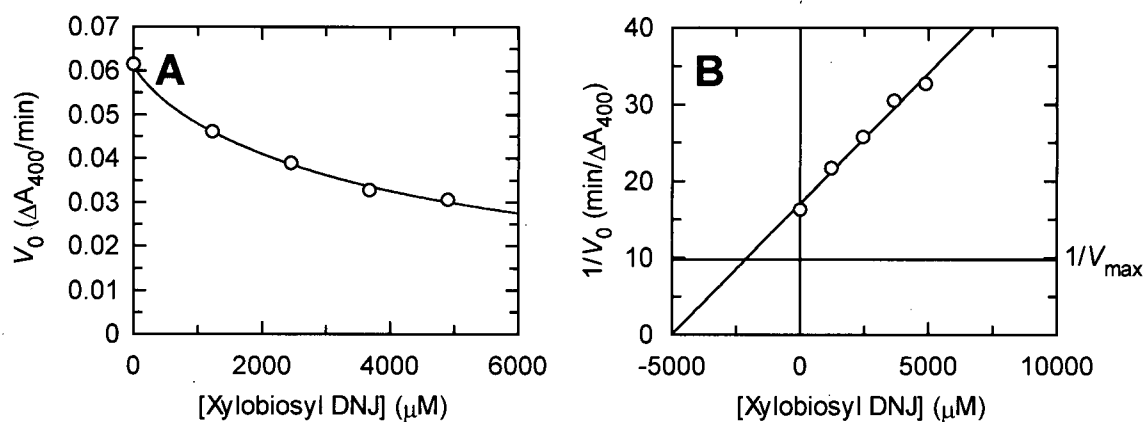


Figure A.109: Inhibition of Cex E43A by Xylobiosyl Deoxynojirimycin.

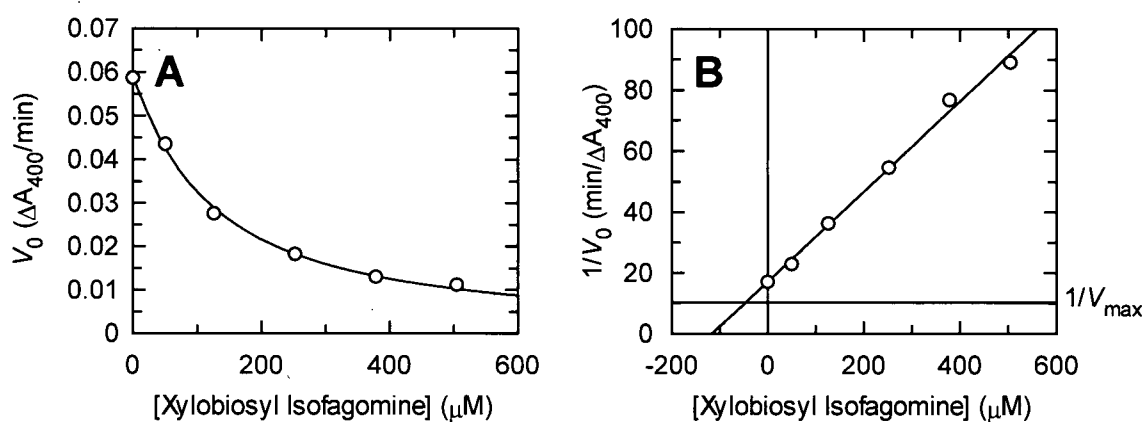


Figure A.110: Inhibition of Cex E43A by Xylobiosyl Isogagomine.

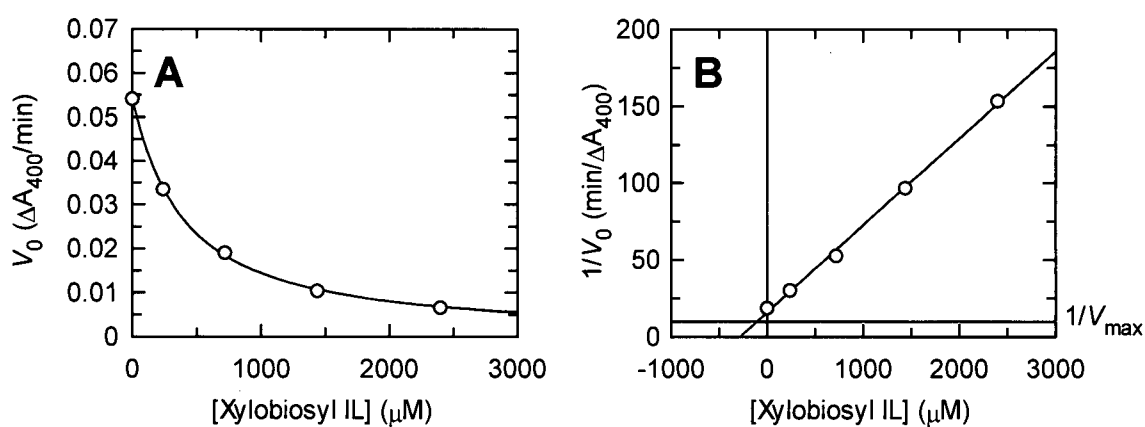
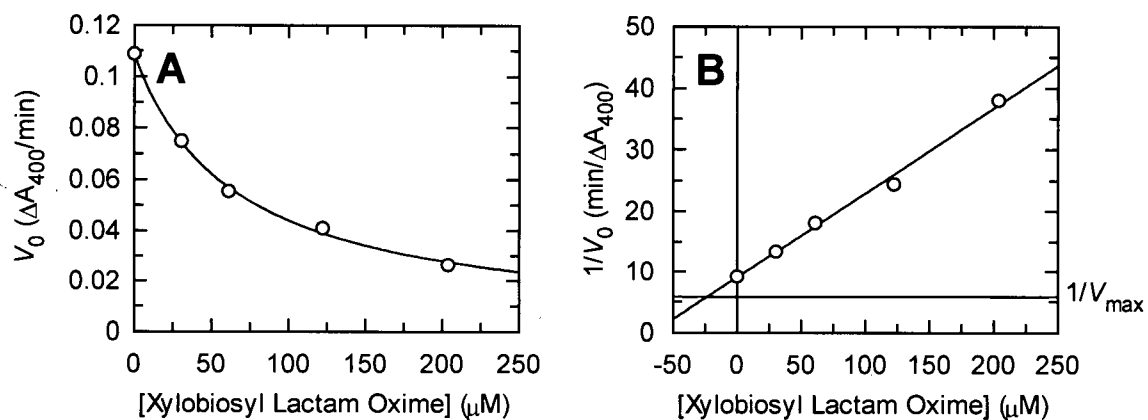
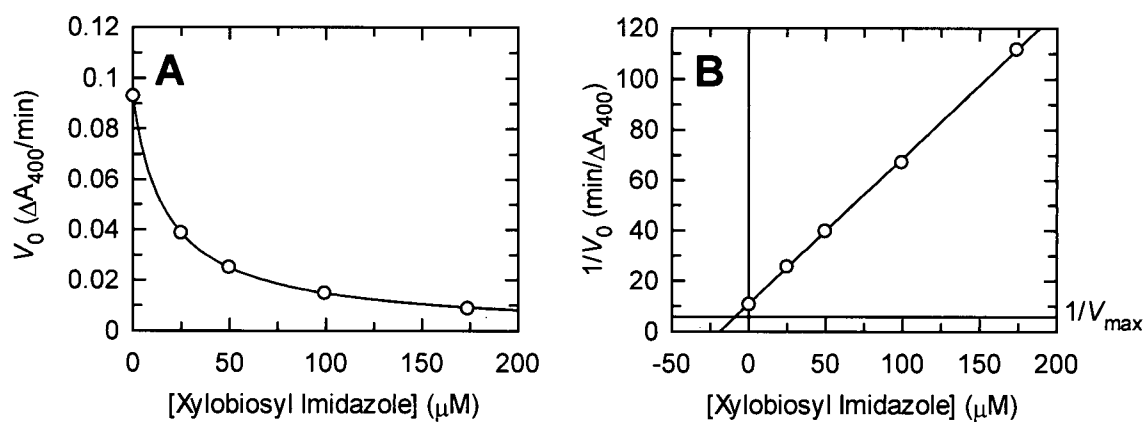
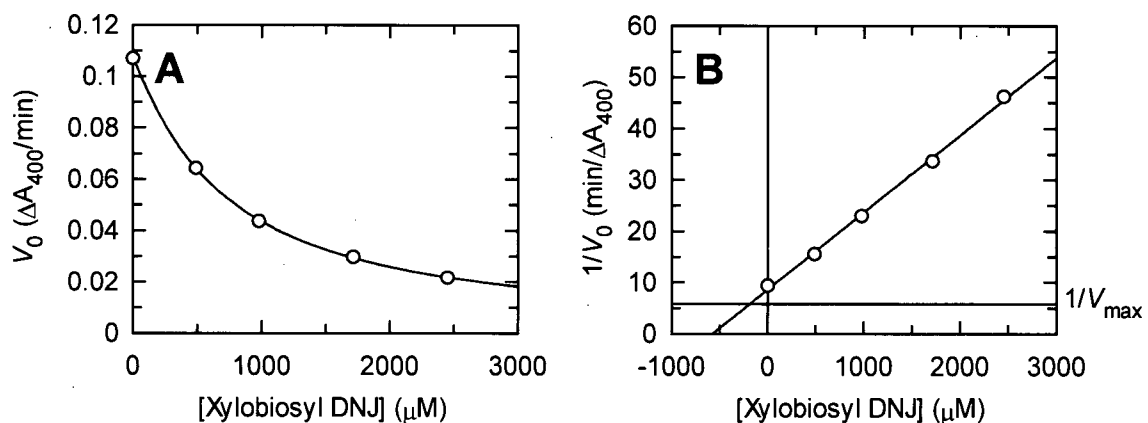


Figure A.111: Inhibition of Cex E43A by Xylobiosyl Isogagomine Lactam.

A.2.2 Cex N44A**Figure A.112: Inhibition of Cex N44A by Xylobiosyl Lactam Oxime.****Figure A.113: Inhibition of Cex N44A by Xylobiosyl Imidazole.****Figure A.114: Inhibition of Cex N44A by Xylobiosyl Deoxynojirimycin.**

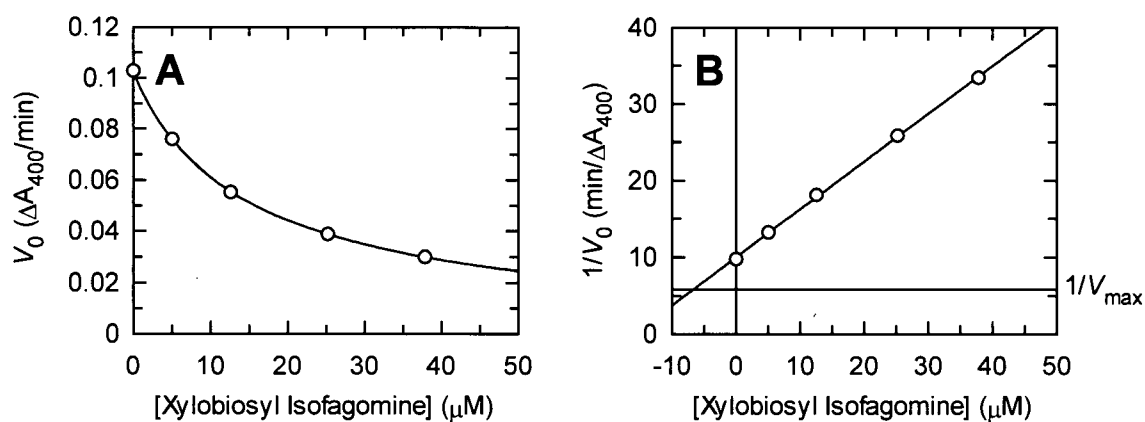


Figure A.115: Inhibition of Cex N44A by Xylobiosyl Isogomine.

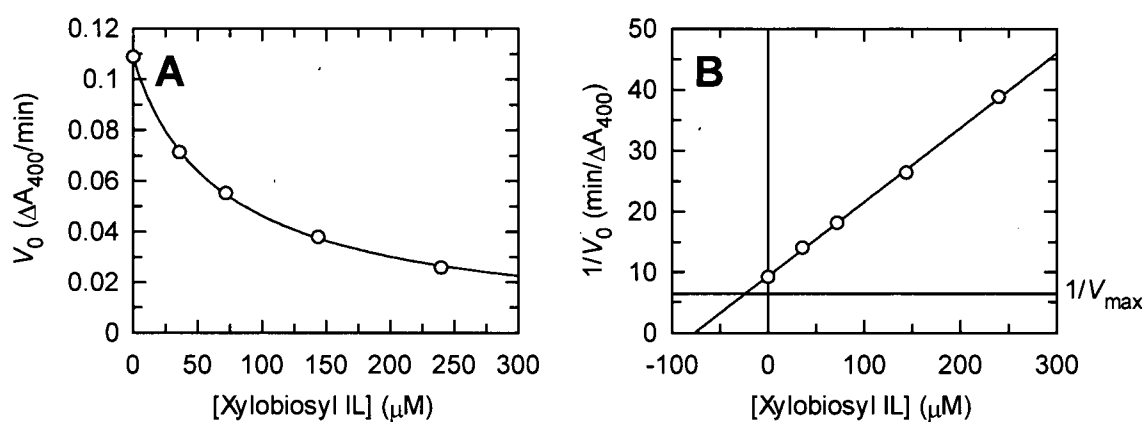
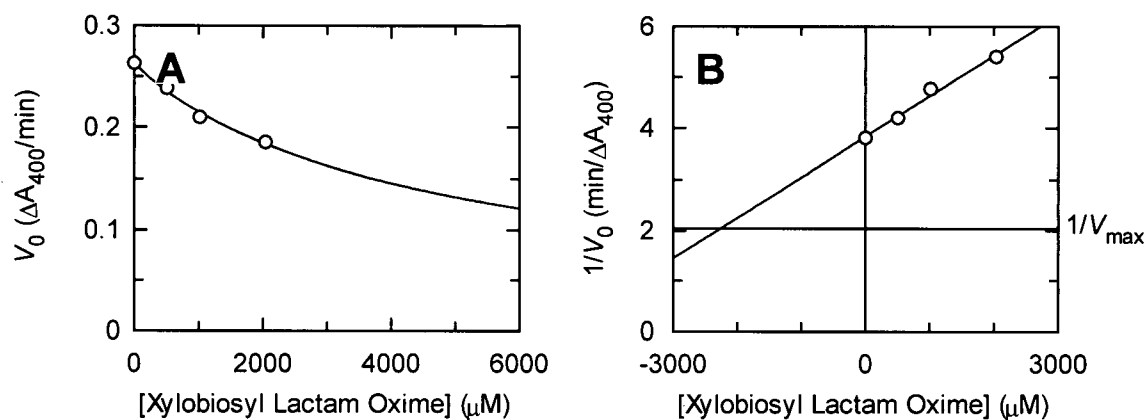
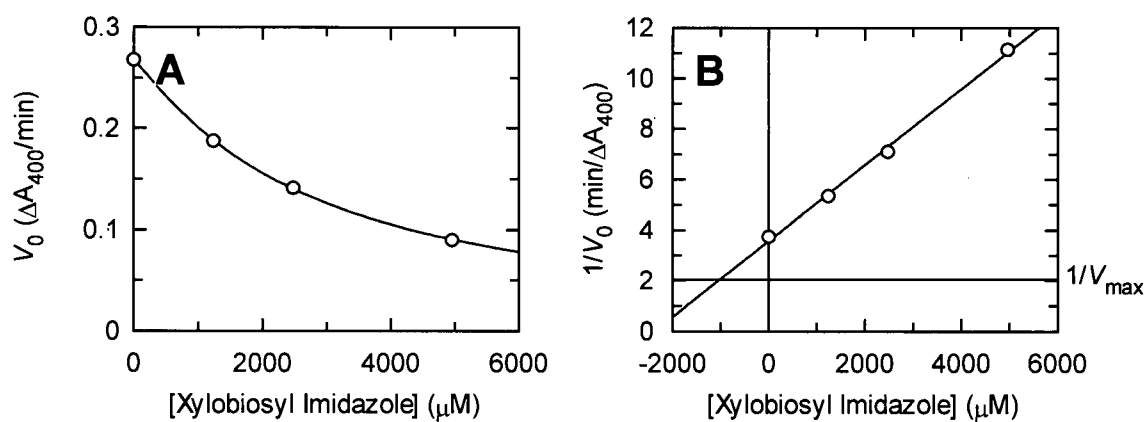
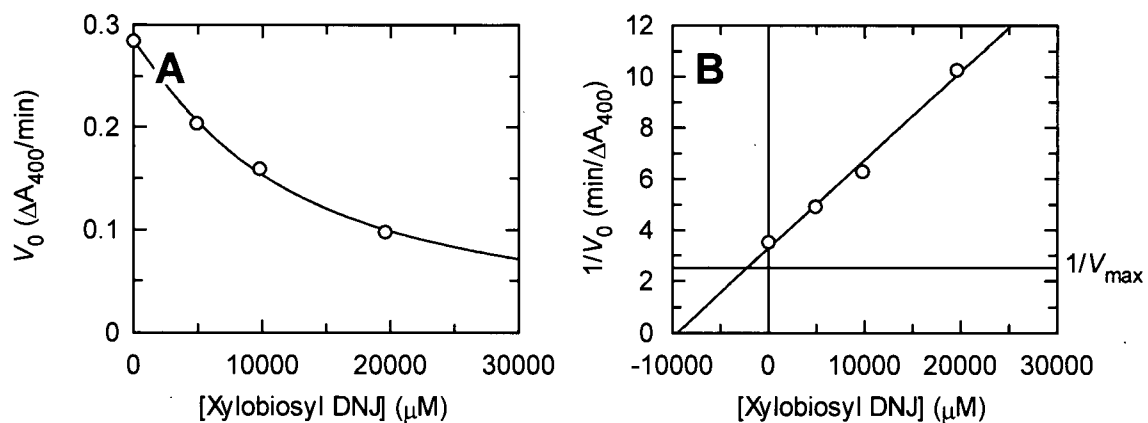


Figure A.116: Inhibition of Cex N44A by Xylobiosyl Isogomine Lactam.

A.2.3 Cex K47A**Figure A.117: Inhibition of Cex K47A by Xylobiosyl Lactam Oxime.****Figure A.118: Inhibition of Cex K47A by Xylobiosyl Imidazole.****Figure A.119: Inhibition of Cex K47A by Xylobiosyl Deoxynojirimycin.**

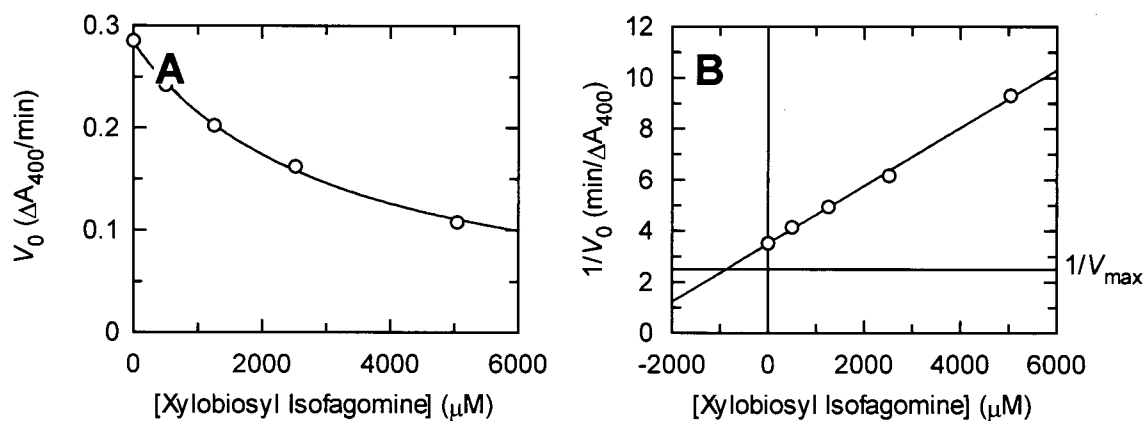


Figure A.120: Inhibition of Cex K47A by Xylobiosyl Isogomine.

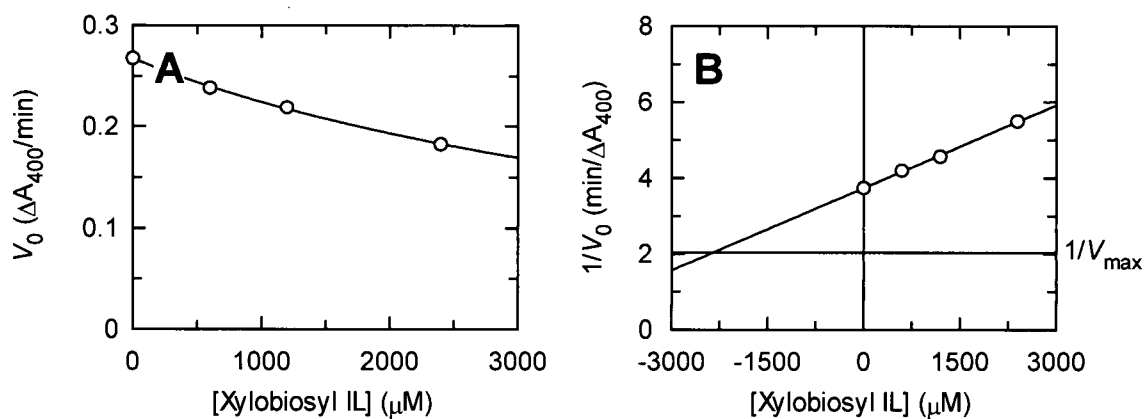
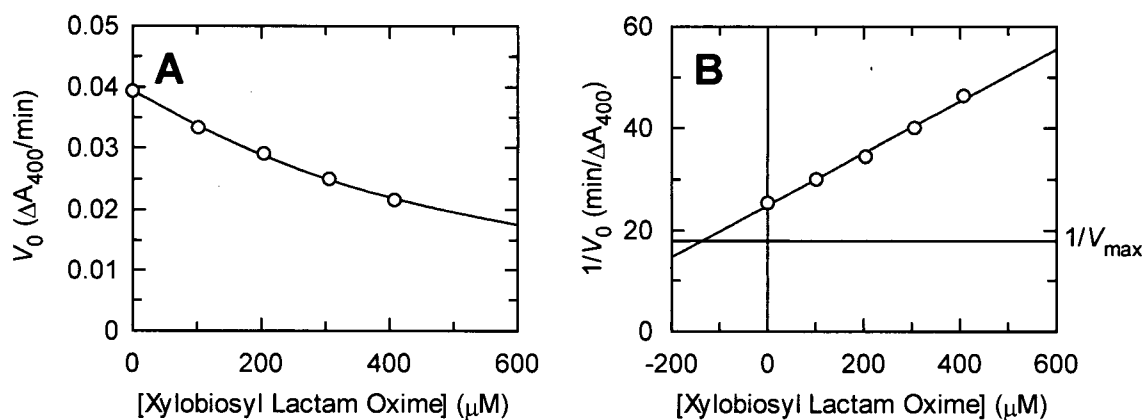
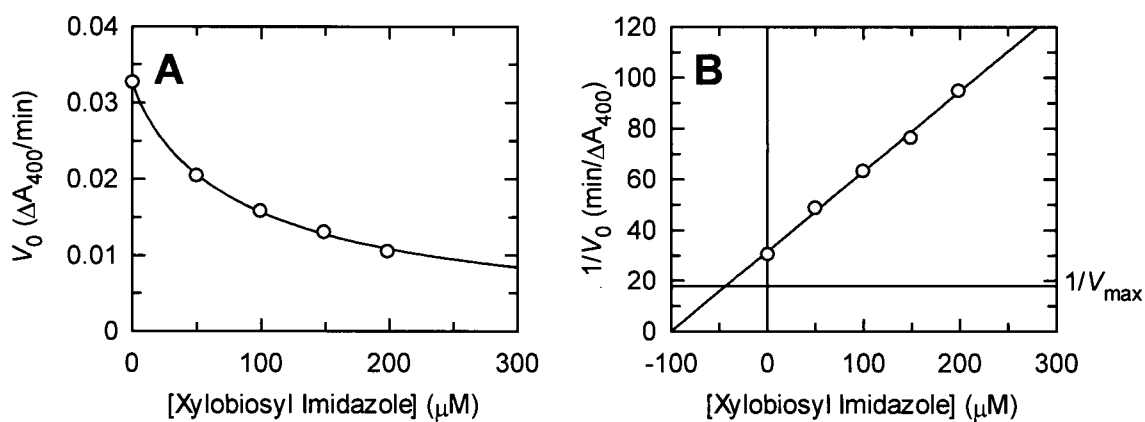
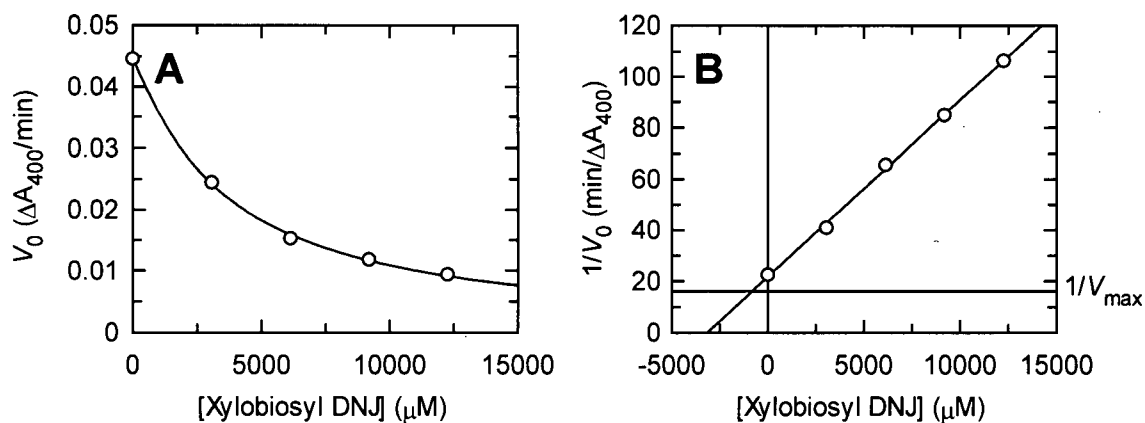


Figure A.121: Inhibition of Cex K47A by Xylobiosyl Isogomine Lactam.

A.2.4 Cex H80A**Figure A.122: Inhibition of Cex H80A by Xylobiosyl Lactam Oxime.****Figure A.123: Inhibition of Cex H80A by Xylobiosyl Imidazole.****Figure A.124: Inhibition of Cex H80A by Xylobiosyl Deoxynojirimycin.**

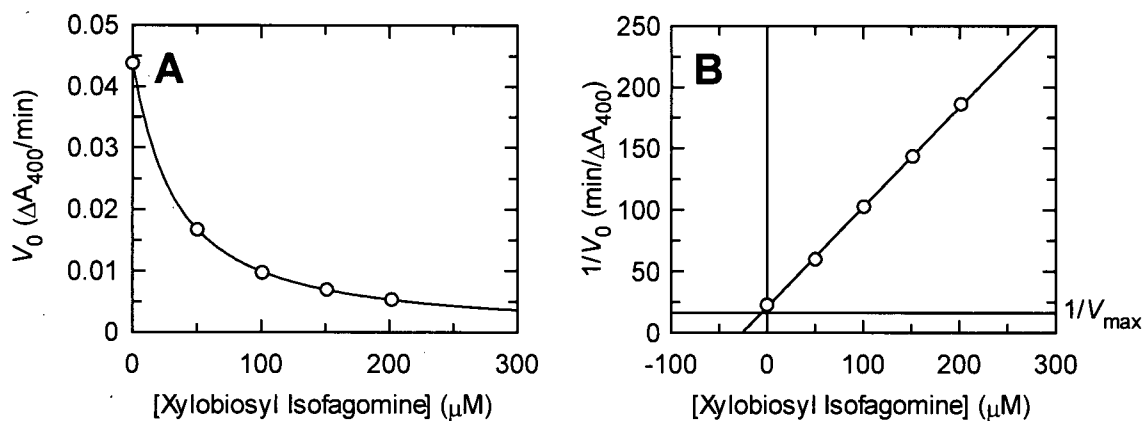


Figure A.125: Inhibition of Cex H80A by Xylobiosyl Isfagomine.

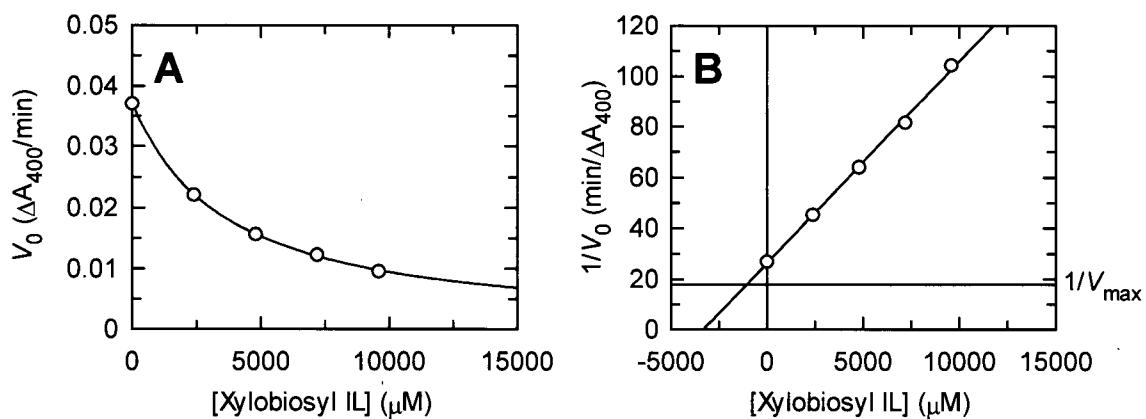
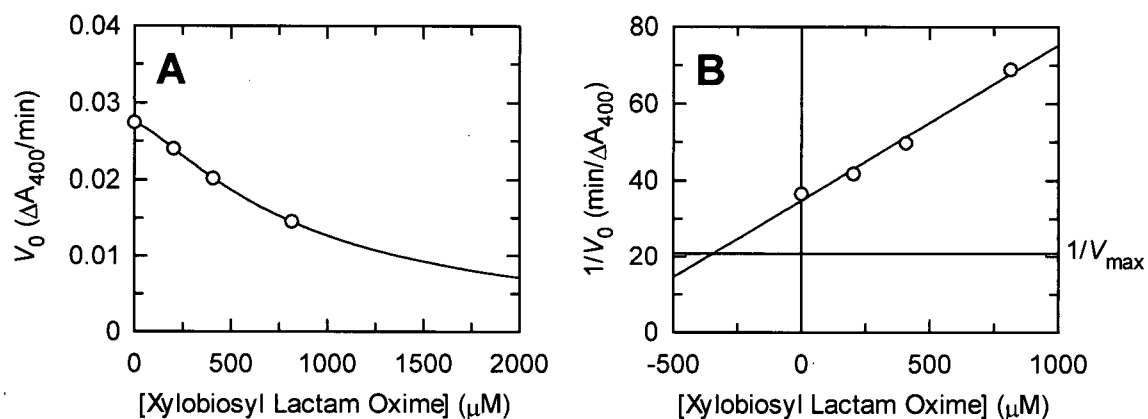
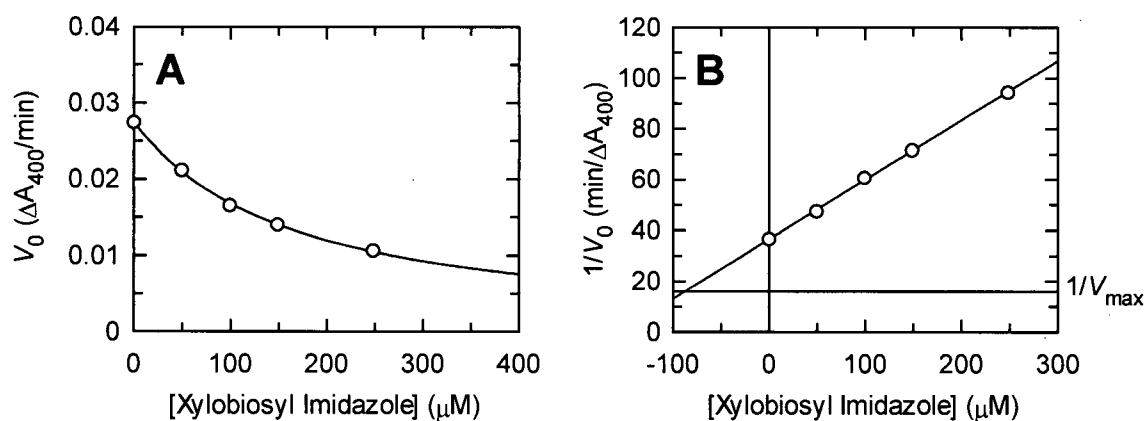
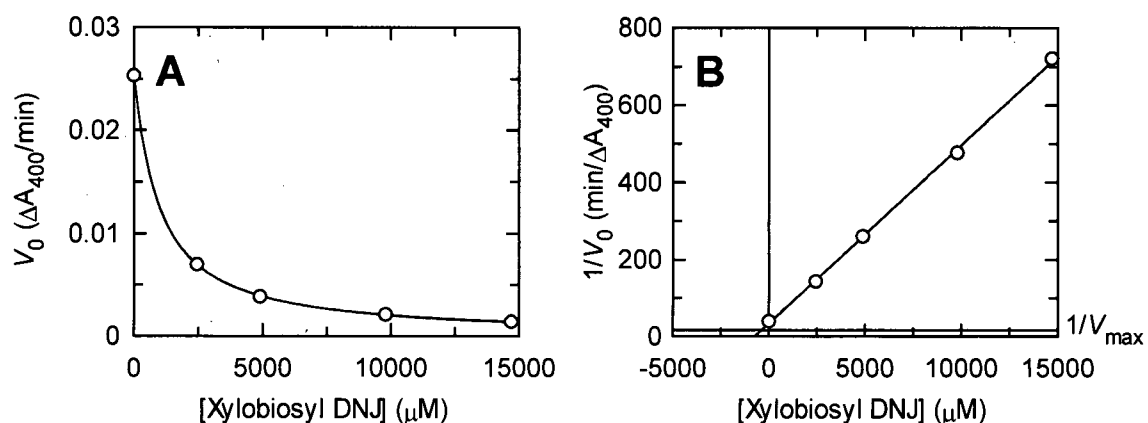


Figure A.126: Inhibition of Cex H80A by Xylobiosyl Isfagomine Lactam.

A.2.5 Cex H80N**Figure A.127: Inhibition of Cex H80N by Xylobiosyl Lactam Oxime.****Figure A.128: Inhibition of Cex H80N by Xylobiosyl Imidazole.****Figure A.129: Inhibition of Cex H80N by Xylobiosyl Deoxynojirimycin.**

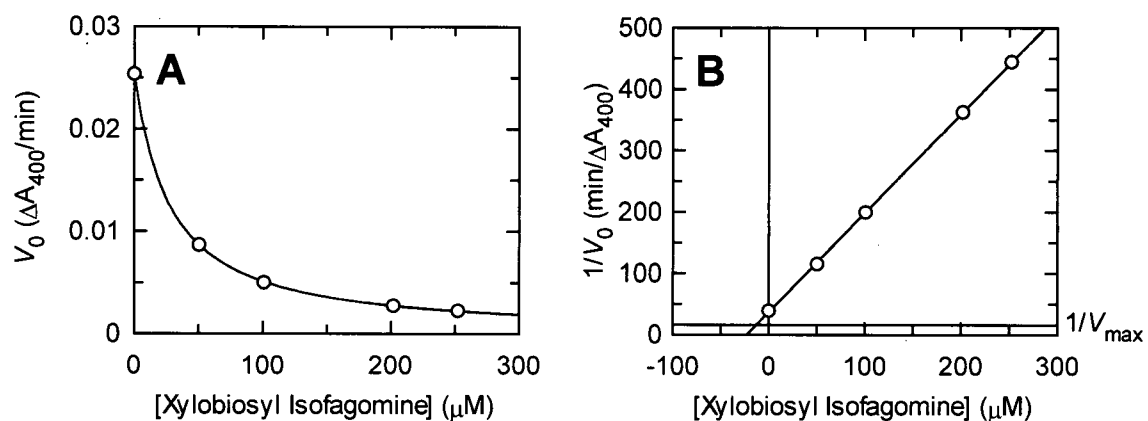


Figure A.130: Inhibition of Cex H80N by Xylobiosyl Isogomine.

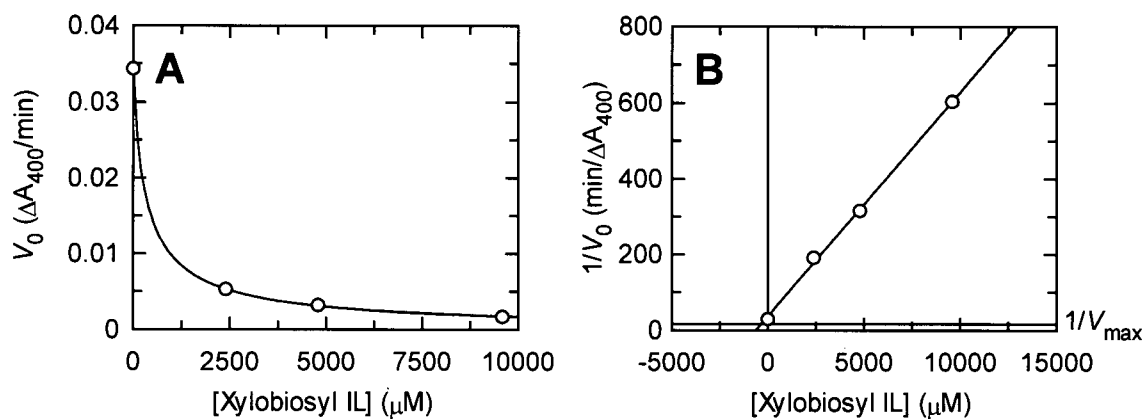
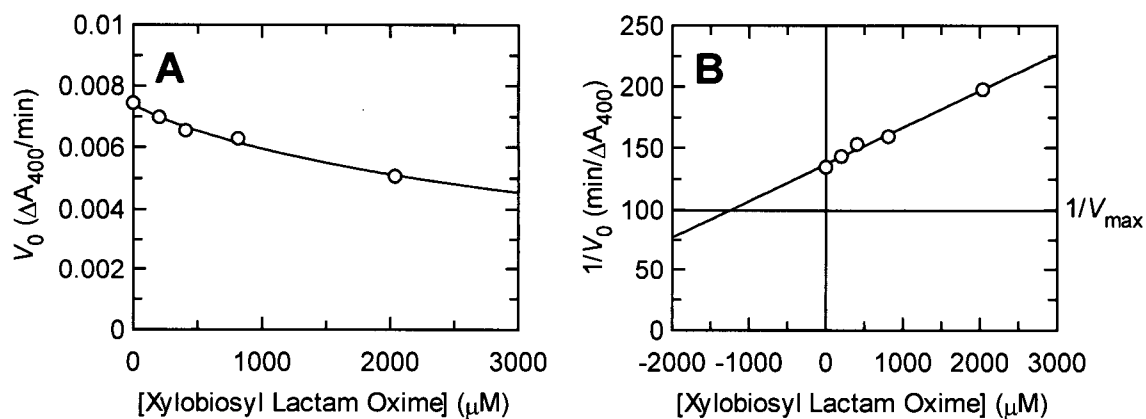
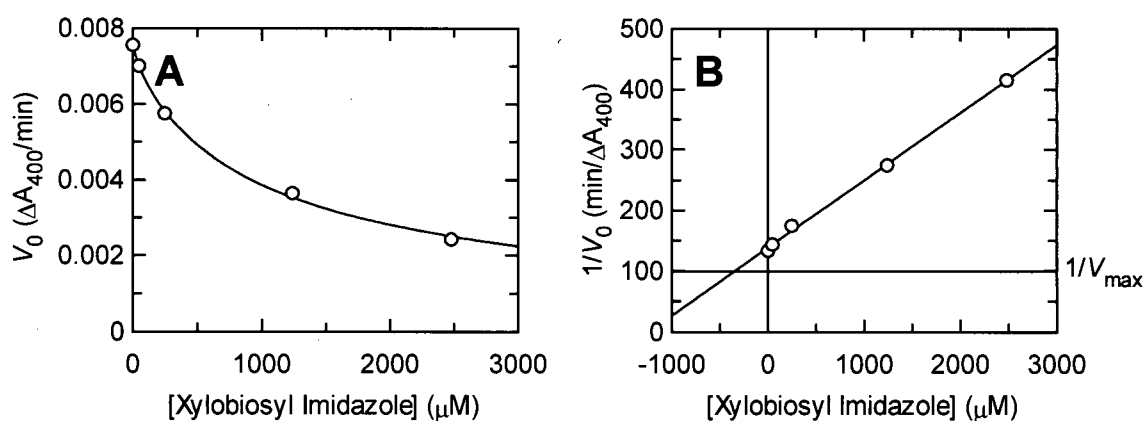
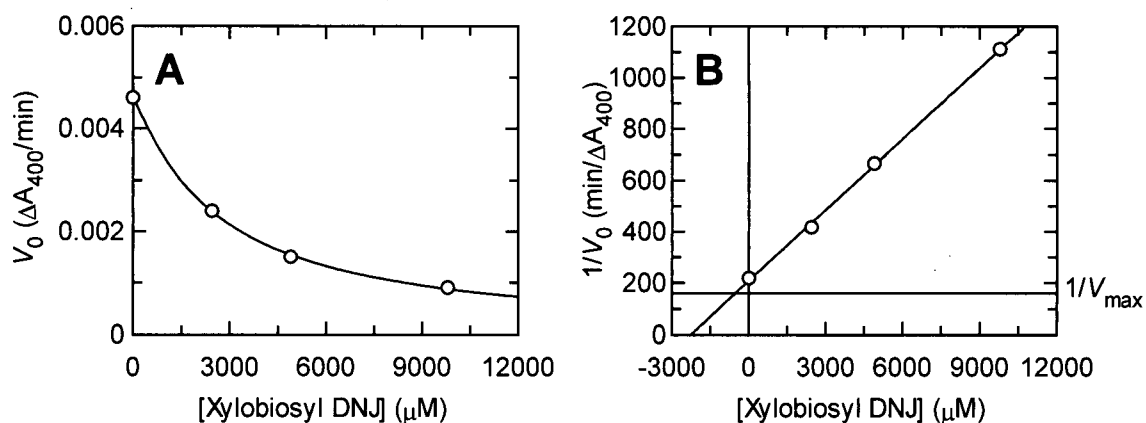


Figure A.131: Inhibition of Cex H80N by Xylobiosyl Isogomine Lactam.

A.2.6 Cex H80Q**Figure A.132: Inhibition of Cex H80Q by Xylobiosyl Lactam Oxime.****Figure A.133: Inhibition of Cex H80Q by Xylobiosyl Imidazole.****Figure A.134: Inhibition of Cex H80Q by Xylobiosyl Deoxynojirimycin.**

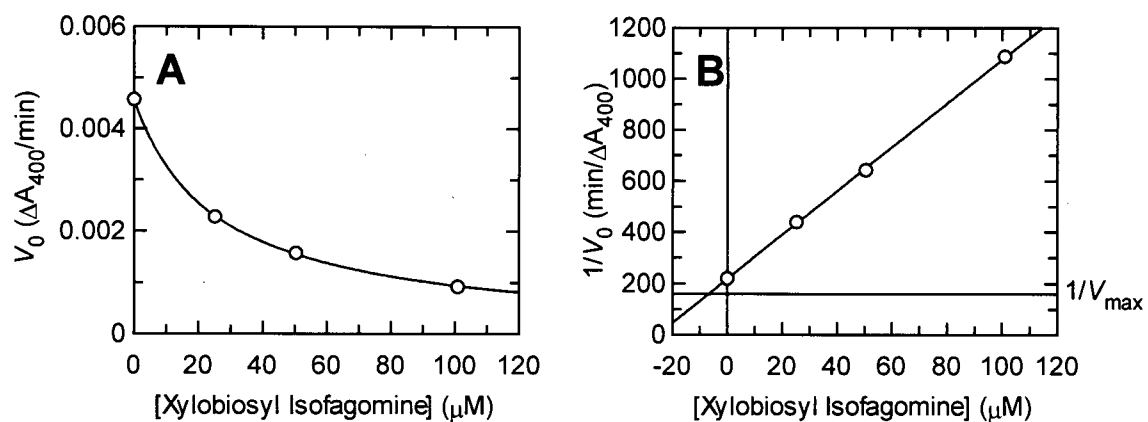


Figure A.135: Inhibition of Cex H80Q by Xylobiosyl Isogomine.

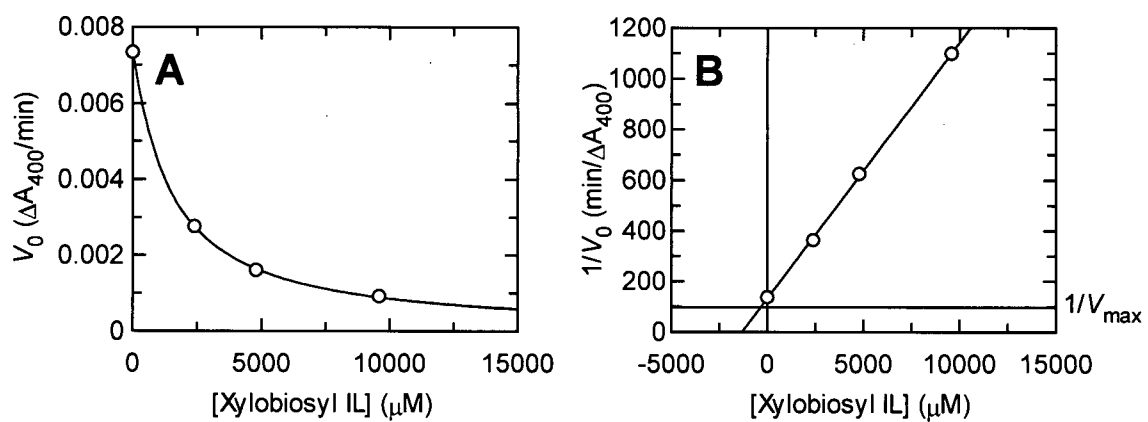
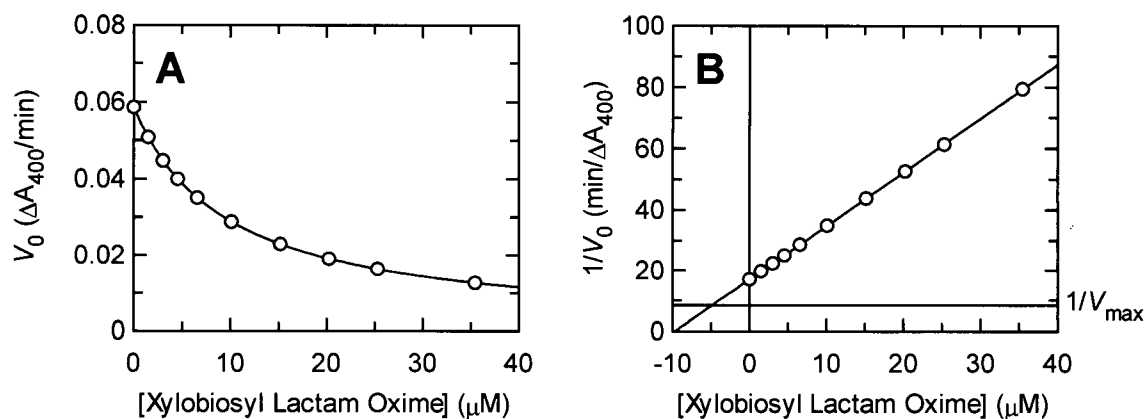
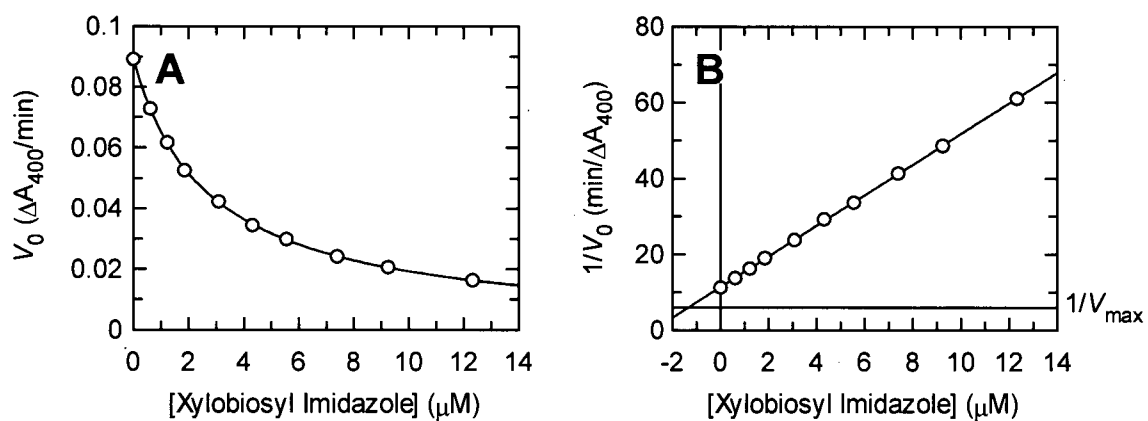
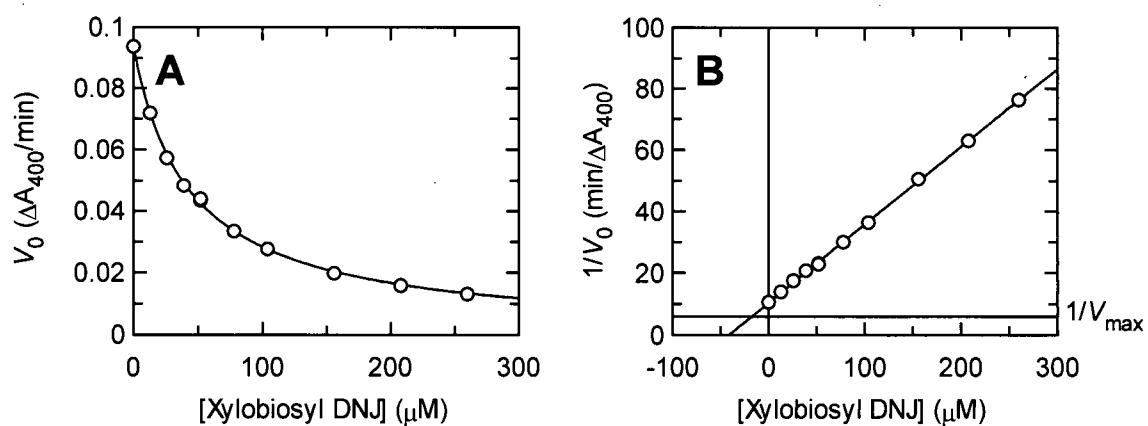


Figure A.136: Inhibition of Cex H80Q by Xylobiosyl Isogomine Lactam.

A.2.7 Cex Q87M**Figure A.137: Inhibition of Cex Q87M by Xylobiosyl Lactam Oxime.****Figure A.138: Inhibition of Cex Q87M by Xylobiosyl Imidazole.****Figure A.139: Inhibition of Cex Q87M by Xylobiosyl Deoxynojirimycin.**

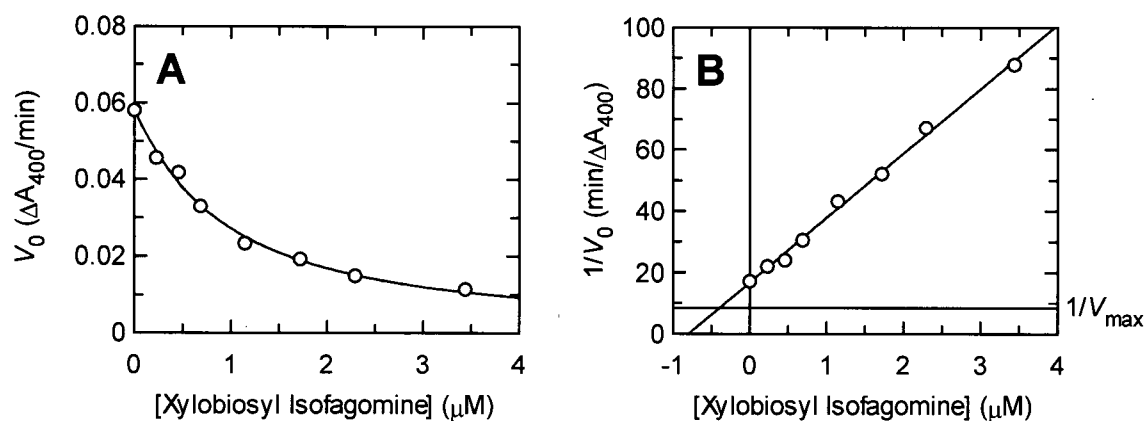


Figure A.140: Inhibition of Cex Q87M by Xylobiosyl Isogomine.

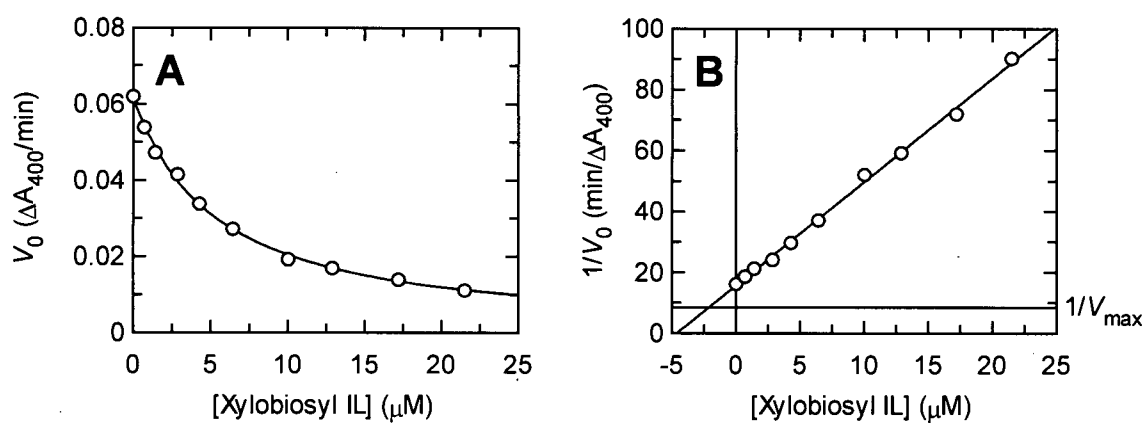


Figure A.141: Inhibition of Cex Q87M by Xylobiosyl Isogomine Lactam.

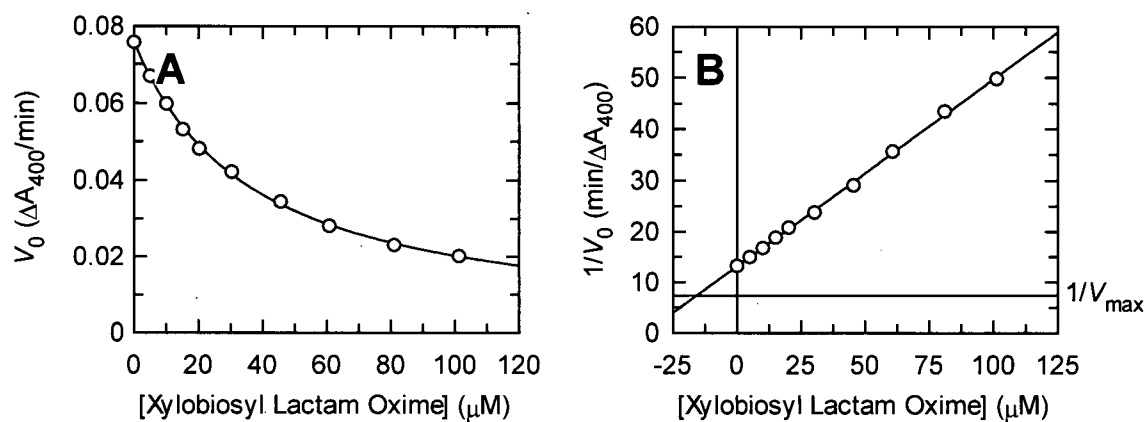
A.2.8 Cex Q87Y

Figure A.142: Inhibition of Cex Q87Y by Xylobiosyl Lactam Oxime.

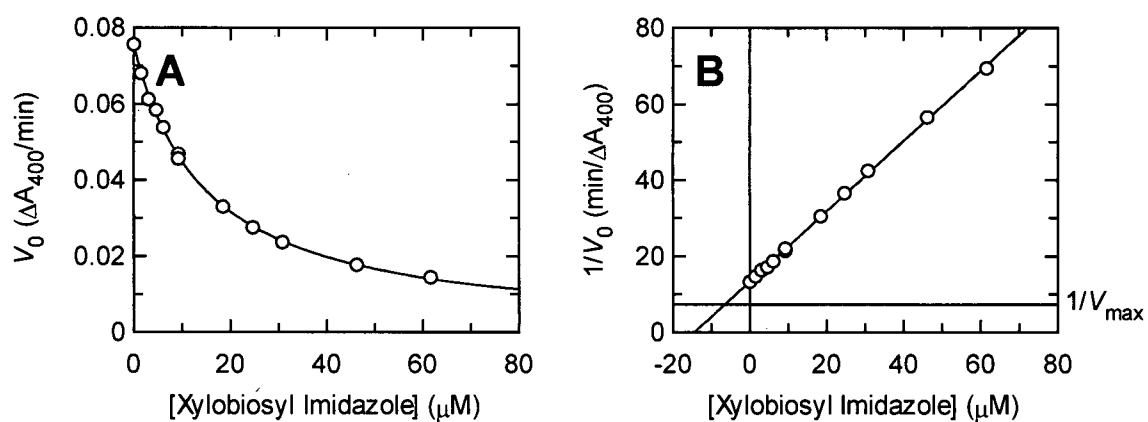


Figure A.143: Inhibition of Cex Q87Y by Xylobiosyl Imidazole.

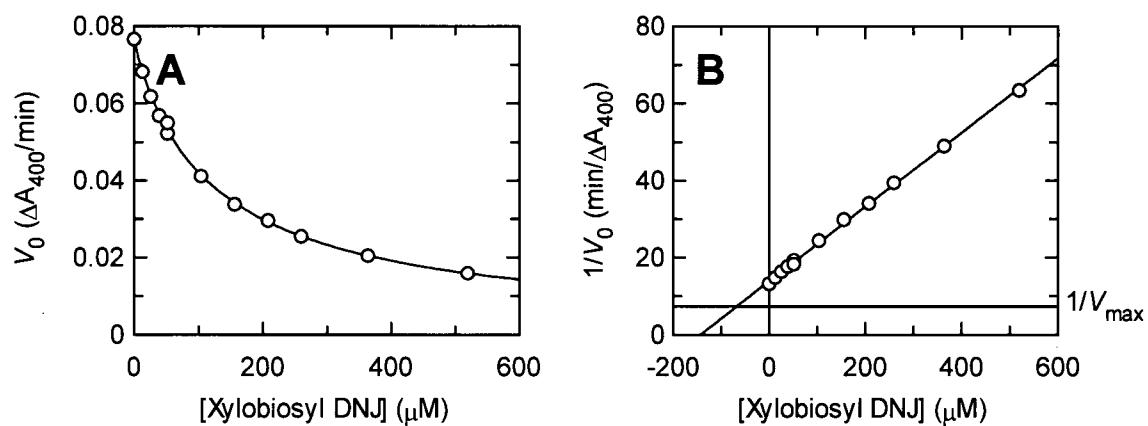


Figure A.144: Inhibition of Cex Q87Y by Xylobiosyl Deoxynojirimycin.

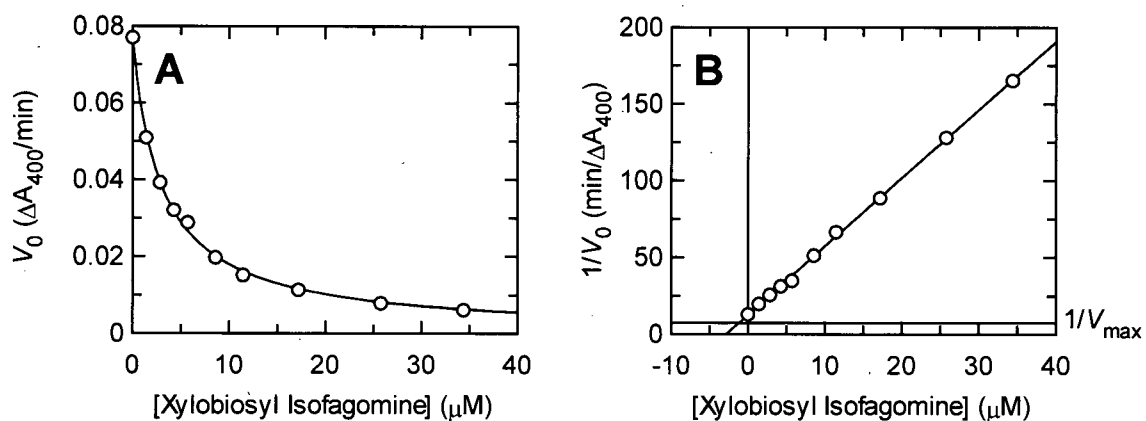


Figure A.145: Inhibition of Cex Q87Y by Xylobiosyl Isfagomine.

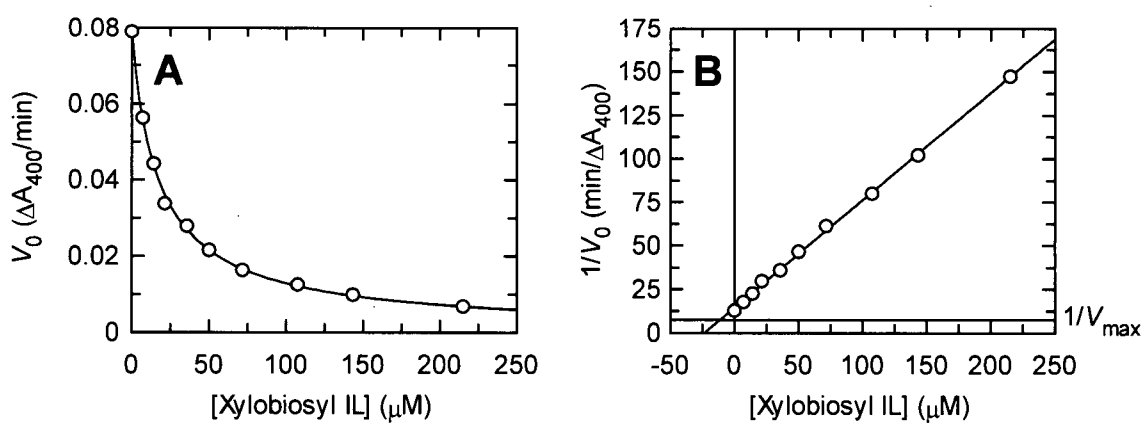
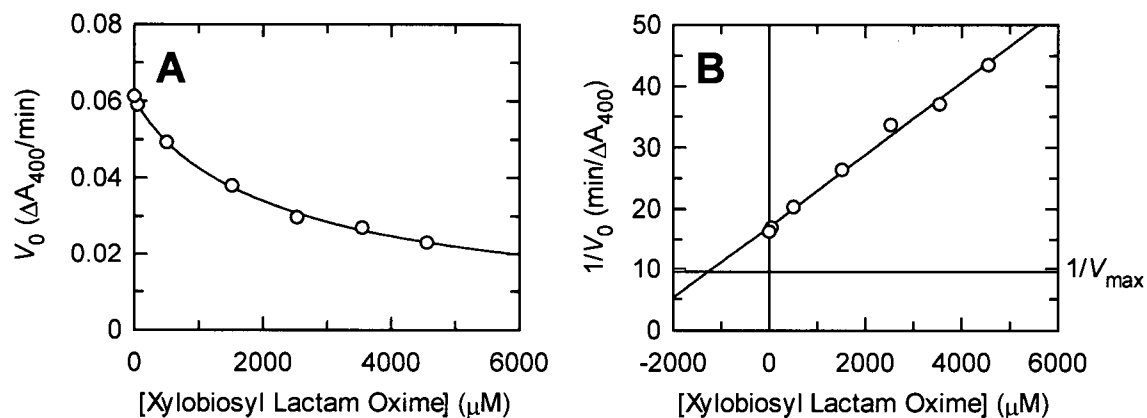
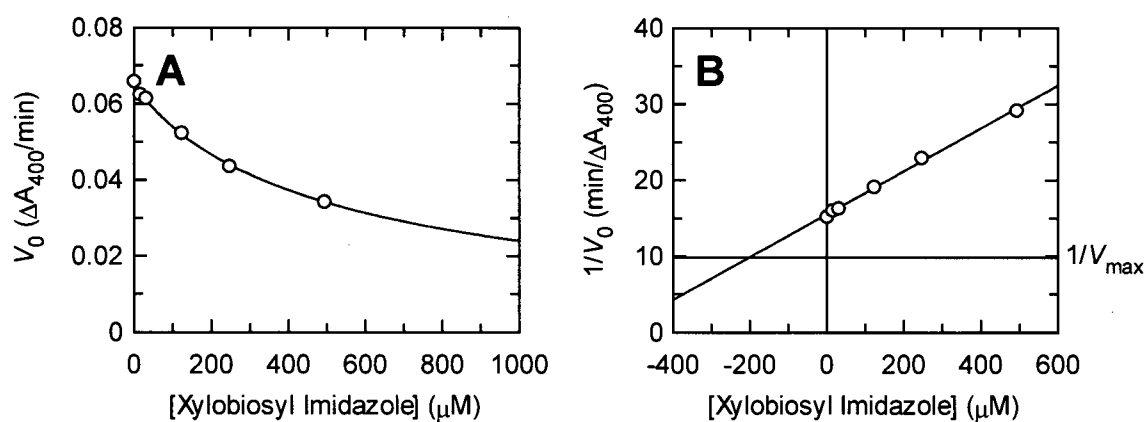
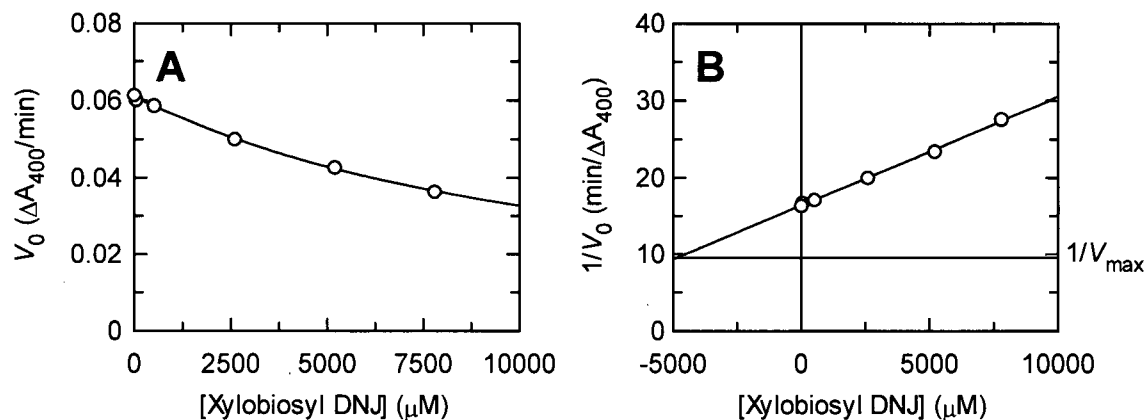


Figure A.146: Inhibition of Cex Q87Y by Xylobiosyl Isfagomine Lactam.

A.2.9 Cex N126A**Figure A.147: Inhibition of Cex N126A by Xylobiosyl Lactam Oxime.****Figure A.148: Inhibition of Cex N126A by Xylobiosyl Imidazole.****Figure A.149: Inhibition of Cex N126A by Xylobiosyl Deoxynojirimycin.**

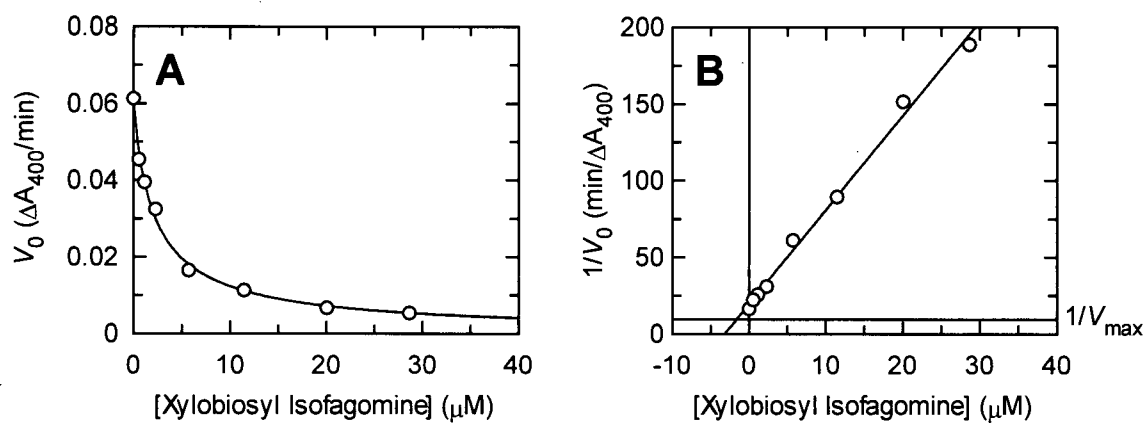


Figure A.150: Inhibition of Cex N126A by Xylobiosyl Isogomine.

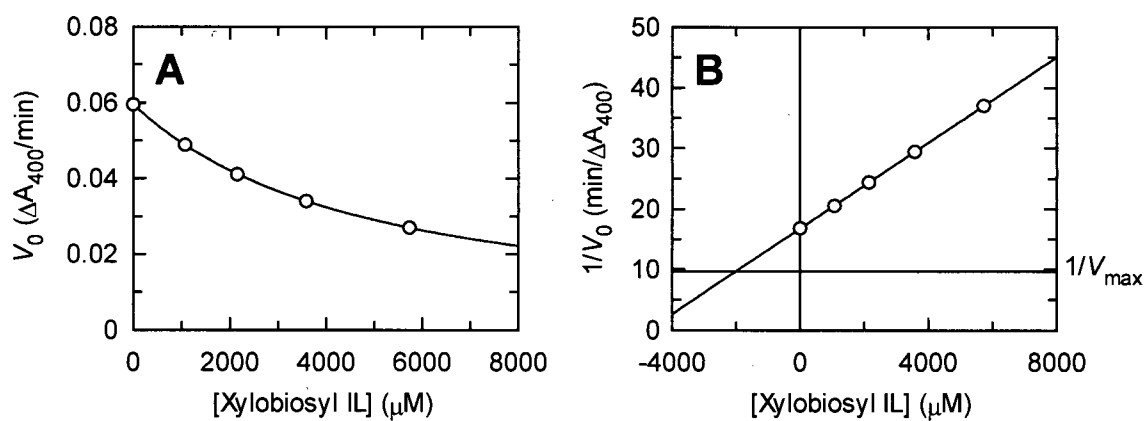
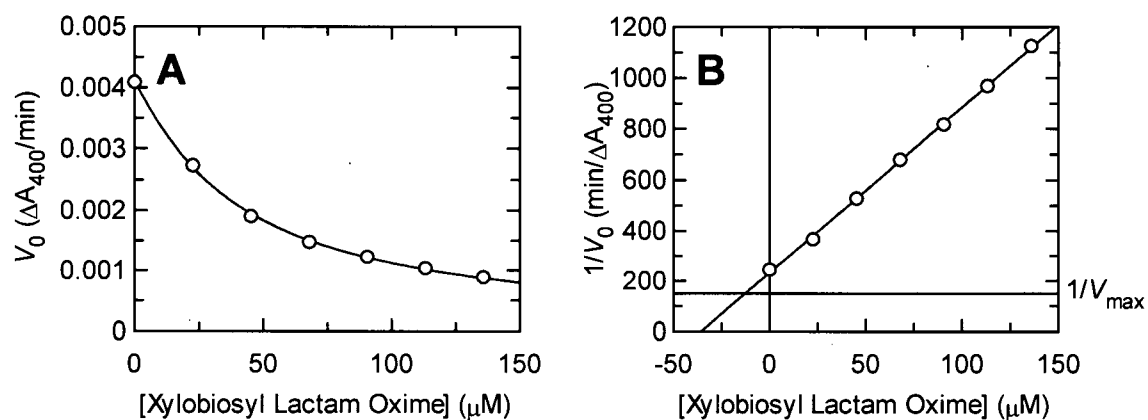
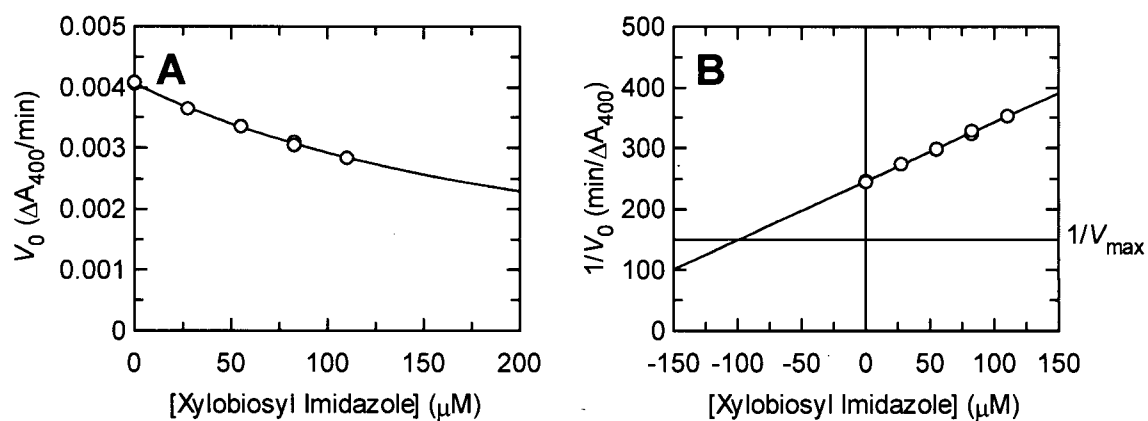
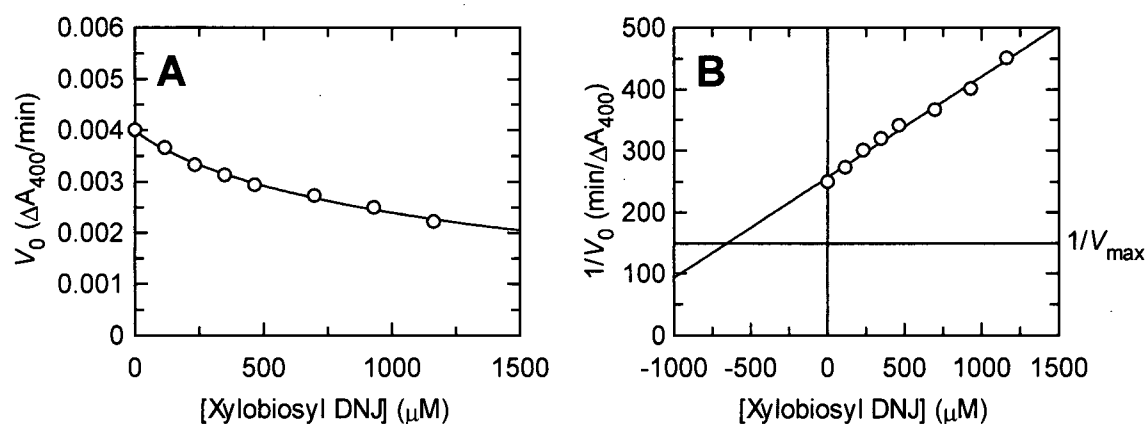


Figure A.151: Inhibition of Cex N126A by Xylobiosyl Isogomine Lactam.

A.2.10Cex E127A**Figure A.152: Inhibition of Cex E127A by Xylobiosyl Lactam Oxime.****Figure A.153: Inhibition of Cex E127A by Xylobiosyl Imidazole.****Figure A.154: Inhibition of Cex E127A by Xylobiosyl Deoxynojirimycin.**

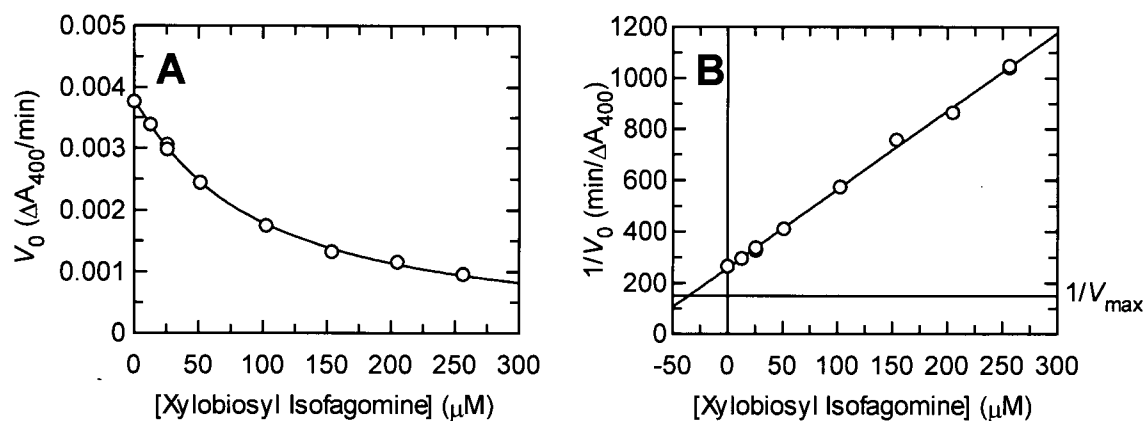


Figure A.155: Inhibition of Cex E127A by Xylobiosyl Isfagomine.

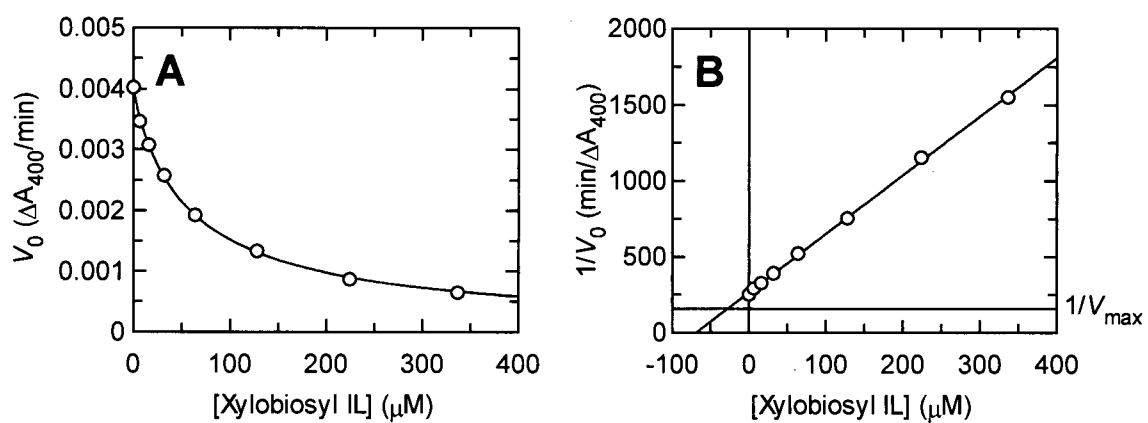


Figure A.156: Inhibition of Cex E127A by Xylobiosyl Isfagomine Lactam.

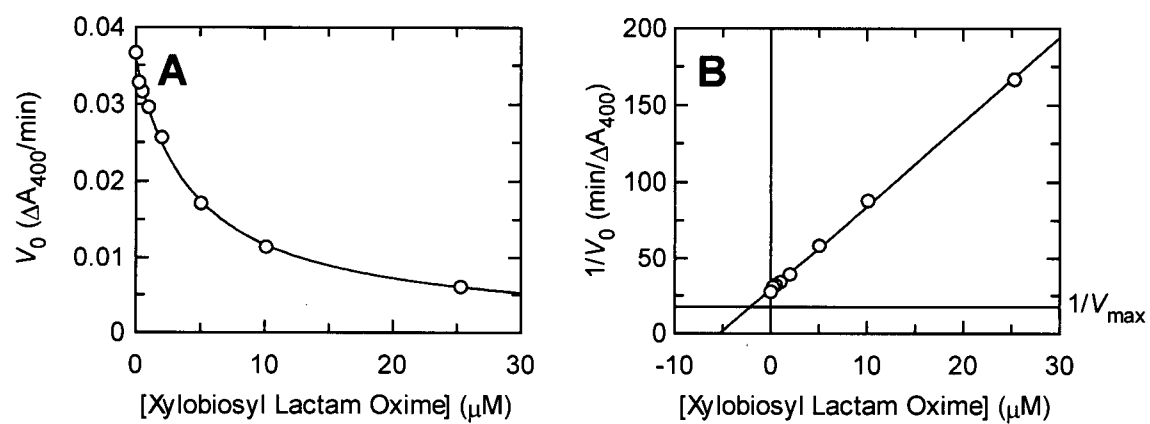
A.2.11Cex N169A

Figure A.157: Inhibition of Cex N169A by Xylobiosyl Lactam Oxime.

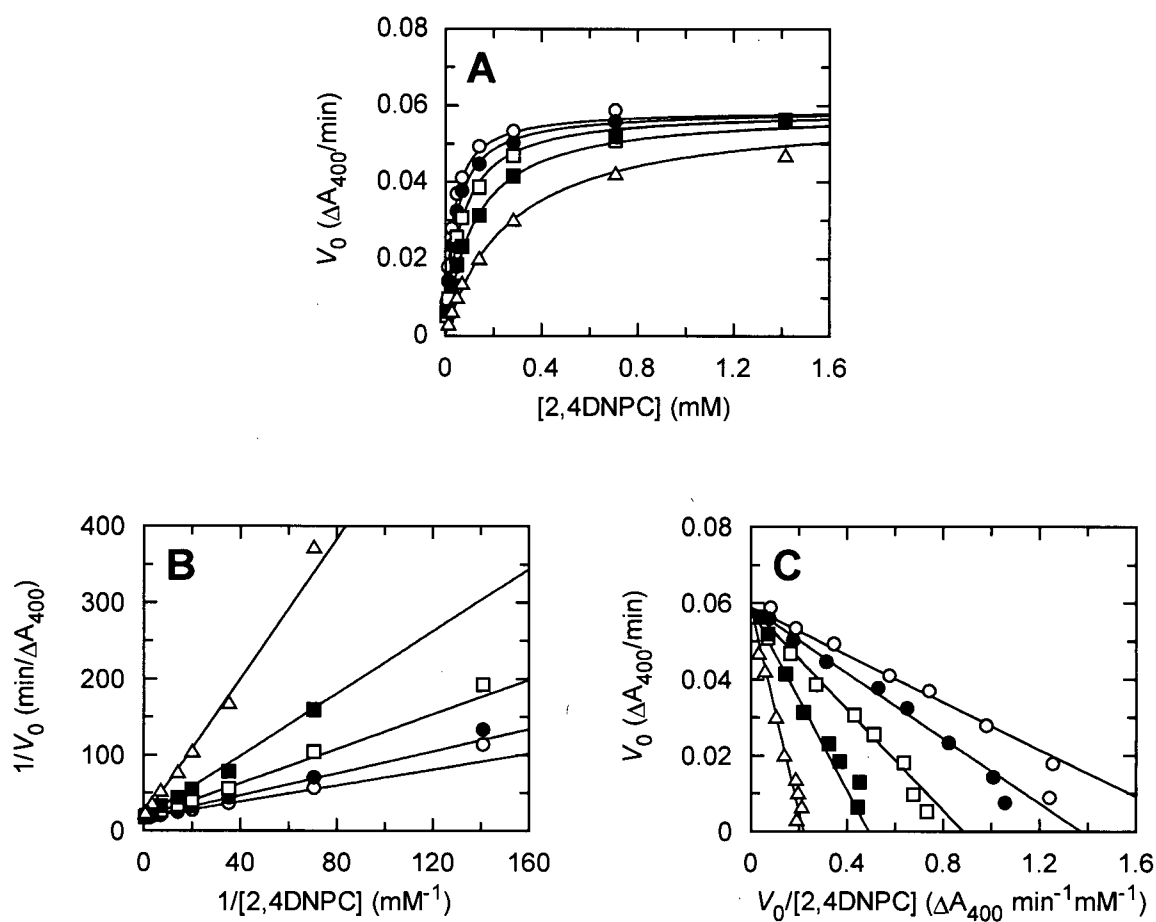


Figure A.158: Inhibition of Cex N169A by Xylobiosyl Imidazole at varying concentrations of 2,4DNPC. Plot A is the Michaelis-Menten plot, plot B is the Lineweaver-Burk plot, and plot C is the Eadie-Hofstee plot. The concentrations of xylobiosyl imidazole were 0 (○), 0.123 (●), 0.370 (□), 0.925 (■), and 2.47 μM (Δ).

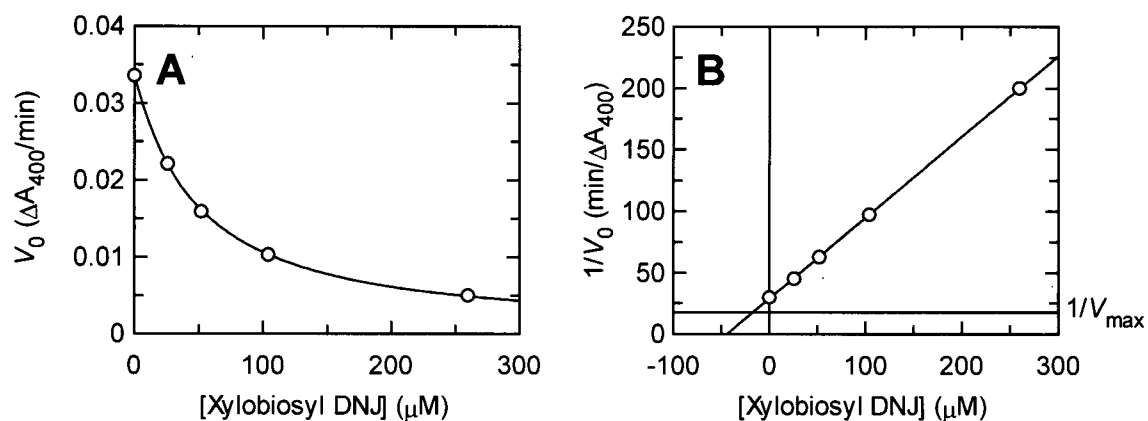


Figure A.159: Inhibition of Cex N169A by Xylobiosyl Deoxynojirimycin.

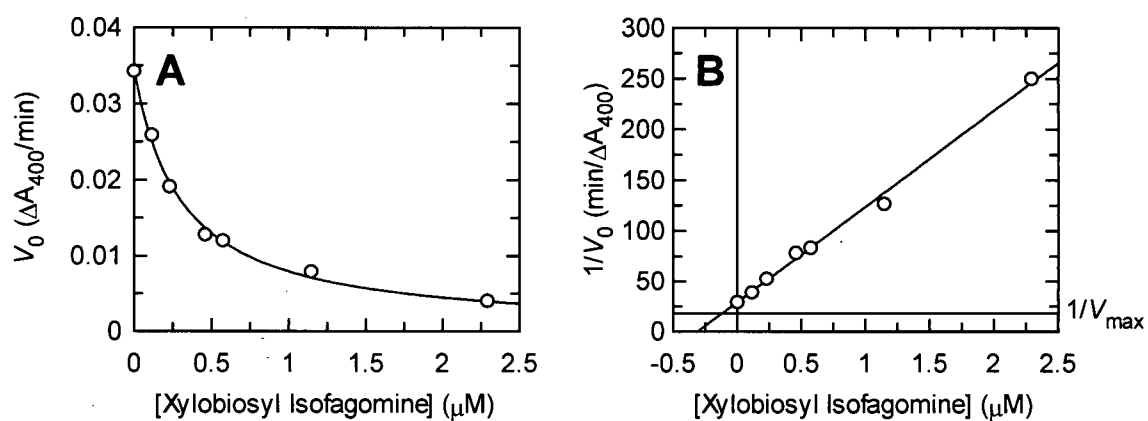


Figure A.160: Inhibition of Cex N169A by Xylobiosyl Isfagomine.

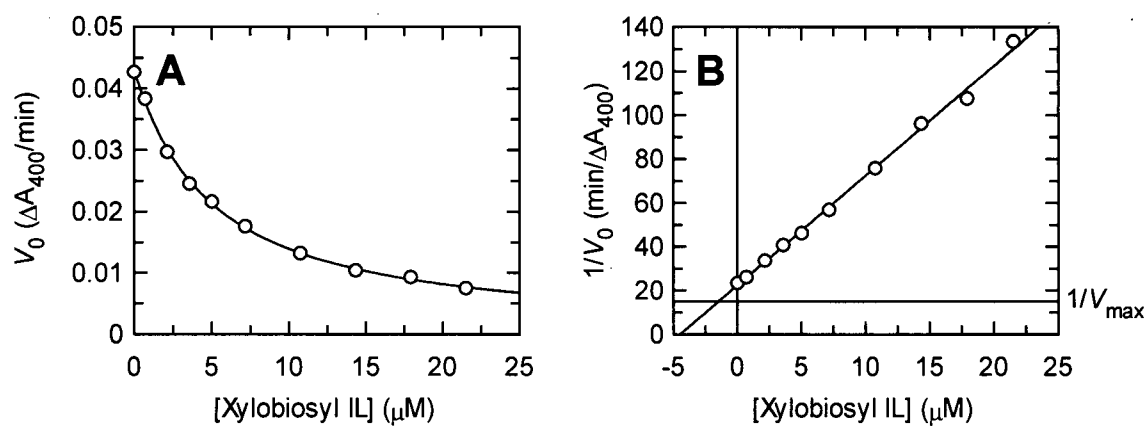


Figure A.161: Inhibition of Cex N169A by Xylobiosyl Isfagomine Lactam.

A.3 pH Dependencies of k_{cat}/K_m for the Hydrolysis of Xylobiosides or Cellobiosides by Native and Mutant Cex

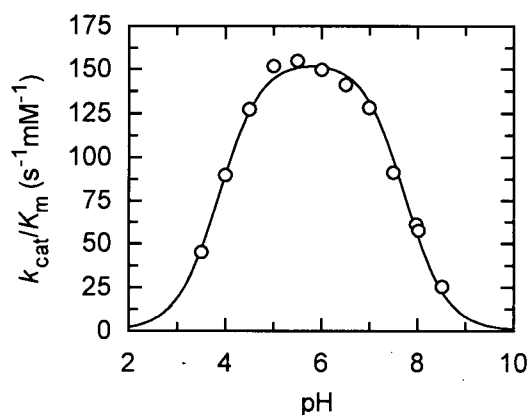


Figure A.162: pH dependence of k_{cat}/K_m for the hydrolysis of 2,4DNPC catalyzed by wild-type Cex.

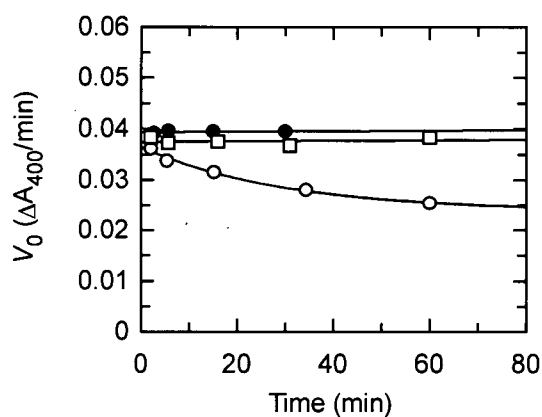


Figure A.163: pH stability of wild-type Cex at pH 3.0 (○), 3.5 (●), and 10.0 (□).

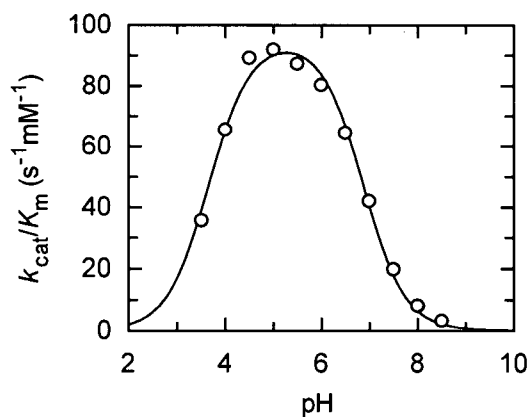


Figure A.164: pH dependence of k_{cat}/K_m for the hydrolysis of 2,4DNPC catalyzed by Cex E43A.

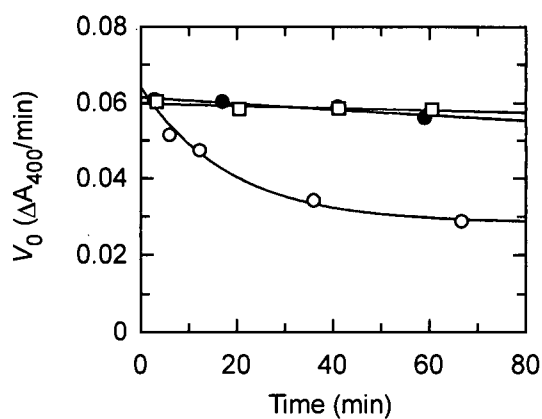


Figure A.165: pH stability of Cex E43A at pH 3.0 (○), 3.5 (●), and 10.0 (□).

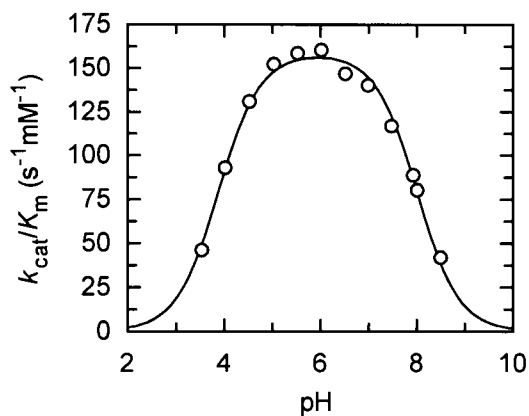


Figure A.166: pH dependence of k_{cat}/K_m for the hydrolysis of 2,4DNPC catalyzed by Cex N44A.

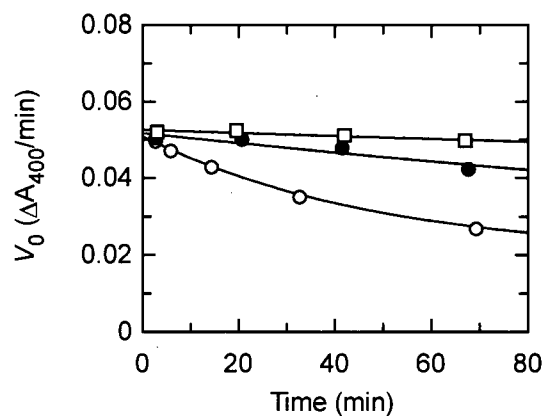


Figure A.167: pH stability of Cex N44A at pH 3.0 (O), 3.5 (●), and 10.0 (□).

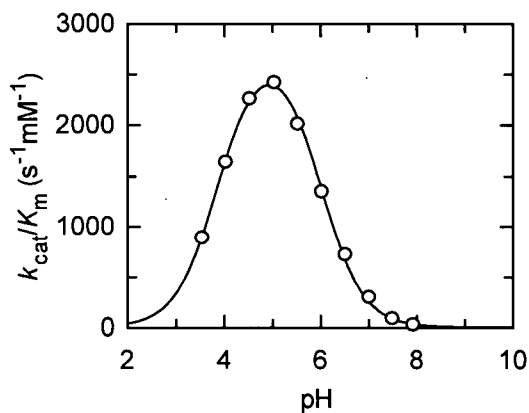


Figure A.168: pH dependence of k_{cat}/K_m for the hydrolysis of 2,5DNPX₂ catalyzed by Cex K47A.

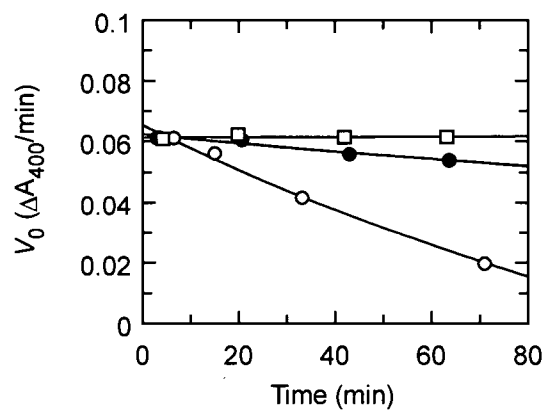


Figure A.169: pH stability of Cex k47A at pH 3.0 (O), 3.5 (●), and 10.0 (□).

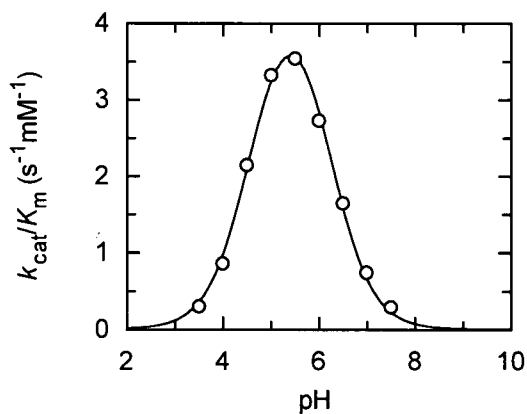


Figure A.170: pH dependence of k_{cat}/K_m for the hydrolysis of PNPX₂ catalyzed by Cex H80A.

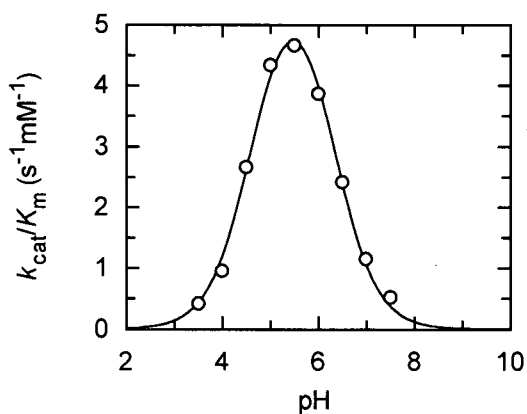


Figure A.171: pH dependence of k_{cat}/K_m for the hydrolysis of PNPX₂ catalyzed by Cex H80N.

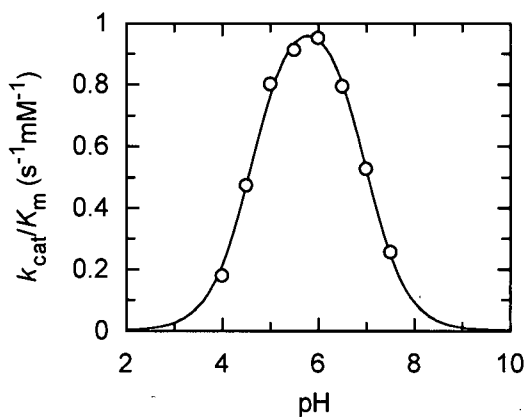


Figure A.172: pH dependence of k_{cat}/K_m for the hydrolysis of PNPX₂ catalyzed by Cex H80Q.

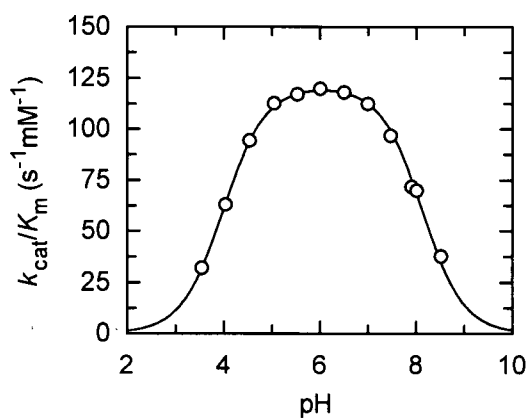


Figure A.173: pH dependence of k_{cat}/K_m for the hydrolysis of 2,4DNPC catalyzed by Cex Q87M.

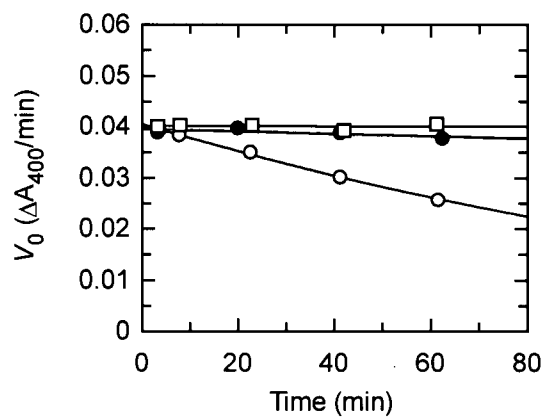


Figure A.174: pH stability of Cex Q87M at pH 3.0 (O), 3.5 (●), and 10.0 (□).

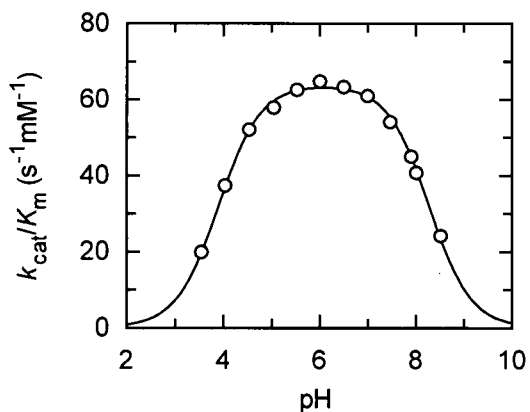


Figure A.175: pH dependence of k_{cat}/K_m for the hydrolysis of 2,4DNPC catalyzed by Cex Q87Y.

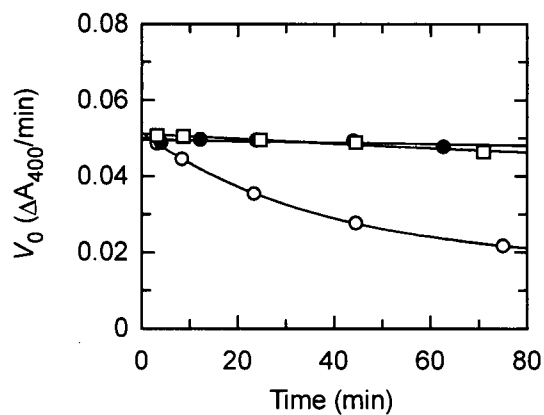


Figure A.176: pH stability of Cex Q87Y at pH 3.0 (O), 3.5 (●), and 10.0 (□).

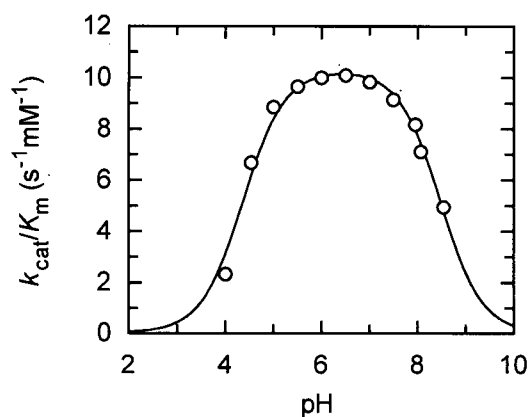


Figure A.177: pH dependence of k_{cat}/K_m for the hydrolysis of 2,4DNPC catalyzed by Cex N126A.

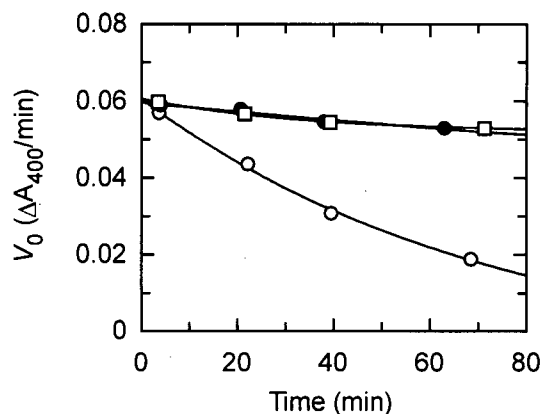


Figure A.178: pH stability of Cex N126A at pH 3.0 (O), 3.5 (●), and 10.0 (□).

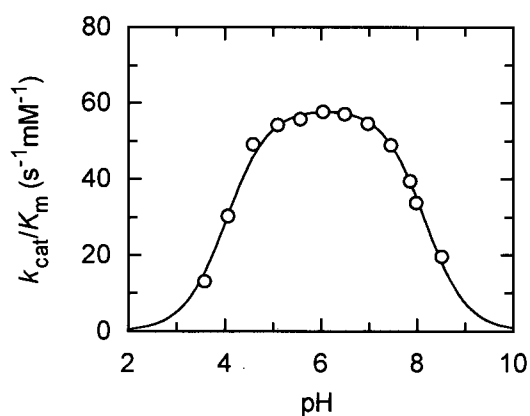


Figure A.179: pH dependence of k_{cat}/K_m for the hydrolysis of 2,4DNPC catalyzed by Cex N169A.

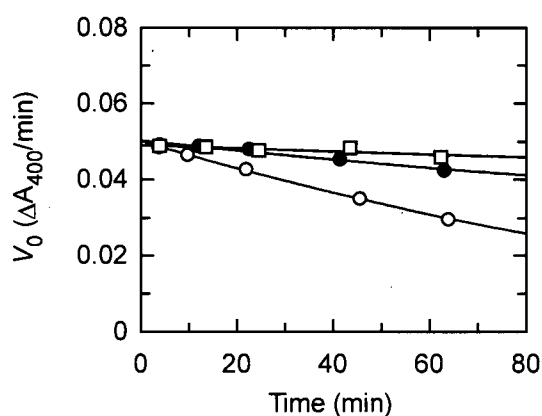


Figure A.180: pH stability of Cex N169A at pH 3.0 (O), 3.5 (●), and 10.0 (□).

APPENDIX B

COMPILATION OF CEX DATA

B Compilation of Cex Data

B.1 Tables

Table B.1: Dependence upon pH of kinetic parameters by *C. fimi* xylanase and mutants.

Enzyme	Kinetic Parameter	pK_{a1}	pK_{a2}	Conditions	
				Substrate	pH Range
Wild-Type	k_{cat}/K_m	3.9	7.7	2,4DNPC	3.5-8.5
	k_{cat}^a	~	~	2,4DNPC	4.5-9.5
	k_{cat}/K_m^a	4.1	7.7	2,4DNPC	4.5-9.5
	k_{cat}/K_m^b	5.0	7.3	PNPC	4.0-8.5
Glu43Ala	k_{cat}/K_m	3.7	6.9	2,4DNPC	3.5-8.5
Asn44Ala	k_{cat}/K_m	3.9	8.0	2,4DNPC	3.5-8.5
Lys47Ala	k_{cat}/K_m	3.9	6.0	2,5DNPX ₂	3.5-8.0
His80Ala	k_{cat}/K_m	4.6	6.2	PNPX ₂	3.5-7.5
His80Asn	k_{cat}/K_m	4.6	6.3	PNPX ₂	3.5-7.5
His80Gln	k_{cat}/K_m	4.6	7.0	PNPX ₂	4.0-7.5
Gln87Met	k_{cat}/K_m	4.0	8.1	2,4DNPC	3.5-8.5
Gln87Tyr	k_{cat}/K_m	3.9	8.3	2,4DNPC	3.5-8.5
Asn126Ala	k_{cat}/K_m	4.4	8.5	2,4DNPC	4.0-8.5
Asn169Ala	k_{cat}/K_m	4.0	8.2	2,4DNPC	3.5-8.5
His205Ala ^b	k_{cat}/K_m	~	6.2	PNPC	4.0-8.5
His205Asn ^b	k_{cat}/K_m	~	~	PNPC	4.0-8.5
Glu127Ala ^c	k_{cat}	~	5.0	2,4DNPC	4.5-9.0
	k_{cat}/K_m	5.9	~	PNPC	5.5-9.5
Glu233Asp ^c	k_{cat}	~	~	2,4DNPC	4.5-8.0
	k_{cat}/K_m	~	~	2,4DNPC	4.5-8.0

^a Data taken from Tull and Withers (1).

^b Data taken from Notenboom *et al.* (2).

^c Data taken from MacLeod *et al.* (3).

Table B.2: Brønsted relationships for the hydrolysis of various glycosides by *C. fimi* xylanase and mutants.

Enzyme	Substrate	Kinetic Parameter	β_{lg}	pK _a Range
Wild-Type	Aryl β -D-Glucosides	k_{cat}	-1^a	4.0-8.4
		k_{cat}/K_m	-1^a	4.0-8.4
	Aryl β -Cellobiosides	k_{cat}	0^a	4.0-8.0
		k_{cat}	-0.3^a	8.0-9.3
		k_{cat}/K_m	-0.3^a	4.0-9.3
		k_2	-0.3^a	4.0-7.2
		k_2/K_S	-0.3^a	4.0-7.2
		k_{cat}/K_m (pH 7.0)	-0.23^b	4.0-7.2
		k_{cat}/K_m (pH 5.5)	-0.29^b	4.0-7.2
	Aryl β -D-Xylosides	k_{cat}	-0.8^c	4.9-8.5
		k_{cat}/K_m	-0.9^c	4.9-8.5
	Aryl β -Xylobiosides	k_{cat}	0^c	5.2-7.2
		k_{cat}/K_m	\sim^c	5.2-7.2
Glu233Asp	Aryl β -Cellobiosides	k_{cat}	0^d	4.0-9.3
		k_{cat}/K_m	-0.3^d	4.0-9.3
Glu127Ala	Aryl β -Cellobiosides	k_{cat}	0^d	4.0-7.5
		k_{cat}/K_m	-1.0^d	4.0-9.3
		k_2	-0.8^d	4.0-7.2
		k_2/K_S	-0.7^d	4.0-7.2
		k_{cat} (pH 7.0)	0^b	4.0-7.2
His205Ala	Aryl β -Cellobiosides	k_{cat}/K_m (pH 7.0)	-0.64^b	4.0-7.2
		k_{cat} (pH 5.5)	0^b	4.0-7.2
		k_{cat}/K_m (pH 5.5)	-0.69^b	4.0-7.2
		k_{cat} (pH 7.0)	0^b	4.0-7.2
His205Asn	Aryl β -Cellobiosides	k_{cat}/K_m (pH 7.0)	-0.43^b	4.0-7.2
		k_{cat} (pH 5.5)	0^b	4.0-7.2
		k_{cat}/K_m (pH 5.5)	-0.46^b	4.0-7.2
		k_{cat} (pH 7.0)	0^b	4.0-7.2

^a Data taken from Tull and Withers (1).^b Data taken from Notenboom *et al.* (2).^c Data taken from Tull, D. (1995) Ph.D. Thesis, UBC.^d Data taken from MacLeod *et al.* (3).

Table B.3: Inactivation parameters for *C. fimi* xylanase and mutants.

Enzyme	Inactivator	k_i (min^{-1})	K_i (mM)	k_i/K_i ($\text{min}^{-1}\text{mM}^{-1}$)	$k_{\text{hydrolysis}}$ (min^{-1})
Wild-Type	2F-DNPG ^a	2.5×10^{-4}	4.5	5.56×10^{-5}	1.3×10^{-5}
	2F-DNPC ^b	6.7×10^{-2}	0.11	6.12×10^{-1}	8.5×10^{-6}
	2F-DNPX ₂ ^c	5.7×10^{-2}	0.0035	16	nd ^f
Glu127Ala	2F-DNPC ^d	nd ^f	nd ^f	1.6	nd ^f
His205Asn	2F-DNPC ^e	1.3×10^{-3}	nd ^f	nd ^f	nd ^f

^a Data taken from Tull *et al.* (4).^b Data taken from Tull and Withers (1).^c Data taken from Ziser *et al.* (5).^d Data taken from MacLeod *et al.* (6).^e Data taken from Notenboom *et al.* (2).^f nd indicates that this kinetic parameter was not determined.**Table B.4: Secondary deuterium kinetic isotope effects measured with *C. fimi* xylanase and mutants.**

Enzyme	Substrate	RDS ^a	k_H/k_D
Wild-Type ^b	2,4DNPG	degly	1.12
	PNPG	gly	1.12
	2,4DNPC	degly	1.10
	PNPC	degly	1.10
	4BrPC	gly	1.06
Glu233Asp ^c	2,4DNPC	degly	1.09
Glu127Ala ^c	2,4DNPC	degly	1.08
His205Ala ^d	2,4DNPC	degly	1.12
His205Asn ^d	2,4DNPC	degly	1.02

^a RDS, rate-determining step.^b Data taken from Tull and Withers (1).^c Data taken from MacLeod *et al.* (3).^d Data taken from Birsan, C. (1996) M.Sc. Thesis, UBC.

Table B.5: Michaelis–Menten parameters for the hydrolysis of 2,4-dinitrophenyl β -cellobioside by *C. fimi* xylanase and mutants.

Enzyme	k_{cat} (s^{-1})	K_{m} (mM)	$k_{\text{cat}}/K_{\text{m}}$ ($\text{s}^{-1} \text{mM}^{-1}$)
Wild-Type	8.5	0.068	120
	12.9 ^a	0.11 ^a	117 ^a
	7.0 ^b	0.06 ^b	116 ^b
	3.9 ^c	0.12 ^c	32 ^c
Glu43Ala	4.9	0.19	27
Asn44Ala	9.4	0.070	130
Lys47Ala	4.2	2.6	1.6
His80Ala	0.088	0.0071	12
His80Asn	0.056	0.0051	11
His80Gln	0.012	0.0019	6.1
Gln87Met	8.8	0.056	160
Gln87Tyr	7.0	0.11	66
Asp123Ala	5.4 ^c	0.53 ^c	10 ^c
Asn126Ala	0.49	0.047	10
Glu127Ala	0.040 ^b	0.0003 ^b	130 ^b
Glu127Asp	0.027 ^b	0.0017 ^b	16 ^b
Glu127Gly	0.035 ^b	0.0004 ^b	92 ^b
Asn169Ala	2.9	0.036	81
His205Ala	0.00082 ^c	0.007 ^c	0.12 ^c
His205Asn	0.00049 ^c	0.03 ^c	0.016 ^c
Glu233Asp	0.0031 ^d	0.086 ^d	0.036 ^d

^a Data taken from Tull and Withers (1).

^b Data taken from MacLeod *et al.* (6).

^c Data taken from Notenboom *et al.* (2).

^d Data taken from MacLeod *et al.* (3).

Table B.6: Michaelis–Menten parameters for the hydrolysis of 4-nitrophenyl β -cellobioside by *C. fimi* xylanase and mutants.

Enzyme	k_{cat} (s^{-1})	K_{m} (mM)	$k_{\text{cat}}/K_{\text{m}}$ ($\text{s}^{-1} \text{mM}^{-1}$)
Wild-Type	9.2	0.58	16
	15.8 ^a	0.60 ^a	26 ^a
	11.3 ^b	0.53 ^b	21 ^b
	3.5 ^c	0.56 ^c	6.2 ^c
Glu43Ala	1.3	13	0.10
Asn44Ala	10	1.7	5.8
Lys47Ala	0.020	29	0.00071
His80Ala	0.048	13	0.0037
His80Asn	0.040	6.6	0.0060
His80Gln	0.0064	3.1	0.0021
Gln87Met	9.6	0.35	27
	9.2 ^e	0.34 ^e	27 ^e
Gln87Tyr	7.4	2.6	2.8
Asp123Ala	0.007 ^d	18 ^d	0.0004 ^d
Asn126Ala	0.052	11.8	0.0044
Glu127Ala	0.033	0.020	1.6
	0.038 ^b	0.025 ^b	1.5 ^b
	0.033 ^d	0.020 ^d	1.7 ^d
Glu127Asp	0.055 ^b	1.7 ^b	0.033 ^b
Glu127Gly	0.033 ^b	0.029 ^b	1.2 ^b
Asn169Ala	3.9	0.59	6.59
His205Ala	0.00091 ^c	0.82 ^c	0.0011 ^c
His205Asn	0.00074	1.05	0.00070
	0.00046 ^c	0.67 ^c	0.00069 ^c
Glu233Asp	0.0038 ^d	0.66 ^d	0.0058 ^d

^a Data taken from Tull and Withers (1).

^b Data taken from MacLeod *et al.* (6).

^c Data taken from Notenboom *et al.* (2).

^d Data taken from MacLeod *et al.* (3).

^e Data taken from Notenboom *et al.* (7).

Table B.7: Michaelis–Menten parameters for the hydrolysis of 2,5-dinitrophenyl β -xylobioside by *C. fimi* xylanase and mutants.

Enzyme	k_{cat} (s^{-1})	K_{m} (mM)	$k_{\text{cat}}/K_{\text{m}}$ ($\text{s}^{-1}\text{mM}^{-1}$)
Wild-Type	30	0.015	2100
Glu43Ala	20	0.063	310
Asn44Ala	43	0.038	1100
Lys47Ala	59	0.20	300
His80Ala	0.25	0.0021	120
His80Asn	0.12	0.0012	99
His80Gln	0.034	0.00062	54
Gln87Met	47	0.047	1000
Gln87Tyr	39	0.052	750
Asp123Ala	nd ^a	nd ^a	nd ^a
Asn126Ala	1.3	0.0025	520
Glu127Ala	0.11	<0.0005	>210
Glu127Asp	nd ^a	nd ^a	nd ^a
Glu127Gly	nd ^a	nd ^a	nd ^a
Asn169Ala	19	0.0078	2600
His205Ala	nd ^a	nd ^a	nd ^a
His205Asn	0.00059	0.013	0.044
Glu233Asp	nd ^a	nd ^a	nd ^a

^a nd indicates that this kinetic parameter was not determined.

Table B.8: Michaelis–Menten parameters for the hydrolysis of 4-nitrophenyl β -xylobioside by *C. fimi* xylanase and mutants.

Enzyme	k_{cat} (s^{-1})	K_{m} (mM)	$k_{\text{cat}}/K_{\text{m}}$ ($\text{s}^{-1}\text{mM}^{-1}$)
Wild-Type	32 40 ^a	0.022 0.018 ^a	1500 2200 ^a
Glu43Ala	27	5.4	5.1
Asn44Ala	89	3.6	25
Lys47Ala	0.36	9.6	0.038
His80Ala	0.42	0.59	0.72
His80Asn	0.13	0.099	1.3
His80Gln	0.037	0.061	0.61
Gln87Met	58 ^b	0.12 ^b	480 ^b
Gln87Tyr	nd ^c	nd ^c	nd ^c
Asp123Ala	nd ^c	nd ^c	nd ^c
Asn126Ala	3.5	7.7	0.45
Glu127Ala	nd ^c	nd ^c	nd ^c
Glu127Asp	nd ^c	nd ^c	nd ^c
Glu127Gly	nd ^c	nd ^c	nd ^c
Asn169Ala	nd ^c	nd ^c	nd ^c
His205Ala	nd ^c	nd ^c	nd ^c
His205Asn	nd ^c	nd ^c	nd ^c
Glu233Asp	0.011 ^d	0.018 ^d	0.61 ^d

^a Data taken from Tull and Withers (1).

^b Data taken from Notenboom *et al.* (7).

^c nd indicates that this kinetic parameter was not determined.

^d Data taken from MacLeod *et al.* (3).

Table B.9: Michaelis–Menten parameters for the hydrolysis of 2-nitrophenyl β -xylobioside by *C. fimi* xylanase and mutants.

Enzyme	k_{cat} (s ⁻¹)	K_m (mM)	k_{cat}/K_m (s ⁻¹ mM ⁻¹)
Wild-Type	38 43 ^a	0.068 0.06 ^a	560 720 ^a
Glu43Ala	47	1.6	30
Asn44Ala	80	0.64	130
Lys47Ala	9.7	8.5	1.2
His80Ala	0.33	0.039	8.4
His80Asn	0.14	0.016	8.6
His80Gln	0.039	0.010	3.8
Gln87Met	55	0.13	420
Gln87Tyr	46	0.22	210
Asp123Ala	nd ^b	nd ^b	nd ^b
Asn126Ala	2.9	0.39	7.3
Glu127Ala	0.080	<0.001	>80
Glu127Asp	nd ^b	nd ^b	nd ^b
Glu127Gly	nd ^b	nd ^b	nd ^b
Asn169Ala	29	0.050	580
His205Ala	nd ^b	nd ^b	nd ^b
His205Asn	0.0029	1.1	0.0026
Glu233Asp	nd ^b	nd ^b	nd ^b

^a Data taken from Tull and Withers (1).

^b nd indicates that this kinetic parameter was not determined.

Table B.10: Inhibition constants (K_i) for *C. fimi* xylanase and mutants with various xylobiose-derived iminosugars.

Enzyme	Compound				
	Xylobiosyl Lactam Oxime	Xylobiosyl Imidazole	Xylobiosyl Deoxy- nojirimycin	Xylobiosyl Isofagomine	Xylobiosyl Isofagomine Lactam
	(μ M)	(μ M)	(μ M)	(μ M)	(μ M)
Wild-Type	0.37 ^a	0.15 ^a	5.8 ^a	0.13 ^a	0.34 ^b
Glu43Ala	110	22	2100	45	96
Asn44Ala	23	8.9	180	7.1	24
Lys47Ala	2300	1000	6600	870	2300
His80Ala	140	43	800	5.9	1000
His80Asn	350	87	370	13	340
His80Gln	1300	350	590	6.7	340
Gln87Met	4.9	1.1	18	0.39	2.1
Gln87Tyr	16	6.4	62	1.2	11
Asn126Ala	1300 ^b	200 ^b	4800 ^b	1.6 ^b	2000 ^b
Glu127Ala	13	99	660	35	28
Asn169Ala	2.1	0.41	17	0.12	1.5

^a Data taken from Williams *et al.* (8).

^b Data taken from Williams *et al.* (9).

Table B.11: Pre-steady state kinetic parameters for the hydrolysis of various aryl glycosides by *C. fimi* xylanase and mutants.

Enzyme	Substrate	k_2 (s ⁻¹)	K_S (mM)	k_2/K_S (s ⁻¹ mM ⁻¹)	k_{cat}/K_m (s ⁻¹ mM ⁻¹)
Wild-Type	2,4DNPC ^a	1660	10.0	166	117
	PNPC ^a	244	12.4	20	26
Glu127Ala ^b	2,4DNPC ^b	190	0.68	280	130
	PNPC ^c	0.30	0.17	1.8	1.5

^a Data taken from Tull and Withers (1).^b Data taken from MacLeod *et al.* (3).^c Data taken from MacLeod *et al.* (6).**Table B.12: Michaelis–Menten parameters for the hydrolysis of various aryl glycoside substrates by *C. fimi* xylanase.**

Substrate	k_{cat} (s ⁻¹)	K_m (mM)	k_{cat}/K_m (s ⁻¹ mM ⁻¹)
PNPG ^a	0.033	8.3	0.0041
PNPX ^a	2.6	20	0.13
PNPC ^a	15.8	0.60	26
PNPX ₂ ^a	40	0.018	2200
2,4DNPG ^a	18	1.9	9.5
2,4DNPX	nd ^b	nd ^b	nd ^b
2,4DNPC ^a	12.9	0.11	117
2,4DNPX ₂	nd ^b	nd ^b	nd ^b

^a Data taken from Tull and Withers (1).^b nd indicates that this kinetic parameter was not determined.

Table B.13: Michaelis–Menten parameters for the hydrolysis of various aryl glycoside substrates by several family 10 xylanases.

Substrate	Enzyme	k_{cat} (s^{-1})	K_m (mM)	k_{cat}/K_m ($s^{-1}mM^{-1}$)
PNPG	Cex, <i>C. fimi</i> ^a	0.033	8.3	0.0041
	Xyl10A, <i>S. lividans</i> ^b	0.011	180	0.00069
	Xyl10A, <i>P. cellulosa</i> ^c	ND ^d	ND ^d	ND ^d
PNPX	Cex, <i>C. fimi</i> ^a	2.6	20	0.13
	Xyl10A, <i>S. lividans</i> ^b	0.32	380	0.00081
	Xyl10A, <i>P. cellulosa</i> ^c	0.15	310	0.00048
PNPC	Cex, <i>C. fimi</i> ^a	15.8	0.60	26
	Xyl10A, <i>S. lividans</i> ^b	3.6	51	0.071
	Xyl10A, <i>P. cellulosa</i> ^c	2.6	50	0.052
PNPX ₂	Cex, <i>C. fimi</i> ^a	40	0.018	2200
	Xyl10A, <i>S. lividans</i> ^b	29	0.58	51
	Xyl10A, <i>P. cellulosa</i> ^c	86	0.57	150

^a Data taken from Tull and Withers (1).

^b Data taken from Ducros *et al.* (10).

^c Data taken from Charnock *et al.* (11).

^d ND, not detectable.

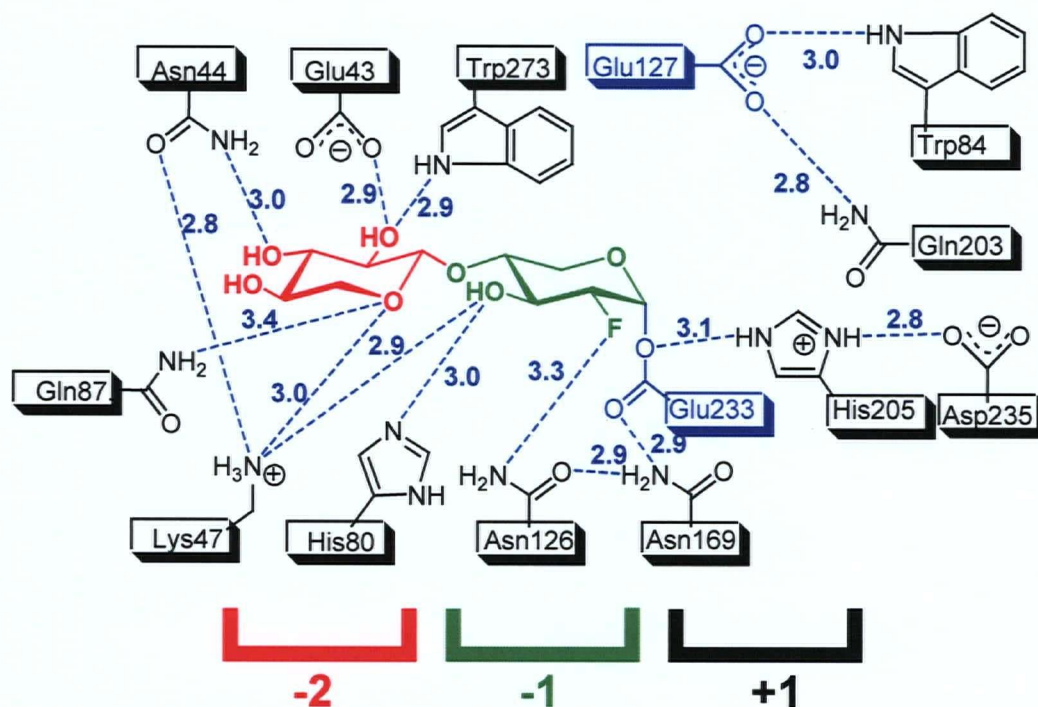


Figure B.1: Scheme of protein–carbohydrate interactions in the active site region of 2F-xylobiosyl–Cex-cd complex observed by three-dimensional structural analysis (7). Hydrogen-bonding interactions between heteroatoms are in Angstroms. The distance between 2F and the carbonyl oxygen of Glu233 is 2.6 Å (not shown).

B.2 References

1. Tull, D., and Withers, S. G. (1994) Mechanisms of cellulases and xylanases: a detailed kinetic study of the exo- β -1,4-glycanase from *Cellulomonas fimi*. *Biochemistry*. 33, 6363-6370.
2. Notenboom, V., Birsan, C., Nitz, M., Rose, D. R., Warren, R. A. J., and Withers, S. G. (1998) Insights into transition state stabilization of the β -1,4-glycosidase Cex by covalent intermediate accumulation in active site mutants. *Nat. Struct. Biol.* 5, 812-818.
3. MacLeod, A. M., Tull, D., Rupitz, K., Warren, R. A. J., and Withers, S. G. (1996) Mechanistic consequences of mutation of active site carboxylates in a retaining β -1,4-glycanase from *Cellulomonas fimi*. *Biochemistry*. 35, 13165-13172.
4. Tull, D., Withers, S. G., Gilkes, N. R., Kilburn, D. G., Warren, A. J., and Aebersold, R. (1991) Glutamic acid 274 is the nucleophile in the active site of a "retaining" exoglucanase from *Cellulomonas fimi*. *J. Biol. Chem.* 266, 15621-15625.
5. Ziser, L., Setyawati, I., and Withers, S. G. (1995) Syntheses and testing of substrates and mechanism-based inactivators for xylanases. *Carbohydr. Res.* 274, 137-153.
6. MacLeod, A. M., Lindhorst, T., Withers, S. G., and Warren, R. A. J. (1994) The acid/base catalyst in the exoglucanase/xylanase from *Cellulomonas fimi* is glutamic acid 127: evidence from detailed kinetic studies of mutants. *Biochemistry*. 33, 6371-6376.
7. Notenboom, V., Birsan, C., Warren, R. A. J., Withers, S. G., and Rose, D. R. (1998) Exploring the cellulose/xylan specificity of the β -1,4-glycanase Cex from *Cellulomonas fimi* through crystallography and mutation. *Biochemistry*. 37, 4751-4758.
8. Williams, S. J., Hoos, R., and Withers, S. G. (2000) Nanomolar versus millimolar inhibition by xylobiose-derived azasugars: significant differences between two structurally distinct xylanases. *J. Am. Chem. Soc.* 122, 2223-2235.
9. Williams, S. J., Notenboom, V., Wicki, J., Rose, D. R., and Withers, S. G. (2000) A new, simple, high-affinity glycosidase inhibitor: analysis of binding through X-ray crystallography, mutagenesis, and kinetic analysis. *J. Am. Chem. Soc.* 122, 4229-4230.
10. Ducros, V., Charnock, S. J., Derewenda, U., Derewenda, Z. S., Dauter, Z., Dupont, C., Shareck, F., Morosoli, R., Kluepfel, D., and Davies, G. J. (2000) Substrate specificity in glycoside hydrolase family 10. Structural and kinetic analysis of the *Streptomyces lividans* xylanase 10A. *J. Biol. Chem.* 275, 23020-23026.
11. Charnock, S. J., Spurway, T. D., Xie, H., Beylot, M.-H., Virden, R., Warren, R. A. J., Hazlewood, G. P., and Gilbert, H. J. (1998) The topology of the substrate binding clefts of glycosyl hydrolase family 10 xylanases are not conserved. *J. Biol. Chem.* 273, 32187-32199.

APPENDIX C

FUNDAMENTALS OF ENZYME KINETICS

C Fundamentals of Enzyme Kinetics

C.1 Basic Enzyme Kinetics

In 1913, L. Michaelis and M. L. Menten* proposed the following scheme:



The typical enzyme-catalyzed reaction occurs in two steps. The enzyme reversibly forms an initial complex with the substrate to give an enzyme–substrate complex, ES. Also known as the Michaelis complex, ES subsequently decomposes to products and enzyme in a second step with the first-order rate constant k_{cat} .

The general expression for enzyme kinetics is known as the Michaelis–Menten equation where v is the initial velocity of the reaction; $[E]_0$ is the total enzyme concentration; $[S]$ is the substrate concentration; k_{cat} is the catalytic constant; and K_m is the Michaelis constant.

$$v = \frac{[E]_0[S]k_{cat}}{K_m + [S]} \quad (C.2)$$

The Michaelis–Menten equation makes two assumptions. First, the enzyme concentration is assumed to be negligible compared to that of the substrate. This is generally true since enzymes catalyze reactions with high efficiency. Second, the reverse reaction can be ignored since the velocity measured is the initial rate of product release. Thus, there is no significant accumulation of products or depletion of substrates, and the change in substrate concentration is generally linear with time.

* Michaelis, L.; Menten, M. L. *Biochem. Z* **49**, 333 (1913).

The Michaelis–Menten mechanism assumes that the enzyme–substrate complex is in thermodynamic equilibrium with free enzyme and substrate, which is true only if $k_2 \ll k_{-1}$ in the following scheme:



In Briggs-Haldane kinetics*, $K_m = \frac{k_{-1} + k_2}{k_1}$. Nonetheless, the K_m is the substrate concentration when the reaction velocity is half the maximum velocity ($v = V_{\max}/2$). It may be treated as an apparent dissociation constant of all enzyme-bound species and as such is expressed as:

$$K_m = \frac{[E][S]}{\sum [ES]} \quad (\text{C.4})$$

Therefore, in the simple Michaelis mechanism, the K_m simplifies to $K_s = \frac{k_{-1}}{k_1}$ and as such is a measure of the enzyme affinity for the substrate. A low K_m indicates that the enzyme has a high affinity for the substrate.

At low substrate concentration, where $[S] \ll K_m$, the Michaelis–Menten equation simplifies to

$$v = \frac{[E]_0 [S] k_{\text{cat}}}{K_m} \quad (\text{C.5})$$

whereas at saturating concentrations, where $[S] \gg K_m$, the equation becomes

$$v = V_{\max} = k_{\text{cat}} [E]_0 \quad (\text{C.6})$$

* Briggs, G. E.; Haldane, J. B. S. *Biochem. J.* **19**, 338 (1925).

The Michaelis–Menten expression above describes a rectangular hyperbola such as is plotted in Figure C.1.

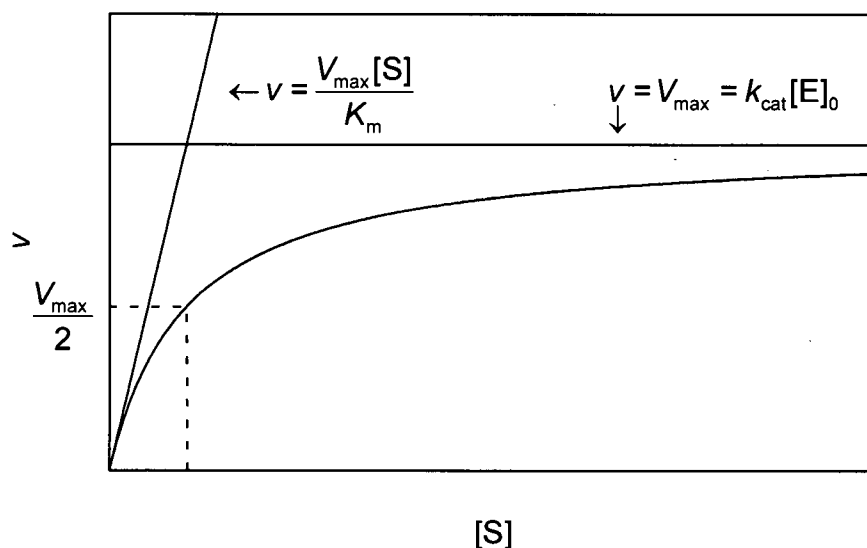


Figure C.1: Plot of reaction rate v versus substrate concentration $[S]$ for a typical enzymatic reaction obeying Michaelis–Menten kinetics.

At low $[S]$ the enzyme is largely unbound such that the total concentration, which is a sum of the concentration of the free and bound enzyme, can be approximated to the concentration of the free enzyme, $[E]$. The Michaelis–Menten equation under these conditions is expressed as

$$v = \frac{[E][S]k_{\text{cat}}}{K_m} \quad (\text{C.7})$$

The k_{cat}/K_m from the above equation is an apparent second-order rate constant that relates the reaction rate to the concentration of *free* enzyme and *free* substrate. This kinetic parameter is also referred to as a specificity constant that is a measure of the catalytic efficiency for the substrate. It is not a true microscopic rate constant except in

the case in which the rate-determining step in the reaction is the encounter of enzyme and substrate. The rate constant is then said to be diffusion-controlled and has been found experimentally to be in the range of 10^6 to $10^9 \text{ s}^{-1} \text{ M}^{-1}$.*

The Michaelis–Menten equation is often transformed into a linear form that is useful for the graphical analysis of the data and detection of deviations from ideal behaviour. The double-reciprocal or Lineweaver–Burk plot[†] is a common method of graphical analysis that is obtained by inverting both sides of the Michaelis–Menten equation.

$$\frac{1}{v} = \frac{1}{V_{\max}} + \frac{K_m}{V_{\max} [S]} \quad (\text{C.8})$$

Plotting $1/v$ as a function of $1/[S]$ (Figure C.2) gives an intercept of $1/V_{\max}$ on the y axis and $-1/K_m$ on the x axis. The slope of the line is K_m/V_{\max} .

* Eigen, M.; Hammes, G. G. *Adv. Enzymol.* **25**, 1 (1963).

† Lineweaver, H.; Burk, D. *J. Am. Chem. Soc.* **56**, 658 (1934).

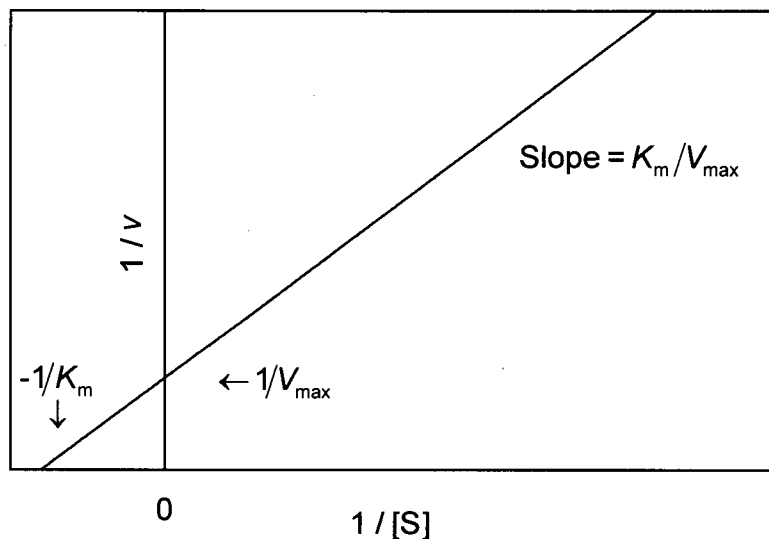
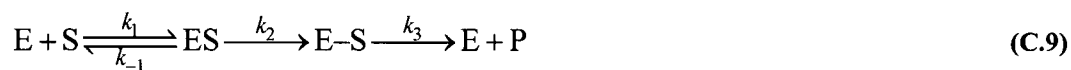


Figure C.2: A Lineweaver–Burk plot for an enzymatic reaction.

C.2 The Significance of Michaelis–Menten Parameters

The Michaelis–Menten equation remains applicable to a variety of cases in which additional intermediates occur on the reaction pathway, although k_{cat} and K_m are now a combination of various rate and equilibrium constants.

The general double-displacement mechanism for glycoside hydrolysis by a retaining glycosidase, originally proposed by Koshland,^{*} proceeds through equation C.9 below.



The formation of the Michaelis–Menten complex ES is referred to as the association step. The conversion of ES to the covalent intermediate $E-S$ is known as the glycosylation step, while the release of product is referred to as the deglycosylation step.

^{*} Koshland, D. E. *Biol. Rev.* **28**, 416 (1953).

Assuming a steady state concentration of ES and E-S is reached during the reaction, the Michaelis–Menten equation is given by

$$v = \frac{\frac{k_2 k_3}{k_2 + k_3} [E]_0 [S]}{\frac{k_3 (k_{-1} + k_2)}{k_1 (k_2 + k_3)} + [S]} \quad (\text{C.10})$$

The equation above follows the standard form of the Michaelis–Menten equation with the following kinetic parameters for the mechanism:

$$k_{\text{cat}} = \frac{k_2 k_3}{k_2 + k_3} \quad (\text{C.11})$$

$$K_m = \frac{k_3 (k_{-1} + k_2)}{k_1 (k_2 + k_3)} \quad (\text{C.12})$$

$$\frac{k_{\text{cat}}}{K_m} = \frac{k_1 k_2}{k_{-1} + k_2} \quad (\text{C.13})$$

It may be shown that k_{cat} is the rate constant for the rate-determining step of the reaction and will always be associated with the highest free energy step in the pathway. The pseudo second-order rate constant, k_{cat}/K_m , refers to the properties and the reactions of the free enzyme and free substrate proceeding to the transition state of the first irreversible step.

Glycosylation becomes rate determining when the rate of deglycosylation is much greater than glycosylation ($k_3 \gg k_2$). Furthermore, if association of enzyme and substrate are rapid and reversible ($k_{-1} \gg k_2$), the kinetic parameters reduce to

$$k_{\text{cat}} = k_2 \quad (\text{C.14})$$

$$K_m = \frac{k_{-1}}{k_1} = K_s \quad (\text{C.15})$$

$$\frac{k_{\text{cat}}}{K_m} = \frac{k_1 k_2}{k_{-1}} = \frac{k_2}{K_s} \quad (\text{C.16})$$

and the Eyring equations are

$$k_{\text{cat}} = \left(\frac{kT}{h} \right) \exp \left(- \frac{(G_{\text{ES}}^{\ddagger} - G_{\text{ES}})}{RT} \right) = \left(\frac{kT}{h} \right) \exp \left(- \frac{\Delta G_{\text{c}}^{\ddagger}}{RT} \right) \quad (\text{C.17})$$

$$\frac{k_{\text{cat}}}{K_m} = \left(\frac{kT}{h} \right) \exp \left(- \frac{(G_{\text{ES}}^{\ddagger} - G_{\text{E+S}})}{RT} \right) = \left(\frac{kT}{h} \right) \exp \left(- \frac{\Delta G_{\text{T}}^{\ddagger}}{RT} \right) \quad (\text{C.18})$$

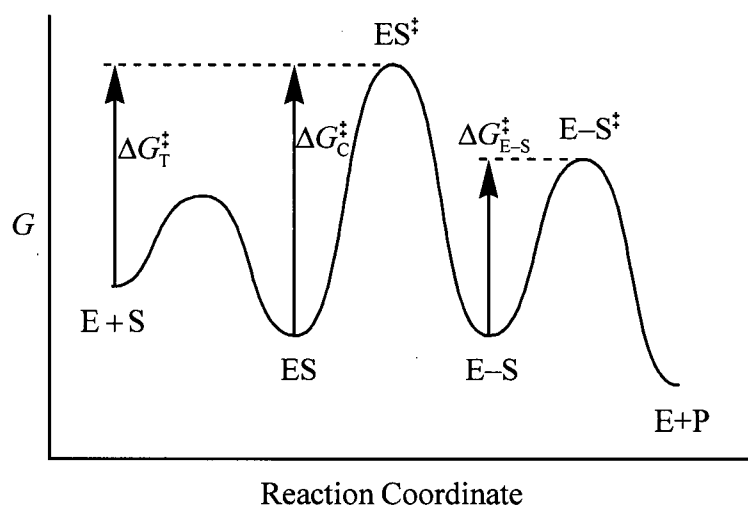


Figure C.3: Hypothetical Gibbs free energy diagram for a retaining glycosidase showing rate-limiting glycosylation ($k_2 \ll k_3$).

In this case, the kinetic parameters, k_{cat} and k_{cat}/K_m , both provide information pertaining to the transition state of the glycosylation step. However, the initial reference

point for k_{cat} is the ES complex and for k_{cat}/K_m , it is free enzyme (E) and free substrate (S).

If, however, the rate of deglycosylation becomes rate determining when the rate of glycosylation is much greater than deglycosylation ($k_2 \gg k_3$), and association of enzyme and substrate are rapid and reversible ($k_{-1} \gg k_2$), the kinetic parameters are reduced to

$$k_{\text{cat}} = k_3 \quad (\text{C.19})$$

$$K_m = \frac{k_{-1}k_3}{k_1k_2} = K_S \frac{k_3}{k_2} \quad (\text{C.20})$$

$$\frac{k_{\text{cat}}}{K_m} = \frac{k_1k_2}{k_{-1}} = \frac{k_2}{K_S} \quad (\text{C.21})$$

which in Eyring form become

$$k_{\text{cat}} = \left(\frac{kT}{h} \right) \exp \left(- \frac{(G_{\text{E-S}}^{\ddagger} - G_{\text{E-S}})}{RT} \right) = \left(\frac{kT}{h} \right) \exp \left(- \frac{\Delta G_{\text{E-S}}^{\ddagger}}{RT} \right) \quad (\text{C.22})$$

$$\frac{k_{\text{cat}}}{K_m} = \left(\frac{kT}{h} \right) \exp \left(- \frac{(G_{\text{ES}}^{\ddagger} - G_{\text{E+S}})}{RT} \right) = \left(\frac{kT}{h} \right) \exp \left(- \frac{\Delta G_{\text{T}}^{\ddagger}}{RT} \right) \quad (\text{C.23})$$

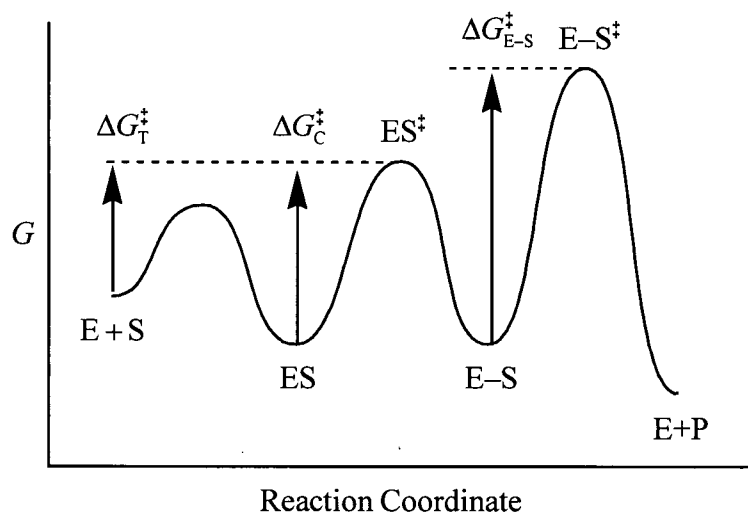


Figure C.4: Hypothetical Gibbs free energy diagram for a retaining glycosidase showing rate-limiting deglycosylation ($k_3 \ll k_2$).

In this case, k_{cat} refers to the transition state of deglycosylation with the covalent intermediate complex as the initial reference point and k_{cat}/K_m refers to the transition state of the glycosylation step with free enzyme [E] and free substrate [S] as the initial reference points.

Thus, in these examples, k_{cat} refers to the rate-determining step while k_{cat}/K_m corresponds to the first irreversible step in the reaction with free enzyme and free substrate as the reference states. In general, $\frac{k_{\text{cat}}}{K_m} = \frac{k_2}{K_s}$, except for the Briggs-Haldane mechanism in which the enzyme-substrate complex is *not* in thermodynamic equilibrium with the free enzyme and substrate.

If the first chemical step of the reaction accelerates to such an extent that the encounter of the enzyme and the substrate become rate determining ($k_{-1} \ll k_2$), the apparent second-order rate constant k_{cat}/K_m approaches the diffusion-controlled limit of

$10^9 \text{ s}^{-1} \text{ M}^{-1}$. The k_{cat} is unaffected and is dependent on whether glycosylation or deglycosylation is the rate-determining step of the reaction. Assuming product release is rate determining, the kinetic parameters reduce to

$$k_{\text{cat}} = k_3 \quad (\text{C.24})$$

$$K_m = \frac{k_3}{k_1} \quad (\text{C.25})$$

$$\frac{k_{\text{cat}}}{K_m} = k_1 \quad (\text{C.26})$$

which in Eyring form become

$$k_{\text{cat}} = \left(\frac{kT}{h} \right) \exp \left(-\frac{(G_{\text{E-S}}^* - G_{\text{E-S}})}{RT} \right) = \left(\frac{kT}{h} \right) \exp \left(-\frac{\Delta G_{\text{E-S}}^*}{RT} \right) \quad (\text{C.27})$$

$$\frac{k_{\text{cat}}}{K_m} = \left(\frac{kT}{h} \right) \exp \left(-\frac{(G_{\text{ES}}^* - G_{\text{E+S}})}{RT} \right) = \left(\frac{kT}{h} \right) \exp \left(-\frac{\Delta G_{\text{r}}^*}{RT} \right) \quad (\text{C.28})$$

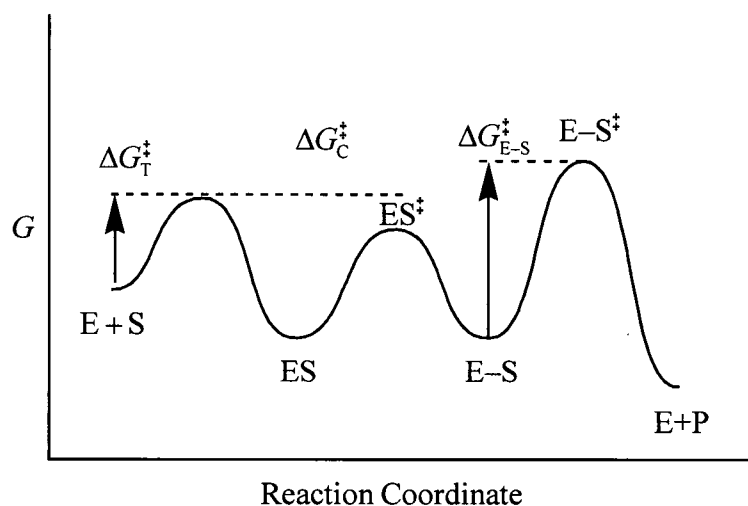


Figure C.5: Hypothetical Gibbs free energy diagram for a retaining glycosidase showing rate-limiting association ($k_{-1} \ll k_2$).

C.3 Enzyme Inhibition

Enzymes may be *reversibly* inhibited by the non-covalent binding of inhibitors according to four binding modes.

C.3.1 Competitive inhibition

An inhibitor is said to be a *competitive* inhibitor when it binds reversibly to the active site of an enzyme and prevents the substrate S from binding and *vice versa* (Figure C.6).

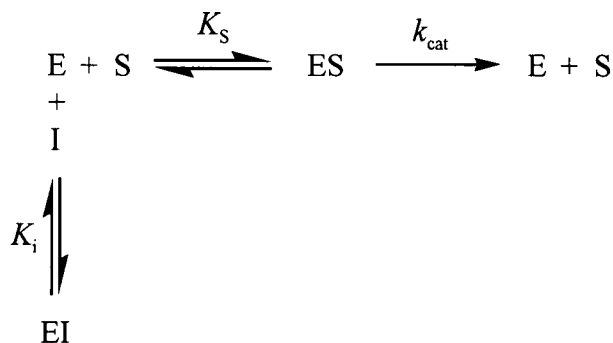


Figure C.6: The simple Michaelis–Menten mechanism showing an addition equilibrium where $K_i = [\text{E}][\text{I}]/[\text{EI}]$.

The Michaelis constant K_m appears to increase by a factor of $(1 + [\text{I}]/K_i)$ as in the equation below.

$$v = \frac{[\text{E}]_0 [\text{S}] k_{\text{cat}}}{[\text{S}] + K_m (1 + [\text{I}]/K_i)} \quad (\text{C.29})$$

Infinitely high concentrations of S displace I from the enzyme, therefore competitive inhibition affects only K_m and not V_{max} .

C.3.2 Noncompetitive, uncompetitive, and mixed inhibition

Simultaneous binding of I and S to the enzyme instead of competition for the same binding site results in different inhibition patterns (Figure C.7).

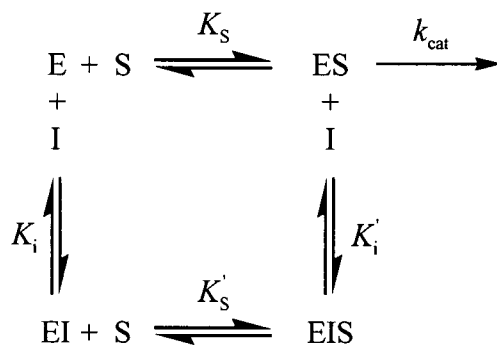


Figure C.7: Thermodynamic box where the inhibition constant of the free enzyme is K_i ; that of the enzyme–substrate complex is K'_i ; and the dissociation constants of EIS and ES are K'_S and K_S , respectively.

Noncompetitive inhibition occurs when the dissociation constant of S from ES is the same as that from EIS (that is, $K_S = K'_S$), and EIS does not react so that

$$v = \frac{[E]_0[S]k_{\text{cat}}/(1 + [I]/K_i)}{[S] + K_m} \quad (\text{C.30})$$

In the above case of noncompetitive inhibition, k_{cat} is lowered by a factor of $(1 + [I]/K_i)$ and K_m is unaffected. *Mixed inhibition* occurs when the dissociation constant of S from ES is different than that from EIS ($K_S \neq K'_S$), and results in altered values of K_m and k_{cat} . *Uncompetitive inhibition* occurs when I binds to ES but not to E. In this case, both K_m and k_{cat} are altered by the same factor, therefore k_{cat}/K_m remains unchanged.

C.4 Binding Energy and Enzyme Catalysis

In 1978 Schowen* proposed "...that the entire and sole source of catalytic power is the stabilization of the transition state; that reactant-state interactions are by nature inhibitory and only waste catalytic power."

Enzymes, like other catalysts, increase reaction rates by lowering activation energies. A unique feature of enzyme catalysis is that the enzyme binds specifically to the substrate and the binding energies involved are used to lower activation energies. However, since the structure of the substrate changes during the reaction, the enzyme can be complementary to only the ground-state or transition-state form of the substrate. It will be shown that it is catalytically advantageous for the enzyme to be complementary to the transition-state structure rather than to the ground-state form of the substrate.

Consider a typical enzymatic reaction consisting of a binding step followed by a catalytic step such as that shown below.



The energy diagram for this reaction is illustrated in Figure C.8 where $k_{-1} \gg k_2$, so that $K_m = K_S$ and the kinetic parameters may be expressed as the following.

$$K_m = \left(\frac{kT}{h} \right) \exp \left(- \frac{\Delta G_S}{RT} \right) \quad (C.32)$$

$$k_{cat} = \left(\frac{kT}{h} \right) \exp \left(- \frac{\Delta G_C^\ddagger}{RT} \right) \quad (C.33)$$

* Schowen, R. L. *Transition States of Biochemical Processes*, Plenum, New York (1978).

$$\frac{k_{\text{cat}}}{K_{\text{m}}} = \left(\frac{kT}{h} \right) \exp \left(-\frac{\Delta G_{\text{T}}^{\ddagger}}{RT} \right) \quad (\text{C.34})$$

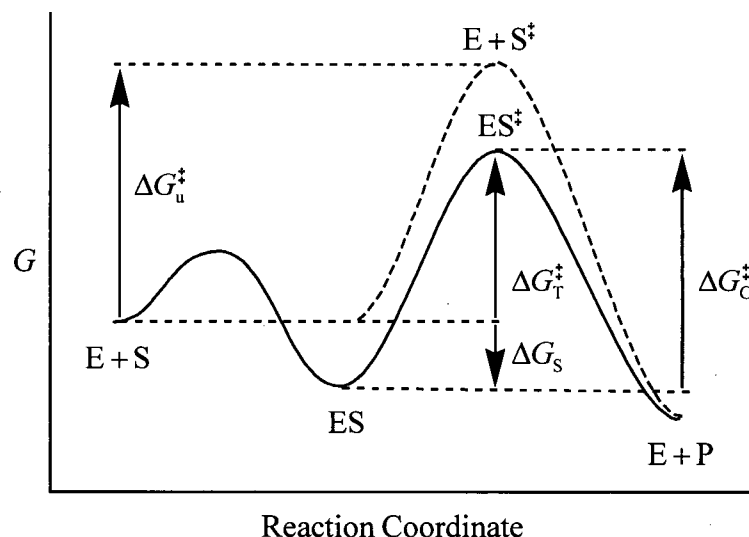


Figure C.8: The reaction coordinate diagram for a typical reaction (solid line) and the corresponding uncatalyzed reaction (dashed line).

Consider the above situation when an additional amount of binding energy, ΔG_{R} , has become available in the form of a hydrogen bond between the enzyme and the substrate. If that extra binding energy is realized in the enzyme–substrate (ES) complex (Figure C.9, left) rather than the transition-state (ES^{\ddagger}) complex, then the ground state is stabilized and ΔG_{S} increases by ΔG_{R} resulting in a decrease of K_{m} . The value of k_{cat} is also reduced since $\Delta G_{\text{C}}^{\ddagger}$ (enzyme–substrate complex, ES, proceeding to the transition state, ES^{\ddagger}) is increased by the ground-state stabilization, ΔG_{R} . However $k_{\text{cat}}/K_{\text{m}}$ is unaffected as this is the rate constant for free enzyme (E) and free substrate (S) proceeding to the transition state (ES^{\ddagger}). Therefore, if the enzyme is complementary to the ground state, then there is tighter substrate binding but a slower reaction rate, k_{cat} .

Alternatively, if the extra binding energy, ΔG_R , is realized only in the transition-state complex (Figure C.9, right), then the transition state is stabilized and ΔG_C^\ddagger and ΔG_T^\ddagger will be lowered by ΔG_R , thus, k_{cat} and k_{cat}/K_m will be increased. The value of ΔG_S is unchanged, and hence, K_m remains the same. Transition-state stabilization can therefore lower the activation energies of k_{cat} and k_{cat}/K_m , increasing reaction rates as a consequence. Ground-state stabilization has no effect on k_{cat}/K_m , although the k_{cat} is decreased.

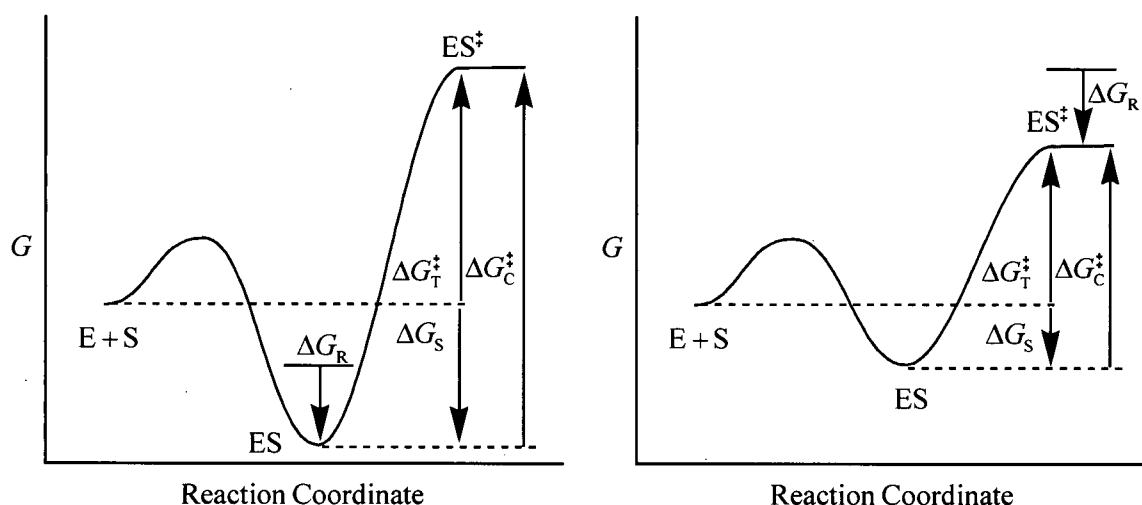


Figure C.9: The reaction coordinate diagram illustrating complementarity of the enzyme to (left) the ground state, and (right) the transition state of the substrate.

C.5 The pH Dependence of Enzyme Catalysis

Enzymes contain a significant number of ionizing groups, some of which are directly involved in catalysis at the active site, while others may be responsible for maintaining the active conformation of the enzyme. Enzyme activity can vary with pH since the active sites contain important acidic or basic groups, where only one protonic

form of the acid or base is catalytically active. Plots of rate against pH take the form of simple single or double ionization curves because, although enzymes contain a multitude of ionizing groups, the only ionizations that are of importance are those of groups that are directly involved in catalysis at the active site.

Four simplifying assumptions include:

1. The groups act as perfectly titrating acids or bases.
2. Only one ionic form of the enzyme is active.
3. Proton transfers are faster than chemical steps.
4. The rate-determining step does not change with pH.

C.5.1 The Michaelis–Menten mechanism

In the simple Michaelis–Menten mechanism, the following equilibria may be set up:

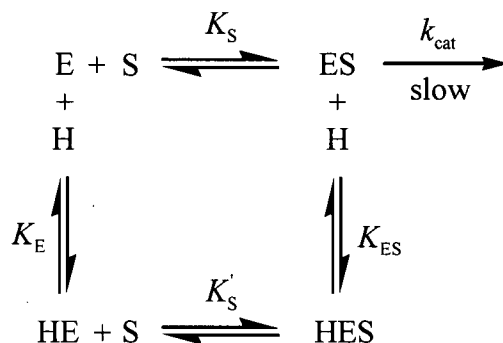


Figure C.10: Thermodynamic box where the ionization constant of the free enzyme is K_E ; that of the enzyme–substrate complex is K_{ES} ; and the dissociation constants of HES and ES are K'_S and K_S , respectively.

Due to the cyclic nature of the equilibria, all four equilibrium constants are related by the equation:

$$K_E K'_S = K_{ES} K_S \quad (\text{C.35})$$

Assuming $K_m = K_S$, the pH dependence of v is given by the following expression:

$$v_H = \frac{k_{\text{cat}} [E]_0 [S]}{K_S + [S] \left(1 + \frac{[H^+]}{K_{ES}} \right) + K_S \frac{[H^+]}{K_E}} \quad (\text{C.36})$$

When $[S] \gg K_S$, the pH dependence of k_{cat} is derived from equation C.36:

$$(V_{\text{max}})_H = [E]_0 (k_{\text{cat}})_H = \frac{k_{\text{cat}} [E]_0 K_{ES}}{K_{ES} + [H^+]} \quad (\text{C.37})$$

The pH dependence of V_{max} or k_{cat} follows the ionization constant of the enzyme-substrate complex, K_{ES} .

The apparent value of K_m (where $K_m = K_S$) at each pH is derived by rearranging equation C.36:

$$(K_m)_H = K_S \frac{\left(1 + \frac{[H^+]}{K_E} \right)}{\left(1 + \frac{[H^+]}{K_{ES}} \right)} \quad (\text{C.38})$$

K_m also follows the ionizations of the enzyme-substrate complex.

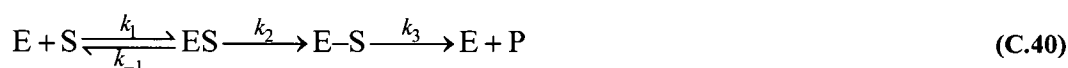
When $[S] \ll K_m$, the pH dependence of k_{cat}/K_m is derived from equation C.36:

$$\left(\frac{k_{\text{cat}}}{K_m} \right)_H = \frac{(k_{\text{cat}}/K_m)}{\left(1 + \frac{[H^+]}{K_E} \right)} \quad (\text{C.39})$$

The pH dependence of k_{cat}/K_m follows the ionizations in the free enzyme and free substrate.

C.5.2 Modifications and breakdown of the Michaelis–Menten mechanism

If a mechanism more complicated than the simple Michaelis–Menten occurs, additional considerations must be taken into account.



The presence of additional intermediates on the reaction pathway does not affect the pH dependence of k_{cat}/K_m . The $\text{p}K_a$'s obtained from the pH profile will correspond to the $\text{p}K_a$'s of the free enzyme and free substrate.* However, the pH dependence of k_{cat} and K_m will give the $\text{p}K_a$'s of the major enzyme-bound species. The pH profiles will give the $\text{p}K_a$'s that are dependent on the concentration of the intermediates and the enzyme–substrate complex.†

When a substrate binds in a non-productive as well as in the productive mode, the pH dependence of k_{cat} or K_m may give an apparent $\text{p}K_a$ that significantly deviates from the real value. This occurs if the ratio of productive to non-productive binding is dependent on ionization of a group in the active site of an enzyme. The pH dependence of k_{cat}/K_m is not affected by non-productive binding modes.‡

* Bender, M. L.; Clement, G. E.; Kézdy, F. J.; Heck, H. d'A. *J. Am. Chem. Soc.* **86**, 3680 (1964).

† Fersht, A. R.; Requena, Y. *J. Am. Chem. Soc.* **93**, 7079 (1971).

‡ Fersht, A. R.; Fastrez, J. *Biochemistry* **12**, 1067 (1973).

The simple rules for pH dependence breakdown in the case of Briggs-Haldane kinetics:*



A change of rate-determining step with pH may give rise to anomalous pK_a 's. When the rate constant for the chemical step is larger than that for the dissociation of the enzyme-substrate complex, k_{cat}/K_m is equal to k_1 , the association rate constant of the enzyme and the substrate. Suppose that the catalytic activity of an enzyme depends on the ionization of a base so that k_2 will be faster than k_{-1} at high pH, but will decrease as the pH is lowered and the base becomes protonated until k_2 is slower than k_{-1} . The apparent pK_a obtained from a pH profile of k_{cat}/K_m results in a *kinetic* pK_a that is lower than the actual pK_a of the group. If the ionization constant of the group on the enzyme is K_a , the apparent ionization constant is given by

$$K_{\text{app}} = \frac{K_a (k_2 + k_{-1})}{k_{-1}} \quad (\text{C.42})$$

* Schmidt, D. E., Jr.; Westheimer, F. H. *Biochemistry* 10, 1249 (1971).

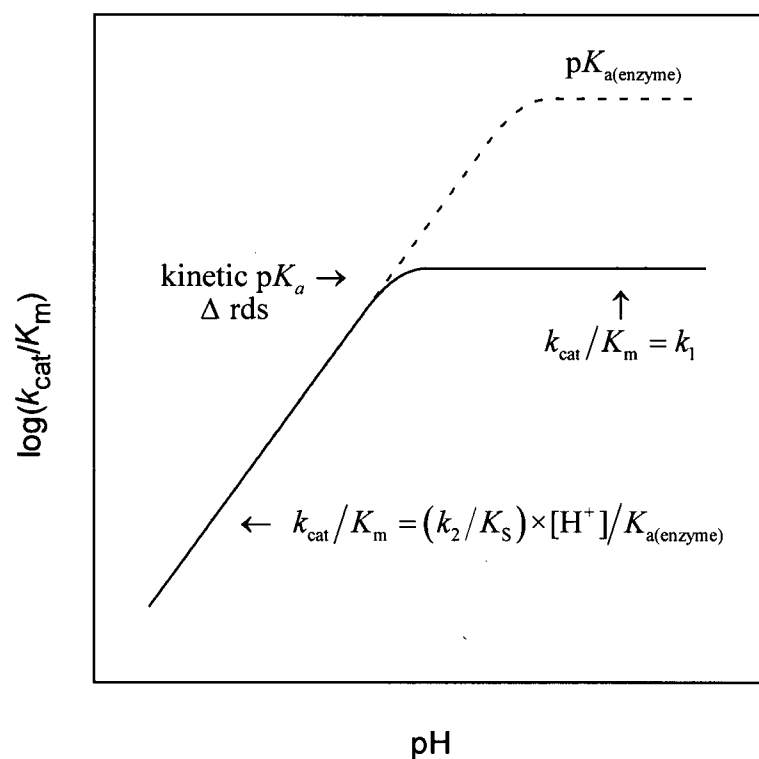


Figure C.11: Illustration of how a change in rate-determining step from a chemical event at low pH to the encounter of enzyme and substrate at high pH may lead to an anomalous pK_a in the k_{cat}/K_m pH profile.*

In general, kinetic pK_a 's occur whenever there is a change of rate-determining step with pH.

* Renard, M.; Fersht, A. R.; *Biochemistry* **12**, 4713 (1973).